

# Quantum Electrodynamics at strong Couplings

Uwe Trittmann and Hans-Christian Pauli  
*Max-Planck-Institut für Kernphysik*  
D-69029 Heidelberg  
(October 8, 2018)

## Abstract

Front form dynamics is not a manifestly rotational invariant formalism. In particular, the requirement of an invariance under rotations around the transverse axes is difficult to fulfill since the corresponding operators are complicated and involve the interaction. All approximations in solving Quantum Field Theories using front form dynamics, as inevitable as they are, are destined to destroy full Poincaré invariance. In the present work it is investigated, to which extent rotational invariance is restored in the solution of a light-cone quantized field theory. The positronium spectrum in full (3+1) dimensions is calculated at an unphysically large coupling of  $\alpha = 0.3$  to be sensitive for terms breaking rotational invariance and to accustomize the theory to future QCD applications. The numerical accuracy of the formalism is improved to allow for the calculation of mass eigenvalues for arbitrary components  $J_z$  of the total angular momentum. We find numerically degenerate eigenvalues as expected from rotationally invariant formalisms and the right multiplet structures up to large principal quantum numbers  $n$ . The results indicate that rotational invariance is unproblematic even in front form dynamics. Another focus of the work relies on the inclusion of the annihilation channel. This enlargement of the model is non-trivial and a consistency check of the underlying theory of effective interactions. The correct numerical eigenvalue shifts, and especially the right hyperfine splitting are obtained. Moreover, the cutoff dependence of the eigenvalues is improved drastically by the annihilation channel for the triplet states. The implications of the applied effective Hamiltonian approach are discussed in detail.

# Contents

<b>Introduction</b>	<b>1</b>
<b>1 Field theories in front form dynamics</b>	<b>6</b>
1.1 Historical survey . . . . .	6
1.2 Problems of front form field theories . . . . .	7
1.3 Preceding work . . . . .	9
<b>2 The positronium model</b>	<b>10</b>
2.1 The model . . . . .	11
2.2 The effective integral equation . . . . .	15
2.3 The positronium mass spectrum . . . . .	17
2.4 Wavefunctions . . . . .	25
<b>3 Angular momentum in front form dynamics</b>	<b>29</b>
3.1 The Poincaré group on the light-cone . . . . .	29
3.1.1 Unitary representations of the Poincaré group . . . . .	29
3.1.2 Connection between canonical spin and front form helicity . . . . .	31
3.1.3 Field theories on the light-cone . . . . .	31
3.2 The Hamiltonian matrix with general $J_z$ . . . . .	34
3.3 The positronium spectrum for general $J_z$ . . . . .	35
3.4 Wavefunctions . . . . .	41
<b>4 The annihilation channel</b>	<b>46</b>
4.1 Introduction . . . . .	46
4.2 Calculation of the matrix elements . . . . .	48
4.3 Spectrum including the annihilation channel . . . . .	50
4.4 Parameter dependence of the spectrum . . . . .	51
<b>5 On the theory of effective interactions</b>	<b>58</b>
5.1 Introduction . . . . .	58
5.2 The method of iterated resolvents . . . . .	59
5.3 QED treated with iterated resolvents . . . . .	61
5.4 Application to a model Hamiltonian . . . . .	64

<b>6</b>	<b>Summary and Outlook</b>	<b>67</b>
<b>A</b>	<b>Notation</b>	<b>72</b>
<b>B</b>	<b>QED(3+1) on the light-cone</b>	<b>74</b>
<b>C</b>	<b>Matrix elements of the light-cone Hamiltonian in QED</b>	<b>79</b>
<b>D</b>	<b>Calculation of effective matrix elements</b>	<b>83</b>
<b>E</b>	<b>Renormalization</b>	<b>87</b>
E.1	The electron sector . . . . .	87
E.2	The positronium sector . . . . .	89
<b>F</b>	<b>Tables of effective matrix elements</b>	<b>90</b>
F.1	Introduction and Notations . . . . .	90
F.2	General helicity table . . . . .	91
F.3	The helicity table for arbitrary $J_z$ . . . . .	92
F.4	Helicity table of the annihilation graph . . . . .	93
<b>G</b>	<b>Numerics</b>	<b>94</b>
G.1	Transformation of the variables . . . . .	94
G.2	Symmetries . . . . .	95
G.3	Coulomb trick . . . . .	98
<b>H</b>	<b>Listing of the computer code</b>	<b>100</b>
H.1	Description of the program . . . . .	100
H.2	Listing . . . . .	101

# Introduction

After a long line of efforts, Quantum Chromodynamics [1, 2, 3, 4] emerged around 1973 as the theory that correctly describes the interaction between *quarks* (fermions), considered to be elementary, through the action of the non-abelian gauge field of *gluons* (bosons). The hierarchy of particles seems to be the following. The *hadrons*, that is baryons (nucleons) and mesons, consist of quarks. The gluons produce the interaction between quarks. They provide the force, a strong analogue of the van-der-Waals force, that allows nucleons to bind together to form the atomic nucleus. This point of view concerning the nuclear forces clarified the former picture that the intermediate boson field is that of the mesons [5].

An open question in modern theoretical physics is the link between the high and the low energy domains of Quantum Chromodynamics. The description of the high energy region, which was inspired by experiments in the late sixties, is well established. Contrary, the low energy region of the theory cannot be attacked by standard perturbation theory because the coupling depends on the scale and grows large in this region. Instead, this region must be described by more phenomenological models such as the constituent quark model, or chiral perturbation theory. A major problem in this undertaking to connect the high and the low energy regimes is the running coupling constant of QCD which depends very strongly on the four momentum transfer between the interacting particles. Moreover, it grows large for small momentum transfer so that perturbation theory breaks down at a certain point. An important task of theoretical high and medium energy physics is therefore the construction of methods that can produce *hadronic* spectra and wavefunctions. The importance of the hadronic properties and their wavefunctions for physical observables, such as structure functions and decay constants, is undeniable. Moreover, their calculation would allow for rigorous tests of assumptions necessary in models of nuclei and hadrons.

The history of methods to calculate quantum mechanical bound states is as old as Quantum Mechanics itself [6]. But in hadronic physics the large coupling implies that bound particles form highly relativistic systems. This fact enforces the rigorous application of covariant field theories. Non-relativistic *potential models* [7, 8, 9] are only applicable for heavy systems, as for instance the  $J/\psi$  [10, 11] or the  $\Upsilon$  [12]. Other covariant methods are *lattice gauge theory* [13] or the evaluation of the *Bethe-Salpeter equation* [14]. Within lattice gauge theories only the ground state or the first few excited states are tractable and structure functions are extremely difficult to observe directly[15]. The application of the Bethe-Salpeter equation[16] suffers the

typical fate of strongly bound systems: The wavefunctions are dominated by relativistic momenta and contain a considerable number of quark-antiquark pairs. Therefore, even the vacuum is very complicated.

The latter point is problematic for all quantum field theories, if a theory is quantized at equal usual time. In *light-cone quantization*, the results are frame independent, as opposed to equal time quantization. There, the Lorentz boosts contain the interaction and are therefore complicated dynamical operators, whereas in light-cone quantization all Lorentz boosts are kinematic [17, Chap. 2.B]. Consequently, light-cone quantized field theories seem to be a promising tool to understand the physics of relativistic QCD-bound states. However, neither have all problems (Poincaré invariance, zero modes, etc.) of this Hamiltonian approach been solved, nor is it clear if and how effective theories [18, 19, 20] which have been proposed to deal with the problems associated to finite cutoffs, will work. Some of these deficiencies are due to the neglect of Hamiltonian field theory in favor of the action-oriented approaches of FEYNMAN, ET. AL [21, 22, 23]. In any case, it is better to establish that a new method works for known problems before applying it to yet unsolved problems. Bearing this in mind, the basic motivation for the present work is twofold. On the one hand, there is the obvious obstacle that light-cone quantized theories are rotationally *not* manifestly invariant *by construction*. One main part of this thesis is consequently dedicated to the investigation of the associated question, what this means to the results of such a theory: do the *results* obey rotational symmetry (as observed in nature) or not? Because we have to compare to other calculations and methods, we choose a realistic, well-understood, but non-trivial problem, namely the QED-bound state *par excellence*: positronium. Our choice has another cause. The formalism to be applied is ideally suited for this case of two particles of same mass. In ordinary approaches, the severe problems of recoil corrections make it much easier to calculate the hydrogen or muonium spectra than to solve for the eigenvalues of positronium.

On the other hand, there is the need for an effective formalism for gauge theories: nobody ever has solved rigorously a relativistic many-body theory in one time and three space dimensions (3+1 dimensional theory). It is therefore necessary to use such an effective approach and to investigate how reasonable its results are. We have done so. But *after* the successfully applying of the effective method, we go one step further in asking how the excellent results can be understood within a much more general formalism, originating in the Lagrangian density of a gauge theory.

## Outline of the present work

This work is structured as follows. We start in Chapter 1 with an overview of the development and difficulties of the approach to field theories in front form dynamics. In Chapter 2, the positronium model used in the present work is introduced. Starting with a Hamiltonian field theory quantized on the light-cone, the steps are described that lead to the formulation of an *effective integral equation* in momentum space. Although

the derivation of the Hamiltonian involved the application of the DLCQ formalism, described in the following section, we stress the fact that we use only the continuum formulation of  $\text{QED}_{(3+1)}$  in front form dynamics in the present work. Discretizations occur only in the context of numerical integrations, which have nothing to do with physical considerations. Errors due to numerical artifacts, such as effects of a finite number of integration points  $N$ , are discussed. Cutoffs determined by physics emerge in two aspects. One is the problem of divergencies occurring because transverse momenta can become infinite. Therefore, one must introduce a regulator. We analyze the results of our model concerning their dependencies on this cutoff. The second is the restriction of *sectors* with different particle content, sometimes referred to as Tamm-Dancoff approach. We will show that (a) a theory truncated in this way is not solvable, (b) there is a possibility to treat the associated singularity by adjusting the form of the effective interaction, and (c) the treatment of the singularity can be understood within a general formalism of effective interactions. The latter point is discussed in Chapter 5.

We improved the numerical methods which were used to solve the effective interaction before [24]. This leads to an improved convergence of the eigenvalues with the number of integration points. However, the basic intention is the need of this improvement to attack the generalization of the model, described in Chapter 3. More effort than in [24] is put in the investigation of higher excited states to show the range of applicability of the model. We find the correct multiplet structure up to a principal quantum number  $n=5$ . Detailed tables allow for the comparison of the results of the present work with those of equal-time perturbation theory. We emphasize the use of a huge coupling constant,  $\alpha=0.3$ , to test our non-perturbative approach: it is approximately 40 times larger than the physical coupling constant of QED. In the calculation of the hyperfine splitting, we point out that the comparison of our results with perturbation theory is problematic, because results of the latter depend noticeably on the order of the calculations at large couplings.

As a main point of the thesis, we generalize the formalism of Chapter 2 to arbitrary  $z$ -components of the total angular momentum,  $J_z$ . This is done in Chapter 3. Before, calculations were performed in the  $J_z=0$  sector of the theory only. To interpret the results, the theory of the Poincaré group is studied in the introductory section of this chapter in the context of front form dynamics. We find that states with the same total angular momentum  $J$ , but different  $J_z$ , are numerically degenerate. This result is expected from physical considerations, but surprising because the associated operators of transverse rotations are dynamical in front form dynamics although they do commute with the light-cone Hamiltonian. As a consequence of our calculations, we can classify the positronium eigenstates according to their quantum numbers of  $J^2$  and  $J_z$ , just as in the equal-time formalism. The wavefunctions are analyzed concerning their symmetry properties. Besides, we show that the wavefunctions are *not* rotationally invariant in any sector of  $J_z$ .

After the application of effective interactions and the generalization of the theory to arbitrary  $J_z$ , the next crucial point is the introduction of the annihilation channel into the theory (Chapter 4). We enlarge the Fock basis by the one-photon state,

typical for QED and absent in QCD. It is shown that the degeneracy of states is maintained. This is astonishing, because we find a total separation of the dynamic and instantaneous diagrams involved in the different  $J_z$  sectors. Another consequence of the implementation of the annihilation channel is the stabilizing of eigenvalues, concerning their dependence on the cutoff  $\Lambda$ .

Chapter 5 deals with the problems constructing effective interactions in front form dynamics. We show that the prescription to treat the singularity attached to a truncation of the Fock space is a consequence of the formalism of effective interactions. A summary and a discussion of our results follow.

All basics and technical details are consequently cast into the appendices to achieve a clear and structured line of arguments in the main part of the thesis. We address the attention of the reader especially to Appendix B where QED on the light-cone is described, and to Appendix G where the numerical methods are explained. The latter should be studied when details of calculations seem unclear in the main text. In Appendix E the applied renormalization scheme is described. The other appendices mainly supply necessary formulæ. The source code of the computer program developed in the present work is listed in Appendix H.

## Methodological sketch

This section describes in short the methods applied in the thesis and their subtle points.

- The underlying picture of a composed system in front form dynamics is that of a state consisting of valence particles carrying its outer quantum numbers, and of arbitrarily many virtual particles, be it gauge particles or fermion-antifermion pairs. A state is written in Fock-space representation as

$$|\psi\rangle = \psi_g|\psi_g\rangle + \psi_{q\bar{q}}|\psi_{q\bar{q}}\rangle + \psi_{q\bar{q}\gamma}|\psi_{q\bar{q}\gamma}\rangle + \psi_{q\bar{q}gg}|\psi_{q\bar{q}gg}\rangle + \dots$$

Here,  $g$  denotes a gauge boson (photon or gluon) and  $q$  a fermion (electron or quark). In QCD, the first term in this expansion is absent because it is not color neutral.

- To construct the Hamiltonian, the following steps are performed. First, starting with the Lagrangian density, the generators of the Poincaré group are calculated.<sup>1</sup> Next, the dependent fields are expressed in terms of the dynamic fields.
- The independent fields are expanded in plane waves and are discretized by imposing periodic or anti-periodic boundary conditions along all space-like directions in a given volume.

---

<sup>1</sup>In actual calculations, one restricts oneself to calculating the momenta  $P^\mu$ , because the angular momentum tensor  $M^{\mu\nu}$  is irrelevant for the mass spectrum. Sometimes  $J_z$  is constructed.

- It is important that the expansion into plane waves takes place in *momentum* space. By this, assuming a reasonable choice of boundary conditions, all points in this space are equivalent and the momentum of the center of mass is well-defined. The enormous improvement of convergence achieved by such a prescription is seen already in non-relativistic many body theory [25].
- When working in the light-cone gauge,  $A_+ = 0$ , the theory is consistent in the *normal mode* sector only (cf. next section). The *zero modes* are important for the vacuum structure [26], but most probably not for bound state spectra.
- Having quantized the theory by postulating canonical commutation relations for the creation and destruction operators, the Poincaré generators are written as functionals of these operators.
- The reference state, “the vacuum”, is an eigenstate of the Hamiltonian with eigenvalue zero. This follows from the fact, that creation of particles out of the vacuum is forbidden because of the conservation of longitudinal momentum.
- Spectrum and wavefunctions are obtained by solving the eigenvalue problem

$$P^+ P^- |\psi_n\rangle = M_n^2 |\psi_n\rangle,$$

where the  $\psi_n$  are eigenfunctions to the mass (squared) eigenvalue  $M_n$ . This matrix equation and its solution by diagonalization are the endpoint of the so-called DLCQ formalism. We discuss its difficulties in the next chapter.

- We can perform the continuum limit of this matrix equation. This is possible in a direct way, as opposed to the non-trivial continuum limit, for example, of lattice gauge theories. The matrix equation is mapped into an integral equation.
- The task is now to find an appropriate scheme to solve for the spectrum of this (infinite dimensional) operator. We use a restriction of the Fock space together with an effective interaction to account for the effects of the truncated states, and an explicit cutoff because of the unrestricted transverse momenta. To exploit and to justify this approach is the main part of the present work.
- The so-obtained *effective integral equation* is solved with the appropriate method of Gaussian quadratures, which leads in the end to the diagonalization of a finite dimensional matrix.
- The dependence of the solutions on the unphysical parameters (cutoffs, etc.) has to be investigated to test the significance of the obtained results.



# Chapter 1

## Field theories in front form dynamics

### 1.1 Historical survey

Light-cone coordinates<sup>1</sup> were introduced into the Hamiltonian field theory by DIRAC [27] in 1949. According to his definition an operator is called a *Hamiltonian* if it propagates a physical system in a fixed direction in space-time. This direction is subject to certain constraints, but not unique. DIRAC listed three different possibilities<sup>2</sup> in selecting such a “general time”. The most prominent ones are the usual time  $x^0$  (*instant form dynamics*) and the light-cone time  $x^+$  (*front form dynamics*). This *Hamiltonian* formalism attracted little attention because of the spectacular achievements (e.g. [28, the anomalous magnetic moment of the electron, Eq. (1.112)]) of the *action-oriented* work of TOMONAGA [21], SCHWINGER [23, 28], and FEYNMAN [22], launched at the same time.

The rejuvenation of the Hamiltonian method in field theory, in particular studying front form dynamics, came in several steps. First, WEINBERG [29], using  $\phi^3$  theory in the *infinite momentum frame*, discovered that the creation and annihilation of particles out of the vacuum is forbidden for  $p_z \rightarrow \infty$  and that the corresponding divergencies are absent in this frame. After the derivation of the rules for front form perturbation theory [30], it was an important success to show the equivalence of this theory with the Feynman rules of ordinary perturbation theory[31][32]. The treatment of non-abelian gauge theories and the description of exclusive QCD processes are described in [33, 34].

To render the theory tractable and to finally implement it on a computer, the ambitious program of **D**iscretized **L**ight-**C**one **Q**uantization[35] was proposed by PAULI and BRODSKY in 1985. The formalism was applied first to the Yukawa model in  $(1+1)$  dimensions, then to scalar QED<sub>(1+1)</sub> [36], followed by calculations of the  $\phi^4_{(1+1)}$  theory [37], and QCD<sub>(1+1)</sub>[38, 39]. Commencing with a paper by ELLER, PAULI and BRODSKY

---

<sup>1</sup>The coordinate vector is  $x = (x^+, x^-, x_\perp)$  with  $x^\pm = x^0 \pm x^3$ ,  $x_\perp = (x_1, x_2)$ . Cf. Appendix A.

<sup>2</sup>Actually, there are five such quantization surfaces [17].

[40], there is a large literature discussing the (massive) *Schwinger model* [41, 42, 43].

All of the above examples have been studied in 1+1 dimensions. Quantum Electrodynamics was the first realistic gauge theory in physical space-time to be treated with DLCQ [24, 44, 45], where results were compared with experimental data or other theoretical work. Subsequently, an attempt was made to apply this method to  $\text{QCD}_{(3+1)}$  [46]. Most recently, this was done to a large extent in the so-called *collinear model* [47, 48], *i.e.* effectively in lower dimensions. Here, the method of the *transverse lattice* [49, 50] seems to open a promising way to proceed, but is still under construction. Nevertheless,  $\text{QED}_{(3+1)}$  is a “milestone” for non-perturbative approaches in light-cone quantization on the way to understand full QCD. QED contains most of the fundamental difficulties found in QCD and can be attacked likewise in a truncated Fock basis.

## 1.2 Problems of front form field theories

The disadvantages using front form dynamics include a certain non-conformity of the inertial system used, especially the counter-intuitive missing of a well-defined angular momentum. As mentioned in the introduction, the operators of rotations around the transverse axes are complicated, *i.e.* contain the interaction. Consequently, although the rotation operator  $\mathcal{J}_3$  is kinematic, the states of a system cannot be classified with respect to total angular momentum  $J^2$ . Of course, this is not necessary from the outset, and calculations have been performed without using equal-time quantum numbers, for example by restricting to a sector of a definite  $z$ -component of the total angular momentum  $J_z$ . However, the physical results of a calculation should be independent of the mathematical method applied. *A priori* it is not clear in front form dynamics, if the results of a calculation will be rotationally invariant. It seems to be impossible to show *analytically* that these solutions do indeed obey rotational symmetry. This would require the diagonalization of an operator at least as complicated as the light-cone Hamiltonian itself. The problem, though fundamental for all Hamiltonian formulations of field theories, was not of primary interest before, since calculations were often performed using lower (typically 1+1) dimensional models. It has been shown [51, 52] that Lorentz covariance, and in particular rotational symmetry, is explicitly violated, if one evaluates front form perturbation theory at the one- and two-loop levels. Non-covariant counterterms have to be constructed to restore covariance.

Because of its long term use, many phenomena have been investigated within equal-time formulation. The number of calculations is understandably much smaller in light-cone quantization. Much effort has been made therefore, to reproduce the results of *instant form dynamics* on the light-cone. A considerable difficulty in light-cone quantization is the rôle of the so-called *zero modes*. The zero mode of a function  $f(x^-, \vec{x}_\perp)$  in a fixed space direction  $y$  with interval length  $L_y$  is defined as (cf. *e.g.* [47, Eq. (4)])

$$\langle f(\vec{x}) \rangle_0 := \frac{1}{2L_y} \int_{-L_y}^{L_y} dy f(\vec{x}, y),$$

where it is *not* integrated over the remaining space directions  $\bar{x}$ . As a first step, the zero modes were omitted in actual calculations, because they are a set of measure zero among the modes of all fields. Their influence on the spectra of bound systems was considered to be negligible.

However, it was found that the convenient *light-cone gauge*  $A^+ \equiv 0$  is inconsistent with the inclusion of the zero modes into the formalism. In non-abelian gauge theories, for instance, the zero mode of the gauge field  $A^+$  cannot be gauged away [47]. It was often seen that by working in the light-cone gauge in the front form dynamics, spurious operators which are singular in the limit  $k^+ \rightarrow 0$  are created [53]. The renormalization of these ultraviolet (UV) and infrared (IR) divergencies was investigated in perturbation theory by MUSTAKI ET AL. [54]. Although the most divergent contributions are cancelled in the graphs of lowest order, the IR singularity remains. For example, the photon propagator picks up an additional  $1/k^+$  singularity. After regularization, it gives rise to difficulties only in higher orders, because then one must integrate over the photon momentum. A naive regularization via principal value runs into difficulties which can be overcome by the LEIBBRANDT-MANDELSTAM prescription [55]. This method for Hamiltonian non-abelian gauge theories was derived by BASETTO ET AL. [56].

To put the former results of calculations in light-cone quantization on a formally correct basis, the influence of the zero modes was examined systematically after pragmatically ignoring them. To name a few, PAULI, PINSKY and KALLONIATIS [47, 57], WERNER, HEINZL ET AL. [58], and MCCARTOR [59] have made important contributions to this subject. The problem of zero modes in QED is discussed by KALLONIATIS and ROBERTSON in [60]. Recently, these more formal examinations have been accompanied by numerical calculations. VÖLLINGER [43] found in his investigation of the massive Schwinger model a vanishing influence of the zero modes concerning the spectrum of this model. However, he considered a vacuum wavefunction that is independent of the variable  $\theta$ , parameterizing the vacuum states. In literature [61], the vacuum is found to be dependent on this parameter (“ $\theta$ -vacuum”) which can have an effect on the spectrum. As an important result, VAN DE SANDE [62] was able to show that DLCQ does give the correct linear increase of the squared mass eigenvalues with the fermion mass in this model. The work of ELSER [42] displayed a quadratic rise of this squared mass with the fermion mass. This effect was falsely attributed to the zero modes. The results of ELSER were numerically unsatisfactory and the latter interpretation could be excluded in Ref. [43], where the method of VAN DE SANDE was used. It was proven that in the continuum limit the right slope is reached and is hidden by an extremely slow convergence typical of DLCQ. The solution to this problem resides in the use of counterterms.

In conclusion, one has strong evidence for a small effect of the zero modes on the physics important for the spectra of bound systems. An application of the light-cone gauge, or equivalently, the consideration of the normal mode sector only, seems to be justified, at least in the QED case. Of course, in QCD there are large effects coming from the vacuum structure, such as chiral symmetry breaking. The origin of these effects has to be investigated separately.

## 1.3 Preceding work

The investigation of QED within the DLCQ formalism dates back to roughly 1988. In 1990, TANG [44] set up a *matrix equation* for  $\text{QED}_{(3+1)}$  by truncating the Fock space to the sectors  $|e\bar{e}\rangle$  and  $|e\bar{e}\gamma\rangle$ . In order to solve the associated eigenvalue problem, he used the diagonalization of the discretized Hamiltonian, and variational methods. With help of the latter, he was only able to produce an *upper limit* for the mass-squared eigenvalue of the triplet ground state of positronium, three percent larger than the BOHR value at  $\alpha = 0.6$ . But compared to the standard results of perturbation theory [63], this upper limit is already below the well-known value for this triplet term. To produce significant results by diagonalizing the Hamiltonian matrix, TANG [44, Ref. 1, p. 46], following his own estimates, would have had to include roughly 11 million Fock states for the large coupling constant  $\alpha = 0.3$ . The main cause for this negative conclusion was the slow numerical convergence of the method applied.

With the solution of the Coulomb problem in momentum space [64], the method of *Coulomb counterterms* was introduced to improve numerical convergence. KRAUT-GÄRTNER [24] applied this method to  $\text{QED}_{(3+1)}$ . He used an *effective* interaction, obtained from a projection of the  $|e\bar{e}\gamma\rangle$ -sector onto the  $|e\bar{e}\rangle$ -sector. The corresponding effective integral equation was solved using Gauss-Legendre quadrature. His results show excellent convergence and coincide to a high degree of accuracy with the expected values. It is worth mentioning that, for the first time, not only the complete *Bohr* spectrum is obtained, but also relativistic effects, like the hyperfine splitting, are correctly described within a non-perturbative approach in front form dynamics.

KALUŽA [45] applied the counterterm technique to the calculation of the spectrum of the light-cone Schrödinger equation. He calculated an eigenvalue for the positronium ground state that coincides approximately with the BOHR value at  $\alpha = 0.3$ . For the calculation of relativistic spectra, KALUŽA improved the diagonalization technique to enlarge the Fock space feasible with the computer equipment used. The convergence of his spectra is rather poor, because he did not use counterterms for the singularity of the relativistic problem. For a comparison with the light-cone Schrödinger equation, only the ground state is considered, which is certainly too large.

WÖLZ [46] subsequently tried to solve the analogous problem for QCD. To include typical QCD effects (self-coupling of the gluons) he enlarged the Fock basis implementing the  $|q\bar{q}gg\rangle$ -sector. In order to solve for the eigenvalues, he applied a hybrid method by projecting the new Fock sector unto the other two sectors, considering the so-derived eigenvalue problem as a matrix equation. His results [46] converge too slowly and suffer strong fluctuations as functions of the changing Fock space size. This is due to the fact that the counterterm technique included in the computer code is not applied in the final calculations because the necessary two dimensional numerical integration are too time consuming.

# Chapter 2

## The positronium model

When quantizing a field theory on the light-cone, it is convenient to work in the usual Fock basis. Consequently, one thinks of a composite physical system, *e.g.* a meson or a baryon, as consisting of fermionic valence particles, bosonic (virtual) gauge particles, and virtual particle-antiparticle pairs. Considering positronium as the physical system of special interest for the present work, the wavefunction reads:

$$|positronium\rangle = \psi_\gamma|\psi_\gamma\rangle + \psi_{e\bar{e}}|\psi_{e\bar{e}}\rangle + \psi_{e\bar{e}\gamma}|\psi_{e\bar{e}\gamma}\rangle + \psi_{e\bar{e}\gamma\gamma}|\psi_{e\bar{e}\gamma\gamma}\rangle + \dots$$

The exact wavefunction is an infinite series and one has to impose simplifying restrictions in actual calculations. The obtained results have to be investigated concerning their dependencies on these restrictions.

The Hamiltonian operators ruling the dynamics of a system can be derived using light-cone quantization. A rough sketch of the procedure is given in the introduction and its application to QED<sub>(3+1)</sub> is described in more detail in Appendix B. It is important that in this work the *continuum* formulation of a light-cone quantized field theory is used. All discretizations come from numerical integrations, cf. Appendix G. The operator

$$H_{LC} := P^\mu P_\mu$$

is commonly called the invariant mass (squared) operator. For convenience I will refer to it as the *light-cone Hamiltonian*, although in the sense of DIRAC [27] only  $P^-$  is a Hamiltonian. The light-cone Hamiltonian is obviously a Lorentz scalar, and so are its eigenvalues, which have the dimension of a mass squared.

Our main task is to set up an *effective, relativistic* Hamiltonian operator, tractable either analytically or with the help of a computer, and to solve the eigenvalue equation

$$H_{LC}|\psi_n\rangle = M_n^2|\psi_n\rangle, \tag{2.1}$$

whose solutions yield the mass (squared) eigenvalues and the corresponding eigenfunctions of our positronium model. The relevant matrix elements of this Hamiltonian are tabulated in Appendix C. The full Hamiltonian matrix elements for QED and QCD are given in [44] and [45, 65], respectively.

## 2.1 The model

To construct a manageable physical model for positronium, we proceed as follows. One is free to divide the Fock space into two arbitrary subspaces, called the *P-space* and the *Q-space*. Restricting the full Fock space to two sectors, being explicit, one with an electron positron pair and one with an additional photon, the associated projection operators onto these subspaces are defined to be

$$\hat{P} := \sum_{\substack{n \\ \text{all QN}}} |(e\bar{e})_n\rangle\langle(e\bar{e})_n| \quad (2.2)$$

and

$$\hat{Q} := \sum_{\substack{n \\ \text{all QN}}} |(e\bar{e}\gamma)_n\rangle\langle(e\bar{e}\gamma)_n|. \quad (2.3)$$

Within this limited Fock space, the model positronium cannot decay into photons, contrary to observation. Moreover, a virtual photon as an intermediate state in an interaction is impossible. The part of the hyperfine splitting connected to this annihilation graph is missing. The inclusion of this graph into the theory is the topic of Chapter 4. Nonetheless, the vector space is well-defined mathematically, and we can proceed to solve the eigenvalue equation (2.1). In our restricted Fock-space we have a  $2 \times 2$  block matrix

$$H_{\text{LC}} = \begin{pmatrix} H_{PP} & H_{PQ} \\ H_{QP} & H_{QQ} \end{pmatrix}. \quad (2.4)$$

Of course, this truncation of the Fock space violates gauge invariance. It will be shown in Chapter 5 that one can treat the consequences of this violation within a general theory of effective interactions.

The attempts to solve for the spectrum of this operator in a matrix equation [44, 45] were bound to fail, as described in Chapter 1, because of computer capacity limitations. We apply a projection method [24] (also used in many body theory<sup>1</sup>) to eliminate the *Q*-space at the expense of an in general more complicated *effective* Hamiltonian operating in *P*-space only. Formally, one can describe the projection as the solution of a system of coupled linear equations. The last of the two equations of the eigenvalue problem Eq. (2.1) with the Hamiltonian (2.4) reads explicitly

$$H_{QP}|e\bar{e}\rangle + H_{QQ}|e\bar{e}\gamma\rangle = M_n^2|e\bar{e}\gamma\rangle.$$

We therefore solve for the state  $\hat{Q}|\psi\rangle = |e\bar{e}\gamma\rangle$  and express it with the help of an inverse Hamiltonian, or resolvent:

$$G(\omega) := \hat{Q}(\omega - H_{\text{LC}})^{-1}\hat{Q}, \quad (2.5)$$

and obtain

$$\hat{Q}|\psi_n\rangle = G(\omega)H_{\text{LC}}\hat{P}|\psi_n\rangle.$$

---

<sup>1</sup>It is described as mathematical method in [66] and applied to problems in nuclear theory by TAMM [67] and DANCOFF [68].

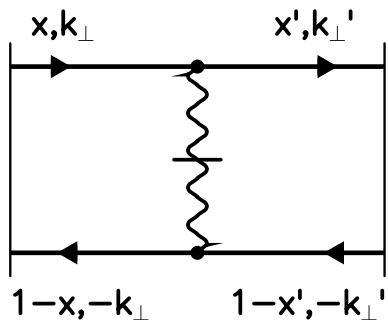


**Figure 2.1:** The seagull graph in  $P$ -space.

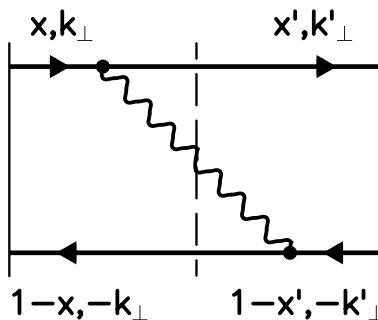


**Figure 2.2:** The iterated vertex interaction ( $x > x'$ ) in  $P$ -space.

The *a priori* unknown eigenvalue  $M_n^2$  was substituted by  $\omega$ , referred to in the remainder of this work as *redundant parameter*. This parameter has to be fixed by an additional condition.

Which interactions can occur in the effective  $|e\bar{e}\rangle$ -sector? The only possible graph in  $P$ -space is shown in Figure (2.1). Because of the projection, one also has iterated graphs, like the one displayed in Figure (2.2). The  $Q$ -space seems quite complicated at first glance, but only one graph, the lower right one of Figure (2.3), survives the so-called *gauge principle* of DLCQ formulated by TANG ET AL. [44, Ref. 2]. The main idea is to restore gauge invariance at tree level, which was destroyed by the Fock space truncation. The recipe is to omit all graphs which have intermediate states that are not contained in the (restricted) Fock space. Instantaneous particles are counted as real particles in this procedure.

Still not all non-diagonal graphs in  $Q$ -space vanish. To simplify the problem, in [24] the remaining seagull graph was omitted on an *ad hoc* basis. We shall show in Chapter 5, using the formalism set up in [20], that this omission is not an assumption, but is a natural consequence of the projection mechanism. We arrive at the *nonlinear* equation

$$H_{\text{LC}}^{\text{eff}}(\omega)|\psi_n(\omega)\rangle = M_n^2(\omega)|\psi_n(\omega)\rangle,$$

where the states, the effective Hamiltonian

$$H_{\text{LC}}^{\text{eff}}(\omega) := \hat{P}H_{\text{LC}}\hat{P} + \hat{P}H_{\text{LC}}\hat{Q}(\omega - H_{\text{LC}})^{-1}\hat{Q}H_{\text{LC}}\hat{P} \quad (2.6)$$

and the mass eigenvalue  $M_n^2$  depend on the redundant parameter  $\omega$ . In principle, we also have to satisfy the obvious constraint that

$$M_n^2(\omega) = \omega.$$

Although the fixing of the parameter  $\omega$  is explained in Chapter 5, we introduce a method of calculating an analytic expression for this parameter. This method is the way the so-called  $\omega^*$ -trick was introduced before the work of PAULI on the Method of Iterated Resolvents [20]. The derivation given here should be considered as a *plausibility*

## 2.1. The model

---

*argument* rather than as a strict proof. Nevertheless, it gives some intuition concerning the physics behind the procedure.

A word on notation seems in order<sup>2</sup>. We label the *fermion mass* with  $m_f$ , the *longitudinal momentum fraction* with  $x$ , the *transverse momentum* with  $\vec{k}_\perp$ , and the *helicity* of a particle with  $\lambda$ . The corresponding quantum numbers after an interaction have a prime ( $x', \vec{k}'_\perp; \lambda'$ ).

We have seen that the energy denominator contains the unknown (parameterized) eigenvalue  $\omega$  of the whole eigenvalue problem and the sector-Hamiltonian operating in  $Q$ -space. The latter consists of a kinetic part  $M_Q^2$ , *i.e.* the free mass (squared) of the  $Q$ -space, and an interaction  $V_Q$ :

$$H_{LC,Q} = M_Q^2 + V_Q.$$

As pointed out above, this poses a difficult problem: a non-diagonal operator has to be inverted *and* as a constraint it has to be guaranteed that the masses should be equal to the mass parameter. The latter results in a mathematical fixpoint equation. To avoid at least the first of these difficulties, one can divide the interaction into a diagonal part  $\langle V_Q \rangle$  and a non-diagonal part  $\delta V_Q$

$$V_Q = \langle V_Q \rangle + \delta V_Q.$$

By defining *formally*

$$T^* := \omega - \langle V_Q \rangle = c\mathbf{I}, \quad c \in \mathbf{R}, \quad (2.7)$$

I changed the notation of [24, Eq. (5.9)] to stress two points. Firstly,  $T^*$  is not just a fixed value of  $\omega$ . This would be inconsistent, because  $\omega$  is a real number, whereas  $T^*$  is a function of the light-cone momenta. Secondly,  $T^*$  is a *kinetic energy* according to Eq. (2.7), where a potential energy is subtracted from a total energy. One can expand the resolvent around the diagonal interaction  $\langle V_Q \rangle$

$$\begin{aligned} \frac{1}{\omega - H_Q} &= \frac{1}{T^* - M_Q^2 - \delta V_Q} \\ &= \frac{1}{T^* - M_Q^2} + \frac{1}{T^* - M_Q^2} \delta V_Q \frac{1}{T^* - M_Q^2 - \delta V_Q}, \end{aligned} \quad (2.8)$$

As a first approximation we consider the first term of the expansion only. It does not contain any non-diagonal terms and is a simple c-number. We label

$$\mathcal{D}(x, x'; T^*) := |x - x'| (T^* - M_Q^2). \quad (2.9)$$

This approximation has severe consequences: a collinear singularity occurs. It is proportional to

$$\frac{1}{\mathcal{D}} \frac{\Delta(x, k_\perp, x', k'_\perp; T^*)}{|x - x'|}.$$

---

<sup>2</sup>Cf. Appx. A.



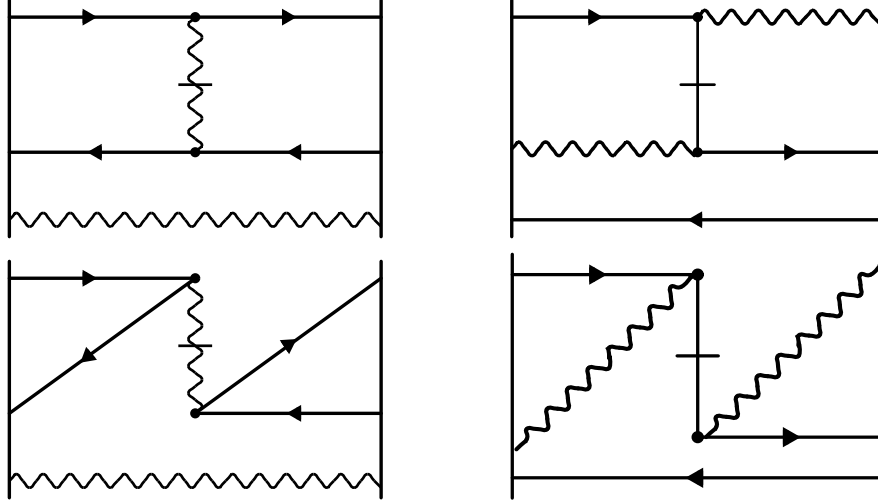


**Figure 2.3:** Graphs of the instantaneous interaction in  $Q$ -space.

We identify now the  $|e\bar{e}\rangle$ -sector with the  $P$ -space and the  $|e\bar{e}\gamma\rangle$ -sector with the  $Q$ -space to calculate the function  $\Delta$  by evaluating the two graphs Fig. (2.1) and Fig. (2.2) according to the rules of front form perturbation theory given in Refs. [33, 65], but using the expression in Eq. (2.9) for the summation over the intermediate states. One obtains

$$\Delta(x, k_{\perp}, x', k'_{\perp}; T^*) = M_{e\bar{e}\gamma}^2 - \omega - \frac{(\vec{k}_{\perp} - \vec{k}'_{\perp})^2}{x - x'} - \frac{1}{2} (l_e^- - l_{\bar{e}}^-),$$

where  $l_e^{\mu} := (k'_e - k_e)^{\mu}$  and  $l_{\bar{e}}^{\mu} := (k_{\bar{e}} - k'_{\bar{e}})^{\mu}$  are the momentum transfers of the electron and positron. One can use this singularity induced by the truncation of the series (2.8) to determine the parameter  $\omega$  in the problem. One simply demands that this *collinear* singularity vanishes:

$$\Delta(x, \vec{k}_{\perp}, x', \vec{k}'_{\perp}; T^*) = 0, \quad \forall x, x', \vec{k}_{\perp}, \vec{k}'_{\perp}.$$

We are even forced to proceed this way to ensure the solubility of the problem. One has to fix  $\omega$  to the expression

$$T^*(x, \vec{k}_{\perp}; x', \vec{k}'_{\perp}) = \frac{1}{2} \left( \frac{m_f^2 + \vec{k}_{\perp}^2}{x(1-x)} + \frac{m_f^2 + \vec{k}'_{\perp}^2}{x'(1-x')} \right), \quad (2.10)$$

which indeed has the form of a kinetic energy. Although it can be shown that the two kinetic energies of this sum must be the same, I wrote  $T^*$  here in the equivalent suggestive form of an *average*. It cannot be overstated that exactly this form of the expression (2.10) follows from the structure of the effective theory [20].

The physical interpretation of this procedure is not easy. One can imagine that the  $Q$ -space contains all interactions of the higher Fock sectors by effectively summing them. In this complicated effective interaction, we disregard all non-diagonal contributions.

## 2.2. The effective integral equation

---

But on the other hand, this is partly compensated by the special choice  $\omega \equiv T^*$ . One can therefore state that  $T^*$  contains an approximation of the summed interactions of the higher Fock states.

## 2.2 The effective integral equation

We can proceed by calculating the matrix elements of the now well-defined effective Hamiltonian. It operates only in  $P$ -space. To read off the actual definition of the matrix elements, we have to write down the integral equation in which they are contained. The continuum version of Eq. (2.1) is

$$\begin{aligned} & \left( \frac{m_f^2 + \vec{k}_\perp^2}{x(1-x)} - M_n^2 \right) \psi_n(x, \vec{k}_\perp; \lambda_1, \lambda_2) \\ & + \frac{g^2}{16\pi^3} \sum_{\lambda'_1, \lambda'_2} \int_D \frac{dx' d^2 \vec{k}'_\perp}{\frac{1}{2}(l_e^2 + l_{\bar{e}}^2)} \frac{\langle x, \vec{k}_\perp; \lambda_1, \lambda_2 | j(l_e)^\mu j(l_{\bar{e}}) | x', \vec{k}'_\perp; \lambda'_1, \lambda'_2 \rangle}{\sqrt{xx'(1-x)(1-x')}} \psi_n(x', \vec{k}'_\perp; \lambda'_1, \lambda'_2) = 0. \end{aligned} \quad (2.11)$$

This form of the *effective integral equation* is very useful for a comparison with the matrix elements calculated in [24], see also Appx. D. However, a main topic of the present work is the investigation of rotational invariance, or in general Poincaré invariance, of QED on the light-cone. In this context, it is helpful to write the interaction term of Eq. (2.11) a covariant way. The integrand reads now

$$\frac{g^2}{16\pi^3} \sum_{\lambda'_1, \lambda'_2} \int_D \frac{dx' d^2 \vec{k}'_\perp}{\sqrt{xx'(1-x)(1-x')}} \frac{j^\mu(l_e, \lambda_e) j_\mu(l_{\bar{e}}, \lambda_{\bar{e}})}{l_e^\mu l_{e,\mu}} \psi_n(x', \vec{k}'_\perp; \lambda'_1, \lambda'_2), \quad (2.12)$$

which makes it obvious that the effective interaction<sup>3</sup>

$$U_{\text{eff}} := \frac{j^\mu(l_e, \lambda_e) j_\mu(l_{\bar{e}}, \lambda_{\bar{e}})}{l_e^\mu l_{e,\mu}}$$

is gauge invariant and a Lorentz scalar. We restrict the integration domain  $D$  using the covariant cutoff of BRODSKY and LEPAGE [33]:

$$\frac{m_f^2 + \vec{k}_\perp^2}{x(1-x)} \leq \Lambda^2 + 4m^2, \quad (2.13)$$

which allows for states having a kinetic energy below the cutoff  $\Lambda$ . The matrix elements are given in some detail in Appendix D. The explicit functions are listed in Appendix F.

---

<sup>3</sup>Instead of providing the arguments of the currents  $j^\mu$  by bras and kets like in Eq. (2.11), we wrote them into brackets.

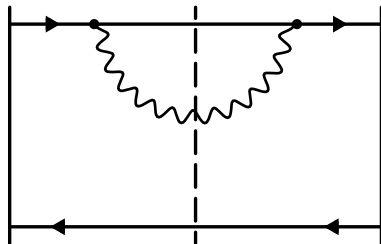


**Figure 2.4:** Diverging diagrams in  $P$ -space: self energy diagram.

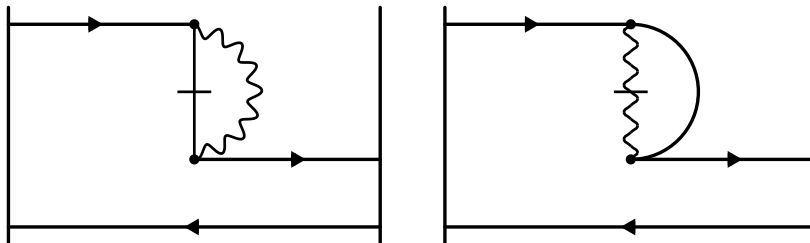


**Figure 2.5:** Diverging diagrams in  $P$ -space: contraction contributions.

So far, we have considered only the problems that occur due to the projection of  $Q$ -space onto  $P$ -space. But already in  $P$ -space we have to face severe singularities stemming from the graphs of the electromagnetic self energy, Fig. (2.4), and the contraction graphs, Fig. (2.5).

A renormalization scheme is necessary to remove the divergencies. It is described in Appendix E and can be summarized as follows. Although each of these graphs is quadratically divergent in the cutoff  $\Lambda$ , their sum is only logarithmically divergent. The arguments used in the proof assume the formulation of the theory in the *continuum*. In the discretized theory the arguments do not necessarily hold.

Before addressing to solve the effective integral equation (2.11), let us briefly review the steps that lead to its derivation and compare the method of this work to other attempts to solve for the positronium spectrum. First, we restricted the Fock space to the sectors  $|e\bar{e}\rangle$  and  $|e\bar{e}\gamma\rangle$ . By this, we arrived at a positronium model with one dynamical photon. This constitutes a matrix equation ( $2 \times 2$  block Hamiltonian). The advantage of this matrix equation is that all interactions in the  $Q$ -space are explicitly taken care of, whereas in our model their contributions are occluded by the determination of the redundant parameter  $\omega$ . However, efforts to extract the spectrum and wavefunction from the matrix equation have failed. In the case of QED, TANG [44] and KALUŽA [45] produced results with no clear significance. This was due to the convergence problems, because they did not include counterterms for the Coulomb singularity. The counterterm technique used in the present work is described in Appendix G. Calculating the counterterms, one faces in general numerical integrations in two or three dimensions, which must be performed for each diagonal matrix element. The numerical effort increases tremendously with the matrix dimensions [46]. We wish

### 2.3. The positronium mass spectrum

---

to avoid the disadvantages of the matrix equation. Therefore we have performed the continuum limit of the DLCQ formalism and obtained a coupled system of integral equations. The effective integral equation (2.11) was derived by casting the effects of higher Fock states into the  $Q$ -space by fixing  $\omega$  to  $T^*$ . Then the  $Q$ -space is projected onto the  $P$ -space as a second step.

If one considers the non-relativistic limit of the interaction in the effective integral equation (2.12), one arrives at the so-called *light-cone Schrödinger equation*. The main point in this calculation is the relation between the longitudinal momentum fraction  $x$  in light-cone coordinates and the equal-time momentum in  $z$ -direction,  $k_z$

$$x = x(k_z) = \frac{1}{2} \left( 1 + \frac{k_z}{\sqrt{m^2 + \vec{k}_\perp^2 + k_z^2}} \right) \simeq \frac{1}{2} \left( 1 + \frac{k_z}{m} \right).$$

The calculation of the non-relativistic limit is then straightforward. The solution of the light-cone Schrödinger equation, which has analytically integrable Coulomb counterterms, was given in [24, Fig. 8], shows very good convergence, and yields the correct eigenvalue spectrum. If one fully reduces the effective integral equation to the non-relativistic limit, one arrives at the well-known Coulomb equation in momentum space, solved numerically and discussed in Ref. [64].

## 2.3 The positronium mass spectrum

The solution to Eq. (2.11) was given in [24]. In contrast to the light-cone Schrödinger or the Coulomb equation, the counterterms for the Coulomb singularity cannot be calculated analytically. As can be seen in the helicity tables in Appendix F, in the case  $J_z=0$  essentially two different diagonal matrix elements occur: one for parallel, the other for anti-parallel helicities. KRAUTGÄRTNER [73] was able to integrate out analytically one of two variables contained in the continuous part of the counterterm for anti-parallel helicities. As a result, he only had to integrate over one dimension numerically. However, he did not succeed in analytically integrating out this variable from both matrix elements and consequently had to use the same counterterm for both diagonal matrix elements. The convergence and the spectra he obtained with this method were reasonably good. Indeed, the use of identical counterterms in this case ( $J_z=0$ ) is well justified since both functions have the same singularity structure and comparable values. We note that this becomes problematic in the case of non-vanishing  $J_z$ , where one has four distinct diagonal matrix elements, one of which is much smaller than the others.

We calculate in this chapter the spectrum of the positronium model described in [24] with an improved counterterm technique. This means a rigorous calculation of *all four* counterterms corresponding to the individual diagonal matrix elements. The prize is an entirely numerical two dimensional integration rather than a one dimensional analytic integration over the variable<sup>4</sup>  $\cos\theta$ , followed by a numerical integration of

---

<sup>4</sup>For the definition of the variables used in the calculations on the computer, see Appx. G.

the off-shell mass  $\mu$ . The effect is an even better convergence of the spectra with the number of integration points, as one can see by comparing Fig. (2.6) with Fig. (2.7). In particular, one notes a better convergence for a principal quantum number  $n \geq 2$  and a number of integration points  $N \leq 13$ . The lowest states for  $n=2$  converge much better when the entirely numerically integrated counterterms are used. This is the result of the afore mentioned small, but distinct difference between the diagonal matrix elements. If only one counterterm, adjusted to the singularity structure of one special diagonal matrix element, is used, the Coulomb singularity of the other diagonal element is over-compensated. As a consequence, the calculated eigenvalue is smaller than it should be. This is exactly the effect observed in the spectra.

We recall the analytic results<sup>5</sup> for the singlet and triplet states [63][71, p. 10] to order  $\mathcal{O}(\alpha^4)$  and write it in the form of BETHE and SALPETER [72, §23]:

$$E_{n,l} = -\frac{1}{2}Ry \left[ \frac{1}{n^2} - \frac{11}{32} \frac{\alpha^2}{n^4} + \left( \epsilon_{l,S,J} - \frac{1}{2l+1} \right) \frac{\alpha^2}{n^3} \right].$$

with the principal quantum number  $n$  and the Rydberg constant  $Ry = m_f \alpha^2 / 2$ . The singlet terms have

$$\epsilon_{l,S=0,J} = 0,$$

and the triplets

$$\epsilon_{l,S=1,J} = \frac{7}{6} \delta_{l0} + \frac{1 - \delta_{l0}}{2(2l+1)} \begin{cases} \frac{3l+4}{(l+1)(2l+3)} & \text{if } J = l+1 \\ -\frac{1}{l(l+1)} & \text{if } J = l \\ -\frac{3l-1}{l(2l-1)} & \text{if } J = l-1. \end{cases}$$

For a comparison of our results to “experiment”, *i.e.* to perturbation theory with a strong coupling constant,  $\alpha = 0.3$ , we have compiled the positronium mass spectrum in Table (2.2). Usually one classifies the states according to their quantum numbers of

---

<sup>5</sup>The “state of the art” theoretical results are given by GUPTA ET AL.[69]. For the triplets they have

$$\begin{aligned} E(n^3S_1) &= -\frac{1}{2}Ry \frac{1}{n^2} + 2Ry \alpha^2 \frac{1}{n^3} \left( \frac{1}{12} + \frac{11}{64n^4} \right) \\ &+ \frac{1}{4\pi} Ry \alpha^3 \frac{1}{n^3} \left[ -\frac{7}{3}a_n - \frac{109}{15} + \frac{2}{3} \ln 2 + 6 \ln \alpha^{-1} - \frac{16}{3} \ln k_0(n) \right] \\ &+ \frac{1}{6} Ry \alpha^4 \frac{1}{n^3} \ln \alpha + \dots, \end{aligned}$$

with the SALPETER terms

$$a_{1S} = -2 \ln 2 - 3, \quad a_{2S} = -\frac{9}{2}, \quad \dots,$$

and the BETHE logarithms

$$\ln k_0(1) = 2.9841285558\dots, \quad \ln k_0(2) = 2.8117698931\dots, \quad \ln k_0(3) = \dots$$

A review of experimental results can be found in [70, Chap. 15].

### 2.3. The positronium mass spectrum

---

total angular momentum  $J$ , orbit angular momentum  $L$ , and total spin  $S$ . This is valid only for rotationally invariant systems, or, in our case, in the non-relativistic limit. These quantum numbers constitute the spectroscopic notation  $^{2S+1}L_J$ . We choose a convention for the time reversal operation

$$V_{\mathcal{H}}|J, J_z\rangle := (-1)^{(J-J_z)}|J, J_z\rangle \quad (2.14)$$

to classify the states likewise. The singlet states are known as *parapositronium*, the triplet states as *orthopositronium*. We display the non-relativistic notation for the states in Table (2.2) to make the comparison to other data easier. The eigenvalues are listed in the form of binding coefficients  $B_n$ , defined as

$$B_n := 4 \frac{2 - M_n}{\alpha^2} \quad (2.15)$$

for all eigenvalues.

The finite  $N$  error estimates given in the table were obtained by comparing the results for the maximum number of integration points with those for the next highest number of points. The actual errors are definitely smaller, because the eigenvalues converge exponentially with the number of integration points  $N$ . We will comment on this in detail, when we have completed our model by introducing the annihilation channel in Chapter 4. A word seems in order on the magnitude of the errors. Surprisingly, the largest errors are those of the states with the largest binding coefficients, in particular of the ground state. The explanation is that we work in momentum space. Consequently, the higher excited states, widely spread in coordinate space, are condensed in momentum space and therefore in the region of many integration points.

Note the good agreement in Table (2.2), including excited states. The singlets  $^1S_0$  tend to be calculated as too weakly bound, especially for  $n=1$  and  $n=2$ . This effect is reversed for the triplets  $^3S_1$ . In principle, the whole bound state spectrum is accessible with our method, not only the first few states. To support this statement, it is instructive to investigate the properties of the higher states.

The main features of a detailed study of the multiplet structure of the spectrum are the following and can be seen from Table (2.2):

- There is a well-defined number of states for each fixed principal quantum number  $n$ . In the case considered here ( $J_z=0$ ), there are  $4(n-1)+2$  states. This number should be reproduced for as large an  $n$  as possible. It turns out that the multiplets contain the correct number of states in our model up to at least  $n=5$ .
- Each state has defined quantum numbers concerning the charge conjugation  $\pi_{\mathcal{C}}$  and  $\mathcal{T}$ -parity  $\pi_{\mathcal{H}}$ , cf. Eqs. (G.6) and (G.7). These quantum numbers can be obtained from the non-relativistic notation  $^{2S+1}L_J$  by

$$\pi_{\mathcal{C}} = (-1)^{L+1} \quad \text{and} \quad \pi_{\mathcal{H}} = (-1)^{J+L+1},$$

using the convention (2.14). It is an important result that only those combinations of quantum numbers  $\pi_{\mathcal{C}}$  and  $\pi_{\mathcal{H}}$  which are expected from the theory, occur in each set of eigenvalues for any given  $n$  in our calculations.

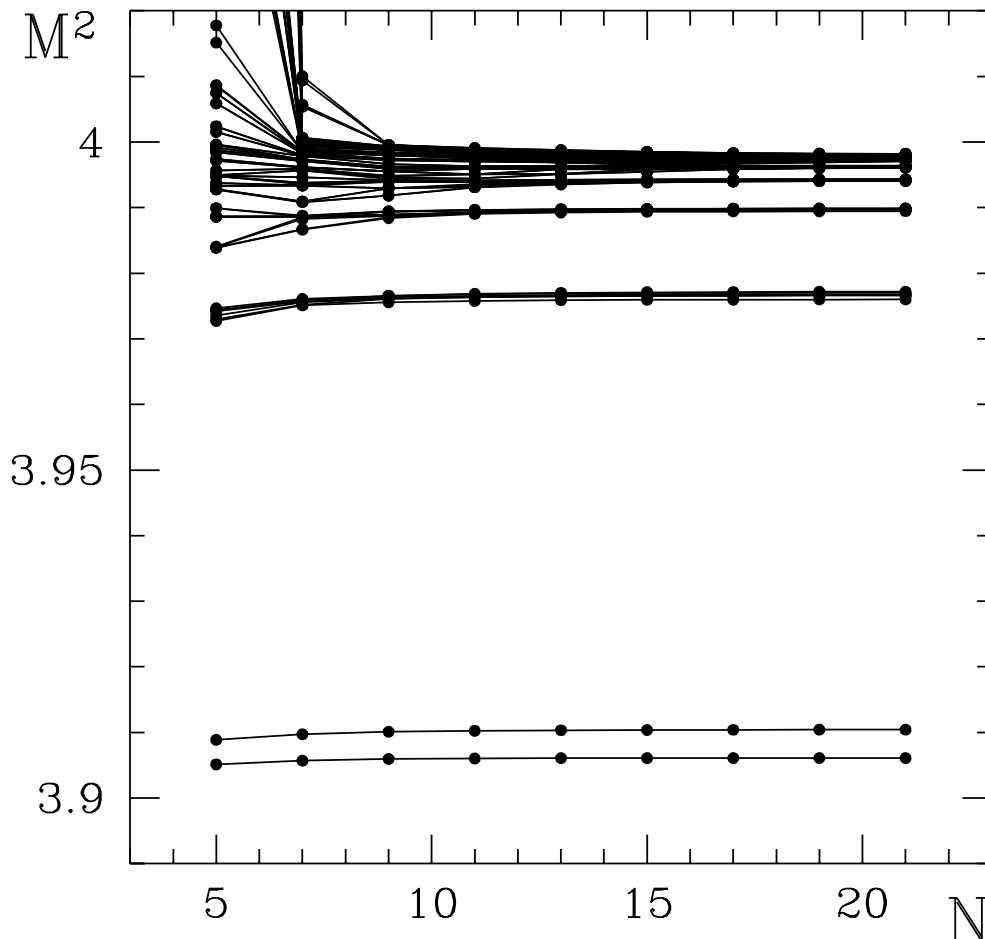


**Figure 2.6:** The spectrum of the effective integral equation for  $\alpha = 0.3, \Lambda = 1.0 m_f, J_z = 0$ . The mass squared eigenvalues  $M_n^2$  in units of the electron mass  $m_f^2$  are shown as functions of the number of integration points  $N \equiv N_1 = N_2$ . The calculation was done using the entirely numerically integrated Coulomb counterterms. Note the improved convergence of the states with  $n \geq 2$  in comparison with Fig. (2.7). The 100 lowest eigenvalues are displayed.

- The ordering of the multiplets seems to have minor errors. For instance, the  $2^1S_0$  state and the  $2^3P_0$  state are permuted, cf. Table (2.2): the S-state should be the lowest according to perturbation theory up to order  $\mathcal{O}(\alpha^4)$ . This finite cutoff effect is explained in next paragraph.

## Cutoff dependence

It is stated in Appendix E that there is, due to the renormalization scheme used, a logarithmic divergence of the eigenvalues with the cutoff  $\Lambda$ . This was already found in [73, Fig. 7]. In Fig. (2.8) and (2.9) the eigenvalues are shown as functions of the cutoff for  $n=1$  and  $n=2$ , respectively. It is obvious that the different eigenstates diverge linearly with the logarithm of the cutoff, and that the coefficients of these divergencies

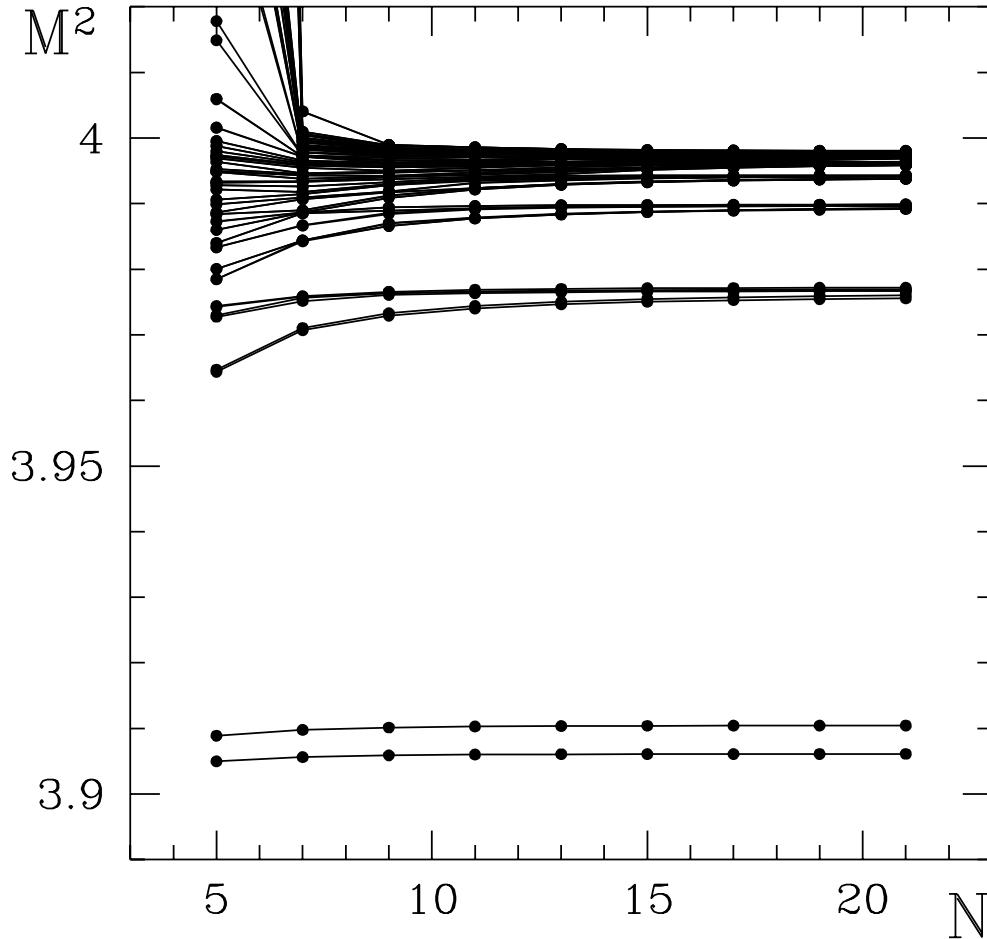


**Figure 2.7:** The spectrum of the effective integral equation for  $\alpha = 0.3, \Lambda = 1.0 m_f, J_z = 0$ . The mass squared eigenvalues  $M_n^2$  in units of the electron mass  $m_f^2$  are shown as functions of the number of integration points  $N \equiv N_1 = N_2$ . The calculation was done using the half-analytical Coulomb counterterms of Ref. [24]. The convergence of states with  $n \geq 2$  is not as good as in Fig. (2.6). The 100 lowest eigenvalues are displayed.

are different. It is reasonable to fit the curves of Fig. (2.8) with a polynomial in  $\log \Lambda$ , because this is the behavior expected from the renormalization scheme. If one omits the points for  $\Lambda > 20 m_f$ , because there the entirely numerical counterterm integrations become problematic, one gets good agreement with the calculated curves if one uses

$$\begin{aligned} M_{singlet}^2(\Lambda) &= 3.90545 - 0.0350983 \log \Lambda + 0.00745955 \log^2 \Lambda, \\ M_{triplet}^2(\Lambda) &= 3.90976 - 0.0185787 \log \Lambda + 0.00788614 \log^2 \Lambda. \end{aligned} \quad (2.16)$$

The small coefficient of the  $\log^2 \Lambda$  term verifies the logarithmic dependence of the eigenvalues on the cutoff. We will see in Chapter 4 that the dependence on  $\Lambda$  becomes even weaker if one includes the annihilation channel.

One notices several level crossings for  $n=2$ . As was stated in the last paragraph, the ordering of the eigenvalues of  $n=2$  for  $\Lambda=1.0 m_f$  turns out to be wrong for the



Cutoff: $\Lambda$	$B_s$	$B_t$	$C_{hf}$
1.0	1.04903964	1.00046227	0.13493713
1.8	1.16373904	1.06860934	0.26424917
3.6	1.25570148	1.10111328	0.42941166
5.4	1.29978050	1.11163578	0.52262422
7.2	1.32941912	1.11782782	0.58775360
9.0	1.35223982	1.12233652	0.63862028
10.8	1.37112216	1.12596311	0.68099735
12.6	1.38744792	1.12904455	0.71778713
14.4	1.40198469	1.13175363	0.75064183
16.2	1.41520247	1.13419048	0.78058886
18.0	1.42740143	1.13641774	0.80828803
ETPT	1.11812500	0.99812500	0.33333333
$\mathcal{O}(\alpha^6 \ln \alpha)$			0.23792985

**Table 2.1:** The binding coefficients of the singlet ( $B_s$ ) and the triplet states ( $B_t$ ) for  $\alpha = 0.3$ ,  $N_1 = 25$ ,  $N_2 = 21$  as functions of the cutoff  $\Lambda$  in electron masses. Additionally the values for equal-time perturbation theory up to order  $\mathcal{O}(\alpha^4)$  (ETPT) and up to order  $\mathcal{O}(\alpha^6 \ln \alpha)$  (cf. Eq. [2.17]) are shown.

two lowest states of this multiplet because of the crossing. That the levels do indeed cross can be proven by tracing them back to their sectors of definite  $\mathcal{C}$ - and  $\mathcal{H}$ -quantum numbers. A consequence of these crossings is the fact that the order of the eigenvalues is correct in the region between the crossings of the  $2^1S_0/2^1P_0$  and the  $2^3P_1/2^1P_0$  states,  $1.5 \leq \Lambda \leq 7$ . A further investigation of these crossings up to  $n=4$  show, that the states with  $\pi_{\mathcal{C}} = +1$  and  $\pi_{\mathcal{H}} = -1$  are those that fall off fastest with  $\Lambda$  and tend to cross other levels.

An important *ratio* of eigenvalues to be compared to results of other calculations is the hyperfine splitting. The hyperfine coefficient

$$\begin{aligned}
 C_{hf} &= (M_{triplet} - M_{singlet}) / \alpha^4 \\
 &= \frac{1}{2} \left[ \frac{2}{3} + \left( \frac{1}{2} \right) - \frac{\alpha}{\pi} \left( \ln 2 + \frac{16}{9} \right) - \frac{5}{12} \alpha^2 \ln \alpha + K \alpha^2 + K' \alpha^3 \right] \quad (2.17)
 \end{aligned}$$

was introduced by FERMI[74] in 1930. FERMI calculated  $C_{hf} = \frac{1}{3}$  for hydrogen-like atoms<sup>6</sup>, which is the exact result up to order  $\mathcal{O}(\alpha^4)$ . The second line of Eq. (2.17) shows the ‘state of the art’ result of equal time perturbation theory [75, p. 759]. The term in brackets is the contribution from the one-photon annihilation. This coefficient is listed in Table (2.1) together with the binding coefficients (2.15). They will be compared to the values obtained by including the annihilation channel in Chapter 4. The

---

<sup>6</sup> He investigated the cases of Sodium and Caesium, e.g. he naturally did *not* consider the possible annihilation of a bound particle-antiparticle system.

### 2.3. The positronium mass spectrum

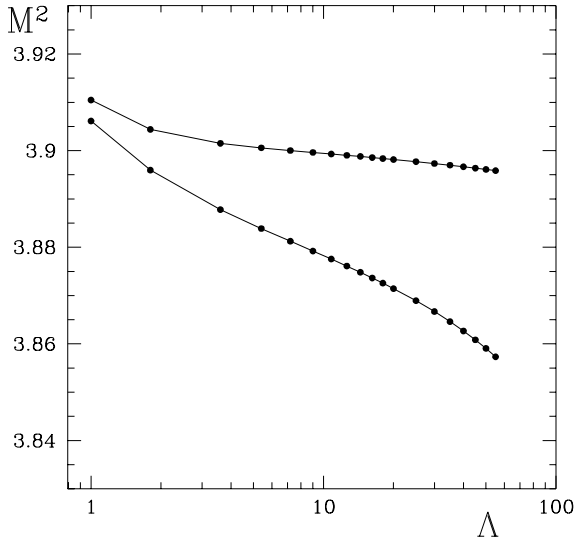


**Figure 2.8:** Cutoff dependence of the triplet (upper curve) and singlet (lower curve) ground state,  $\alpha = 0.3$ . The cutoff is given in units of the electron mass.

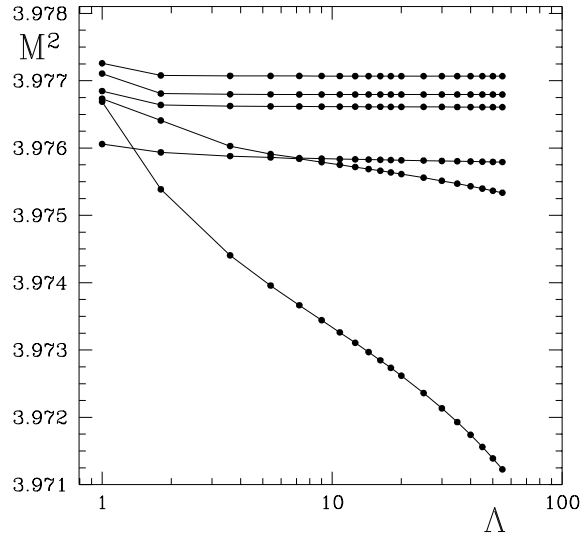


**Figure 2.9:** Cutoff dependence of the first excited states ( $n=2$ ) for  $\alpha = 0.3$ . The cutoff is given in units of the electron mass. Note the level crossings.

coefficients were calculated with the improved counterterms, as opposed to [24, Table V.]. Comparing with the values given there, one notices that the singlet falls off slower with  $\Lambda$  for the old counterterms. Consequently the values for the hyperfine coefficient  $C_{hf}$  are smaller there. The value of this coefficient, using Eq. (2.17) without the annihilation contribution, is displayed, too. In the region of large couplings considered in this work, also higher orders in the coupling constant are important. Note the remarkable effect: the value  $C_{hf}$  is 40% larger up to  $\mathcal{O}(\alpha^4)$  than up to  $\mathcal{O}(\alpha^6 \ln \alpha)$ !

Concluding, one can state that the best values as compared to equal time perturbation theory are obtained for  $\Lambda \simeq 1.5 m_f$ : the hyperfine splitting has the right order of magnitude, the order of the eigenvalues is correct, and the ground state is at the value of perturbative calculations. Although one can think of fitting the obtained data to the results of perturbation theory, I decided to follow the renormalization scheme of Appx. E to show the consistency of the positronium model described in this chapter, rather than to produce results competing with the accuracy of elaborate perturbative calculations. Moreover, it is not clear in the regime of a large coupling, how reliable the results of ETPT are, as we have seen from the significant dependence of the value for  $C_{hf}$  on the order of perturbative calculations.

$n$	Term	$\pi_{\mathcal{C}}$	$\pi_{\mathcal{H}}$	$B_{ETPT,n}$	$B_{theor,n}$	$\Delta B$	$\frac{100 \times \Delta B}{B_{exp,n}}$
1	$1^1S_0$	+1	-1	1.11812500	$1.04955251 \pm 0.00001714$	0.068572	6.13
2	$1^3S_1$	-1	+1	0.99812500	$1.00101171 \pm 0.00011090$	-0.002887	0.29
3	$2^1S_0$	+1	-1	0.26863281	$0.26023681 \pm 0.00016870$	0.008396	3.13
4	$2^3S_1$	-1	+1	0.25363281	$0.25380363 \pm 0.00021696$	-0.000171	0.07
5	$2^1P_1$	-1	-1	0.25363281	$0.25796923 \pm 0.00016055$	-0.004336	1.71
6	$2^3P_0$	+1	+1	0.26113281	$0.26706985 \pm 0.00015593$	-0.005937	2.27
7	$2^3P_1$	+1	-1	0.25550781	$0.25966695 \pm 0.00020629$	-0.004159	1.63
8	$2^3P_2$	+1	+1	0.25100781	$0.25525791 \pm 0.00017678$	-0.004250	1.69
9	$3^1S_0$	+1	-1	0.11701389	$0.11520626 \pm 0.00031353$	0.001808	1.54
10	$3^3S_1$	-1	+1	0.11256944	$0.11344082 \pm 0.00036304$	-0.000871	0.77
11	$3^1P_1$	-1	-1	0.11256944	$0.11448968 \pm 0.00026966$	-0.001920	1.71
12	$3^3P_0$	+1	+1	0.11479167	$0.11713342 \pm 0.00027062$	-0.002342	2.04
13	$3^3P_1$	+1	-1	0.11312500	$0.11512731 \pm 0.00032573$	-0.002002	1.77
14	$3^3P_2$	+1	+1	0.11179167	$0.11371654 \pm 0.00028065$	-0.001925	1.72
15	$3^1D_2$	+1	-1	0.11168056	$0.11281562 \pm 0.00015011$	-0.001135	1.02
16	$3^3D_1$	-1	+1	0.11168056	$0.11342693 \pm 0.00015480$	-0.001746	1.56
17	$3^3D_2$	-1	-1	0.11179167	$0.11297755 \pm 0.00016091$	-0.001186	1.06
18	$3^3D_3$	-1	+1	0.11136310	$0.11251082 \pm 0.00015641$	-0.001148	1.03
19	$4^1S_0$	+1	-1	0.06507080	$0.06549049 \pm 0.00058804$	-0.000420	0.64
20	$4^3S_1$	-1	+1	0.06319580	$0.06478625 \pm 0.00059833$	-0.001590	2.52
21	$4^1P_1$	-1	-1	0.06319580	$0.06500267 \pm 0.00046706$	-0.001807	2.86
22	$4^3P_0$	+1	+1	0.06413330	$0.06611514 \pm 0.00046966$	-0.001982	3.09
23	$4^3P_1$	+1	-1	0.06343018	$0.06533105 \pm 0.00048739$	-0.001901	3.00
24	$4^3P_2$	+1	+1	0.06286768	$0.06469966 \pm 0.00047847$	-0.001832	2.91
25	$4^1D_2$	+1	-1	0.06282080	$0.06396765 \pm 0.00029377$	-0.001147	1.83
26	$4^3D_1$	-1	+1	0.06282080	$0.06426183 \pm 0.00030846$	-0.001441	2.29
27	$4^3D_2$	-1	-1	0.06286768	$0.06409883 \pm 0.00031866$	-0.001231	1.96
28	$4^3D_3$	-1	+1	0.06268687	$0.06386407 \pm 0.00030333$	-0.001177	1.88
29	$4^1F_3$	-1	-1	0.06266009	$0.06314142 \pm 0.00009618$	-0.000481	0.77
30	$4^3F_2$	+1	+1	0.06266009	$0.06329675 \pm 0.00011207$	-0.000637	1.02
31	$4^3F_3$	+1	-1	0.06267683	$0.06323357 \pm 0.00011899$	-0.000557	0.89
32	$4^3F_4$	+1	+1	0.06258754	$0.06309753 \pm 0.00010310$	-0.000510	0.81
33	$5^1S_0$	+1	-1	0.04134100	$0.04325281 \pm 0.00125908$	-0.001912	4.62
34	$5^3S_1$	-1	+1	0.04038100	$0.04291300 \pm 0.00127772$	-0.002532	6.27
35	$5^1P_1$	-1	-1	0.04038100	$0.04283966 \pm 0.00064062$	-0.002459	6.09

**Table 2.2:** The positronium spectrum for  $\alpha = 0.3$ ,  $\Lambda = 1.0 m_f$ ,  $N_1 = N_2 = 21$ . The  $n^{2S+1}L_J$  notation, the quantum numbers under charge conjugation,  $\mathcal{C}$ , and  $\mathcal{T}$ -parity,  $\mathcal{H}$ , are shown in the first columns. The first row of binding coefficients ( $B_{ETPT,n}$ ) comes from equal time perturbation theory calculations up to order  $\mathcal{O}(\alpha^4)$ . In the following row our results are listed with an estimate of finite  $N$  errors. Also shown is the difference  $\Delta B := B_{ETPT,n} - B_{theor,n}$ . The last row contains the relative discrepancy to perturbation theory in percent.

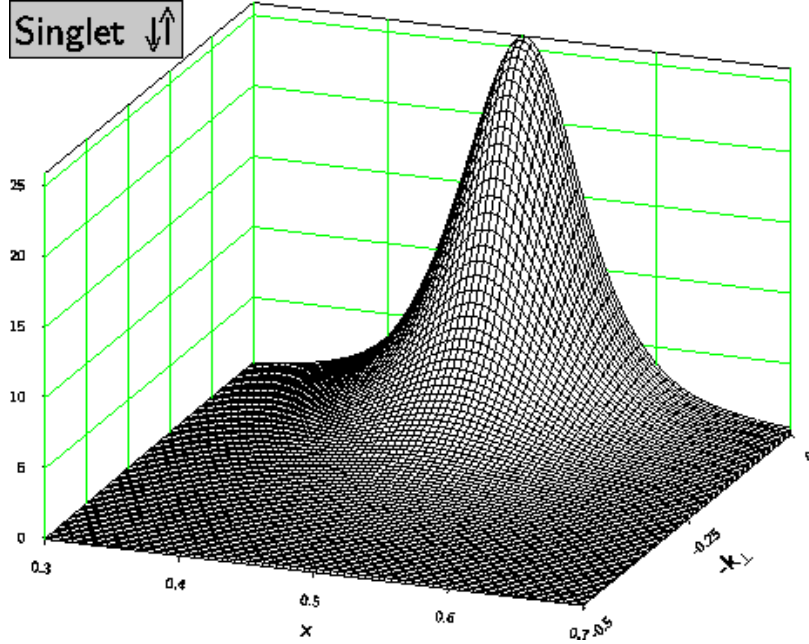


**Figure 2.10:** The singlet wavefunction for anti-parallel spins as a function of the longitudinal momentum fraction  $x$  and the transverse momentum  $k_{\perp}$ , omitting the dependence on the angle  $\varphi$ . The calculation was done with  $\alpha = 0.3$ ,  $\Lambda = 1.0 m_f$ ,  $J_z = 0$ ,  $N_1 = 41$ ,  $N_2 = 11$ .

## 2.4 Wavefunctions

A big advantage of the Hamiltonian method applied in the calculations of the spectrum is the fact that the wavefunctions of positronium are obtained in the same calculation as the spectrum. The wavefunctions for the singlet and the triplet components are displayed in this section. Similar plots in Ref. [73] seem to indicate numerical problems of that work, because they show some internal structure. It turns out that this is due merely to mistakes in the graphing package used. The smoothing functions are quite sensitive to the data and boundary conditions employed<sup>7</sup>.

The wavefunctions have two components: one with parallel ( $\uparrow\uparrow$ ) and the other with anti-parallel ( $\uparrow\downarrow$ ) helicities. For the displayed singlet and triplet wavefunctions, the decomposition in terms of spin components (cf. Eqs. [G.6] and [G.7]) read

$$|\psi_{\text{sing}}(\uparrow\downarrow)\rangle = \frac{1}{2} \sum_{i=1}^{N_1} \sum_{j=1}^{(N+1)/2} \left[ \psi b_1^{\dagger}(\uparrow) d_2^{\dagger}(\downarrow) - \psi^* b_1^{\dagger}(\downarrow) d_2^{\dagger}(\uparrow) - \psi b_2^{\dagger}(\downarrow) d_1^{\dagger}(\uparrow) + \psi^* b_2^{\dagger}(\uparrow) d_1^{\dagger}(\downarrow) \right] |0\rangle,$$

$$|\psi_{\text{sing}}(\uparrow\uparrow)\rangle = \frac{1}{2} \sum_{i=1}^{N_1} \sum_{j=1}^{(N+1)/2} \left[ \psi b_1^{\dagger}(\uparrow) d_2^{\dagger}(\uparrow) + \psi^* b_1^{\dagger}(\downarrow) d_2^{\dagger}(\downarrow) - \psi b_2^{\dagger}(\uparrow) d_1^{\dagger}(\uparrow) - \psi^* b_2^{\dagger}(\downarrow) d_1^{\dagger}(\downarrow) \right] |0\rangle,$$

<sup>7</sup> For our purpose GLE 3.3 by C. PUGMIRE yielded the best results together with the smoothing function grid of PLOTDATA.

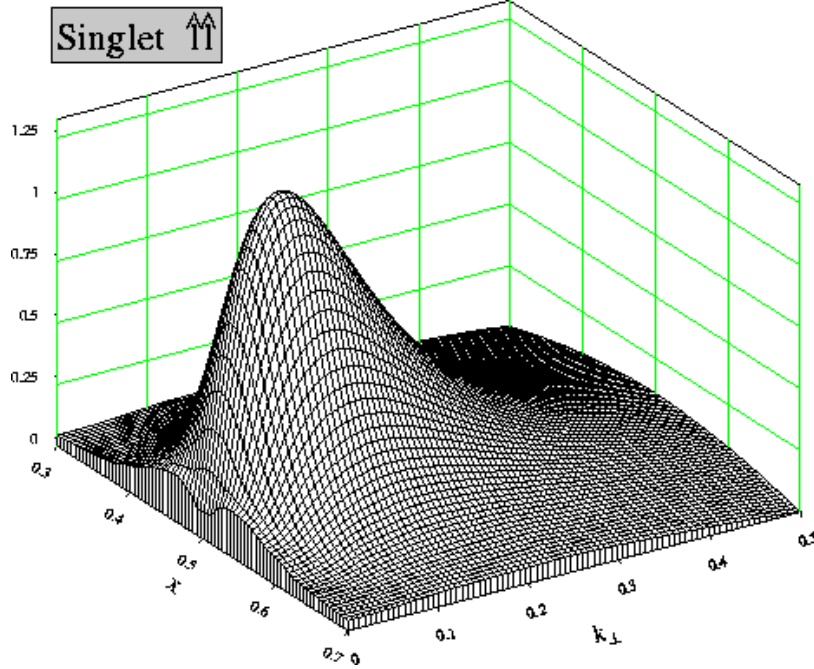


**Figure 2.11:** The singlet wavefunction for parallel spins as a function of the longitudinal momentum fraction  $x$  and the transverse momentum  $k_{\perp}$ , omitting the dependence on the angle  $\varphi$ . The calculation was done with  $\alpha = 0.3$ ,  $\Lambda = 1.0 m_f$ ,  $J_z = 0$ ,  $N_1 = 41$ ,  $N_2 = 11$ .

$$|\psi_{\text{trip}}(\uparrow\downarrow)\rangle = \frac{1}{2} \sum_{i=1}^{N_1} \sum_{j=1}^{(N+1)/2} \left[ \psi b_1^{\dagger}(\uparrow) d_2^{\dagger}(\downarrow) + \psi^* b_1^{\dagger}(\downarrow) d_2^{\dagger}(\uparrow) + \psi b_2^{\dagger}(\downarrow) d_1^{\dagger}(\uparrow) + \psi^* b_2^{\dagger}(\uparrow) d_1^{\dagger}(\downarrow) \right] |0\rangle,$$

$$|\psi_{\text{trip}}(\uparrow\uparrow)\rangle = \frac{1}{2} \sum_{i=1}^{N_1} \sum_{j=1}^{(N+1)/2} \left[ \psi b_1^{\dagger}(\uparrow) d_2^{\dagger}(\uparrow) - \psi^* b_1^{\dagger}(\downarrow) d_2^{\dagger}(\downarrow) + \psi b_2^{\dagger}(\uparrow) d_1^{\dagger}(\uparrow) - \psi^* b_2^{\dagger}(\downarrow) d_1^{\dagger}(\downarrow) \right] |0\rangle,$$

The wavefunctions are normalized in the polar coordinates  $\mu$  and  $\cos\theta$ , such that

$$\sum_{i=1}^{N_1} \sum_{j=1}^{(N_2+1)/2} [\psi(\mu_i, \cos\theta_j; \lambda_1 = \lambda_2) + \psi(\mu_i, \cos\theta_j; \lambda_1 = -\lambda_2)] = 1. \quad (2.18)$$

where

$$\begin{aligned} b_1^{\dagger} &= b^{\dagger}(x, k_{\perp}, \varphi) = b^{\dagger}(\mu, \cos\theta, \varphi), \\ d_2^{\dagger} &= d^{\dagger}(1-x, k_{\perp}, \varphi) = d^{\dagger}(\mu, -\cos\theta, \varphi + \pi). \end{aligned}$$

and discretized variables  $\mu_i, \cos\theta_j$  are used. For all details on the numeric aspects of the calculations see Appx. G.

Figure (2.14) shows the decrease of the singlet wavefunction with anti-parallel helicities as the off-shell mass  $\mu$  increases. The graph, calculated with entirely numerical counterterms, is almost the same as that in [24, Fig. (11), bottom] with half-analytical

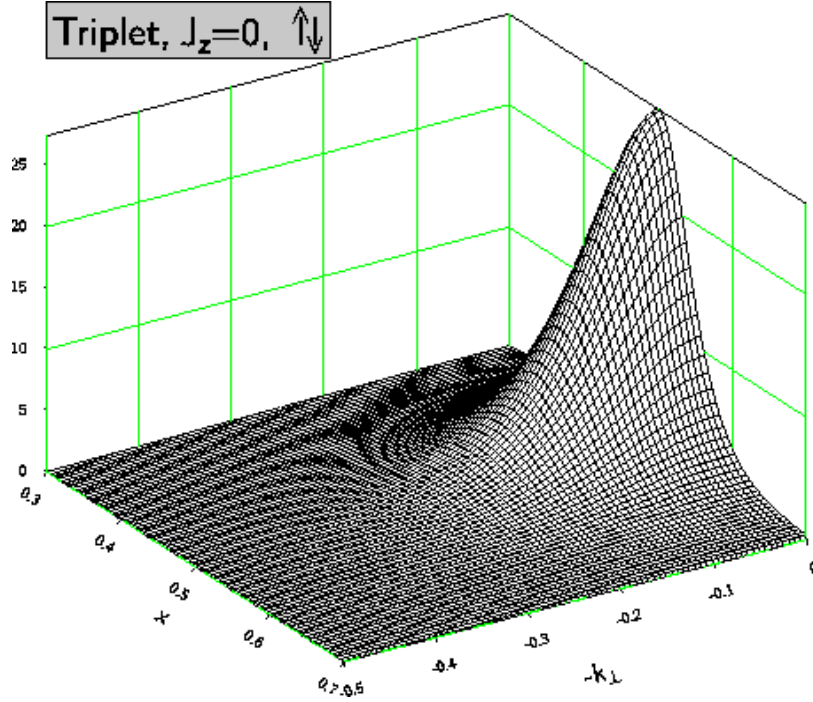


**Figure 2.12:** The triplet wavefunction for anti-parallel spins as a function of the longitudinal momentum fraction  $x$  and the transverse momentum  $k_{\perp}$ , omitting the dependence on the angle  $\varphi$ . The calculation was done with  $\alpha = 0.3$ ,  $\Lambda = 1.0 m_f$ ,  $J_z = 0$ ,  $N_1 = 41$ ,  $N_2 = 11$ .

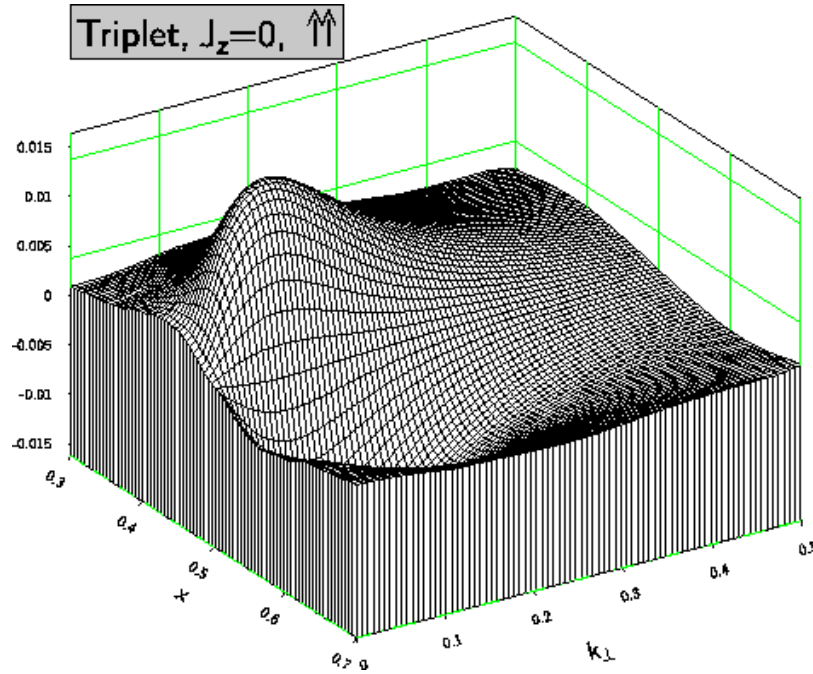


**Figure 2.13:** The triplet wavefunction for parallel spins as a function of the longitudinal momentum fraction  $x$  and the transverse momentum  $k_{\perp}$ , omitting the dependence on the angle  $\varphi$ . The calculation was done with  $\alpha = 0.3$ ,  $\Lambda = 1.0 m_f$ ,  $J_z = 0$ ,  $N_1 = 41$ ,  $N_2 = 11$ .

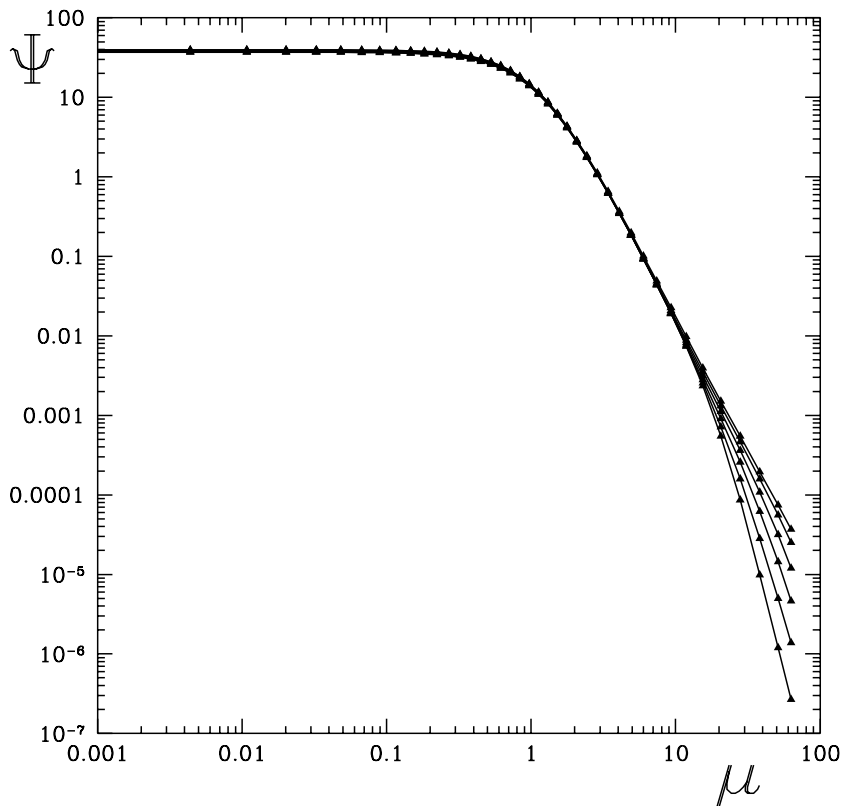


**Figure 2.14:** The decrease of the  $J_z = 0$  singlet ground state with anti-parallel helicities as function of the off-shell mass variable  $\mu$ , Eq. mu. The parameters used are  $N_1 = 41$ ,  $N_2 = 11$ ,  $\Lambda = 1.0 m_f$ ,  $\alpha = 0.3$ . Plotted are the six different decreases corresponding to the six non-positive values of the discretized angle variable  $\cos \theta$ . One notices the deviations from rotational symmetry for  $\mu \geq 10$ .

counterterms, since a large number of integration points ( $N_1 = 41$ ,  $N_2 = 11$ ) were used to calculate the results. It can be seen that rotational invariance is broken. This component of the S-wave state does not depend on any angle and should therefore decrease independently of  $\cos \theta$ . The broken rotational invariance is no surprise. One reason is the fact that the associated operators  $F_1$  and  $F_2$  of rotations around the transverse axes are dynamical, *i.e.* contain the interaction, cf. Table (3.1). The other argument uses the transformation to equal-time coordinates

$$dx d^2 \vec{k}_\perp = \left| \frac{\partial x}{\partial k_z} \right| = \frac{1}{2E} \left( 1 - \frac{k_z^2}{E^2} \right) d^3 \vec{k}. \quad (2.19)$$

One sees directly that the term proportional to  $\frac{k_z^2}{E^2}$  breaks rotational invariance.

It is worth mentioning that the breaking of rotational invariance is noticeable only for large cutoffs  $\Lambda$ . With a cutoff of  $\Lambda = 1.0 m_f$ , the deviation of curves with different  $\cos \theta$  is not visible. In the next chapter, we investigate the same properties of the corresponding wavefunction for  $J_z=1$ .

# Chapter 3

## Angular momentum in front form dynamics

### 3.1 The Poincaré group on the light-cone

To provide the theoretical background for our numerical calculations, we review the properties of angular momenta on the light-cone. The material presented here was inspired by a section on the same subject in [76].

#### 3.1.1 Unitary representations of the Poincaré group

The Poincaré group has 10 generators: the four-momentum  $P^\mu$ , and the generalized angular momenta, constituting an anti-symmetric tensor  $M^{\mu\nu} = -M^{\nu\mu}$ . They are subject to the commutation relations

$$\begin{aligned} [P^\mu, P^\nu] &= 0, \\ [M^{\mu\nu}, P^\rho] &= i(g^{\mu\nu}P^\rho - g^{\rho\mu}P^\nu), \\ [M^{\mu\nu}, M^{\rho\sigma}] &= i(g^{\mu\sigma}M^{\nu\rho} - g^{\mu\rho}M^{\nu\sigma} - g^{\nu\sigma}M^{\mu\rho} + g^{\nu\rho}M^{\mu\sigma}). \end{aligned}$$

The Poincaré group has two Casimir operators, *i.e.* two invariant functions of the generators. One is the *mass* (squared) operator

$$M^2 := P^\mu P_\mu,$$

which cannot be confused with the *indexed* tensor of angular momenta  $M^{\mu\nu}$ . The other is the square of the *Pauli-Lubanski vector* [77]

$$W_\nu := \frac{1}{2}\epsilon_{\rho\sigma\mu\nu}P^\rho M^{\sigma\mu}.$$

The components of this vector obey the commutation relations

$$[W^\mu, W^\nu] = i\epsilon_{\mu\nu\rho\sigma}W^\rho P^\sigma, \tag{3.1}$$



and commute with  $P^\mu$ . The spin operator  $\vec{j}$  can be defined [76, Eq. (6)] as

$$j_i := u_i^\mu(P) \frac{W_\mu}{M}, \quad i = 1, 2, 3. \quad (3.2)$$

It is therefore a linear function of the Pauli-Lubanski vector. The coefficients  $u_i$  are three orthonormal, operator valued, space-like basis vectors, orthogonal to  $P^\mu$ . They have the properties

$$u_i^\mu(P) u_{j,\mu}(P) = \delta_{ij}, \quad \text{and} \quad \sum_{i=1}^3 u_i^\mu(P) u_i^\nu(P) = g^{\mu\nu} - \frac{P^\mu P^\nu}{P^2}. \quad (3.3)$$

The basis vectors transform under a Lorentz transformation like

$$U^\dagger(\Lambda) u_i(P) U(\Lambda) = u_i(\Lambda P) \neq \Lambda u_i(P).$$

These two basis systems are related by a rotation, since  $u_i(\Lambda P)$  and  $\Lambda u_i(P)$  are both orthonormal space-like vectors, orthogonal to  $\Lambda P^\mu$ . This transformation is referred to as a *Wigner rotation* by COESTER [76]

$$\mathcal{R}_W(\Lambda, P)_{ij} := u_i^\mu(\Lambda P) \Lambda u_{j\mu}(P).$$

One can show that the Lorentz transformation of the spin operator is equivalent to a Wigner rotation of its components

$$U^\dagger(\Lambda) \vec{j}(P) U(\Lambda) = \mathcal{R}_W(\Lambda, P) \vec{j}.$$

This follows from the definition (3.2) of the spin operator and holds for every vector  $b_i(P) = u_i^\mu(P) V_\mu$ , where  $V_\mu$  is an arbitrary four-vector. The spin operator has the correct SU(2) commutation relations, as can be proven using (3.1) and the properties of the basis vectors, Eqs. (3.3). Lorentz transformations  $\Lambda$  have the general property

$$\Lambda_\mu{}^\rho g_{\rho\sigma} \Lambda_\nu{}^\sigma = g_{\mu\nu}. \quad (3.4)$$

If one defines  $u_0 := \frac{P}{M}$ , one can re-write Eq. (3.3) into a four dimensional equation

$$u_\mu{}^\rho u_\nu{}^\sigma g_{\rho\sigma} = g_{\mu\nu},$$

which has the same structure as Eq. (3.4). The operator valued matrix  $u_\mu{}^\nu$  is thus an  $SO(1, 3)$  representation of some Lorentz transformation  $B(P)$  which can be interpreted with some care as the Lorentz transformation to the rest frame of P:  $u_\mu{}^\nu(P) P_\nu = g_{\mu 0} M$ . The spin operator  $\vec{j}$  can be written, apart from the form given in Table (3.1), in terms of the basis vectors

$$j_i = \frac{1}{2} u_0{}^\mu(P) u_i{}^\nu(P) \epsilon_{\mu\nu\rho\sigma} M^{\rho\sigma}.$$

We are interested in bound state calculations, *i.e.* in composite systems. One can define the relative momenta  $k_n$  of a subsystem by

$$k_{n,i} := u_i^\nu(P) p_{n,\nu}, \quad p_n^\mu = \sum_i u_i^\mu(P) k_{n,i},$$

where  $P = \sum_n p_n$  is the (absolute) momentum of the system.

#### 3.1.2 Connection between canonical spin and front form helicity

So far, everything was independent of the choice of the basis vectors  $u_\alpha(P)$ , *i.e.* of the form of the Hamiltonian dynamics. The implications for *instant form* and *front form*, the two kinds of dynamics of interest for the present work, are compared now. The major features of the two types of dynamics are listed in Table (3.1).

The instant form, *i.e.* canonical, choice of the basis  $\bar{u}_\alpha(P)$  is related to the front form basis  $\check{u}_\alpha(P)$  by the so-called *Melosh rotation* [78]

$$\mathcal{R}_M(P)_{ij} := \bar{u}_i(P) \cdot \check{u}_j(P).$$

Its  $SU(2)$  representation is

$$D^{1/2}[\mathcal{R}_M(P)] = \frac{M + P^+ - i\vec{\sigma} \cdot (\hat{z} \times \vec{P}_\perp)}{\sqrt{(M + P^+)^2 + P_\perp^2}}.$$

The essential observation for a relation between instant form spin and light-cone helicity is that the canonical spin of the  $n$ -th particle of a composite system can be expressed in the front form basis

$$\bar{s}_{n,i} = \bar{u}_i(\bar{k}_n) \cdot \bar{B}(P) \frac{W_n}{M_n} = \mathcal{R}_M(P) \bar{u}_i(\check{k}_n) \cdot \check{B}(P) \frac{W_n}{M_n}.$$

The translation of the total angular momentum from equal time to light-cone coordinates is therefore obtained by a Melosh rotation, cf. Table (3.1).

#### 3.1.3 Field theories on the light-cone

There are two different ways to construct front form particle dynamics. One approach starts from the mass and spin operators which have to fulfill some constraints on their commutation relations. The three Hamiltonians of front form dynamics can then be expressed as functions of the kinematic generators and of the mass and spin operators

$$\begin{aligned} P^- &= \frac{M^2 + P_\perp^2}{P^+}, \\ F_1 &= \frac{2(M\check{j}_2 + P_2\check{j}_3)}{P^+} + \frac{P^-}{P^+} E_1 + \frac{2P_1}{P^+} K_z, \\ F_2 &= -\frac{2(M\check{j}_1 + P_1\check{j}_3)}{P^+} + \frac{P^-}{P^+} E_2 + \frac{2P_2}{P^+} K_z. \end{aligned}$$

The dynamical operators commute with each other

$$[P^-, \vec{F}_\perp] = [F_1, F_2] = 0. \quad (3.5)$$

The other approach is that of Fock space field theories. Here, the fundamental quantities are the Hamiltonians which are derived from a Lagrangian density. The spin operators are then formulated in terms of the Hamiltonians

$$\begin{aligned}\check{j}_z = \frac{W^+}{P^+} &= M_z - \frac{\hat{z} \cdot (\vec{E}_\perp \times \vec{P}_\perp)}{P^+}, \\ \check{j}_\perp &= \frac{\vec{W}_\perp}{M} - \frac{\vec{P}_\perp W^+}{MP^+},\end{aligned}$$

where

$$\vec{W}_\perp = \frac{1}{2}P^+\hat{z} \times (\vec{F} - \vec{E}) + \frac{1}{2}(P^+ - P^-)\hat{z} \times \vec{E}_\perp - (\hat{z} \times \vec{P}_\perp) K_z,$$

and  $\hat{z}$  is the unit vector in  $z$ -direction. Very important is the fact that Poincaré invariance is destroyed, as soon as truncations of the Fock space or regularizations of Fock sectors are implemented. In particular, the requirement of an invariance under rotations around the transverse axes is difficult to fulfill since the corresponding operators are complicated and involve the interaction. Even worse, in a truncated Fock space formalism the full Poincaré invariance is absent if it is not restored by an additional (*ad hoc*) prescription [76, p. 11]!

It is therefore impossible for our positronium model to be Poincaré *invariant*. I shall rather show its *covariance* by looking at the results, *i.e.* at the physical observables such as the invariant mass spectrum. If full rotational invariance is restored in the solution, the states of same total angular momentum  $J$  but different  $J_z$ , become degenerate.

The most direct way would of course be to construct the operators  $F_1$  and  $F_2$  explicitly and then to diagonalize the operator of total angular momentum  $\mathcal{J}^2$ . This has not been done up to now. Because of the vanishing commutators of the dynamical operators with  $P^-$ , Eq. (3.5), it is clear that the diagonalization of the rotation operators will be much simpler with an already diagonal Hamiltonian  $H_{LC}$ : only the states with degenerate mass eigenvalues will be coupled by  $\vec{F}_\perp$ .

However, we restrict ourselves in the present work to the calculation of the spectrum of the light-cone Hamiltonian and will find that we can classify the eigenstates with regard to  $J^2$  even without constructing or diagonalizing the rotation operators  $\vec{F}_\perp$ .

### 3.1. The Poincaré group on the light-cone

	instant form dynamics	front form dynamics
Kinematic operators	6 operators: $\vec{P}, \vec{J} := (M^{23}, M^{31}, M^{12})$	7 operators: $\vec{P}, K_z := \frac{1}{2}M^{+-}, \vec{E}_\perp := M^{\perp+}, J_z$
Dynamic operators	4 operators: $P^0, \vec{K}$	3 operators: $P^-, \vec{F}_\perp := M^{\perp-}$
Conditions on basis	$\bar{B}(P)$ are rotationless Lorentz transformations	$\check{B}(P)$ are null-plane boosts
Basis	$\bar{u}_i := e_i + \frac{e_i^\mu P_\mu}{M - e_0^\mu P_\mu} \left( \frac{P}{M} + e_0 \right)$	$\check{u}_\perp := e_\perp + \frac{e_\perp^\mu P_{\perp\mu}}{n^\mu P_\mu} n,$ $\check{u}_3 := \frac{M}{n^\mu P_\mu} \left( n - \frac{(n^\mu P_\mu)P}{P^2} \right)$
Wigner rotation	$\bar{\mathcal{R}}_W(\mathcal{R}, P) = \mathcal{R}$	$\check{\mathcal{R}}_W(\check{\Lambda}_{boost}, P)_{\alpha\beta} = \delta_{\alpha\beta}$
Angular momentum	$\vec{j} = \frac{\vec{W}}{M} - \frac{\vec{P}W_0}{M(M + P^0)}$	$\check{j} = \mathcal{R}_M^{-1}(P)\vec{j}$
Spin operator	$\vec{s}_i = \bar{\mathcal{R}}_W(P, p_i)\vec{j}_i$	$\check{s}_i = \mathcal{R}_M^{-1}(P)\vec{s}_i$
Notations	$e_\sigma^\mu := g_\sigma^\mu, \quad n^\mu := (1, -\hat{z}), \quad \check{\Lambda}_{boost} \in \{\vec{E}_\perp, K_z\}$	

**Table 3.1:** Major properties of instant form and front form dynamics.

## 3.2 The Hamiltonian matrix with general $J_z$

The material presented in the previous section shows that the definition of angular momentum operators in front form dynamics is problematic since they include the interaction. It is therefore a subject of its own merit to study the properties of angular momentum within a well-defined model on the light-cone. Consequently, we investigate the case of a non-vanishing  $z$ -component of the total angular momentum in our positronium model.

The way to proceed is inferred from the definition of the integral used to integrate out the angular degree of freedom ( $\varphi$ ) and substitute it with the discrete quantum number  $J_z$

$$\langle x, \vec{k}_\perp; J_z, \lambda_1, \lambda_2 | \tilde{V}_{\text{eff}} | x', \vec{k}'_\perp; J'_z, \lambda'_1, \lambda'_2 \rangle := \frac{1}{2\pi} \int_0^{2\pi} d\varphi e^{-iL_z\varphi} \int_0^{2\pi} d\varphi' e^{iL'_z\varphi'} \langle x, k_\perp, \varphi; \lambda_1, \lambda_2 | V_{\text{eff}} | x', k'_\perp, \varphi'; \lambda'_1, \lambda'_2 \rangle. \quad (3.6)$$

We listed the general matrix elements  $\langle x, \varphi; s_1, s_2 | V_{\text{eff}} | x', \varphi'; s'_1, s'_2 \rangle$  in Table (F.1). In general, the functions displayed there contain a dependence on the angles. Hence, it is not clear how the general  $\varphi$  dependence of the matrix elements will look like, if one inserts an arbitrary  $L_z = J_z - S_z$  into Eq. (3.6). Fortunately, a simple scheme can be set up to construct the functions for all  $J_z = n, n \in \mathbf{Z}$ . In particular, one can prove that the matrix elements can only depend on the difference  $\varphi - \varphi'$ . The general function has the shape

$$F(x, k_\perp, x', k'_\perp; \lambda_1, \lambda_2) = \frac{1}{2\pi} \int_0^{2\pi} d\varphi \int_0^{2\pi} d\varphi' \frac{\tilde{F}(x, \vec{k}_\perp, x', \vec{k}'_\perp; \lambda_1, \lambda_2)}{a - 2k_\perp k'_\perp \cos(\varphi - \varphi')} e^{in(\varphi - \varphi')},$$

where  $n \in \mathbf{Z}$  and

$$a = (x - x')^2 \frac{m_f^2}{2} \left( \frac{1}{xx'} + \frac{1}{(1-x)(1-x')} \right) + k_\perp^2 + k'_\perp{}^2 - \frac{1}{2}(x - x') \left[ k_\perp'^2 \left( \frac{1}{1-x'} - \frac{1}{x'} \right) - k_\perp^2 \left( \frac{1}{1-x} - \frac{1}{x} \right) \right].$$

It is straightforward to evaluate this expression with the decomposition  $\exp\{\pm ix\} = \cos x \pm i \sin x$  and the integrals

$$\begin{aligned} \frac{1}{2\pi} \int_0^{2\pi} d\varphi \int_0^{2\pi} d\varphi' \frac{\cos\{n(\varphi - \varphi')\}}{a - 2k_\perp k'_\perp \cos(\varphi - \varphi')} &= 2\pi (-A)^{-|n|+1} \left( \frac{B}{k_\perp k'_\perp} \right)^{|n|}, \\ \frac{1}{2\pi} \int_0^{2\pi} d\varphi \int_0^{2\pi} d\varphi' \frac{\sin\{n(\varphi - \varphi')\}}{a - 2k_\perp k'_\perp \cos(\varphi - \varphi')} &= 0. \end{aligned}$$

Here, the definitions

$$A = \frac{1}{\sqrt{a^2 - 4k_\perp^2 k'_\perp{}^2}} \quad \text{and} \quad B = \frac{1}{2} (1 - aA),$$

were used. Using these relations, one can calculate the matrix elements for arbitrary  $J_z$ . The results are listed in Table (F.2).

### 3.3 The positronium spectrum for general $J_z$

The positronium spectrum is calculated numerically from the matrix elements of Table (F.2). Although we implemented a more general counterterm technology, described in Chapter 1, which automatically accounts for the new features of the diagonal matrix elements for  $J_z \neq 0$ , we must be even more careful. In the former calculations ( $J_z = 0$ ), we made use of the *discrete* symmetries  $\mathcal{C}$  and  $\mathcal{H}$ , as described in Appendix G, §2. These symmetry properties are not explicitly conserved for the more general case  $J_z \neq 0$ . To be careful, we ignore possible point symmetries in the problem, and solve for the spectrum without symmetrizing the Hamiltonian. We will see in the next section how justified our extra care was. The numerical effort increases enormously. With the unsymmetrized Hamiltonian, the dimensions of the matrices to be diagonalized are four times larger. Since the number of operations grows with the third power of the matrix dimensions in a standard diagonalization algorithm, the CPU time used is 16 times longer.

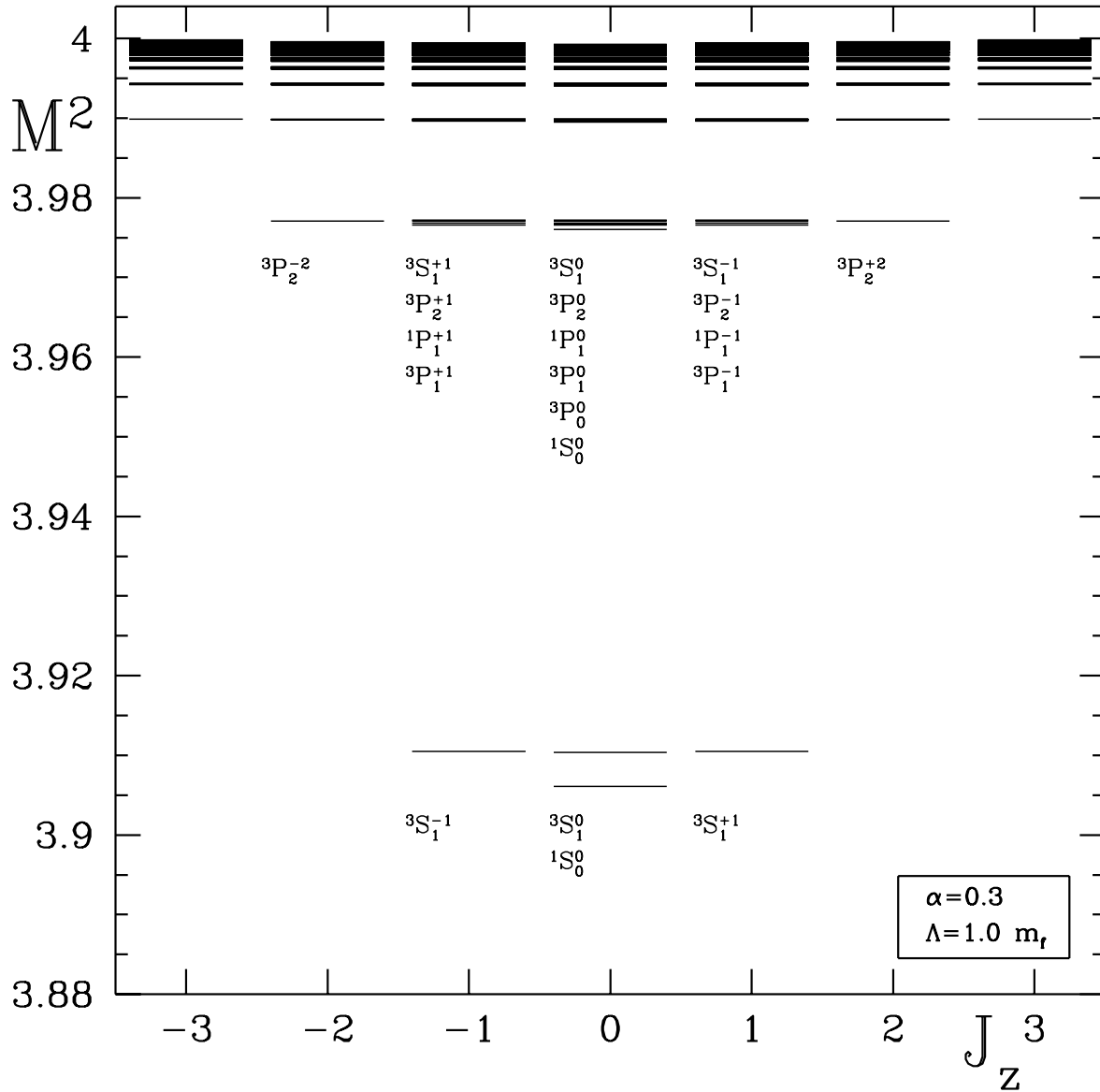
We calculated spectra for the seven different values,  $J_z = -3, -2, \dots, +3$ . It is found that the eigenvalues are *identical* for  $J_z = +n$  and  $J_z = -n$  as can be seen from Fig. (3.1). The individual spectra and the convergence can be seen from Figures (3.2)–(3.4). In particular, one notices that the singlet ground state is absent from all three plots, and that for  $J_z=2$  and  $J_z=3$  even more states are absent. The explanation is the impossibility to have states with  $J_z = n$  in multiplets with  $J < n$ . The numerical stability (*i.e.* convergence) is very good: in each of the figures the lowest eigenvalue is almost independent of the number of integration points. In fact, the eigenvalues converge exponentially with the number of integration points, as we will show in Chapter 4. This is the more surprising, as we adjusted the Coulomb counterterm<sup>1</sup>, based on the non-relativistic ground state wavefunction, and the excited state wavefunctions are quite different.

Fig. (3.1), the summary of the spectra for different  $J_z$ , is central to this chapter. What can we learn from it? It has two prominent features. Firstly, there are multiplets of states with different  $J_z$  that are degenerate. We shall discuss the numerical evidence in what follows. Secondly, there is a limited odd number of degenerate states for each eigenvalue. The interpretation of these facts is obvious. The positronium mass spectrum is a physical observable, Lorentz invariant and therefore independent of the mathematical algorithm applied and of the Lorentz frame used. Central forces are rotationally invariant, and this should be observed in the spectrum of an electromagnetic bound system, too. Rotational symmetry tells us that there has to be a defined number of degenerate states for each fixed value of the total angular momentum  $\vec{J}$ . Conversely, since this is exactly what we observe here, we can infer the quantum number  $J$  from the number of degenerate states for a fixed eigenvalue  $M_n^2$ . Concluding, the 1, 3, 5, ... degenerate states constitute the singlets, triplets, pentuplets, ... of a  $J = 0, 1, 2, \dots$  multiplet.

In Table (3.2), the spectrum obtained for  $J_z=1$  is compiled to compare it with the

---

<sup>1</sup>*i.e.*, the converging function  $g(p, p')$  was chosen in this manner, cf. Appendix G.



**Figure 3.1:** Compiled spectra of positronium with different  $J_z = -3, -2, \dots, +3$ . All spectra have been calculated with  $\alpha = 0.3, \Lambda = 1.0 m_f, N_1 = N_2 = 21$ . The mass squared eigenvalues  $M_n^2$  in units of the electron mass  $m_f^2$  are shown. The notation for the states is  ${}^{3S+1}L_{J_z}^{J_z}$ . The resolution of the plot is inadequate for the multiplets. Nevertheless, the numerical degeneracy of the three triplet ground states  ${}^3S_{-1}^{-1}, {}^3S_1^0$ , and  ${}^3S_1^+1$  becomes very clear.

### 3.3. The positronium spectrum for general $J_z$

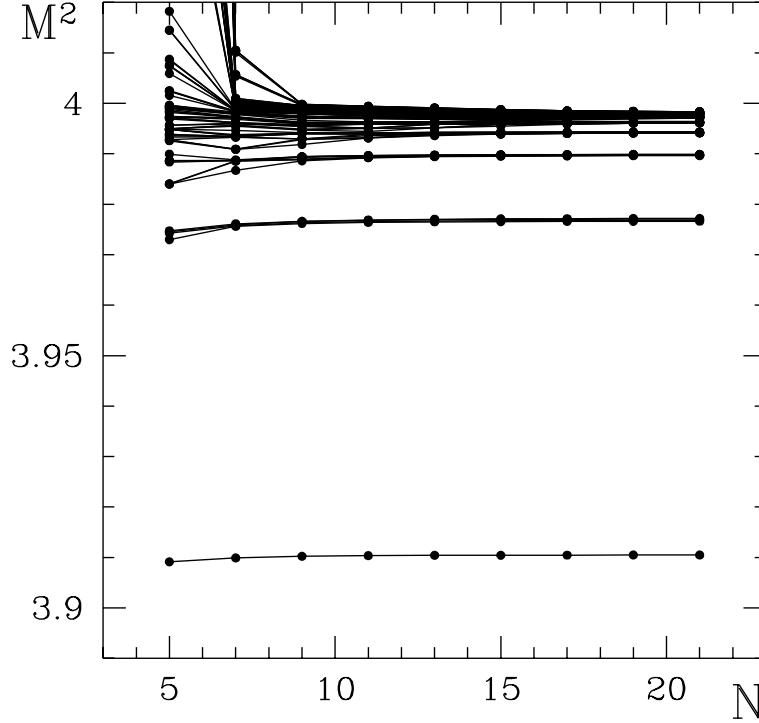


**Figure 3.2:** The spectrum of the effective integral equation for  $\alpha = 0.3, \Lambda = 1.0 m_f, J_z = 1$ . The mass squared eigenvalues  $M_n^2$  in units of the electron mass  $m_f^2$  are shown as functions of the number of integration points  $N \equiv N_1 = N_2$ . The calculation was done using the entirely numerically integrated Coulomb counterterms. Note that the singlet ground state is absent. For  $n=1$  only the triplet  ${}^3S_1$  survives the projection on the  $J_z=1$  sector. Cf. Fig. (2.6).

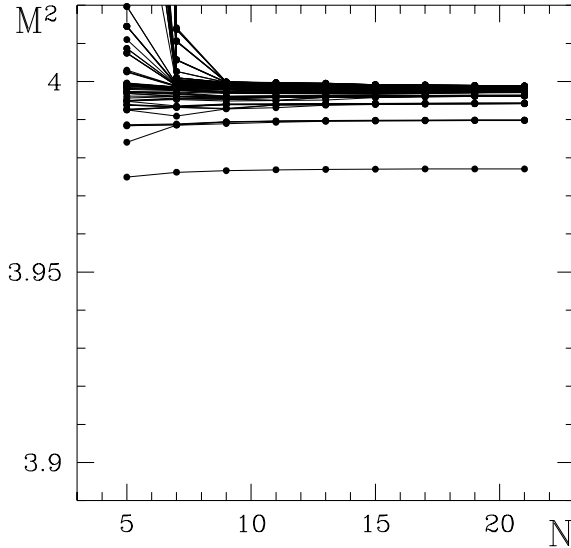


**Figure 3.3:** The spectrum of the effective integral equation for  $\alpha = 0.3, \lambda = 1.0 m_f, J_z = 2$ . Note the total absence of any  $n = 1$  state.

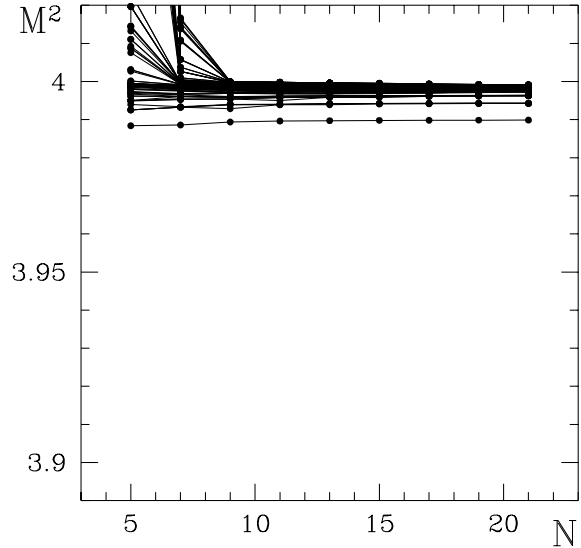


**Figure 3.4:** The spectrum of the effective integral equation for  $\alpha = 0.3, \Lambda = 1.0 m_f, J_z=3$ . Even more states are not compatible with  $J_z=3$ .



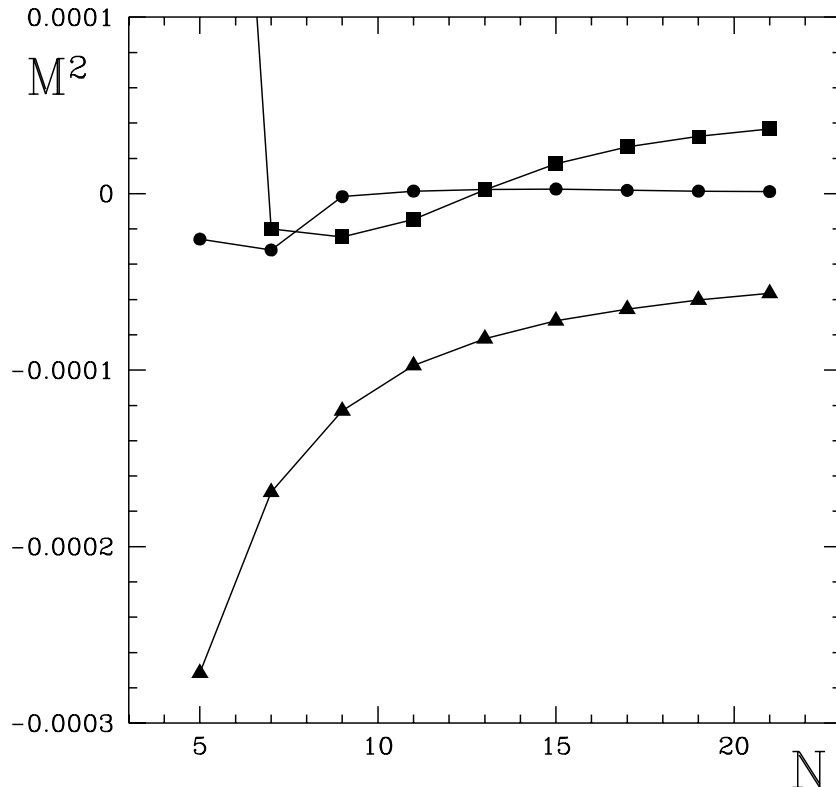


**Figure 3.5:** Deviation of corresponding eigenvalues for  $J_z=0$  and  $J_z=1$  multiplets ( $\alpha = 0.3, \Lambda = 1.0 m_f$ ) with growing number of integration points. The graphs show  $\Delta M^2 := M_n^2(J_z=0) - M_n^2(J_z=1)$  for the states  $1^3S_1$  ( $\Delta$ ),  $2^3P_1$  ( $\square$ ), and  $2^1P_1$  ( $\circ$ ).

eigenvalues for  $J_z=0$ . Apart from the absence of the states with  $J=0$ , the table displays an almost complete coincidence of the corresponding states. Only for the triplet  $1^3S_1$ , the gap between the two states of different  $J_z$  is bigger, though the numerical error is actually smaller.

We have to investigate the significance of the degeneracy with respect to the number of integration points and with respect to the cutoff  $\Lambda$ . To find out if this discrepancy is merely a numerical artifact, or a property of the positronium model, consider Figure (3.5). Here, the mass (squared) discrepancy between the  $J_z=0$  and  $J_z=1$  eigenvalues is plotted versus the number of integration points  $N$  for three different states. One notices the convergence of  $\Delta M^2(1^3S_1)$  with  $N$ . The curve does not converge to zero, as one would want, but to a value of  $\Delta M^2(1^3S_1) \simeq -5 \times 10^{-5}$ . The mass gap for  $2^1P_1$  does, however, go to zero as  $N$  grows large. The mass gap of the other helicity-triplet state  $2^3P_1$  has the same increase as  $\Delta M^2(1^3S_1)$ , if one disregards the behavior of the corresponding graph for the untrustworthy values  $N=5$  and  $N=7$ . It converges to  $4 \times 10^{-5}$  as  $N$  increases. We mention that KALUŽA and PIRNER [52] find that in light-cone perturbation theory there is a discrepancy between the case of  $J_z=0$  and  $J_z=1$ . This is due to the perturbative method applied there and even expected from

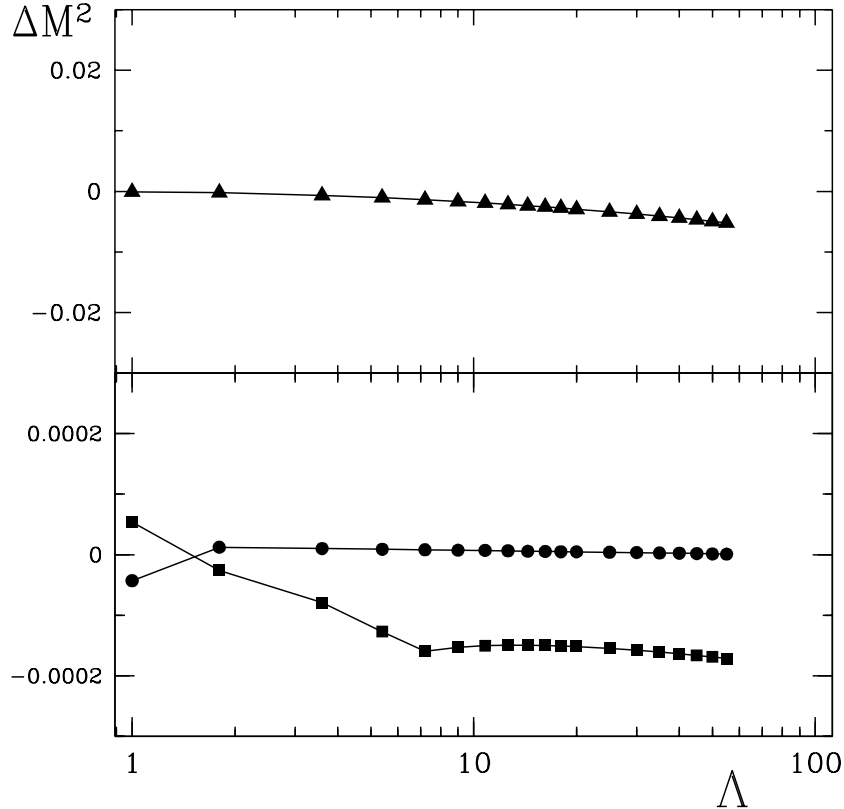


**Figure 3.6:** Deviation of corresponding eigenvalues for  $J_z=0$  and  $J_z=1$  ( $\alpha = 0.3$ ) as functions of the cutoff  $\Lambda$ . The graphs show  $\Delta M^2 := M_n^2(J_z=0) - M_n^2(J_z=1)$  for the states  $1^3S_1$  ( $\Delta$ ) [upper box], and  $2^3P_1$  ( $\square$ ), and  $2^1P_1$  ( $\circ$ ) [lower box]. Note that the scales of the two boxes differ by a factor of 100!

the point of view taken in the present work. Perturbation theory to any finite order breaks the symmetries of the theory. Since rotations contain the interaction in front form dynamics, the associated symmetry will be broken in a perturbative approach.

### Cutoff dependence

For the cutoff dependence of the eigenvalues for non-vanishing  $J_z$  the statements given in the context of Chapter 2 hold equally. A main result of the present work is the documentation of the restoration of rotational symmetry in the solution in front form dynamics. Consequently, the investigation of the degeneracy of eigenvalues of same total angular momentum, but different  $J_z$  is crucial. The discrepancy between corresponding eigenvalues of  $J_z=0$  and  $J_z=1$  as functions of the cutoff is displayed in Fig. (3.6). One notices that there is a slight deviation of the cutoff dependence of the triplets  $1^3S_1$  for different  $J_z$ . The deviations of the other states ( $2^3P_1$  and  $2^1P_1$ ) are suppressed by roughly a factor of 100.

This weak dependence of  $\Delta M_n^2$  on the cutoff will be suppressed even more, if the annihilation channel is included.

$n$	Term	$B_n(J_z=0)$	$B_n(J_z=+1)$	$10^5 \Delta B_n$
1	$1^1S_0$	$1.049553 \pm 0.000017$	—	—
2	$1^3S_1$	$1.001012 \pm 0.000111$	$1.000376 \pm 0.000071$	63.53
3	$2^1S_0$	$0.260237 \pm 0.000169$	—	—
4	$2^3S_1$	$0.253804 \pm 0.000217$	$0.253720 \pm 0.000208$	8.33
5	$2^1P_1$	$0.257969 \pm 0.000161$	$0.257982 \pm 0.000166$	-1.30
6	$2^3P_0$	$0.267070 \pm 0.000156$	—	—
7	$2^3P_1$	$0.259667 \pm 0.000206$	$0.260075 \pm 0.000159$	-40.80
8	$2^3P_2$	$0.255258 \pm 0.000177$	$0.255253 \pm 0.000172$	0.47
9	$3^1S_0$	$0.115206 \pm 0.000314$	—	—
10	$3^3S_1$	$0.113441 \pm 0.000363$	$0.113413 \pm 0.000261$	2.79
11	$3^1P_1$	$0.114490 \pm 0.000270$	$0.114529 \pm 0.000282$	-3.96
12	$3^3P_0$	$0.117133 \pm 0.000271$	—	—
13	$3^3P_1$	$0.115127 \pm 0.000326$	$0.115116 \pm 0.000273$	1.13
14	$3^3P_2$	$0.113717 \pm 0.000281$	$0.113719 \pm 0.000280$	-0.26
15	$3^1D_2$	$0.112816 \pm 0.000150$	$0.112842 \pm 0.000158$	-2.66
16	$3^3D_1$	$0.113427 \pm 0.000155$	$0.113496 \pm 0.000277$	-6.90
17	$3^3D_2$	$0.112978 \pm 0.000161$	$0.112982 \pm 0.000162$	-0.43
18	$3^3D_3$	$0.112511 \pm 0.000156$	$0.112515 \pm 0.000158$	-0.41
19	$4^1S_0$	$0.065490 \pm 0.000588$	—	—
20	$4^3S_1$	$0.064786 \pm 0.000598$	$0.064774 \pm 0.000596$	1.25
21	$4^1P_1$	$0.065003 \pm 0.000467$	$0.065062 \pm 0.000486$	-5.91
22	$4^3P_0$	$0.066115 \pm 0.000470$	—	—
23	$4^3P_1$	$0.065331 \pm 0.000487$	$0.065282 \pm 0.000475$	4.88
24	$4^3P_2$	$0.064700 \pm 0.000478$	$0.064706 \pm 0.000480$	-0.65
25	$4^1D_2$	$0.063968 \pm 0.000294$	$0.064041 \pm 0.000317$	-7.32
26	$4^3D_1$	$0.064262 \pm 0.000308$	$0.064371 \pm 0.000348$	-10.97
27	$4^3D_2$	$0.064099 \pm 0.000319$	$0.064088 \pm 0.000314$	1.06
28	$4^3D_3$	$0.063864 \pm 0.000303$	$0.063875 \pm 0.000305$	-1.07
29	$4^1F_3$	$0.063141 \pm 0.000096$	$0.063106 \pm 0.000103$	3.51
30	$4^3F_2$	$0.063297 \pm 0.000112$	$0.063232 \pm 0.000116$	6.52
31	$4^3F_3$	$0.063234 \pm 0.000119$	$0.063210 \pm 0.000118$	2.32
32	$4^3F_4$	$0.063098 \pm 0.000103$	$0.063422 \pm 0.000158$	-32.44
33	$5^1S_0$	$0.043253 \pm 0.001259$	—	—
34	$5^3S_1$	$0.042913 \pm 0.001278$	$0.042915 \pm 0.000740$	-0.19
35	$5^1P_1$	$0.042840 \pm 0.000641$	$0.042905 \pm 0.000675$	-6.53

**Table 3.2:** The positronium spectrum for  $\alpha = 0.3$ ,  $\Lambda = 1.0 m_f$ ,  $N_1 = N_2 = 21$ . The non-relativistic notation for the terms and the binding coefficients for  $J_z=0$  and  $J_z=+1$  are shown. The numerical errors are estimated from the difference between the values for maximum and next to maximum number of integration points. In fact they are smaller, because the eigenvalues converge exponentially with the number of integration points.

## 3.4 Wavefunctions

The  $J_z \neq 0$  wavefunctions show more structure than those with  $J_z=0$ , due to the lower symmetry. In the  $J_z=0$  case, there are essentially two different components of the wavefunctions: one for parallel, the other for anti-parallel helicities. Consequently, there are only two plots shown for the singlet and triplet wavefunctions in Chapter 1: Figs. (2.10), (2.11) and Figs. (2.12), (2.13), respectively.

This is not a consequence of the symmetrized Hamiltonian. If the non-symmetrized  $J_z=0$  Hamiltonian matrix is diagonalized, the same eigenfunctions are found as in the symmetric case, but twice as many occur. The only difference is a sign, depending on the parity quantum number.

When  $J_z \neq 0$ , we encounter four distinct components of each of the eigenfunctions, corresponding to four different helicity combinations. We elaborate on this subject by considering the components of the triplet wavefunction for  $J_z=1$ , Figs. (3.8)(a)-(d), and that of the next higher state, Figs. (3.9)(a)-(d). In both cases, the components for anti-parallel helicities are identical, though displayed differently to show their full shape. For the triplet, the components with parallel helicities have nothing in common: the ( $\uparrow\uparrow$ )-component peaks at  $x=0.5$ ,  $k_\perp=0$  and is almost rotationally invariant, whereas the ( $\downarrow\downarrow$ )-component vanishes at  $k_\perp=0$  and is shaped more like the components with anti-parallel helicities. Note the extremely differing peak values: the anti-parallel components are suppressed by a factor of 40, compared to the ( $\uparrow\uparrow$ )-component, the ( $\downarrow\downarrow$ )-component even by a factor of 1400! As with the  $J_z=0$  sector, Eq. (2.18), the normalization is

$$\sum_{i=1}^{N_1} \sum_{j=1}^{N_2} \sum_{\lambda_1, \lambda_2} \psi(\mu_i, \cos \theta_j; \lambda_1, \lambda_2) = 1.$$

The missing symmetry of the components is a consequence of the missing symmetry of the  $J_z \neq 0$  sector with respect to  $\mathcal{T}$ -parity. This property is found in all wavefunctions of these sectors. We have displayed here the wavefunction(s) of the next excited state to show another important fact: the wavefunction Fig. (3.9)(a) has a small, but noticeable deviation from the reflection symmetry with respect to the  $x = 0.5$  plane. This symmetry around  $x=0.5$  is due to the charge conjugation symmetry  $\mathcal{C}$ : if one permutes particle and antiparticle, one substitutes  $x$  with  $1 - x$ . The fact that this property is respected by all wavefunctions other than Fig. (3.9)(a) shows, that this symmetry is not broken, even not in the  $J_z \neq 0$  sector. The slight deviations can be explained as numerical errors, or more likely, as errors due to the `grid` function of the graphing package used. Some examples for higher excitations and larger  $J_z$  are given in Fig.(3.10).

The decrease of the triplet wavefunction  $1^3S_1(\uparrow\uparrow)$  with parallel helicities is plotted in Fig. (3.7). These curves for different  $\cos \theta_j$  have to be compared to those of Fig. (2.14). In both cases, rotational symmetry is broken, since the decrease of the wavefunction is not isotropic but depends on the angle  $\theta$ . There are some differences between the sectors  $J_z=0$  and  $J_z=1$ . One is the fact that the smallest value of the wavefunction for  $J_z=1$  is roughly  $9 \times 10^{-6}$ , whereas for  $J_z=0$  its approximately three times smaller.

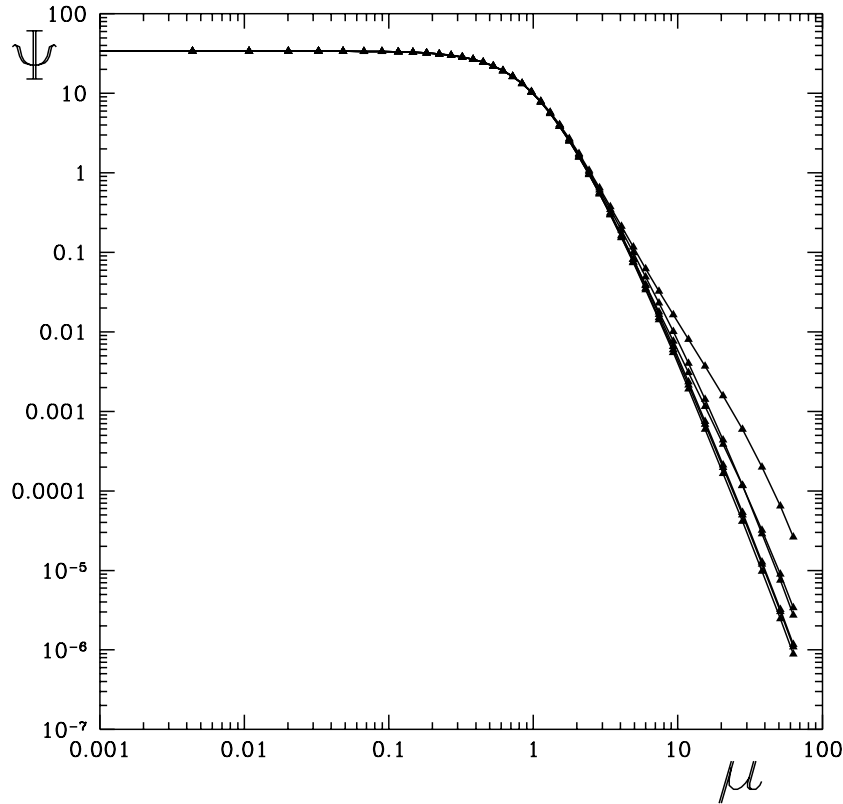


**Figure 3.7:** The decrease of the  $J_z = +1$  triplet ground state wavefunction with parallel helicities as a function of the momentum variable  $\mu$ . The parameters are  $\alpha = 0.3$ ,  $\Lambda = 20.0 m_f$ ,  $N_1 = 41$ ,  $N_2 = 11$ . There are six different curves corresponding to six values of the discretized angle variable,  $\theta$ : they show the decrease in  $\psi$  with increasing  $\mu$ . Notice the deviations from rotational symmetry for  $\mu \geq 10$ .

Another difference is the value of  $\mu$  from that on the deviations in the decreases become noticeable. For  $J_z=0$  this value is at  $\mu \simeq 10$ , contrary to  $\mu \simeq 3$  in the  $J_z=1$  sector. Moreover, the curves of different  $\cos \theta$  seem to be grouped for  $J_z=1$ . In any case, the important result is the same as in the case of  $J_z=0$ : the wavefunctions are not rotationally invariant.

### 3.4. Wavefunctions

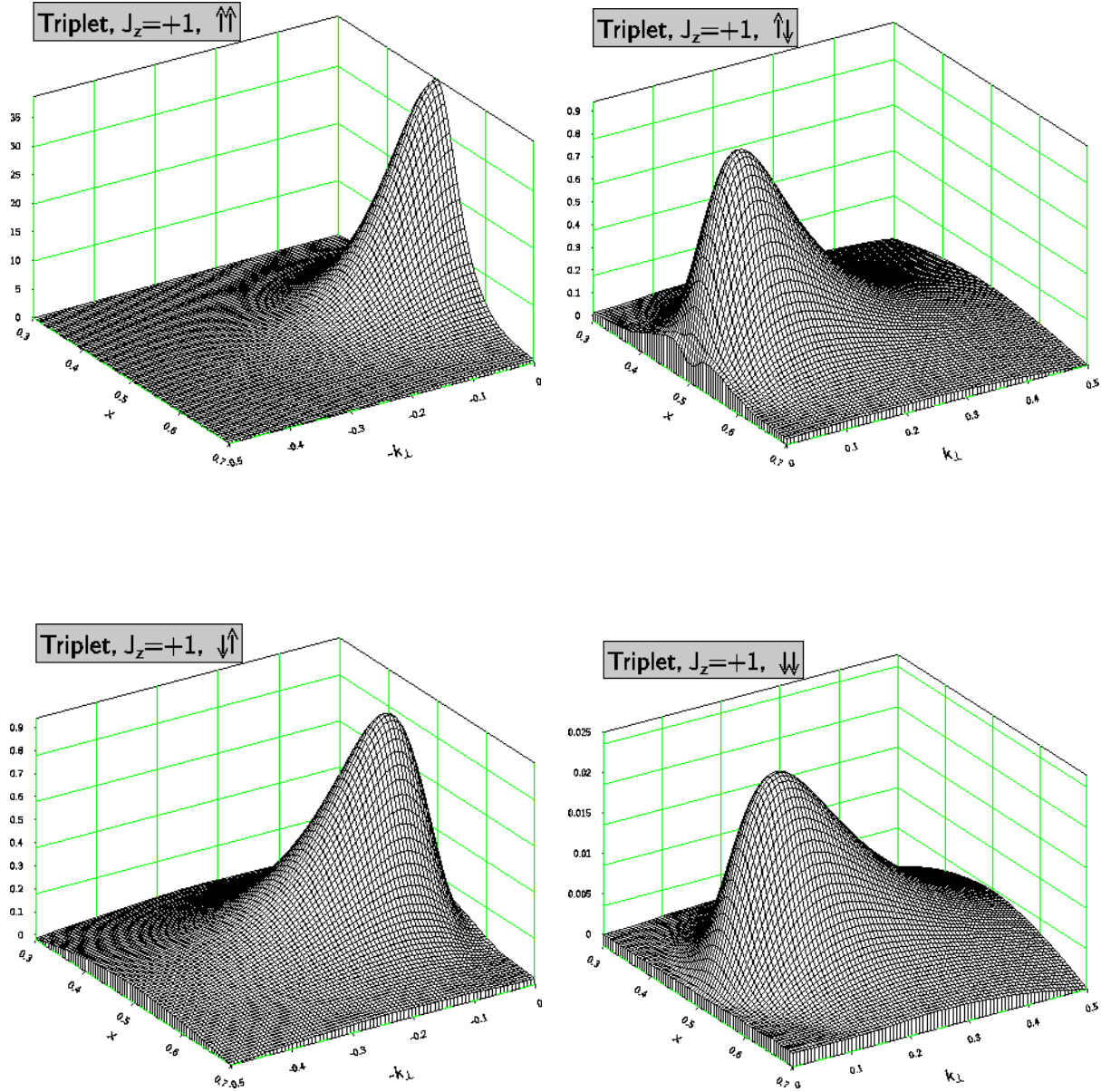


**Figure 3.8:** The triplet ground state wavefunction for  $J_z = +1$  as a function of the longitudinal momentum fraction  $x$  and the transverse momentum  $k_{\perp}$ , omitting the dependence on the angle  $\varphi$ . The calculation was done with  $\alpha = 0.3$ ,  $\Lambda = 1.0 m_f$ ,  $N_1 = 41$ ,  $N_2 = 11$ . Shown are: (a)  $(\uparrow\uparrow)$ -component, (b)  $(\uparrow\downarrow)$ -component, (c)  $(\downarrow\uparrow)$ -component, (d)  $(\downarrow\downarrow)$ -component.

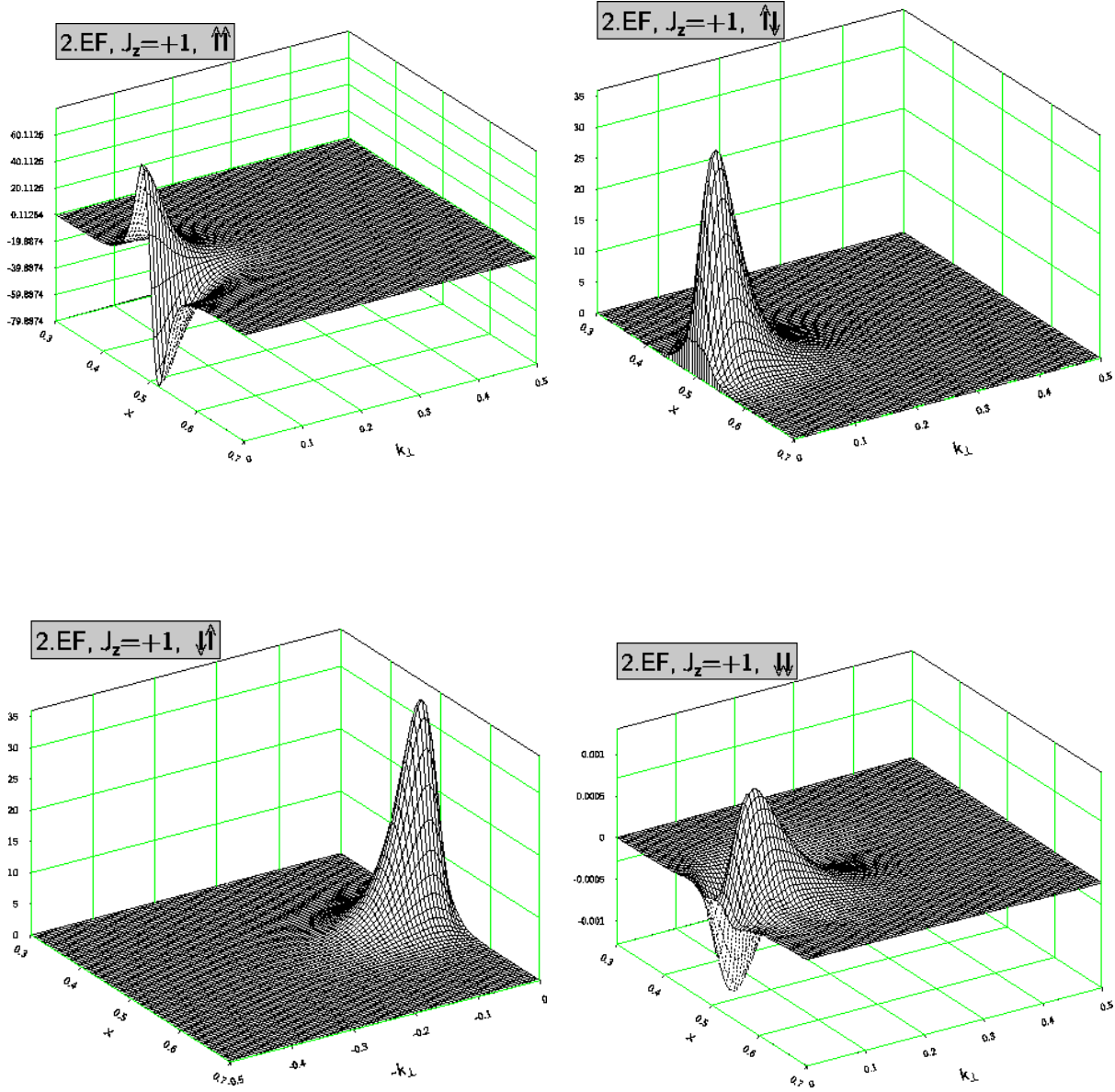


**Figure 3.9:** The  $2^3P_1$  wavefunction for  $J_z = +1$  as a function of the longitudinal momentum fraction  $x$  and the transverse momentum  $k_\perp$ , omitting the dependence on the angle  $\varphi$ . The calculation was done with  $\alpha = 0.3, \Lambda = 1.0 m_f, N_1 = 41, N_2 = 11$ . Shown are: (a) ( $\uparrow\uparrow$ )-component, (b) ( $\uparrow\downarrow$ )-component, (c) ( $\downarrow\uparrow$ )-component, (d) ( $\downarrow\downarrow$ )-component.

### 3.4. Wavefunctions

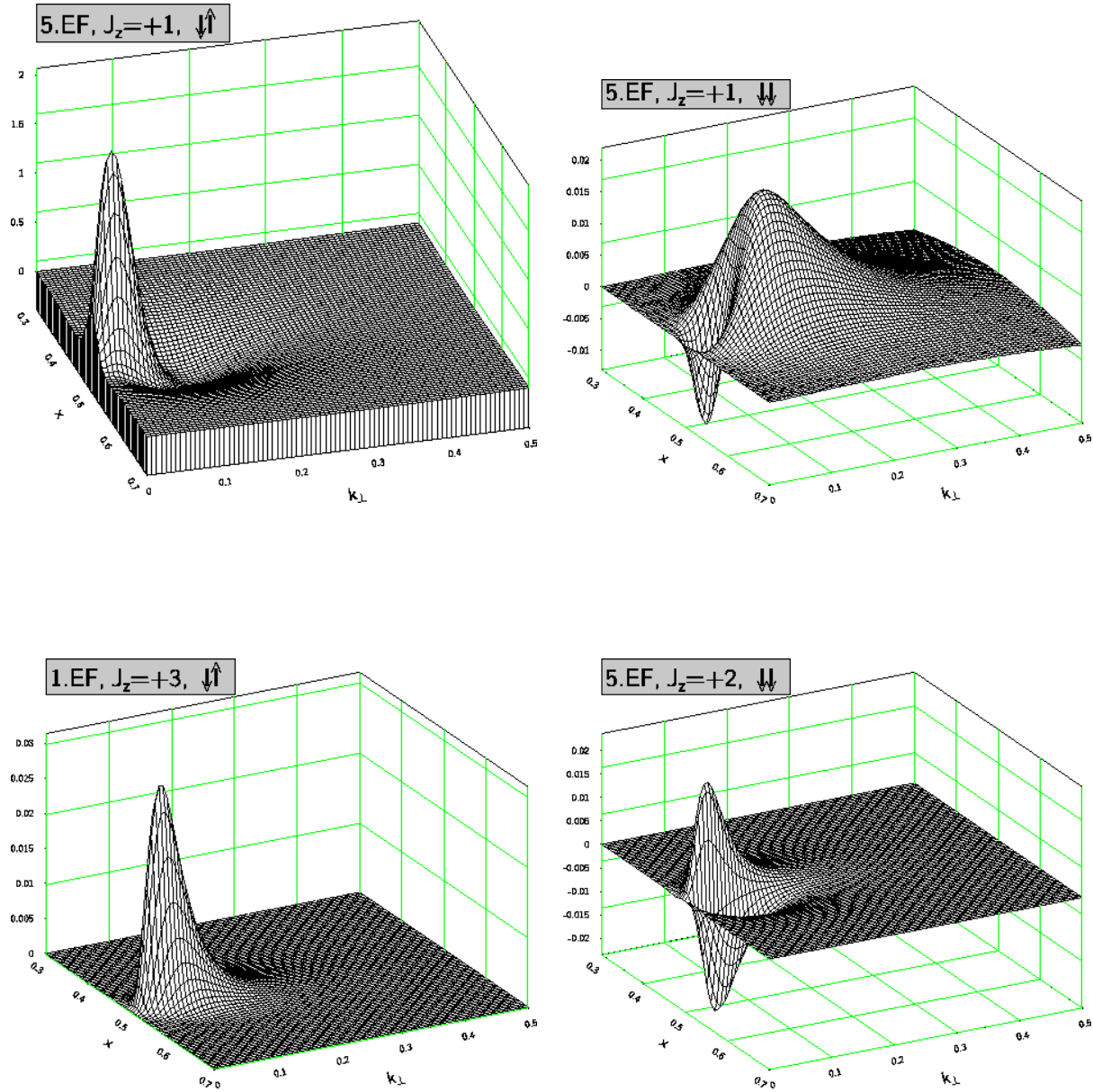


**Figure 3.10:** Components of wavefunctions for larger values of  $J_z$  as a function of the longitudinal momentum fraction  $x$  and the transverse momentum  $k_{\perp}$ , omitting the dependence on the angle  $\varphi$ . The calculation was done with  $\alpha = 0.3, \Lambda = 1.0 m_f, N_1 = 41, N_2 = 11$ . Shown are: (a)  $(\uparrow\uparrow)$ -component of  $2^3S_1$ , (b)  $(\downarrow\downarrow)$ -component of  $2^3S_1$ , (c)  $(\uparrow\downarrow)$ -component of  $3^3D_3$ , (d)  $(\downarrow\downarrow)$ -component of  $3^1D_2$ .



# Chapter 4

## The annihilation channel

### 4.1 Introduction

So far, we have considered an effective Fock space, consisting of two sectors  $|e\bar{e}\rangle$  and  $|e\bar{e}\gamma\rangle$ . We shall justify the absence of any higher<sup>1</sup> Fock state in Chapter 5 from the structure of the applied formalism of effective interactions. The general formalism [20] is set up for a non-abelian  $SU(N)$  gauge theory. Unlike QED, the one boson state is absent in these theories because of color neutrality. Nevertheless, one has to take care of the one photon state  $|\gamma\rangle$  in QED, and the proceeding to include it is as follows.

Firstly, it is important to notice not only the differences between the QED Table (4.1) and the analogous QCD table in [20, Fig. 1], but also the similarities. Some of the graphs occurring in the QCD case are absent in QED, in particular those graphs with a three- or four-boson interaction and the instantaneous interactions connecting four bosons. But, although an additional sector occurs as a first row and a first column in the QED table, neither is a change in the higher Fock sectors observed, nor is the ordering altered in any way.

In addition to Eqs. (2.2) and (2.3), the  $N$ -space (*i.e.* the sector containing the  $|\gamma\rangle$  states) is added to the system. The corresponding projector is

$$\hat{N} := \sum_{\text{all } n_{\text{QN}}} |(\gamma)_n\rangle\langle(\gamma)_n|.$$

The whole procedure of subsequent projections of higher Fock states onto the remaining Hilbert space of states can be carried out like before until one arrives at a  $(2 \times 2)$  matrix analogous to (2.4), but operating in the  $N$ - and  $P$ -space rather than in the  $P$ - and  $Q$ -space

$$H_{\text{LC}} \psi = \begin{pmatrix} H_{NN} & H_{NP} \\ H_{PN} & H_{PP} \end{pmatrix} \begin{pmatrix} \psi_\gamma \\ \psi_{e\bar{e}} \end{pmatrix} = \omega \begin{pmatrix} \psi_\gamma \\ \psi_{e\bar{e}} \end{pmatrix}. \quad (4.1)$$

From Table (4.1) one can read off the interaction of the one photon state with all other sectors: the vertex interaction annihilates the photon into an electron-positron pair

---

<sup>1</sup>Or rather the substitution of effects of higher Fock sectors with the use of *effective* matrix elements in the remaining sectors. “Higher” here in the sense of ascending  $n$  in Table (4.1).

## 4.1. Introduction

Sector	$n$	0	1	2	3	4	5	6	7	8	9	10	11	12	13
$ \gamma\rangle$	0	•	V	•	F	•	•	•	•	•	•	•	•	•	•
$ e\bar{e}\rangle$	1	V	•	S	V	F	•	F	•	•	•	•	•	•	•
$ \gamma\gamma\rangle$	2	•	S	•	V	•	V	F	•	•	•	•	•	•	•
$ e\bar{e}\gamma\rangle$	3	F	V	V	•	V	S	V	F	•	•	•	•	•	•
$ e\bar{e}e\bar{e}\rangle$	4	•	F	•	V	•	•	S	V	F	•	•	F	•	•
$ \gamma\gamma\gamma\rangle$	5	•	•	V	S	•	•	V	•	•	V	F	•	•	•
$ e\bar{e}\gamma\gamma\rangle$	6	•	F	F	V	S	V	•	V	•	S	V	F	•	•
$ e\bar{e}e\bar{e}\gamma\rangle$	7	•	•	•	F	V	•	V	•	V	•	S	V	F	•
$ e\bar{e}e\bar{e}e\bar{e}\rangle$	8	•	•	•	•	F	•	•	V	•	•	•	S	V	F
$ \gamma\gamma\gamma\gamma\rangle$	9	•	•	•	•	•	V	S	•	•	•	V	•	•	•
$ e\bar{e}\gamma\gamma\gamma\rangle$	10	•	•	•	•	•	F	V	S	•	V	•	V	•	•
$ e\bar{e}e\bar{e}\gamma\gamma\rangle$	11	•	•	•	•	F	•	F	V	S	•	V	•	V	•
$ e\bar{e}e\bar{e}e\bar{e}\gamma\rangle$	12	•	•	•	•	•	•	•	F	V	•	•	V	•	V
$ e\bar{e}e\bar{e}e\bar{e}e\bar{e}\rangle$	13	•	•	•	•	•	•	•	•	F	•	•	•	V	•

**Figure 4.1:** The Hamiltonian matrix for QED. The sectors  $n$  are numbered starting at zero. The vertex, seagull and fork interactions are denoted by V, S, F respectively. Diagonal matrix elements are symbolized by •. This table is courtesy of H.-C. PAULI.

and a fork interaction scatters it into the sector  $|e\bar{e}\gamma\rangle$ . The latter interaction is already contained in the effective interaction Eq. (4.1) because of the projection of the  $Q$ -space.

Although we always projected the higher Fock sectors onto the lower ones up to now, one is, of course, free to project the (lower)  $|\gamma\rangle$ -sector onto the (higher)  $|e\bar{e}\rangle$ -sector, and obtains

$$H_{\text{eff}}(\omega) = H_{PP} + H_{PN} \frac{1}{\omega - H_{NN}} H_{NP} + H_{PQ} \frac{1}{\omega - H_{QQ}} H_{QP}$$

Of course we do this for convenience; we could just as well solve the eigenvalue problem of Eq. (4.1). The projection is depicted in two graphs. One is the *dynamic annihilation graph*, Fig. (4.2), the other is the corresponding *seagull annihilation graph*,

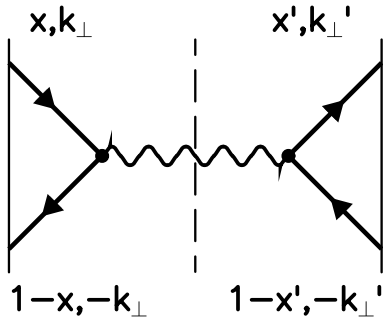


**Figure 4.2:** The dynamical annihilation graph.

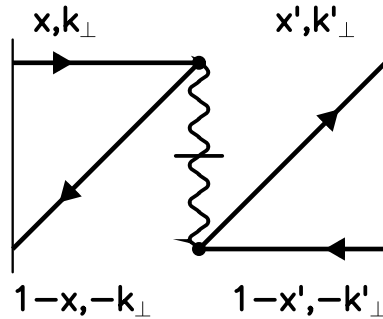


**Figure 4.3:** The seagull graph of the annihilation channel.

Fig. (4.3). The latter is a  $P$ -space graph and was absent before because of the gauge principle of TANG.

## 4.2 Calculation of the matrix elements

The calculation is straightforward. The matrix elements of the canonical Hamiltonian are given in Appendix C. Up to now, we had to consider merely the first type of vertex interaction, cf. Table (C.1), where a photon is irradiated from a fermion. Now the other graph must be evaluated. The calculation of the graphs [Fig. (4.2)–(4.3)] is performed in the ( $J_z=0$ ) and ( $J_z=\pm 1$ ) sectors. The graph is absent in all other sectors because of the helicity of the photon: no angular momentum larger than  $J = 1$  is possible. The functions derived depend on the light-cone momenta ( $x, \vec{k}_\perp$ ). They are given in Table (F.3) and have to be added to those of Table (F.2). The energy denominator in the one photon sector is simple because the photon has zero mass:

$$G(\omega) = \frac{1}{\omega - H_\gamma} = \frac{1}{T^*}, \quad (4.2)$$

where we used the definition (2.10). Note that this denominator does *not* depend on the directions of the vectors  $\vec{k}_\perp, \vec{k}'_\perp$ , *i.e.* on the angles  $\varphi, \varphi'$ .

The calculation of the dynamic annihilation graph follows the steps described in Appendix D. We mention only some aspects here. The transversal photon momentum vanishes:

$$\vec{k}_{\perp\gamma} = \vec{k}_{\perp e} + \vec{k}_{\perp \bar{e}} = 0,$$

and the longitudinal momentum  $x_\gamma$  is unity. Consequently, all expressions of the form

$$\frac{\vec{k}_{1\perp}}{x_1} \equiv 0$$

vanish and  $1/\sqrt{x_1} \equiv 1$  becomes trivial. The matrix elements of the vertex interaction  $V_{g \rightarrow q\bar{q}}$  [Table (C.2)], split up into their three components with different helicity factors, are

$$\begin{aligned} \langle e\bar{e}|V_A|\gamma\rangle &= -m\sqrt{\beta} \left( \frac{1}{x} + \frac{1}{1-x} \right) \times \delta_{+\lambda_2}^{+\lambda_1} \delta_{+\lambda_3}^{+\lambda_1}, \\ \langle e\bar{e}|V_B|\gamma\rangle &= -\sqrt{\beta} \frac{k_\perp}{1-x} e^{+i\lambda_2\varphi} \times \delta_{+\lambda_2}^{+\lambda_1} \delta_{-\lambda_3}^{+\lambda_1}, \\ \langle e\bar{e}|V_C|\gamma\rangle &= \sqrt{\beta} \frac{k_\perp}{x} e^{-i\lambda_2\varphi} \times \delta_{-\lambda_2}^{+\lambda_1} \delta_{+\lambda_3}^{+\lambda_1}. \end{aligned}$$

The complete matrix elements are obtained by symmetry, since  $\langle e\bar{e}|V_i|\gamma\rangle = \langle \gamma|V_i|e\bar{e}\rangle^*$ . To substitute the angles, we multiply the functions  $\langle e\bar{e}|V_i|\gamma\rangle G(\omega) \langle \gamma|V_j|e\bar{e}\rangle$  by

$$e^{-i(L_z\varphi - L'_z\varphi')} \quad (4.3)$$

## 4.2. Calculation of the matrix elements

final : initial	$(\lambda'_1, \lambda'_2) = \uparrow\uparrow$	$(\lambda'_1, \lambda'_2) = \uparrow\downarrow$	$(\lambda'_1, \lambda'_2) = \downarrow\uparrow$	$(\lambda'_1, \lambda'_2) = \downarrow\downarrow$
$(\lambda_1, \lambda_2) = \uparrow\uparrow$	$W_{AA}$	$W_{AB}$	$W_{AC}$	0
$(\lambda_1, \lambda_2) = \uparrow\downarrow$	$W_{BA}$	$W_{BB}$	$W_{BC}$	0
$(\lambda_1, \lambda_2) = \downarrow\uparrow$	$W_{CA}$	$W_{CB}$	$W_{CC}$	0
$(\lambda_1, \lambda_2) = \downarrow\downarrow$	0	0	0	0

**Table 4.1:** Symbolic helicity table for the dynamic annihilation graph. The functions  $W_{ii}$  are identical with the expressions  $F_i$  listed in Table (F.3). Here, terms proportional to  $\delta_{|J_z|,0}$  are omitted.

following Eq. (3.6) and integrate over  $\varphi$  and  $\varphi'$ . It turns out that because of the simple energy denominator (4.2), the only dependence on the angles comes from the factor (4.3) and is proportional to  $\cos\{\varphi - \varphi'\}$  or  $\sin\{\varphi - \varphi'\}$ . As a result, all matrix elements of the *dynamic* annihilation graph for  $J_z=0$  vanish when integrated over the angles. Only for  $J_z = \pm 1$  do some of the matrix elements survive the integration.

Because of the combination of matrix elements with the factor (4.3), two types of functions emerge for  $J_z = \pm 1$ : one is independent of the angles, the other has a dependence proportional to  $\exp\{\pm 2i(\varphi - \varphi')\}$ . The latter vanishes after angular integration. The helicity table (4.1) is given to illustrate the helicity dependencies. It holds for  $J_z = +1$ . The analogous table for  $J_z = -1$  is obtained by the operation

$$W_{ij}(J_z=+1; \lambda_1, \lambda_2) = -\lambda_1 W_{ij}(J_z=-1; -\lambda_1, -\lambda_2).$$

The simple kinematics ( $x_e + x_{\bar{e}} = 1$ ) of the seagull annihilation graph, Fig.(4.3), result in a constant contribution of this graph to the Hamiltonian matrix. It is

$$\langle e\bar{e}|S|e\bar{e}\rangle = -2\beta\delta_{-\lambda_1}^{+\lambda_2}\delta_{-\lambda'_1}^{+\lambda'_2}. \quad (4.4)$$

Because of its helicity factors, the graph acts only between states with

$$S_z = S'_z = 0. \quad (4.5)$$

This means that the seagull graph does not contribute when  $J_z \neq 0$  because it has a factor proportional to  $(\varphi - \varphi')$  resulting from (4.5). A rather surprising consequence is that the dynamic graph is the only annihilation channel contribution in the  $J_z = \pm 1$  sector, whereas in the  $J_z = 0$  sector the instantaneous graph is the only one. This is necessary for rotational invariance: both diagrams must yield the same value, though one shows much more structure than the other, since degeneracy of the orthopositronium ground state with respect to  $J_z$  is found without the annihilation channel and inclusion must not destroy it.

At first glance, there seems to be a manifest breaking of rotational symmetry: the helicity table (4.1) separates between states with  $(\lambda_1, \lambda_2) = (\uparrow\uparrow)$  and  $(\lambda_1, \lambda_2) = (\downarrow\downarrow)$ . But this is only a consequence of the integration over the angles: for  $J_z = +1$  the  $(\downarrow\downarrow)$ -combination gives no contribution, and likewise does the  $(\uparrow\uparrow)$ -combination for  $J_z = -1$ .

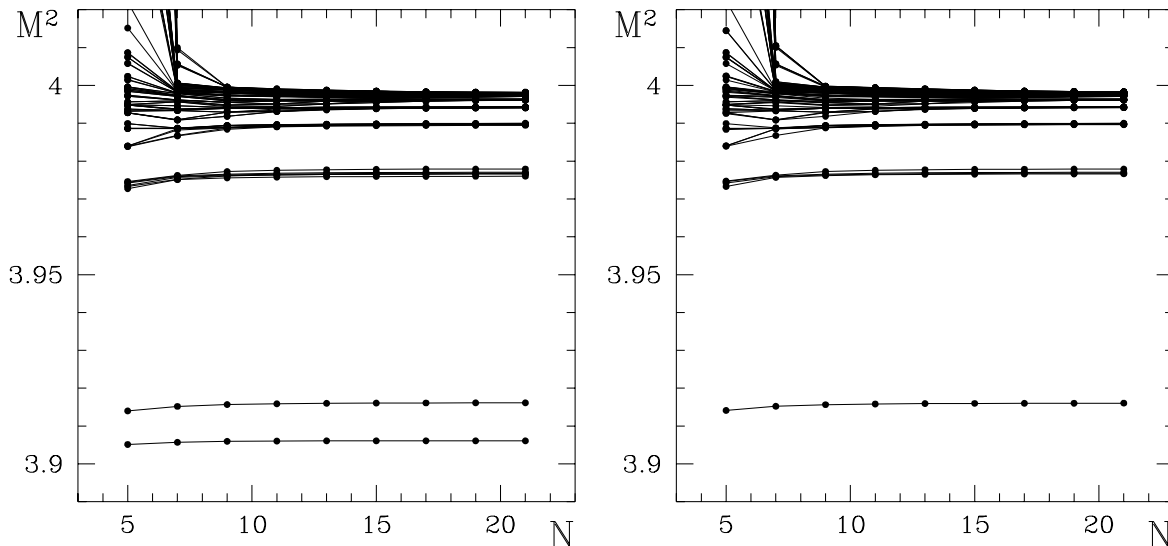


**Figure 4.4:** The positronium spectrum including the annihilation channel: (a)  $J_z=0$  sector, (b)  $J_z=+1$  sector. Parameters of the calculation:  $\alpha = 0.3, \Lambda = 1.0 m_f$ . The mass squared eigenvalues  $M_n^2$  in units of the electron mass  $m_f^2$  are shown as functions of the number of integration points  $N \equiv N_1 = N_2$ . The triplet states, especially  $1^3S_1$ , are lifted up, the singlet mass eigenvalues are the same as without annihilation channel. Cf. (2.6) and Table (4.3).

### 4.3 Spectrum including the annihilation channel

The spectrum including the annihilation channel shows the expected properties: the singlet eigenvalues remain unchanged, only the triplet states do change at all. An essential point in the actual calculations is that one has to use the same counterterms for the Coulomb singularity as used *without* the annihilation channel. This is due to the fact that the one photon annihilation part of the interaction has no additional singularity that needs to be taken care of numerically, because of the simple energy denominator (4.2). We compiled our results in the form of binding coefficients in Table (4.3). We have used there, contrary to previous chapters, the bracket convention for the errors to suppress the zeros.

One notes a slightly larger breaking of rotational symmetry. The triplet ground states of different  $J_z$  are still approximately degenerate, but the discrepancy is bigger than without the annihilation channel. The dependence of these discrepancies between corresponding eigenvalues for  $J_z=0$  and  $J_z=1$  on the number of integration points is shown in Fig. (4.5). The behavior of the curves is similar to those of the calculations without annihilation channel, Fig. (3.5). An additional plot, Fig. (4.5), shows the dependence of the rotational symmetry breaking on the cutoff  $\Lambda$ . The discrepancies of corresponding eigenvalues are almost independent of the cutoff  $\Lambda$ .

To make a comparison of our results to those of perturbation theory easier, we show in Fig (4.7) the eigenvalues for a principal quantum number  $n=2$  for both theories graphically. The structure of the two plots is almost the same, only the  $2^1S_0$  state and the  $2^3P_0$  state are exchanged in our results. This is due to the cutoff dependence of

#### 4.4. Parameter dependence of the spectrum

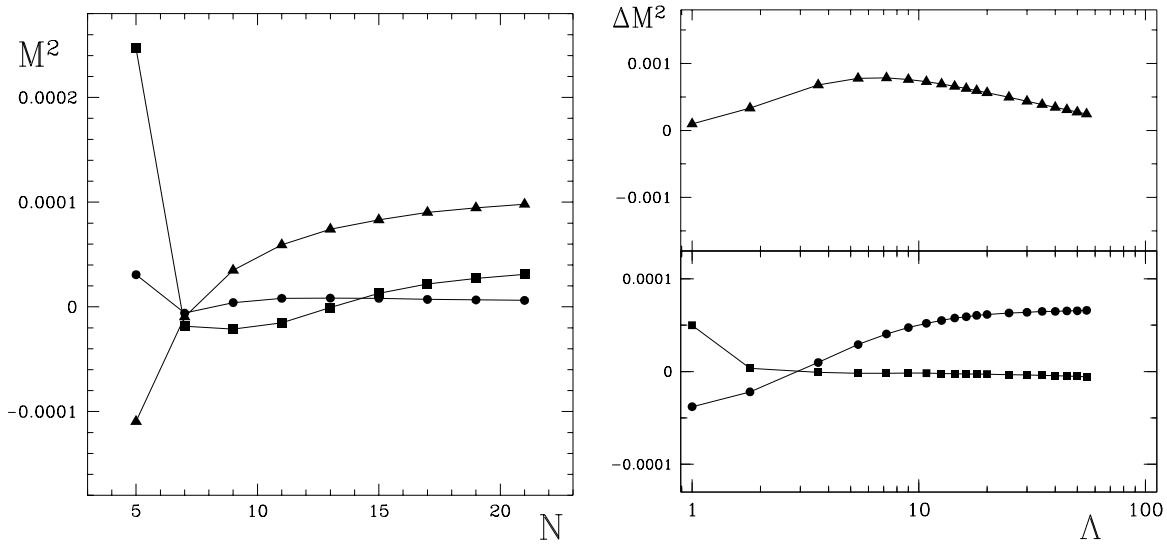


**Figure 4.5:** Deviation of corresponding eigenvalues for  $J_z = 0$  and  $J_z = 1$  including the annihilation channel ( $\alpha = 0.3, \Lambda = 1.0 m_f$ ): (a) as a function of the number of integration points  $N$ , (b) as a function of the cutoff  $\Lambda$ . The graphs show  $\Delta M^2 := M_n^2(J_z = 0) - M_n^2(J_z = 1)$  for the states  $1^3S_1$  ( $\Delta$ ),  $2^3P_1$  ( $\square$ ), and  $2^1P_1$  ( $\circ$ ).

the S-state, which is larger than that of the other states (cf. Fig. (4.6)(b) and next paragraph). We stress that the results of the perturbative calculations change considerably, when the next higher order in  $\alpha$  is considered. For example, the mass squared of the triplet  $2^3S_1$  is, according to FULTON and MARTIN [79],  $M^2(2^3S_1) = 3.9780186070$  up to order  $\alpha^3 Ry$ , which is nearer to our result than the value of perturbative calculations up to order  $\mathcal{O}(\alpha^4)$  as displayed in Fig. (4.7).

#### 4.4 Parameter dependence of the spectrum

The convergence of the eigenvalues with growing number of integration points  $N$  is the same as the case of no annihilation channel. To be explicit, the convergence of the eigenvalues can be shown to be exponential. One can fit the singlet ground state eigenvalue excellently with the function

$$M^2(N) = M^2(21) - [M^2(21) - M^2(5)] e^{-(N-5)/2.2}.$$

We did not perform the limit  $N \rightarrow \infty$ , because the accuracy of the results for  $N > 20$  suffices to compare to other data.

The cutoff dependence of the positronium spectrum including the annihilation channel is comparable to that of the spectrum without it. However, a striking difference occurs: the inclusion of the annihilation channel stabilizes the cutoff dependence of the eigenstates. In particular, the triplet ground state in Fig. (4.6)(a) shows only a small dependence on the cutoff, when one compares it to the behavior of the same state in Fig. (2.8). One can fit these curves with a polynomial in  $\log \Lambda$ . The singlet ground

Cutoff: $\Lambda$	$B_s$	$B_t$	$C_{hf}$
1.8	1.16373904	0.96234775	0.55942025
3.6	1.25570163	0.96446614	0.80898748
5.4	1.29978067	0.96482118	0.93044303
7.2	1.32941926	0.96541695	1.01111752
9.0	1.35224000	0.96603457	1.07279285
10.8	1.37112216	0.96661006	1.12364471
12.6	1.38744792	0.96713137	1.16754595
14.4	1.40198469	0.96760110	1.20662108
16.2	1.41520247	0.96802548	1.24215830
18.0	1.42740143	0.96841025	1.27497551
ETPT	1.11812500	0.90812500	0.58333333
$\mathcal{O}(\alpha^6 \ln \alpha)$			0.48792985

**Table 4.2:** The binding coefficients of the singlet ( $B_s$ ), the triplet ( $B_t$ ), and the hyperfine coefficient  $C_{hf}$  are listed for  $\alpha = 0.3$ ,  $N_1 = 41$ ,  $N_2 = 11$ .

state eigenvalues are the same as without the annihilation graph and for the triplet one obtains

$$M_{triplet}^2(\Lambda) \simeq 3.91392 - 0.000288079 \log \Lambda + 0.000147268 \log^2 \Lambda.$$

Comparison with Eq. (2.16) shows that the decrease of the triplet with  $\log \Lambda$  is suppressed by including the annihilation channel by a factor of 60. Also the excited states,  $n=2$ , show a different behavior, as compared to Fig. (2.8). Here, only one state shows level crossing as  $\Lambda$  grows large. The eigenvalue of the  $2^3P_1$  state, however, depends only weakly on the cutoff here.

The values for the binding coefficients  $B_n$  and the coefficient of the hyperfine splitting  $C_{hf}$  are presented in Table (4.2). The values are correct for a cutoff  $\Lambda \simeq 2m_f$  when compared to results of perturbation theory up to  $\mathcal{O}(\alpha^4)$ . However, the effects of higher order correction to perturbative calculations are significant for a large coupling such as  $\alpha = 0.3$ . The result of perturbation theory to  $\mathcal{O}(\alpha^6 \ln \alpha)$  for the coefficient  $C_{hf}$  is considerably smaller than that to order  $\mathcal{O}(\alpha^4)$ .

Concluding, we state that the cutoff dependence of the spectrum is improved as compared with the case of missing annihilation channel. This makes it evident that the annihilation channel is a necessary part of the theory.

As a last investigation of the properties of our model, we will vary the coupling constant and interpret the spectrum. A similar procedure was performed by DYKSHOORN ET AL. [80], who studied coupled integral equations for QED-bound states in equal-time quantization with a variational ansatz. They calculate masses for the lowest eigenstates of positronium with and without the annihilation channel and plot them versus the coupling constant. The prominent feature of their figures is the occurrence of

#### 4.4. Parameter dependence of the spectrum

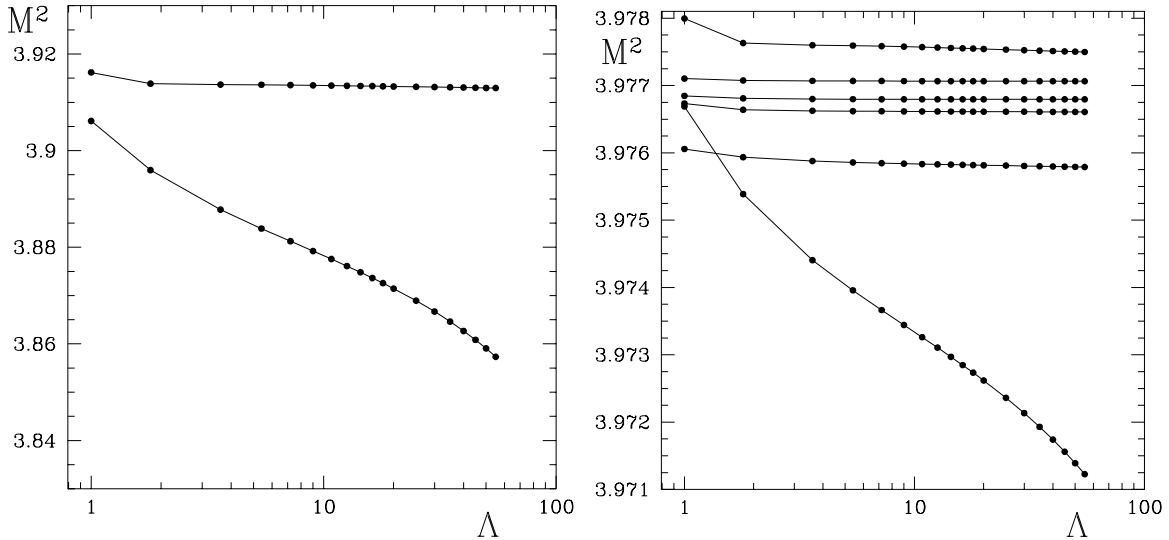


**Figure 4.6:** The spectrum with annihilation channel as a function of the cutoff  $\Lambda$ : (a) ground states ( $n=1$ ), (b) first radial excited states ( $n=2$ ). The parameters for the calculation are  $\alpha = 0.3$ ,  $J_z = 0$ ,  $N_1 = 25$ ,  $N_2 = 21$ . One notices a better behavior of the curves with growing  $\Lambda$  compared to Figs. (2.8) and (2.9): the decrease of the eigenvalues is smaller, especially for the ground state triplet  $1^3S_1$ . Moreover, there are no level crossings for  $n=2$ , except the crossing of the singlet S-state at  $\Lambda = 1.5$  (not visible in this plot).

a critical coupling at which the masses become smaller than zero. We have performed the analogous calculations within our approach. It seems at first glance [Fig. (4.9)(a)] as if the eigenvalues, after decreasing quadratically with the coupling as expected by perturbation theory, stabilize at a coupling  $\alpha \simeq 1.5$ . However, further investigation shows that this is merely an effect of the cutoff dependence of the spectrum. The eigenvalues in Fig. (4.9)(a) were calculated with a cutoff  $\Lambda = 1.0 m_f$ , which is too small for an coupling constant of  $\alpha = 1.0$ , since then the Bohr momentum is of the same order as the cutoff. Fig. (4.9)(b) shows clearly that there is a critical coupling. The masses calculated with a cutoff of  $\Lambda = 20 m_f$  tend to zero at  $\alpha \simeq 0.5$ . A similar value was found in [80, Ref. 2].



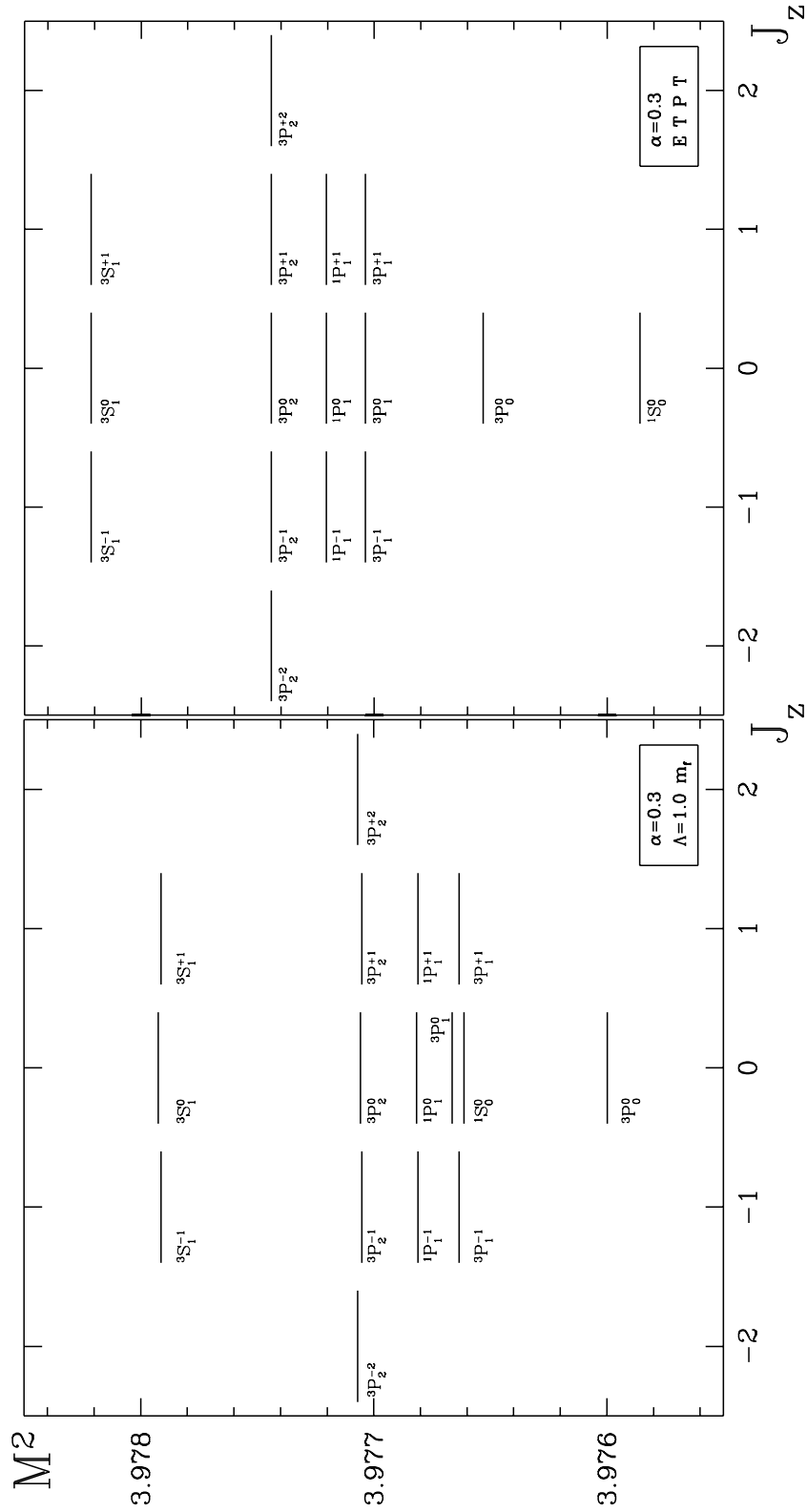


**Figure 4.7:** Comparison of multiplets for  $n=2$ : (a) results of the present work with  $\alpha = 0.3$ ,  $\Lambda = 1.0 m_f$ ,  $N_1 = N_2 = 21$ ; (b) equal-time perturbation theory (ETPT) up to order  $\mathcal{O}(\alpha^4)$ .

#### 4.4. Parameter dependence of the spectrum

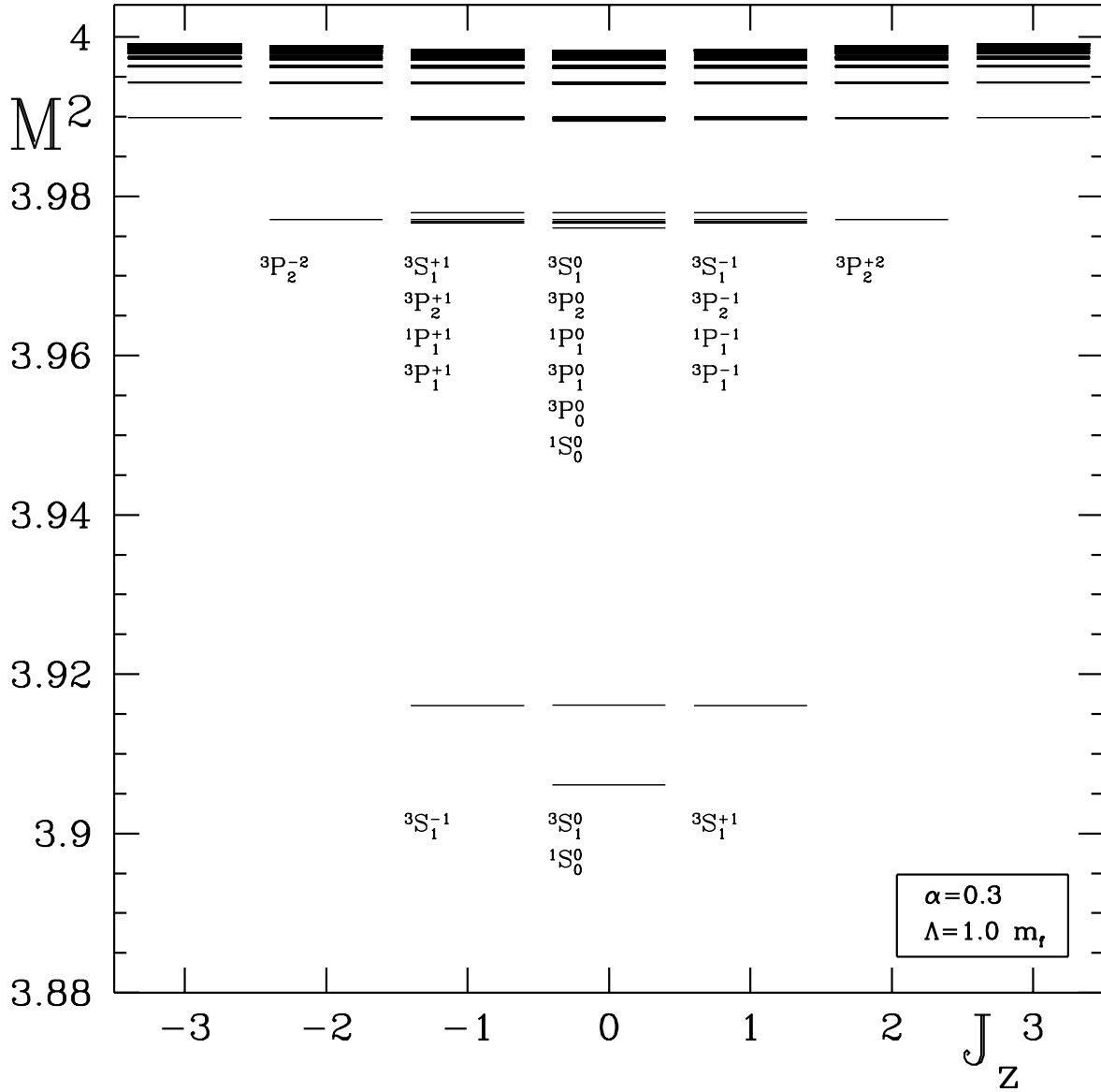


**Figure 4.8:** Compiled spectra of positronium with different  $J_z = -3, -2, \dots, +3$  including the annihilation channel. All spectra have been calculated with  $\alpha = 0.3$ ,  $\Lambda = 1.0 m_f$ ,  $N_1 = N_2 = 21$ . The mass squared eigenvalues  $M_n^2$  in units of the electron mass  $m_f^2$  are shown. The notation for the states is  $^{3S+1}L_J^{J_z}$ . The resolution of the plot is inadequate for the multiplets. Nevertheless, the numerical degeneracy of the three triplet ground states  $^3S_1^{-1}$ ,  $^3S_1^0$ , and  $^3S_1^{+1}$  becomes very clear.

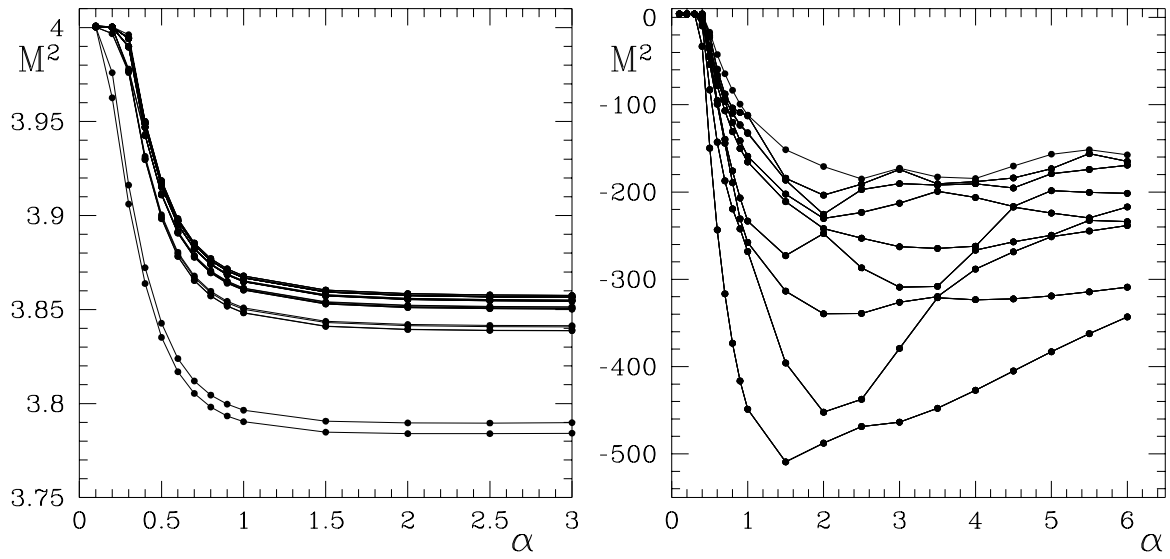


**Figure 4.9:** The spectrum as a function of the coupling constant: (a)  $\Lambda = 1.0 m_f$ , (b)  $\Lambda = 20.0 m_f$ . In (a), the eigenvalues seem to converge to a stable value as  $\alpha$  grows large. However, this is just an effect of the cutoff dependence of the spectrum: for a larger cutoff  $\Lambda = 20 m_f$ , (b), the eigenvalues become negative at a critical coupling  $\alpha_c \simeq 0.5$ .

#### 4.4. Parameter dependence of the spectrum

---

$n$	Term	$B_n(J_z=0)$	$B_n(J_z=+1)$	$\Delta B_n$
1	$1^1S_0$	1.049552(17)	—	—
2	$1^3S_1$	0.936800(189)	0.937902(151)	-0.001102
3	$2^1S_0$	0.260237(169)	—	—
4	$2^3S_1$	0.255292(184)	0.255359(179)	-0.000067
5	$2^1P_1$	0.257969(160)	0.258037(168)	-0.000068
6	$2^1P_1$	0.267090(160)	—	—
7	$2^3P_1$	0.259667(206)	0.260013(163)	-0.000346
8	$2^3P_2$	0.245615(239)	0.245755(228)	-0.000140
9	$3^1S_0$	0.115206(314)	—	—
10	$3^3S_1$	0.113434(156)	0.113497(179)	-0.000063
11	$3^1P_1$	0.114490(269)	0.114521(283)	-0.000032
12	$3^1P_1$	0.117142(272)	—	—
13	$3^3P_1$	0.115127(326)	0.115102(275)	0.000025
14	$3^3P_2$	0.113731(284)	0.113753(283)	-0.000023
15	$3^1D_2$	0.112816(150)	0.112842(158)	-0.000027
16	$3^3D_1$	0.112977(161)	0.112987(164)	-0.000010
17	$3^3D_2$	0.112520(158)	0.112524(160)	-0.000004
18	$3^3D_3$	0.111027(377)	0.111072(373)	-0.000045
19	$4^1S_0$	0.065490(588)	—	—
20	$4^3S_1$	0.064707(480)	0.064723(481)	-0.000016
21	$4^1P_1$	0.065003(467)	0.065061(486)	-0.000059
22	$4^1P_1$	0.066119(470)	—	—
23	$4^3P_1$	0.065331(487)	0.065276(475)	0.000055
24	$4^3P_2$	0.064265(309)	0.064372(348)	-0.000107
25	$4^1D_2$	0.063968(430)	0.064041(363)	-0.000073
26	$4^3D_1$	0.064099(319)	0.064090(325)	0.000009
27	$4^3D_2$	0.063870(391)	0.063881(477)	-0.000011
28	$4^3D_3$	0.063788(387)	0.063807(381)	-0.000019
29	$4^1F_3$	0.063141(96)	0.063112(104)	0.000030
30	$4^3F_2$	0.063299(112)	0.063233(116)	0.000065
31	$4^3F_3$	0.063234(119)	0.063209(119)	0.000024
32	$4^3F_4$	0.063103(104)	0.063422(158)	-0.000319
33	$5^1S_0$	0.043253(806)	—	—
34	$5^3S_1$	0.043046(682)	0.042912(739)	0.000134
35	$5^1P_1$	0.043412(1100)	0.042724(853)	0.000688

**Table 4.3:** The positronium spectrum for  $\alpha = 0.3$ ,  $\Lambda = 1.0 m_f$ ,  $N_1 = N_2 = 21$ . The non-relativistic notation for the terms and the eigenvalues for  $J_z=0$  and  $J_z=+1$  including the annihilation channel are shown. The discrepancy between the eigenvalues is  $\Delta B_n := B_n(J_z=0) - B_n(J_z=+1)$ . The numerical errors are estimated from the difference between the values for maximum and next to maximum number of integration points. The actual errors are smaller due to the exponential convergence of the eigenvalues with  $N$ . The  $k$  numbers in brackets are the errors in the last  $k$  digits.

# Chapter 5

## On the theory of effective interactions

### 5.1 Introduction

The aim of this chapter is to show that fixing the redundant parameter  $\omega$  to the expression (2.10) is *not* an ad hoc assumption, but a consequence of the structure of the theory and of the projection method used. The material presented here follows the line of arguments given in [20], where the method of iterated resolvents was introduced and applied to QCD. The case of QED is discussed in this section.

To understand the following, it is helpful to review the reasoning presented in Chapter 2 and to see things in a more general way. In the description of the positronium model it was pointed out that the unrestricted Fock space can be divided *arbitrarily* into two parts, one called the  $P$ - the other the  $Q$ -space. Since only two Fock sectors ( $|e\bar{e}\rangle, |e\bar{e}\gamma\rangle$ ) were used in the model, it was clear how this separation had to be done.

TAMM [67] and DANCOFF [68] used this method in a different context in the following way. First, they truncated the Fock space to two sectors. Second, they projected one Fock sector onto the other. Third, the emerging energy denominator is *modified* to simplify the calculations. The so-defined procedure fails completely in front form dynamics [24] if the third step is missing. A severe (collinear) singularity occurs that cannot be treated within this approach. TAMM did not recognize this problem, because he considered the modification of the energy denominator rather as a simplification than as an approximation for the effects of the omitted higher Fock states.

What was done in Eq. (2.5) was to introduce a new, redundant parameter  $\omega$  for the *a priori* unknown mass (squared) eigenvalue  $M_n^2$ . This parameter is free and can be fixed on an *ad hoc* basis to remove the collinear singularity. It will be shown that this fixing, Eq. (2.10), is not only the natural choice for this parameter, but that it is a consequence of the structure of the formalism.

## 5.2 The method of iterated resolvents

The essential cause for the failure of a “naive” Tamm-Dancoff approach is the fact that the Fock space truncation is performed too early in the formalism. Because of this, one throws away all possible interactions with the omitted sectors. This gives rise to the problems described above. It is therefore necessary to study the structure of the resolvents to all orders and to investigate possible approximation schemes consistent with the solubility of the whole problem.

Of course, one has to construct a finite dimensional Hamiltonian from the Lagrangian density in the style of the Tamm-Dancoff approach. But a truncation cannot be the first step. Rather one introduces unphysical parameters needed to map the Hamiltonian operator onto a *matrix* in such a way that they remain in the formalism until the end. One can then investigate rigorously the behavior of the theory in the limit when all unphysical parameters are removed.

We consider in this chapter the Hamiltonian within the DLCQ formalism, *i.e.* with discretized momenta. This maps the Hamiltonian operator into a matrix with a denumerable number of columns and rows. It may still be an infinite dimensional matrix. In a Fock basis, the Hamiltonian is naturally decomposed into sectors of different particle content, cf. Table (4.1). Each sector by itself contains an infinite number of states, and is regulated by a cutoff  $\Lambda$ , like in Eq. (2.13). The number of Fock sectors, on the other hand, is limited by the finite longitudinal momentum  $P^+$ , or rather by the *harmonic resolution*  $K = \frac{L}{\pi}P^+$ . The finite dimensional eigenvalue problem reads thus:

$$\begin{pmatrix} \langle 0|H|0\rangle & \langle 0|H|1\rangle & \cdots & \langle 0|H|N\rangle \\ \langle 1|H|0\rangle & \langle 1|H|1\rangle & \cdots & \langle 1|H|N\rangle \\ \vdots & \vdots & \ddots & \vdots \\ \langle N|H|0\rangle & \langle N|H|1\rangle & \cdots & \langle N|H|N\rangle \end{pmatrix} \begin{pmatrix} \langle 0|\psi\rangle \\ \langle 1|\psi\rangle \\ \vdots \\ \langle N|\psi\rangle \end{pmatrix} = \omega \begin{pmatrix} \langle 0|\psi\rangle \\ \langle 1|\psi\rangle \\ \vdots \\ \langle N|\psi\rangle \end{pmatrix}. \quad (5.1)$$

Like in Chapter 2, one can reduce the dimension of the Hamiltonian matrix by projecting the “highest” state  $\langle N|\psi\rangle$  onto the others. One arrives at an effective Hamiltonian, depending on the parameter  $\omega$ , due to the resolvent

$$G_n(\omega) := \langle n| \omega - H |n\rangle, \quad 1 \leq n \leq N.$$

In general, one has the eigenvalue problem

$$\sum_{j=0}^n \langle i|H_n(\omega)|j\rangle \langle j|\psi(\omega)\rangle = E(\omega) \langle i|\psi(\omega)\rangle,$$

where the last state can be expressed by all others

$$\langle N|\psi(\omega)\rangle = G_n(\omega) \sum_{j=0}^{n-1} \langle i|H_n(\omega)|j\rangle \langle j|\psi(\omega)\rangle.$$

Consequently, the effective Hamiltonian in the  $(n-1)$ -sector becomes for each matrix element  $\langle i|H_{n-1}(\omega)|j\rangle$

$$H_{n-1}(\omega) = H_n(\omega) + H_n(\omega)G_n(\omega)H_n(\omega), \quad (5.2)$$

which in a sense is a recursion relation.

One has to find a systematic way to express the effective Hamiltonian after the  $i$ -th projection in terms of the bare Hamiltonian  $H$ . If one applies the relation Eq. (5.2) repeatedly, one obtains

$$H_n = H + \sum_{m=n+1}^N H_m G_m H_m, \quad (5.3)$$

with the bare Hamiltonian  $H$ . For example, for  $n = 3$  one gets

$$H_1 = H_3 + H_3 G_3 H_3 + H_2 G_2 H_2. \quad (5.4)$$

by inserting  $H_2 = H_3 + H_3 G_3 H_3$  into  $H_1 = H_2 + H_2 G_2 H_2$ . The general case can be proven by induction. An illustrative example is given in Section 5.4.

In Eq. (5.3), the effective Hamiltonian in Fock sector  $n$  is expressed in terms of the bare Hamiltonian and scatterings into *higher* Fock sectors. It is important to notice that no scattering into lower Fock sectors occurs. From Eq. (5.4) one can infer how the general structure of the expression for the effective Hamiltonian will be. *Chains* of terms with a different number of resolvents will emerge. In fact, it turns out to be much better to classify those chains by the number of its resolvents than, for example, by the order of the coupling constant. If all chains with  $k$  resolvents are collected in  $H^{(k)}$ , the effective Hamiltonian is the sum

$$H_n = H_n^{(0)} + H_n^{(1)} + H_n^{(2)} + \dots \quad (5.5)$$

This expansion is finite, because the bare Hamiltonian is a finite matrix. With this classification scheme, one obtains a recursion relation for the general term by inserting of Eq. (5.5) into Eq. (5.3)

$$H_n^{(k+1)} = \sum_{l>n} \left( H_l^{(0)} G_l H_l^{(k)} + H_l^{(1)} G_l H_l^{(k-1)} + \dots + H_l^{(k-1)} G_l H_l^{(1)} + H_l^{(k)} G_l H_l^{(0)} \right). \quad (5.6)$$

The first terms read

$$\begin{aligned} H_n^{(1)} &= \sum_{l>n} H_l^{(0)} G_l H_l^{(0)} \quad , \\ H_n^{(2)} &= \sum_{l>n} \left( H_l^{(0)} G_l H_l^{(1)} + H_l^{(1)} G_l H_l^{(0)} \right) . \end{aligned}$$

Note the change in the order of the calculation. At first, the rows of the Hamiltonian were projected from  $N$  to 1 unto one another to derive the expression for the effective Hamiltonian in the lowest sector. Now, the calculations are reversed in the sense that the effective Hamiltonian in the lowest sector is evaluated by longer and longer chains of resolvents, until one reaches the dimension of the bare Hamiltonian. The advantage is obvious: one is able to control the limit in which no truncation is made at all, *i.e.*  $N \rightarrow \infty$ .

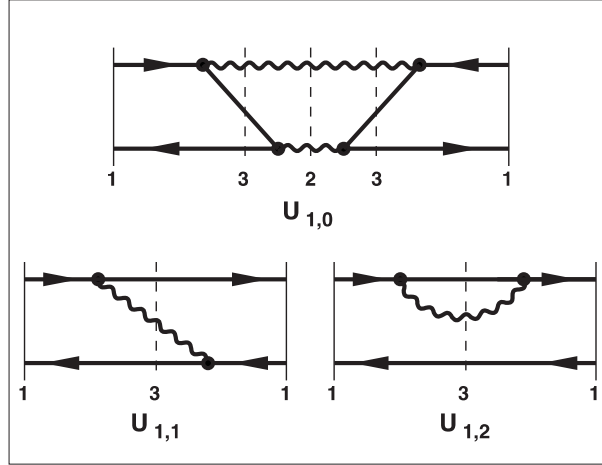


Figure 5.1: The three effective graphs of gauge theories (Courtesy of H.-C. PAULI).

### 5.3 QED treated with iterated resolvents

So far, the general method of how to calculate an effective Hamiltonian out of a finite dimensional Hamiltonian matrix was described. In particular, no assumptions on the matrix elements of the starting Hamiltonian (like the one in Eq. [5.1]) were made. From the structure of the QED Hamiltonian, described in Appendix C and displayed in Table (4.1), it is obvious that most of the matrix elements will be zero, certainly including all those in which the number of partons created or destroyed by the interaction exceeds two. This can clearly lead to significant simplifications. The procedure can be simplified even more by applying a technique of light-cone perturbation theory. There, one takes care of the instantaneous gauge parts of the Hamiltonian, *i.e.* of the *seagulls* and *forks*, only at the end of each calculation by redefining the non-instantaneous propagators [33, Appx. A, Fig. 31]. One adds to the propagators a part containing an instantaneous graph including a  $\theta$ -function for the longitudinal momentum transferred. One can apply the same trick here: one only keeps the *vertex* interaction in the matrix, Table (4.1).

Since we want to calculate mesonic, *i.e.* fermion-antifermion systems, the sector  $|e\bar{e}\rangle$  plays the rôle of a “cornerstone” sector. If one calculates the effective Hamiltonian in this sector one gets

$$H_{q\bar{q}} \equiv H_1 = T_1 + VG_3V + VG_3VG_2VG_3V, \quad (5.7)$$

where  $T_1$  is the kinetic energy in the  $|e\bar{e}\rangle$ -sector. This is an expression with at most three resolvents  $G_j(\omega)$ . The graphs of these fundamental chains are shown in Figure (5.1): the photon exchange graph, the two-photon annihilation graph, and the self energy graph.

It is worth mentioning two things here. Firstly, the resolvents are in general non-diagonal operators. Secondly, a single chain can symbolize more than one graph. For



example, the photon exchange graph and the self energy graph emerge out of the same chain  $VG_3V$ .

The structure of the effective interaction for the  $|e\bar{e}\rangle$  states seems to be very simple. The question arises what the effect of the higher Fock states will be. A first hint can be gained by looking at sectors similar to  $|e\bar{e}\rangle$ , *i.e.* to  $|e\bar{e}\gamma\rangle$ ,  $|e\bar{e}\gamma\gamma\rangle \dots$ ,

$$H_{e\bar{e}\gamma} \equiv H_3 = T_3 + VG_6V + VG_6VG_5VG_6V + VG_4V, \quad (5.8)$$

$$H_{e\bar{e}\gamma\gamma} \equiv H_5 = T_6 + VG_{10}V + VG_{10}VG_9VG_{10}V + VG_7V, \quad (5.9)$$

$$H_{e\bar{e}\gamma\gamma\gamma} \equiv H_{10} = T_{10} + VG_{15}V + VG_{15}VG_{14}VG_{15}V + VG_{11}V. \quad (5.10)$$

The only difference of these expression to Eq. (5.7) is the absence of the last term, the annihilation of a photon into an electron-positron pair. This is because the first sector does not contain a photon.

These sectors seem to be similar to each other. However, they are only a small set in the whole Hamiltonian. Their defining property is that the photons do not interact with the fermion-antifermion system. To classify the sectors, this kind of interactions is named *spectator interaction*  $\bar{U}_n$ . The other class of interactions, where the photons do interact, is called *participant interaction*  $\tilde{U}_n$ . Consequently, the decomposition of the Hamiltonians read

$$H_n = T_n + \bar{U}_n + \tilde{U}_n, \quad n = 3, 6, 10, 15, \dots \quad (5.11)$$

Analogously to Eq. (2.5), where the resolvent was expanded around its diagonal (*i.e.* free) part, the resolvents  $\bar{G}_n$  can be expanded around the part containing the spectator interaction  $\bar{U}_n$

$$\bar{G}_n = \frac{1}{\omega - T_n - \bar{U}_n}. \quad (5.12)$$

The full resolvent is obtained by the infinite series

$$G_n = \bar{G}_n + \bar{G}_n \tilde{U}_n G_n = \bar{G}_n + \bar{G}_n \tilde{U}_n \bar{G}_n + \bar{G}_n \tilde{U}_n \bar{G}_n \tilde{U}_n \bar{G}_n + \dots \quad (5.13)$$

Note that the unperturbed resolvent contains the interaction! Moreover, one observes that in this approach, the system does not leave the sector  $n$ .

Let's repeat what we have achieved up to now. We divided the interaction in one part that acts only between the electron and the positron (spectator interaction) and one part where the photons can interact with the two fermions (participant interaction). We expanded the full resolvent  $G_n$  as an infinite series around the spectator interaction. One can show [20], that the spectator interaction allows for three fundamental graphs only, Fig. (5.1), if one reduces the bare Hamiltonian by subsequent projections to the fermion-antifermion sector. This is the end of the procedure for non-abelian gauge theories. In QED, however, one has an additional sector  $|\gamma\rangle$  responsible for the annihilation diagram, Fig (4.2). The whole spectator interaction resides in the coupling function attached to the vertices.

The question arises, if the spectator interactions in the different sectors are somehow related. Note that the only difference between their diagrams is the different number

### 5.3. QED treated with iterated resolvents

---

of *non-interacting* photons. In fact, this is the crucial point in the formalism. We will give here a *heuristic* explanation, how this can be understood.

Consider the separation of the Fock space into two parts, named  $P$ - and  $Q$ -space, like in Chapter 2. According to the discussion of this chapter, the only interaction in both spaces is the spectator interaction. What does the resolvent look like? It is from Eq. (2.5)

$$G(\omega) := \frac{1}{\omega - H_Q}, \quad (5.14)$$

where  $H_Q = T_Q + V_Q$  is the sector-Hamiltonian of the  $Q$ -space. The redundant parameter  $\omega$  stands for the actual eigenvalue of the whole eigenvalue problem and contains therefore a kinetic and an interaction part

$$\omega = T_{\text{true}} + V_{\text{true}}.$$

The resolvent reads thus

$$G(\omega) = \frac{1}{T_{\text{true}} + V_{\text{true}} - T_Q - V_Q}. \quad (5.15)$$

With the help of two smallness assumptions on the momenta of the photon

$$x_\gamma \ll 1, \quad \text{and} \quad \vec{k}_{\gamma\perp}^2 \ll M_{e\bar{e}}^2. \quad (5.16)$$

it has been shown in [20], that indeed

$$\lim_{N \rightarrow \infty} V_{\text{true}} - V_Q = 0,$$

which is very plausible from what we have stated before: the interactions in the different sectors deviate only by a different number of non-interacting photons. We stress the importance of the continuum limit at this point. If one has a finite number of Fock sectors, the argument does not hold. We obtain finally

$$G(\omega) = \frac{1}{T_{\text{true}} - T_Q} =: \frac{1}{T^*}. \quad (5.17)$$

By this, one has shown that the resolvents are diagonal in the solution if one makes the two smallness assumptions (5.16), which are fully justified within a bound-state formalism. In fact, one makes the surprising observation that the resolvents are totally *independent* of the redundant parameter  $\omega$ . It is clear that this parameter is merely a mathematical tool to perform the calculations in a controlled way.

We recall the result of the plausibility argument in Chapter 2, namely the definition of the energy denominator  $\mathcal{D}$ , Eq. (2.9), together with the analytic expression for  $T^*$ , Eq. (2.10), in the  $|e\bar{e}\gamma\rangle$ -sector. Evaluating Eq. (5.17) in the  $|e\bar{e}\gamma\rangle$ - and  $|e\bar{e}\rangle$ -sector, one gets by the arguments of the general formalism exactly the expression of Chapter 2, Eq. (2.10).

One might wonder why the correct fixing of the redundant parameter  $\omega$  resulting in the diagonal resolvent Eq. (5.17) could appear as an approximation of the expansion Eq. (2.8), or even as an *ad hoc* assumption in [24, Eq. (2.7)]. The answer is that it is very important for the theory, at which the stage the (necessary) truncations are made. If one truncates too early in the formalism, it is clear from the work of TAMM [67] and DANCOFF [68] that other prescriptions, such as *ad hoc* assumptions, have to guarantee the solubility of the equations. This is handled better when the truncation happens in a controlled way as in the formalism of iterated resolvents [20].

The general formalism of effective interactions can be understood as a summation over all intermediate states in the effective fermion-antifermion sector. It is, however, no Tamm-Dancoff truncation, as sometimes referred to in the literature. In fact, the Coulomb potential comes out of the formalism correctly only if one sums over *all* photons and fermion-antifermion pairs, *i.e.* in the limit  $N \rightarrow \infty$ .

Note that the renormalization problem remains unsolved. After having derived the effective interaction within the present formalism, the cutoff dependence of the results have to be investigated. This is still a “stumbling stone” for the case of QCD. In QED the problems are present, but seem to be not as dramatic.

## 5.4 Application to a model Hamiltonian

To give an instructive example of how the method of iterated resolvents works, we solve the eigenvalue equation

$$H^{toy}|\psi\rangle = E|\psi\rangle$$

where the  $5 \times 5$  dimensional toy Hamiltonian is

$$H^{toy} := \begin{pmatrix} D & F & V & S & 0 \\ F & D & V & 0 & F \\ V & V & D & V & 0 \\ S & 0 & V & D & 0 \\ 0 & F & 0 & 0 & D \end{pmatrix} \quad (5.18)$$

with  $D := 10$ ,  $V := 4$ ,  $S := 3$ ,  $F := 1$ . The eigenvalues  $E_i$  can be calculated by standard methods

$$E_i \in \{4.1386, 6.9387, 9.4239, 11.0368, 18.4908\}. \quad (5.19)$$

The space in which this matrix operates is divided into two subspaces  $|1\rangle$  and  $|2\rangle$ , *i.e.*  $N=2$  in Eq. (5.1), so that the diagonal block matrices are

$$\langle 1|H^{toy}|1\rangle = \begin{pmatrix} D & F \\ F & D \end{pmatrix}, \quad \langle 2|H^{toy}|2\rangle = \begin{pmatrix} D & V & 0 \\ V & D & 0 \\ 0 & 0 & D \end{pmatrix}.$$

## 5.4. Application to a model Hamiltonian

---

The effective Hamiltonian in the  $|1\rangle$ -sector, according to the method of iterated resolvents (cf. Eq. [5.3]), is

$$H_1^{toy}(\omega) = H_1^{toy} + \sum_{l_1 > 1}^N H_{l_1}^{toy} G_{l_1}(\omega) H_{l_1}^{toy} = \langle 1 | H^{toy} | 1 \rangle + \langle 1 | H^{toy} | 2 \rangle G_2(\omega) \langle 2 | H^{toy} | 1 \rangle,$$

where the resolvent

$$G_2 = \frac{1}{\omega - \langle 2 | H^{toy} | 2 \rangle} = \begin{pmatrix} \omega - D & V & 0 \\ V & \omega - D & 0 \\ 0 & 0 & \omega - D \end{pmatrix}^{-1}$$

is itself a  $3 \times 3$  matrix. The Hamiltonian to diagonalize is a  $1 \times 1$  block matrix with two columns and rows. The corresponding two eigenvalues, both functions of  $\omega$ , are plotted in Fig. (5.2). Fixing the redundant parameter  $\omega$  by the condition

$$E(\omega) = \omega \tag{5.20}$$

yields exactly the eigenvalues given in Eq. (5.19). Note that the eigenvalue functions for the first and second eigenvalue have continuous transitions. This is due to the diagonalization algorithm used which will always consider the lowest eigenvalue to be the first one. Note also the strange behavior of the curves yielding the second and third eigenvalue of the whole matrix. One sees that the eigenvalues repel each other in the numerical program. However, it is clear that there should be a crossing of the two curves. In fact, we have two functions in the plot, one of which has one and the other has two poles. This yields five intersection points with  $E(\omega) = \omega$ , as expected. Another important observation is the fact that the dependence of the functions on  $\omega$  is rather weak at the intersection points, which yields numerically stable eigenvalues.

The result obtained should be compared with the similar plot in [81, Fig. 5]. There, a  $4 \times 4$  matrix was solved by applying the projection method row by row, and one ended up with an effective  $1 \times 1$  Hamiltonian, a function of  $\omega$ , but nonetheless a real number. Here, we have shown that the formalism can be applied also to matrices: the effective Hamiltonian is a matrix depending on  $\omega$ . But the functions for the different eigenvalues  $E_i(\omega)$  combine in such a way that continuous functions emerge which have  $N$  intersection points with the line defined by Eq. (5.20). This corresponds to the  $N$  eigenvalues of the toy matrix (5.18), just as in the case discussed in [81].

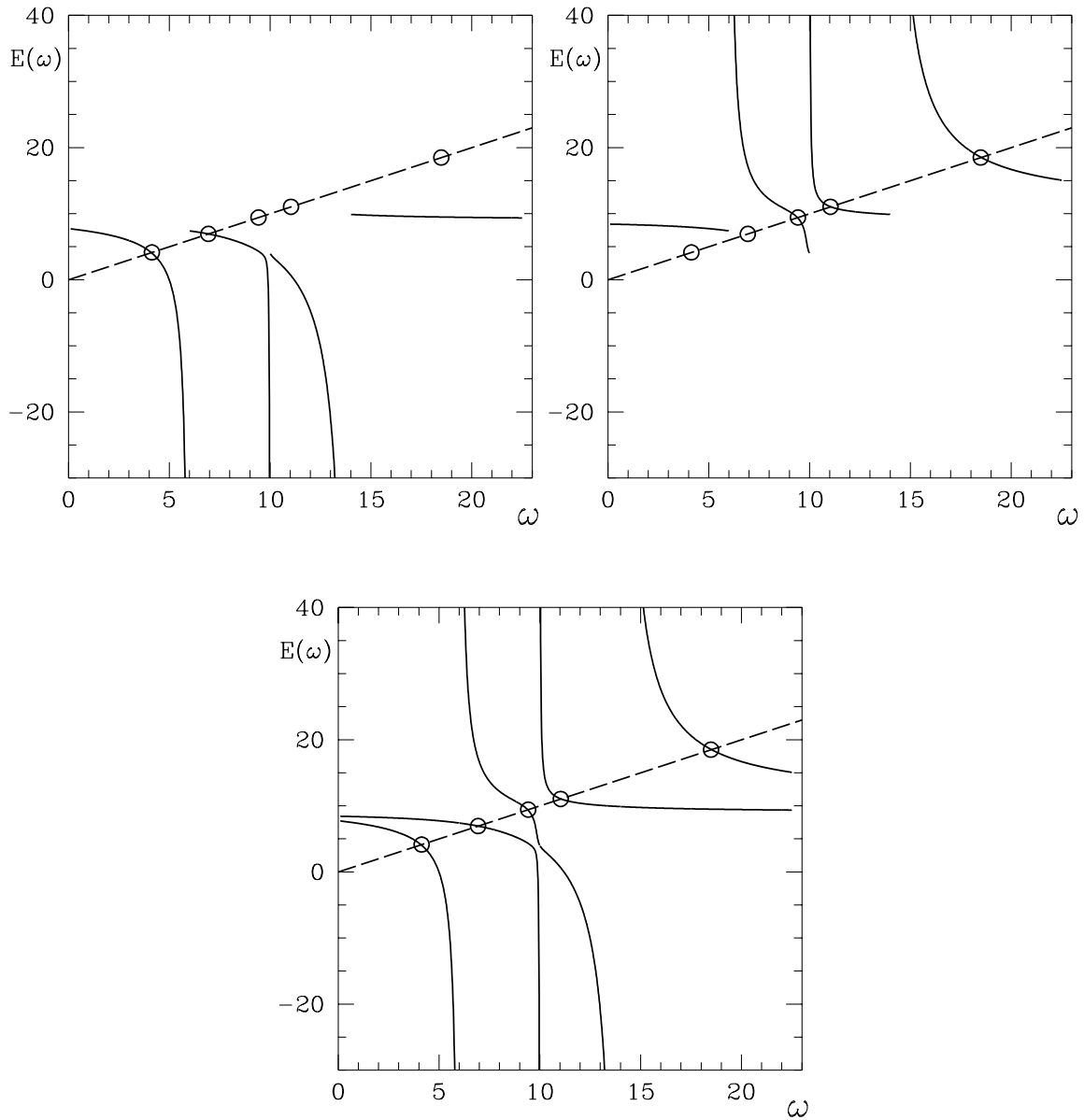


**Figure 5.2:** Eigenvalues of the effective  $2 \times 2$  dimensional toy Hamiltonian as functions of the redundant parameter  $\omega$ : (a) the first, (b) the second eigenvalue, (c) the two plots in one figure. Note the continuous transition from one eigenvalue to the other. The five eigenvalues at the intersection points with the fixing condition  $E(\omega) = \omega$  (dashed line) are encircled.

# Chapter 6

## Summary and Outlook

In this thesis, the calculation of the spectra and the wavefunctions of an electromagnetically bound, relativistic fermion-antifermion system in  $(3 + 1)$  dimensions has been performed. The problem has been solved for all components of the total angular momentum,  $J_z$ , and for an arbitrarily large coupling constant. The latter required the application of non-perturbative methods in quantum field theory. An effective Hamiltonian in the  $|e\bar{e}\rangle$ -sector has been used. The corresponding integral equation is mapped into a matrix eigenvalue problem and solved numerically. The spectrum and the wavefunctions of positronium have been calculated in the regime of an unphysically strong coupling constant,  $\alpha = 0.3$ . A computer code has been created that yielded numerically stable results with a minimized demand on computer equipment. The numerical methods described in [24] have been tested and improved. In particular, the counterterm technology for the Coulomb singularity has been fully implemented. Since the counterterms may in general involve an integral which is not analytically solvable, one can use only numerical integrations and the numerical effort increases. As can be seen by comparing the results of this work with [24], the convergence is improved noticeably. The most prominent aspect of the numerical results is that the spectrum is found to coincide to a very high degree of accuracy with the results of elaborate perturbation techniques. Previous work in this direction (TANG [44], KALUZA [45]) failed to produce significant results because of numerical problems.

Special care has been taken in the comparison of the eigenvalues of the positronium model used with results of perturbation theory. In the sector  $J_z=0$  the Hamiltonian was split up into four block matrices with definite quantum numbers of charge conjugation and  $\mathcal{T}$ -parity. This allows a one-to-one comparison of states with those resulting from perturbation theory, since the symmetry quantum numbers can be related to those used in instant form dynamics. In addition to the fact that the multiplets of a fixed principal quantum number  $n$  contain the correct number of states up to at least  $n = 5$ , we find that the correct combinations of quantum numbers are included in each of these multiplets. A careful study of the higher excited states shows that the calculations of this work are trustworthy even for these states, as opposed to, for example, lattice gauge theories.

As was pointed out, rotational invariance is problematic when using front form dynamics. The operators attached to the transverse rotations are complicated and contain the interaction explicitly. It is therefore important to study the full spectrum of positronium by generalizing the model to a non-vanishing  $J_z$  component of the total angular momentum. We find that the matrix elements can be calculated even for arbitrary  $J_z$ . The improvement of the counterterm technology was crucial in this case. It is important that the counterterms are taken care of individually, because the singularity structures of the diagonal matrix elements differ considerably from each other. We stress the fact that this counterterms are due to numerical problems and have nothing to do with the physics of the positronium model. We *neither* use any special prescription to restore gauge invariance, as suggested by COESTER [76], *nor* do we construct non-covariant counterterms for this purpose, as necessary in front form perturbation theory [51]. One way to study rotational symmetry in front form dynamics requires the diagonalization of operators at least as complicated as the light-cone Hamiltonian itself. We listed these operators in the first section of Chapter 3. It is clear that this is a non-trivial task. Almost all efforts up to date are spend to construct and to diagonalize the light-cone Hamiltonian, and not the other dynamical operators. Surely, the latter is an interesting project. However, we were able to construct an effective Hamiltonian and to solve for its spectrum in all sectors of different  $z$ -components of the total angular momentum. In this way, we can learn from the physical observables (mass squared eigenvalues), how quantum numbers concerning the complicated operators can be attributed to the states. We point out the importance of the non-perturbative approach used in the present work. It has been shown in several models (even QED<sub>3+1</sub>) [51] that perturbation theory in front form dynamics yields results where rotational symmetry is explicitly broken. There are no degeneracies of states with the same total angular momentum. This is clear from our point of view. Exact rotational symmetry is expected only if it is summed over *all* Fock states and *all* momenta. Because we used an effective theory in the present work, where the effects of all Fock states are included in the effective interaction, we observe the desired degeneracies in our approach.

The properties of the spectra calculated for different values of  $J_z$  are the following. Most remarkably, we find that states of different  $J_z$  but same total angular momentum  $J$  are numerically degenerate. There are slight deviations from exact degeneracy also for a large number of integration points. The latter can be explained by the restrictions of the positronium model used, *e.g.* finite cutoff and others. These degeneracies make it possible to classify the states according to their quantum numbers of total angular momentum *a posteriori* and make the diagonalization of the complicated operators of transverse rotations superfluous. Even more, it shows that rotations are unproblematic on the light cone, because rotational symmetry is restored in the solution, a previously worrying fact. The results show very good agreement with the values obtained by equal-time perturbation theory up to order  $\mathcal{O}(\alpha^4)$ .

The model was enlarged by including the one photon annihilation channel. The inclusion is a test for the consistency of the model. In particular, the conception of an effective theory operating with resolvents can be falsified if the annihilation channel

---

cannot be implemented without special assumptions. Our results show that the implementation of the annihilation channel is unproblematic in the sense that the same formalism can be applied as in the case of the projection of the effective  $|e\bar{e}\gamma\rangle$ -sector onto the electron-positron sector. As an interesting property of the annihilation channel we find a strict separation of the instantaneous and the non-instantaneous interaction: the seagull interaction is present only in the  $J_z = 0$  sector, whereas the dynamic graph has non-vanishing matrix elements only for  $J_z = \pm 1$ . Our approach passes another test: both graphs yield the same contributions to the eigenvalues and consequently rotational symmetry is seen also in the spectrum including the annihilation channel. Moreover, the inclusion of the annihilation channel improves the results for the hyperfine splitting.

We stress the point that the implementation of the annihilation channel completes the investigations of how to construct an effective interaction for the electromagnetic fermion-antifermion system in the meaning of the method of iterated resolvents, described in Chapter 5. We have put all effects of higher Fock states into an effective  $|e\bar{e}\gamma\rangle$ -sector, as far as the *spectator interaction* is concerned, *i.e.* the interactions in which the photons are not directly involved. The remainder of the interaction relies in the coupling function of the vertices. A hint to this conclusion is the logarithmic cutoff dependence of our results. It is clear that the coupling constant depends on the cutoff and has to be analyzed. A future aim, beyond the scope of this work, will be to show that the physical results of our model become independent of the cutoff, as soon as renormalization group techniques are consistently applied. This is supported by the fact that we find a stabilizing effect of the annihilation channel on the dependence of the spectrum on the cutoff: all eigenvalues show slower variation with growing cutoff  $\Lambda$  when the annihilation graph is added, in some cases this even prevents level crossings with other states. We therefore conclude that our model is correct as long as the vacuum polarization effects are not considered.

The possibility of one boson annihilation is the main difference between QED and QCD in effectively truncated Fock spaces where the dynamic three- or four-gluon interaction is not possible but resides in the coupling function. The one boson sector exists only in QED because of the constraint of color neutrality in QCD. We showed that this sector can be projected onto the (already) effective electron-positron sector.

In Chapter 5 we described the method of iterated resolvents which allows for the construction of effective interactions on the light-cone. We applied this formalism to our problem. It was shown that the assumption is correct that the effects of the higher Fock states can be accounted for by the fixing the redundant parameter  $\omega$  by a function of the light-cone momenta, Eq. (2.10). The fixing was necessary to derive an effective integral equation starting from the  $\text{QED}_{(3+1)}$  Hamiltonian and is equivalent to the calculation of the effective resolvent in the  $|e\bar{e}\gamma\rangle$ -sector. We showed that this resolvent is indeed diagonal in the Fock basis used and is therefore a function rather than an operator. This fixing procedure was supported before by the numerical precision of the calculations using it as an assumption.

Because of a confusion of technical terms we stress the following in this context. The formalism applied here is misnamed when referred to as a Tamm-Dancoff approach.



The Tamm-Dancoff approach was invented for nuclear forces in instant form dynamics. Its three main steps become very clear in the work of TAMM [67, §2]. The first step is to *truncate* the Fock space to two sectors ( $P$ - and  $Q$ -space). Then a projection of one space onto the other is performed. The emerging energy denominator (or resolvent) is *modified* to render the system solvable as a third step. What we have done is (a) regulation of the number of Fock sectors, (b) derivation of an effective Hamiltonian by subsequent projections of Fock sectors onto another, (c) proof that in the limit of infinitely many Fock sectors, the resolvents become diagonal for bound states. In our approach it is clear that a sheer truncation must fail, because essential parts of the Fock space are missing. It remains to treat the so-derived effective Hamiltonian with a renormalization group analysis. We have shown that the dependence of our results is logarithmic (weak) in the cutoff  $\Lambda$ . The inclusion of the annihilation channel stabilizes the eigenvalues. Whether or not this hints to a weaker dependence of the (running) coupling of QED on the cutoff when compared with the coupling of QCD, where this channel is absent, is subject to further investigation.

This thesis was motivated by the will to understand the problems of non-perturbative methods on the light-cone. The hope is clearly to find an adequate description of the low energy region of QCD and thereby of the QCD bound states, like mesons and hadrons. Front form dynamics offers very promising features, such as a simple vacuum, and more. Other methods have been proposed to deal with these problems, namely approaches which diverge from the constituent quark picture. The method of *similarity transforms* of the bare Hamiltonian proposed by WILSON ET AL. [18] and the *coupling coherence* technique advocated by PERRY ET AL. seem to be very promising. Although the formalism is very elaborate, there are problems in calculating actual numbers. A model of BRISUDOVA ET AL. [82] aims at calculating mesons with one heavy constituent quark with these methods. However, the authors are forced to perform a line of approximations, and end up with a non-relativistic, rotationally non-invariant Schrödinger equation, which makes it hard to tell the actual achievements of the approach apart from the draw-backs of the approximations made. An instructive analytical study is that of JONES ET AL. [83], which makes the approach of WILSON and PERRY very clear. The authors calculate the positronium spectrum up to order  $\mathcal{O}(\alpha^4)$  and show that the results are independent of the cutoff up to order  $\mathcal{O}(\alpha^5)$ . The triplet ground states are degenerate. This is not surprising because the effective interactions are derived for small couplings  $\alpha \ll 1$  and a non-relativistic limit of the theory is considered. It is known (Eq. 2.19) that the term that breaks rotational invariance vanishes in the non-relativistic limit. A similar method is that of WEGNER [84], who uses flow equations to renormalize the bare Hamiltonian. Attempts have been made [85] to apply this formalism to QED and to calculate the positronium spectrum. A link between the DLCQ approach and the method of WILSON ET AL. is the work of AMMONS [86]. There, a Tamm-Dancoff truncation is performed together with an application of the similarity transforms. These approaches are distinct from the one used in the present work in the following sense. First, the Hamiltonian is constructed using renormalization theory, then the associated eigenvalue problem is solved. Up

---

to date, the latter step has been performed using bound state perturbation theory or other *perturbative* methods, although in principle a non-perturbative solution seems possible. Complementary to this formalism, we construct *first* an effective Hamiltonian to account for the many-body aspects of the theory [87], solve for the spectra with a non-perturbative method and *then* have to analyze the results using renormalization techniques to study the implications of Quantum Field Theory.

Concluding, the formalism of DLCQ together with the theory of effective interactions, as described in Chapter 5, can be combined to yield non-perturbative results for a relativistic bound system in very good agreement with other standard methods. Even in (3+1) dimensions it is possible to construct a consistent and solvable model for bound states with an arbitrarily large coupling.

With the results of this work and the computer code at hand, one can now proceed to attack QCD bound states in true (3 + 1) dimensions. Because we have reduced the Fock space by effective methods, the difference between QED and QCD relies in the coupling constant, or rather coupling function. The method of iterated resolvents [20] allows for the calculation of these coupling functions for both QED and QCD, but this is tedious work and has not been tackled. On the other hand, MERKEL ET AL. [88] used a phenomenological running coupling for QCD, inspired by the work of RICHARDSON [7], to construct an integral equation, analogous to the one in the present work, for the bound states of a quark-antiquark system. This equation is solved with variational methods. The fitted meson masses show good agreement with experiment. This phenomenological coupling can now be plugged into the formalism and computer code derived in the present work to solve for the spectrum of a QCD-bound quark-antiquark system. This seems possible, because the full effective Hamiltonian of a gauge theory contains only three essential graphs, which themselves include a coupling *function*. The computer code created in the present work already contains two of these graphs, and the third one (the two gluon annihilation) is known to be less important. Consequently, the first task is to find a reasonable phenomenological running coupling constant to construct such a test. The main problem is to find an appropriate regularization of the severe ( $p^{-4}$ ) singularities occurring. Because of this, the dependence of the results on the regularization scheme used has to be investigated carefully. Nevertheless, this seems a promising way to proceed to understand hadrons as QCD-bound states.

# Appendix A

## Notation

The notations used in this work are compiled in the sequel. New technical terms are *italicized* when first introduced. The conventions used for discretizing the theory can be found in Appendix B.

### Coordinates

The *light-cone coordinates* are defined by

$$x^\pm := (x^0 \pm x^3).$$

We use the *metric*

$$g^{\mu\nu} = \begin{pmatrix} 0 & 0 & 0 & 2 \\ 0 & -1 & 0 & 0 \\ 0 & 0 & -1 & 0 \\ 2 & 0 & 0 & 0 \end{pmatrix}.$$

The *greek* indices run like  $(+, 1, 2, -)$ , *latin* indices denote transversal directions, *e.g.*  $i = 1, 2$ . Analogously the *momentum coordinates* of a particle are  $(p^+, \vec{p}_\perp, p^-)$ . Hence,  $p^-$  is the *light-cone energy* of a particle. An underlined variable denotes a merely spatial vector  $\underline{x} := (x^-, \vec{x}_\perp)$ . Some frequently used symbols are:

$P^+$	total longitudinal momentum
$\vec{P}_\perp := 0$	total transversal momentum
$2L$	longitudinal box length
$2L_\perp$	transversal box length
$K := \frac{L}{\pi} P^+$	harmonic resolution (integer valued)
$\Omega := 2L(2L_\perp)^2$	discretization volume
all QN	summation over all quantum numbers

The relative coordinates of the  $i$ -th particle are

$$x_i := \frac{p_i^+}{P^+}, \quad \text{and} \quad \vec{k}_{\perp i} := x_i P^+ - \vec{p}_{\perp i}, \quad (\text{A.1})$$

referred to as the *longitudinal momentum fraction* and the (relative) *transversal momentum*, respectively. If  $\vec{P}_\perp := 0$ , they have the properties

$$\sum_i x_i = 1, \quad \text{and} \quad \sum_i k_i = 0.$$

### Commutation relations

The commutation relations according to the DIRAC-BERGMANN [89, 90] algorithm are

$$\begin{aligned} \{\psi_{+\alpha}(\underline{x}), \psi_{+\beta}^\dagger(\underline{y})\}_{x^+=x_0^+} &= \frac{1}{2} \Lambda_{+\alpha\beta} \delta(x^- - y^-) \delta^2(\vec{x}_\perp - \vec{y}_\perp), \\ [A^i(\underline{x}), \partial^+ A^j(\underline{y})]_{x^+=x_0^+} &= \frac{i}{2} \delta^{ij} \delta(x^- - y^-) \delta^2(\vec{x}_\perp - \vec{y}_\perp). \end{aligned}$$

To be consistent with these relations, in the expansions of the fields the operator-valued coefficients have to obey

$$\begin{aligned} \{b_{\lambda, \underline{n}}, b_{\lambda', \underline{m}}^\dagger\} &= \{d_{\lambda, \underline{n}}, d_{\lambda', \underline{m}}^\dagger\} = \delta_{\lambda, \lambda'} \delta_{n, m} \delta_{\vec{n}_\perp, \vec{m}_\perp}^2, \\ [a_{\lambda, \underline{p}}, a_{\lambda', \underline{q}}^\dagger] &= \delta_{\lambda, \lambda'} \delta_{p, q} \delta_{\vec{p}_\perp, \vec{q}_\perp}^2. \end{aligned}$$

All other (anti-)commutators vanish.

### Coupling constant

We set

$$\alpha := \frac{g^2}{4\pi}.$$

In QED:  $g \equiv |e_0|$ ,  $\alpha = 1/137.0359895(61) = 0.007297353$ . In the discretized theory we use

$$\beta := \frac{g^2}{4\pi K L_\perp^2}.$$

### Spinors and polarization vectors

The fermion fields are separated into two different helicity eigenstates by

$$\psi_\pm = \Lambda_\pm \psi.$$

Here, the projection operators read

$$\Lambda_\pm := \frac{1}{2} \gamma^0 \gamma^\pm$$

or explicitly

$$\Lambda_+ = \frac{1}{2} \begin{pmatrix} 1 & 0 & 1 & 0 \\ 0 & 1 & 0 & -1 \\ 1 & 0 & 1 & 0 \\ 0 & -1 & 0 & 1 \end{pmatrix}, \quad \Lambda_- = \frac{1}{2} \begin{pmatrix} 1 & 0 & -1 & 0 \\ 0 & 1 & 0 & 1 \\ -1 & 0 & 1 & 0 \\ 0 & 1 & 0 & 1 \end{pmatrix},$$

The explicit form of the spinors and polarization vectors used is given in Eqs. (B.5) and (B.6).

# Appendix B

## QED(3+1) on the light-cone

The Hamiltonian operator of Quantum Electrodynamics in  $(3+1)$  dimensions in front form dynamics is derived. QED describes the interaction of (electrically) charged particles. The interaction is intermediated by the gauge field of the photons. We begin with the *Lagrangian density* of QED<sub>(3+1)</sub>

$$\mathcal{L} = -\frac{1}{4}F_{\mu\nu}F^{\mu\nu} + \frac{i}{2} [\bar{\psi}\gamma^\mu\partial_\mu - (\partial_\mu\bar{\psi})\gamma^\mu] \psi - m_f\bar{\psi}\psi - g\bar{\psi}\gamma^\mu\psi A_\mu.$$

The *field strength tensor* is

$$F^{\mu\nu} := \partial^\mu A^\nu - \partial^\nu A^\mu.$$

The equations of motion emerging for the gauge fields are the *Maxwell equations*

$$\partial_\mu F^{\mu\nu} = j^\nu := g\bar{\psi}\gamma^\nu\psi, \tag{B.1}$$

and for the Fermi fields the *Dirac equation*

$$(i\gamma^\mu D_\mu - m_f)\psi = 0, \tag{B.2}$$

where

$$D_\mu := \partial_\mu + igA_\mu$$

denotes the *covariant derivative*. We use in this work the *light-cone coordinates*

$$x^\pm := x^0 \pm x^3.$$

$x^+$  plays the role of a time,  $x^-$  is a direction of space. To write scalar products involving Dirac matrices likewise, we define

$$\gamma^\pm := \gamma^0 \pm \gamma^3.$$

We use the usual Dirac representation for these matrices. We work in the so-called *light-cone gauge*

$$A^+ = A^0 + A^3 \equiv 0, \tag{B.3}$$

which leads to a consistent theory in the normal mode sector. Deriving the *light-cone energy*  $P^-$ , we shall follow the line of arguments of TANG [44, Ref. 1]. With help of the *projection operators*

$$\Lambda_{\pm} := \frac{1}{2}\gamma^0\gamma^{\pm} = \frac{1}{4}\gamma^{\mp}\gamma^{\pm},$$

we separate the fields into states of different helicity

$$\psi_{\pm} = \Lambda_{\pm}\psi.$$

It turns out that only six out of the twelve fields  $A^{\mu}$ ,  $\psi_+$ ,  $\psi_+^{\dagger}$ ,  $\psi_-$ , and  $\psi_-^{\dagger}$  occurring in the Lagrangian density are independent of the others: the conjugate momenta of  $A^-$ ,  $\psi_-$ , and  $\psi_-^{\dagger}$  vanish. The Euler-Lagrange equations in these fields contain no time derivative, and have the rank of constraints. This is a consequence of the chosen quantization plane. The equations of motion for the dependent fields are

$$\begin{aligned} i\partial^+\psi_- &= \left(-i\partial_i\alpha^i + \beta m_f + gA_i\alpha^i\right)\psi_+, \\ i\partial^+\psi_-^{\dagger} &= -\psi_+^{\dagger}\left(i\overleftarrow{\partial}_i\alpha^i + \beta m_f + gA_i\alpha^i\right), \\ (i\partial^+)^2A^- &= 2\partial^+\partial_iA^i + 4g\psi_+^{\dagger}\psi_+. \end{aligned} \tag{B.4}$$

with the usual Dirac matrices  $\alpha^i, \beta$  and  $\psi_+^{\dagger}\overleftarrow{\partial}_i := \partial_i\psi_+^{\dagger}$ .

To quantize correctly, we have to eliminate all dependent degrees of freedom. This can be achieved either<sup>1</sup> by inverting the equations (B.4) or by applying the Dirac-Bergmann algorithm [89, 91, 90]. The latter leads for a reasonable Lagrange density necessarily to the right commutation relations for the independent fields.

We substitute the dependent fields by functionals of the dynamic degrees of freedom

$$\begin{aligned} \psi_- &= \frac{1}{i\partial^+}\left(-i\partial_i\alpha^i + \beta m_f\right)\psi_+ - \frac{g}{i\partial^+}A^i\alpha^i\psi_+, \\ \psi_-^{\dagger} &= \frac{-1}{i\partial^+}\psi_+^{\dagger}\left(i\overleftarrow{\partial}_i\alpha^i + \beta m_f\right) + \frac{g}{i\partial^+}\psi_+^{\dagger}A^i\alpha^i, \\ A^- &= \frac{2}{(i\partial^+)^2}\partial^+\partial_iA^i + \frac{4g}{(i\partial^+)^2}\psi_+^{\dagger}\psi_+. \end{aligned}$$

The inverse derivatives are defined by Green functions<sup>2</sup>. From the energy-momentum tensor

$$\mathcal{T}^{\mu\nu} = \sum_r \frac{\delta\mathcal{L}}{\delta(\partial_{\mu}\phi_r)}\partial^{\mu}\phi_r - g^{\mu\nu}\mathcal{L},$$

one obtains the momenta  $P^{\mu}$  by integrating over all space directions

$$P^{\mu} = \frac{1}{2}\int_{-\infty}^{\infty}dx^- \int_{-\infty}^{\infty}d^2x_{\perp}\mathcal{T}^{+\mu}.$$

<sup>1</sup>Cf. [44, Chapter 4].

<sup>2</sup>These definitions are not unique [35].

The *light-cone energy*  $P^-$  has the following structure

$$P^- = \frac{1}{2} \int_{-\infty}^{\infty} dx^- \int_{-\infty}^{\infty} d^2 x_{\perp} \mathcal{P}_0^- + g \mathcal{P}_1^- + g^2 \mathcal{P}_2^-.$$

The different terms are

$$\begin{aligned} \mathcal{P}_0^- &= \partial^i A^j \partial^i A^j - \partial^i A^j \partial^j A^i + \left\{ i \partial^+ i \partial_i A^i \frac{1}{(i \partial^+)^2} i \partial^+ i \partial_j A^j \right\}_{sym} \\ &\quad + 2 \left\{ \psi_+^\dagger \left[ -i \partial_i \alpha^i + \beta m_e \right] \frac{1}{i \partial^+} \left[ -i \partial_j \alpha^j + \beta m_e \right] \psi_+ \right\}_{sym} \\ \mathcal{P}_1^- &= -2 \left\{ \psi_+^\dagger A^i \alpha^i \frac{1}{i \partial^+} \left[ -i \partial_i \alpha^i + \beta m_e \right] \psi_+ \right\} \\ &\quad - 2 \left\{ \psi_+^\dagger \left[ i \overleftarrow{\partial}_i \alpha^i + \beta m_e \right] \frac{1}{i \partial^+} A^i \alpha^j \psi_+ \right\} \\ &\quad - 4 \left\{ \psi_+^\dagger \psi_+ \frac{1}{(i \partial^+)^2} i \partial^+ i \partial_i A^i \right\}_{sym} \\ \mathcal{P}_2^- &= 2 \left\{ \psi_+^\dagger A^i \alpha^i \frac{1}{i \partial^+} A^j \alpha^j \psi_+ \right\} + 4 \left\{ \psi_+^\dagger \psi_+ \frac{1}{(i \partial^+)^2} \psi_+^\dagger \psi_+ \right\}_{sym}. \end{aligned}$$

Here, the symmetric brackets are defined by

$$\begin{aligned} \left\{ A \frac{1}{i \partial^+} B \right\}_{sym} &:= \frac{1}{2} \left[ A \frac{1}{i \partial^+} B - \left( \frac{1}{i \partial^+} A \right) B \right], \\ \left\{ A \frac{1}{(i \partial^+)^2} B \right\}_{sym} &:= A \frac{1}{(i \partial^+)^2} B + \left( \frac{1}{i \partial^+} A \right) \left( \frac{1}{i \partial^+} B \right) + \left( \frac{1}{(i \partial^+)^2} A \right) B. \end{aligned}$$

We expand the system in plane waves at light-cone time  $x^+ = 0$ , and work subsequently in momentum space. The notations used here are those of [65]. By restricting the system to a box

$$\begin{aligned} -L_{\perp} &\leq x^i \leq L_{\perp}, \\ -L &\leq x^- \leq L, \end{aligned}$$

we discretize the momenta. We have to impose boundary conditions compatible with the equations of motion (B.1,B.2). The expansions of the dynamical fields with the notation  $\underline{x} := (x^-, \vec{x}_{\perp})$  for space and  $\underline{k} := (k^+, k_{\perp})$  for momentum variables read explicitly

$$\begin{aligned} \psi_+(\underline{x}) &= \frac{1}{\sqrt{\Omega}} \sum_s \sum_{\underline{n}} \left[ b_{\underline{n},s} u_+(\lambda) e^{-i \underline{k} \cdot \underline{x}} + d_{\underline{n},-s}^\dagger v_+(\lambda) e^{i \underline{k} \cdot \underline{x}} \right], \\ A^i(\underline{x}) &= \frac{1}{\sqrt{\Omega}} \sum_{\lambda} \sum_{\underline{p}} \frac{1}{\sqrt{k^+}} \left[ a_{\underline{p},\lambda} \epsilon^i(\lambda) e^{-i \underline{k} \cdot \underline{x}} + a_{\underline{p},\lambda}^\dagger \epsilon^{*i}(\lambda) e^{i \underline{k} \cdot \underline{x}} \right]. \end{aligned}$$

---

Here,  $\Omega = 2L(2L_\perp)^2$  symbolizes the volume of the box, in which the momentum vectors have to lie.

We are forced to demand periodic boundary conditions in all space directions for the gauge fields, since they couple to a bilinear term. The boundary conditions for the fermion fields are not subject to such a constraint. It is convenient to impose antiperiodic boundary conditions merely for the longitudinal fermion field. The zero mode of this field vanishes by that choice. Of course, this is of no importance to us, since we consider *a priori* only the normal mode sector by working in the light-cone gauge. The summations are performed in the following way. For fermions the indices are

$$\begin{aligned} k^+ &= \frac{n\pi}{L} & n &= 1, 3, 5, \dots \\ k^i &= \frac{n^i\pi}{L_\perp} & n^i &= 0, \pm 1, \pm 2, \dots \end{aligned}$$

and photons have

$$\begin{aligned} k^+ &= \frac{p\pi}{L} & p &= 2, 4, 6, \dots \\ k^i &= \frac{p^i\pi}{L_\perp} & p^i &= 0, \pm 1, \pm 2, \dots \end{aligned}$$

The projected spinors are defined according to LEPAGE and BRODSKY [33] to be  $u_+(\lambda) := \chi(\lambda)$  and  $v_+(\lambda) := \chi(-\lambda)$ . The spinors

$$\chi(\uparrow) = \frac{1}{\sqrt{2}} \begin{pmatrix} 1 \\ 0 \\ 1 \\ 0 \end{pmatrix}, \quad \chi(\downarrow) = \frac{1}{\sqrt{2}} \begin{pmatrix} 0 \\ 1 \\ 0 \\ -1 \end{pmatrix} \quad (\text{B.5})$$

obey the relations

$$\begin{aligned} \chi^\dagger(\lambda)\chi(\lambda') &= \delta_{\lambda,\lambda'}, \\ \sum_\lambda \chi_\alpha(\lambda)\chi_\beta^\dagger(\lambda) &= \Lambda_{\alpha\beta}^+. \end{aligned}$$

The polarization vectors

$$\epsilon(\uparrow) := \frac{-1}{\sqrt{2}} \begin{pmatrix} 1 \\ i \end{pmatrix}, \quad \text{and} \quad \epsilon(\downarrow) := \frac{1}{\sqrt{2}} \begin{pmatrix} 1 \\ -i \end{pmatrix}. \quad (\text{B.6})$$

are orthonormal in the transverse space and complete

$$\begin{aligned} \epsilon^*(\lambda)\epsilon(\lambda') &= \delta_{\lambda,\lambda'}, \\ \sum_\lambda \epsilon_i(\lambda)\epsilon_j^*(\lambda) &= \delta_{ij}. \end{aligned}$$



The projected spinor  $\psi_+(x)$  can easily be generalized to a spinor for the full free fermion field  $\psi(x)$  by substituting  $u_+(\lambda)$  and  $v_+(\lambda)$  by

$$\begin{aligned} u(\underline{k}, \lambda) &= \frac{1}{\sqrt{k^+}} \left( k^+ + \beta m_f + \vec{\alpha}_\perp \cdot \vec{k}_\perp \right) \chi(\lambda) \\ v(\underline{k}, \lambda) &= \frac{1}{\sqrt{k^+}} \left( k^+ + \beta m_f + \vec{\alpha}_\perp \cdot \vec{k}_\perp \right) \chi(-\lambda). \end{aligned}$$

The same is true for the gauge field, if the purely transversal vector  $\vec{\epsilon}_\perp(\lambda)$  is substituted by the four vector

$$\epsilon^\mu(\lambda) := \begin{pmatrix} 0 \\ 2 \frac{\vec{\epsilon}_\perp \cdot \vec{k}_\perp}{k^+} \\ \vec{\epsilon}_\perp(\lambda) \end{pmatrix}.$$

We quantize by postulating the usual commutation relations for the coefficients of the Fourier decomposition of the fields. The coefficients become operator valued and obey

$$\{b_{s,\underline{k}}, b_{s',\underline{k}'}^\dagger\} = \{d_{s,\underline{k}}, d_{s',\underline{k}'}^\dagger\} = \delta_{s,s'} \delta_{\underline{k},\underline{k}'}^{(3)}$$

$$[a_{\underline{k},\lambda}, a_{\underline{k}',\lambda'}^\dagger] = \delta_{\lambda,\lambda'} \delta_{\underline{k},\underline{k}'}$$

$$\{b, b\} = \{d, d\} = \{b, d^\dagger\} = [a, b] = [a, d] = [a, b^\dagger] = [a, d^\dagger] = 0.$$

Since we address ourselves in this work to solve an *integral* equation, we additionally list the expansions of the fields in the continuum

$$\begin{aligned} \psi_+(x) &= \frac{1}{\sqrt{2(2\pi)^3}} \sum_\lambda \int_0^\infty dk^+ \int_{-\infty}^\infty d^2k_\perp \frac{1}{\sqrt{k^+}} \left[ b(\underline{k}, \lambda) u_+(\lambda) e^{-i\underline{k} \cdot \underline{x}} + d^\dagger(\underline{k}, \lambda) u_+(\lambda) e^{+i\underline{k} \cdot \underline{x}} \right] \\ A^i(x) &= \frac{1}{\sqrt{2(2\pi)^3}} \sum_\lambda \int_0^\infty dk^+ \int_{-\infty}^\infty d^2k_\perp \frac{1}{\sqrt{k^+}} \left[ a(\underline{k}, \lambda) \epsilon^i(\lambda) e^{-i\underline{k} \cdot \underline{x}} + a^\dagger(\underline{k}, \lambda) \epsilon^{*i}(\lambda) e^{+i\underline{k} \cdot \underline{x}} \right]. \end{aligned}$$

# Appendix C

## Matrix elements of the light-cone Hamiltonian in QED

The matrix elements of the QED<sub>(3+1)</sub> Hamiltonian in light-cone quantization have been derived elsewhere [44]. The light-cone Hamiltonian is defined as

$$H_{\text{LC}} := P^\mu P_\mu = P^+ P^-.$$

It is usually divided into the parts

$$H_{\text{LC}} = T + V + S + F + C,$$

where the *kinetic* energy is

$$T = \sum_q \frac{m_f^2 + \vec{k}_\perp^2}{x_q} (b_q^\dagger b_q + d_q^\dagger d_q) + \sum_q \frac{\vec{k}_\perp^2}{x_q} a_q^\dagger a_q.$$

$V$ ,  $S$ ,  $F$  and  $C$  are the *vertex*-, the *seagull*- and the *fork*-interaction, as well as the *contractions*<sup>1</sup>. The Fork interaction is absent in this work because of the truncation of the Fock space and is not listed.

The creation operators  $b_q^\dagger, d_q^\dagger$  and  $a_q^\dagger$  create plane waves (states) for electrons, positrons and photons, respectively. These particles are characterized by their quantum numbers

$$q := (x, \vec{k}_\perp, \lambda).$$

A particle with *longitudinal momentum fraction*  $x$ , *transversal momentum*  $\vec{k}_\perp$  and *helicity*  $\lambda$  is annihilated by the (annihilation) operators  $b_q, d_q, a_q$ , depending on the nature of the particle, and represented in the graphs of the matrix elements by the following symbols

---

<sup>1</sup> This nomenclature stems from the operator structure of the matrix elements. Is the parton number changed by an interaction by 0, 1 or 2, the operators are called seagull, vertex, or fork, respectively. Contractions occur due to normal ordering of the seagull operators.

## Appendix C. Matrix elements of the light-cone Hamiltonian in QED

$$\begin{array}{ll}
 \longrightarrow & b_q^\dagger = b^\dagger(x, \vec{k}_\perp, \lambda) \quad (\text{electron}), \\
 \longleftarrow & d_q^\dagger = d^\dagger(x, \vec{k}_\perp, \lambda) \quad (\text{positron}), \\
 \text{~~~~~} & a_q^\dagger = a^\dagger(x, \vec{k}_\perp, \lambda) \quad (\text{photon}).
 \end{array}$$

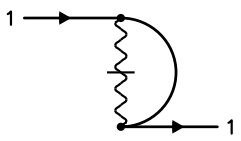
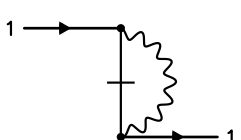
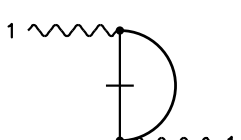
The photons are massless, the fermion mass is  $m_f$ . Creation and annihilation operators obey the usual commutation relations. It is summed over all possible quantum numbers in all expressions.

The matrix elements are listed in the discretized form where the normalization volume is

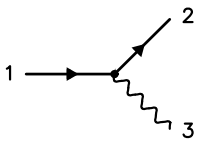
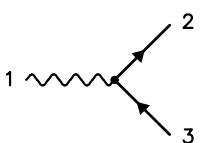
$$\Omega := 2L(2L_\perp)^2,$$

with the half longitudinal and transversal box lengths  $L$  and  $L_\perp$ , respectively. The coupling constant in the tables is  $\tilde{g}^2 = g^2 \frac{2}{P^+ \Omega}$ , the total longitudinal momentum  $P^+ = \frac{\pi}{L} K$ , with the *harmonic resolution*  $K$ . For all other notations see Appendix A. The *continuum limit* is obtained by substituting simultaneously

$$\frac{\tilde{g}^2}{4\pi} \longrightarrow \frac{\alpha}{2\pi^2} \quad \text{and} \quad \sum_{\text{all QN}} \longrightarrow \sum_{\lambda=\pm 1} \int_0^1 dx \int_{-\infty}^{\infty} dk_x \int_{-\infty}^{\infty} dk_y.$$

Graph	Matrix Element
	$C_q^{(g)}(1) = \tilde{g}^2 \sum_{x', \vec{k}'_\perp} \left( \frac{1}{(x_1 - x')^2} - \frac{1}{(x_1 + x')^2} \right)$
	$C_q^{(q)}(1) = \tilde{g}^2 \sum_{x', \vec{k}'_\perp} \left( \frac{1}{x'(x_1 + x')} + \frac{1}{x'(x_1 - x')} \right)$
	$C_g^{(q)}(1) = -\tilde{g}^2 \sum_{x', \vec{k}'_\perp} \left( \frac{1}{x_1(x' + x_1)} + \frac{1}{x_1(x' - x_1)} \right)$
$C = \sum_{\text{all QN}} \left[ (b_1^\dagger b_1 - d_1^\dagger d_1) (C_q^{(g)}(1) + C_q^{(q)}(1)) + a_1^\dagger a_1 C_g^{(q)}(1) \right]$	

**Table C.1:** Matrix elements of the contractions. For further explanations, see text.

Graph	Matrix Element	Helicity
	$ \begin{aligned} V_{q \to qg}(1; 2, 3) = & +\tilde{g} \frac{m_f}{\sqrt{x_1}} \left( \frac{1}{x_2} - \frac{1}{x_3} \right) && \times \delta_{\lambda_2}^{\lambda_1} \delta_{\lambda_3}^{\lambda_1} \\ & +\tilde{g} \sqrt{\frac{2}{x_3}} \vec{\epsilon}_\perp(\lambda_3) \left( \frac{\vec{k}_{\perp 3}}{x_3} - \frac{\vec{k}_{\perp 2}}{x_2} \right) && \times \delta_{\lambda_2}^{\lambda_1} \delta_{-\lambda_3}^{\lambda_1} \\ & +\tilde{g} \sqrt{\frac{2}{x_3}} \vec{\epsilon}_\perp(\lambda_3) \left( \frac{\vec{k}_{\perp 3}}{x_3} - \frac{\vec{k}_{\perp 1}}{x_1} \right) && \times \delta_{-\lambda_2}^{\lambda_1} \delta_{\lambda_3}^{\lambda_1} \end{aligned} $	
	$ \begin{aligned} V_{g \to q\bar{q}}(1; 2, 3) = & \tilde{g} \frac{m_f}{\sqrt{x_1}} \left( \frac{1}{x_2} + \frac{1}{x_3} \right) && \times \delta_{\lambda_2}^{\lambda_1} \delta_{\lambda_3}^{\lambda_1} \\ & -\tilde{g} \sqrt{\frac{2}{x_1}} \vec{\epsilon}_\perp(\lambda_1) \left( \frac{\vec{k}_{\perp 1}}{x_1} - \frac{\vec{k}_{\perp 3}}{x_3} \right) && \times \delta_{\lambda_2}^{\lambda_1} \delta_{-\lambda_3}^{\lambda_1} \\ & -\tilde{g} \sqrt{\frac{2}{x_1}} \vec{\epsilon}_\perp(\lambda_1) \left( \frac{\vec{k}_{\perp 1}}{x_1} - \frac{\vec{k}_{\perp 2}}{x_2} \right) && \times \delta_{-\lambda_2}^{\lambda_1} \delta_{\lambda_3}^{\lambda_1} \end{aligned} $	
$ \begin{aligned} V = & \sum_{\text{all QN}} (b_1^\dagger b_2 a_3 - d_1^\dagger d_2 a_3) V_{q \to qg}(1; 2, 3) \\ & + \sum_{\text{all QN}} (a_3^\dagger b_2^\dagger b_1 - a_3^\dagger d_2^\dagger d_1) V_{q \to qg}^*(1; 2, 3) \\ & + \sum_{\text{all QN}} [a_1^\dagger b_2 d_3 V_{g \to q\bar{q}}^*(1; 2, 3) + d_3^\dagger b_2^\dagger a_1 V_{g \to q\bar{q}}(1; 2, 3)] \end{aligned} $		

**Table C.2:** Matrix elements of the vertex interaction. For further explanations, see text.

Graph	Matrix Element	Helicity
	$S_{q\bar{q} \to q\bar{q}}^{(s)}(1, 2; 3, 4) = \tilde{g}^2 \frac{2}{(x_1 - x_3)^2}$	$\times \delta_{\lambda_3}^{\lambda_1} \delta_{\lambda_4}^{\lambda_2}$
	$S_{q\bar{q} \to q\bar{q}}^{(a)}(1, 2; 3, 4) = \tilde{g}^2 \frac{-2}{(x_1 + x_3)^2}$	$\times \delta_{-\lambda_2}^{\lambda_1} \delta_{-\lambda_4}^{\lambda_3}$
	$S_{qg \to qg}^{(s)}(1, 2; 3, 4) = \tilde{g}^2 \frac{1}{x_1 - x_4} \frac{1}{\sqrt{x_2 x_4}}$	$\times \delta_{\lambda_2}^{\lambda_1} \delta_{\lambda_3}^{\lambda_1} \delta_{\lambda_4}^{\lambda_1}$
	$S_{qg \to qg}^{(a)}(1, 2; 3, 4) = \tilde{g}^2 \frac{1}{x_1 + x_2} \frac{1}{\sqrt{x_2 x_4}}$	$\times \delta_{-\lambda_2}^{\lambda_1} \delta_{\lambda_3}^{\lambda_1} \delta_{-\lambda_4}^{\lambda_1}$
$S = \sum_{\text{all QN}} b_1^\dagger d_2^\dagger b_3 d_4 \left[ S_{q\bar{q} \to q\bar{q}}^{(s)}(1, 2; 3, 4) + S_{q\bar{q} \to q\bar{q}}^{(a)}(1, 2; 3, 4) \right]$ $+ \sum_{\text{all QN}} \left( b_1^\dagger a_2^\dagger b_3 a_4 + d_1^\dagger a_2^\dagger d_3 a_4 \right) \left[ S_{qg \to qg}^{(s)}(1, 2; 3, 4) + S_{qg \to qg}^{(a)}(1, 2; 3, 4) \right]$		

**Table C.3:** Matrix elements of the seagull interaction used or mentioned in the present work. The full table can be found in [65]. For further explanations, see text.

# Appendix D

## Calculation of effective matrix elements

The calculation of the matrix elements of the effective interaction using matrix elements of the canonical Hamiltonian and using currents is described in short. We use the derivation of KRAUTGÄRTNER, PAULI and WÖLZ [24]. The interaction within the positronium system can be expressed via currents [24, Eq. (2.13)]

$$V_{\text{eff}} = \frac{g^2}{\mathcal{D}} j(l_e)^\mu j(l_{\bar{e}})_\mu + \frac{g^2}{\mathcal{D}} \frac{T^* - \omega}{|x - x'|} j(l_e)^+ j(l_{\bar{e}})^+. \quad (\text{D.1})$$

Here the *currents* are

$$\begin{aligned} j(l_e)^\mu &= \bar{u}(k'_e) \gamma^\mu u(k_e), \\ j(l_{\bar{e}})^\mu &= \bar{u}(k'_{\bar{e}}) \gamma^\mu u(k_{\bar{e}}), \end{aligned}$$

the *momentum transfers* read

$$\begin{aligned} l_e^\mu &= (k'_e - k_e)^\mu, \\ l_{\bar{e}}^\mu &= (k_{\bar{e}} - k'_{\bar{e}})^\mu, \end{aligned}$$

and the *energy denominator* is given by

$$\mathcal{D} = |x - x'| (T^* - \omega) - l_e^2, \quad (\text{D.2})$$

using  $l_e^2 \equiv \frac{1}{2} (l_e^2 + l_{\bar{e}}^2)$ . In order to derive (D.1), one evaluates the diagrams shown in Fig. (D.1) according to the rules of light-cone perturbation theory as formulated by LEPAGE and BRODSKY in [33, Appx. A]. In the energy denominator, the average of the energies of the in- and outgoing particles is used instead of the sum of the energies of the incoming particles only. The second term of Eq. (D.1) vanishes, if one fixes  $\omega = T^*$  as described in Chapter 2. The definition of the interaction matrix elements is read off from the integral equation. We follow [33, Eq. (A.5)] and [92, Eq. (3.19)] by setting

$$\left(\frac{m_f^2 + \vec{k}_\perp^2}{x(1-x)} - M_n^2\right) \psi_n(x, \vec{k}_\perp; \lambda_1, \lambda_2) + \frac{g^2}{16\pi^3} \sum_{s'_1, s'_2} \int_D \frac{dx' d^2 \vec{k}'_\perp}{\frac{1}{2}(l_e^2 + l_{\bar{e}}^2)} \frac{\langle x, \vec{k}_\perp; \lambda_1, \lambda_2 | j(l_e)^\mu j(l_{\bar{e}}) | x', \vec{k}'_\perp; s'_1, s'_2 \rangle}{\sqrt{xx'(1-x)(1-x')}} \psi_n(x, \vec{k}_\perp; \lambda_1, \lambda_2) = 0.$$

For the actual calculation of the effective interaction via the currents we need the matrix elements of the Dirac spinors:

$\mathcal{M}$	$\frac{1}{\sqrt{k^+ k'^+}} \bar{u}(k', \lambda') \mathcal{M} u(k, \lambda)$
$\gamma^+$	$2\delta_\lambda^\lambda$
$\gamma^-$	$\frac{2}{k^+ k'^+} \left[ (m^2 + k_\perp k'_\perp e^{+i\lambda(\varphi - \varphi')}) \delta_{\lambda'}^\lambda + m\lambda (k'_\perp e^{+i\lambda\varphi'} - k_\perp e^{+i\lambda\varphi}) \delta_{-\lambda'}^\lambda \right]$
$\gamma_1$	$\left( \frac{k'_\perp}{k'^+} e^{-i\lambda\varphi'} + \frac{k_\perp}{k^+} e^{+i\lambda\varphi} \right) \delta_{\lambda'}^\lambda - m\lambda \left( \frac{1}{k'^+} - \frac{1}{k^+} \right) \delta_{-\lambda'}^\lambda$
$\gamma_2$	$i\lambda \left( \frac{k'_\perp}{k'^+} e^{-i\lambda\varphi'} - \frac{k_\perp}{k^+} e^{+i\lambda\varphi} \right) \delta_{\lambda'}^\lambda - im \left( \frac{1}{k'^+} - \frac{1}{k^+} \right) \delta_{-\lambda'}^\lambda$

**Table D.1:** Matrix elements of the Dirac spinors.

With the notation

$$\langle \mathcal{M}_1 \mathcal{M}_2 \rangle := \frac{\bar{u}(x', k'_\perp, \lambda'_1) \mathcal{M}_1 u(x, k_\perp, \lambda_1) \bar{u}(1-x', -k'_\perp, \lambda'_2) \mathcal{M}_2 u(1-x, -k_\perp, \lambda_2)}{\sqrt{xx'(1-x)(1-x')}},$$

the prescription for the calculation of the matrix elements of the effective interaction reads

$$\begin{aligned} \langle x, \vec{k}_\perp; \lambda_1, \lambda_2 | j^\mu(l_e) j_\mu(l_{\bar{e}}) | x', \vec{k}'_\perp; \lambda'_1, \lambda'_2 \rangle &:= \frac{\langle x, \vec{k}_\perp; \lambda_1, \lambda_2 | j^\mu(l_e) j_\mu(l_{\bar{e}}) | x', \vec{k}'_\perp; \lambda'_1, \lambda'_2 \rangle}{2\sqrt{xx'(1-x)(1-x')}} \\ &= \frac{1}{2} \left( \frac{1}{2} \langle \gamma^+ \gamma^- \rangle + \frac{1}{2} \langle \gamma^- \gamma^+ \rangle - \langle \gamma_1^2 \rangle - \langle \gamma_2^2 \rangle \right). \end{aligned} \tag{D.3}$$

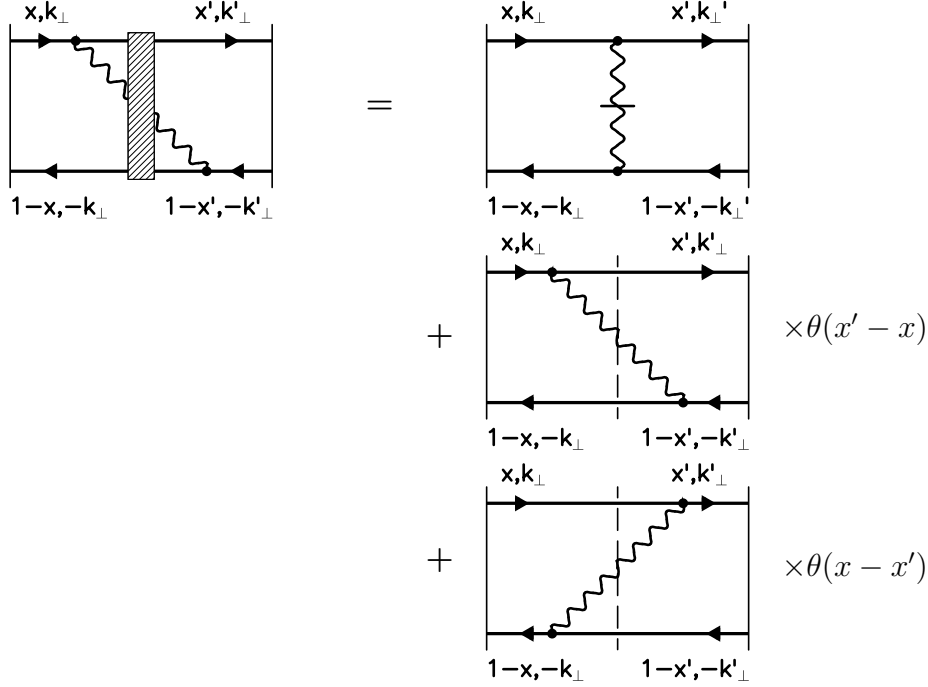


**Figure D.1:** The graphs of the effective interaction. Shown are the graphs with an effective photon (a), the instantaneous seagull-graph (b), and the dynamic graph (c) and (d) with time ordering (I) and (II), respectively.

These functions are listed in Appendix F.

Using canonical Hamiltonian matrix elements, as worked out in detail by TANG ET AL. [44] and listed in Appx. C, one can easily obtain the same results as using currents. As an example, we give the prescription for calculations of effective matrix elements originating in the projection of the  $|e\bar{e}\gamma\rangle$ -sector onto the  $|e\bar{e}\rangle$ -sector of the truncated Fock-space

$$\langle (e\bar{e})_i | V_{\text{eff}} | (e\bar{e})_j \rangle = \sum_k \langle (e\bar{e})_i | V | (e\bar{e}\gamma)_k \rangle \frac{1}{\langle (e\bar{e}\gamma)_k | \omega - H | (e\bar{e}\gamma)_k \rangle} \langle (e\bar{e}\gamma)_k | V | (e\bar{e})_j \rangle, \quad (\text{D.4})$$

where  $V$  is the vertex operator of a fermion irradiating a photon. For the time ordering (I), Fig. (D.1)(c), we obtain

$$\begin{aligned} \langle (e\bar{e}\gamma)' | V | e\bar{e} \rangle &= \sqrt{\beta} \frac{1}{\sqrt{(x-x')}} \left\{ m_f \frac{x-x'}{xx'} \times \delta_{-\lambda_2}^{\lambda_1} \delta_{\lambda_3}^{\lambda_1} \right. \\ &\quad + \frac{\lambda}{x-x'} \left( -k_{\perp} e^{-i\lambda\varphi} + \frac{x}{x'} k'_{\perp} e^{-i\lambda\varphi'} \right) \times \delta_{\lambda_2}^{\lambda_1} \delta_{\lambda_3}^{\lambda_1} \\ &\quad \left. + \frac{\lambda}{x-x'} \left( k'_{\perp} e^{-i\lambda\varphi'} - \frac{x'}{x} k_{\perp} e^{-i\lambda\varphi} \right) \times \delta_{\lambda_2}^{\lambda_1} \delta_{-\lambda_3}^{\lambda_1} \right\} \end{aligned}$$



$$\begin{aligned}
 \langle (e\bar{e})' | V | e\bar{e}\gamma \rangle &= -\sqrt{\beta} \frac{1}{\sqrt{x-x'}} \left\{ m_f \frac{x-x'}{(1-x)(1-x')} \times \delta_{-\lambda_2}^{\lambda_1} \delta_{\lambda_3}^{\lambda_1} \right. \\
 &\quad + \frac{\lambda}{x-x'} \left( k'_\perp e^{+i\lambda\varphi'} - \frac{1-x'}{1-x} k_\perp e^{+i\lambda\varphi} \right) \times \delta_{\lambda_2}^{\lambda_1} \delta_{\lambda_3}^{\lambda_1} \\
 &\quad \left. + \frac{\lambda}{x-x'} \left( -k_\perp e^{+i\lambda\varphi} + \frac{1-x}{1-x'} k'_\perp e^{+i\lambda\varphi'} \right) \times \delta_{\lambda_2}^{\lambda_1} \delta_{-\lambda_3}^{\lambda_1} \right\}.
 \end{aligned}$$

The helicity of the irradiated photon is  $\lambda$ , in all other respects we use the notation of Appx. C for this vertex operator. The matrix elements for time ordering (II) are evaluated in a straightforward way. They evolve from the functions displayed above by exchanging particles and anti-particles<sup>1</sup> and a change of the sign because of the  $\theta$ -function. We have to multiply these functions by the inverse Hamiltonian,

$$\frac{1}{\langle (e\bar{e}\gamma)_k | \omega - H | (e\bar{e}\gamma)_k \rangle},$$

which is the equivalent of the energy denominator, Eq. (D.2), in our case. Together with the much simpler matrix elements of the seagull interaction Fig. (D.1)(b), we obtain the functions of Table (F.1) by substituting all photon helicities by those of fermions. This is in accordance with [24] and our previous treatment via currents in Eq. (D.3).

---

<sup>1</sup>That is,  $(x, \vec{k}_\perp) \leftrightarrow (1-x, -\vec{k}_\perp)$ .



$$\begin{aligned}
 &= \frac{\alpha}{2\pi^2} \int_D dx' d^2 \vec{k}'_{\perp} \frac{1}{1-x'} \left[ \frac{m_f^2 (1-x')^2}{x'^2} + \frac{\vec{k}'_{\perp}{}^2}{(1-x')^2} \left( 1 + \frac{1}{x'^2} \right) \right] \\
 &\quad \times \frac{1}{\omega - \frac{m^2 + \vec{k}'_{\perp}{}^2}{x} + \frac{\vec{k}'_{\perp}{}^2}{1-x'}}.
 \end{aligned}$$

The domain of integration is restricted by imposing the condition

$$\frac{m^2 + \vec{k}'_{\perp}{}^2}{x} + \frac{\vec{k}'_{\perp}{}^2}{1-x'} \leq \Lambda^2 + m_f^2.$$

This means that the difference of the free invariant masses of the states before and after an interaction must not exceed a cutoff  $\Lambda$ , which plays the rôle of a regulator. We use again the fixing of the parameter  $\omega$ , Eq.(2.10), and arrive at

$$W = \frac{\alpha}{2\pi^2} \int_D dx' d^2 \vec{k}'_{\perp} \left( \frac{2m_f^2}{m_f^2 (1-x')^2 + \vec{k}'_{\perp}{}^2} - \frac{1}{x'^2} - \frac{2}{(1-x')^2} \right). \quad (\text{E.1})$$

The evaluation of the contraction terms is achieved in the following way. We extract from Table (C.1) the contributions of the *instantaneous fermion* and *photon* part and perform the continuum limit

$$\begin{aligned}
 C^{(q)}(x, \vec{k}_{\perp}, \lambda) &= \frac{\alpha}{2\pi^2} \int_0^1 dy \int_{-\infty}^{\infty} d^2 \vec{k}'_{\perp} \frac{1}{2} \left[ \frac{1}{y(x-y)} + \frac{1}{y(x-y)} \right], \\
 C^{(g)}(x, \vec{k}_{\perp}, \lambda) &= \frac{\alpha}{2\pi^2} \int_0^1 dy \int_{-\infty}^{\infty} d^2 \vec{k}'_{\perp} \left[ \frac{1}{(x-y)^2} - \frac{1}{(x+y)^2} \right].
 \end{aligned}$$

When we use the *principal value* as a regulator for these integrals [54], we obtain<sup>2</sup>

$$\begin{aligned}
 C^{(q)}(x, \vec{k}_{\perp}, \lambda) &= \frac{\alpha}{2\pi^2} \frac{1}{x} \int_0^1 dy \int_{-\infty}^{\infty} d^2 \vec{k}'_{\perp} \frac{1}{y}, \\
 C^{(g)}(x, \vec{k}_{\perp}, \lambda) &= \frac{\alpha}{2\pi^2} \int_0^{x'} dy \int_{-\infty}^{\infty} d^2 \vec{k}'_{\perp} \frac{2}{y^2}.
 \end{aligned}$$

We have to regulate the integral, since both integrands are singular. If we use here the same integration domain as for the iterated interaction, rename the variables and sum the two contraction contributions

$$C := \frac{\alpha}{2\pi^2} \int_D dx d^2 \vec{k}'_{\perp} \left[ \frac{2}{(1-x')^2} + \frac{1}{1-x'} \right],$$

we find that the quadratically divergent term of the instantaneous photon interaction is compensated exactly by the analogous expression in the iterated vertex interaction,

---

<sup>2</sup>For the subtleties of these integrals cf. [73, Appx. B].

## E.2. The positronium sector

---

Eq. (E.1). Additionally, the fermion part proportional to  $1/1 - x'$  cancels and only a logarithmically divergent term survives. The self mass

$$\begin{aligned}\Delta m^2 := W + C &= \frac{\alpha}{2\pi^2} \int_D dx d^2 \vec{k}'_{\perp} \left( \frac{2m_f^2}{m_f^2(2-x')^2 + \vec{k}'_{\perp}{}^2} \right) \\ &= \frac{\alpha}{2\pi} m_f^2 \left( 3 \ln \frac{\Lambda^2 + m_f^2}{m_f^2} - \frac{\Lambda^2}{m_f^2 + \Lambda^2} \right),\end{aligned}\tag{E.2}$$

is therefore only logarithmically divergent, although its three contributions diverge quadratically with the cutoff  $\Lambda$ .

## E.2 The positronium sector

In the positronium sector as defined in Chapter 2, we have the two states  $|e\bar{e}\rangle$  and  $|e\bar{e}\gamma\rangle$ . The calculations of the contractions and the iterated vertex interaction are performed exactly as in the previous section. The domain of integration is given by

$$\left[ m_f^2(x-x')^2 + (x\vec{k}'_{\perp} - x'\vec{k}_{\perp})^2 \right] \frac{1}{xx'(x-x')} \leq \Lambda^2.$$

The expression for the electromagnetic self mass of the electron (and positron) is

$$\Delta M^2 = \frac{\alpha}{2\pi^2} \int_D dx d^2 \vec{k}'_{\perp} \left( \frac{2m_f^2}{m_f^2(x-x')^2 + (x\vec{k}'_{\perp} - x'\vec{k}_{\perp})^2} - \frac{1}{xx'} + \frac{1}{x(x-x')} \right).$$

We can retrieve an expression similar to Eq. (E.2) by substituting

$$y := \frac{x'}{x} \quad \text{and} \quad \vec{p}_{\perp} := \vec{k}'_{\perp} - y\vec{k}_{\perp},$$

where the self masses are related by

$$\Delta M^2 = \frac{1}{x} \Delta m^2.$$

The renormalization is performed by setting

$$m_f \equiv m_e = 511 \text{ keV},$$

or in other words, we adjust the contraction terms so that their divergent pieces cancel exactly those of the iterated interaction, *i.e.*  $\Delta m^2 \equiv 0$ .

The renormalization is restricted to  $P$ -space. In principle, the counterterms will depend on the Fock sector considered. If one takes into account higher Fock states, these counterterms will in general not be analytically calculable. They are essentially non-perturbative.

# Appendix F

## Tables of effective matrix elements

### F.1 Introduction and Notations

The dependence of the effective interaction on the helicities of in- and out-going particles is displayed in the form of tables. A part of the compiled functions has been discussed by KRAUTGÄRTNER ET AL. [24]. The matrix elements of the effective interaction depend on the one hand on the momenta of the electron and positron, respectively, and on the other hand on their helicities before and after the interaction. The latter dependencies occur during the calculation of these functions  $M(x, \vec{k}_\perp, \lambda_1, \lambda_2; x', \vec{k}'_\perp, \lambda'_1, \lambda'_2)$  as complicated Kronecker deltas. A good survey is obtained, however, when displaying these functions in the form of a table.

In the remainder of this appendix, the tables are given for the general, angle-dependent effective matrix elements, Table (F.1), for the matrix elements of arbitrary  $J_z$ , after integrating over the angles, Table (F.2), and for the matrix elements of the annihilation graph, Table (F.3). The following notation is used for functions of the type  $F(x, \vec{k}_\perp; x', \vec{k}'_\perp)$ :

- An asterisk denotes the permutation of particle and anti-particle.

$$F_3^*(x, \vec{k}_\perp; x', \vec{k}'_\perp) := F_3(1-x, -\vec{k}_\perp; 1-x', -\vec{k}'_\perp).$$

- If the function additionally depends on the component of the total angular momentum  $J_z = n$ , a tilde symbolizes the operation

$$\tilde{F}_i(n) = F_i(-n),$$

## F.2 General helicity table

<b>final : initial</b>	$(\lambda'_1, \lambda'_2) = \uparrow\uparrow$	$(\lambda'_1, \lambda'_2) = \uparrow\downarrow$	$(\lambda'_1, \lambda'_2) = \downarrow\uparrow$	$(\lambda'_1, \lambda'_2) = \downarrow\downarrow$
$(\lambda_1, \lambda_2) = \uparrow\uparrow$	$E_1(\vec{k}, \vec{k}')$	$E_3^*(\vec{k}, \vec{k}')$	$-E_3(\vec{k}, \vec{k}')$	0
$(\lambda_1, \lambda_2) = \uparrow\downarrow$	$\bar{E}_3^*(\vec{k}', \vec{k})$	$E_2(\vec{k}, \vec{k}')$	$E_4(\vec{k}, \vec{k}')$	$E_3(\vec{k}', \vec{k})$
$(\lambda_1, \lambda_2) = \downarrow\uparrow$	$-\bar{E}_3(\vec{k}', \vec{k})$	$E_4(\vec{k}, \vec{k}')$	$E_2(\vec{k}, \vec{k}')$	$-E_3^*(\vec{k}', \vec{k})$
$(\lambda_1, \lambda_2) = \downarrow\downarrow$	0	$\bar{E}_3(\vec{k}, \vec{k}')$	$-\bar{E}_3^*(\vec{k}, \vec{k}')$	$E_1(\vec{k}, \vec{k}')$

**Table F.1:** General helicity table of the effective interaction.

A description of the calculation of the functions displayed in the above table was given in some detail in Appendix D. Note that these matrix elements depend in general on the *vectors*  $\vec{k}_\perp$  and  $\vec{k}'_\perp$ . The functions  $E_i(\vec{k}, \vec{k}') := E_i(x, \vec{k}_\perp; x', \vec{k}'_\perp)$  read

$$\begin{aligned}
 E_1(x, \vec{k}; x', \vec{k}') &= \frac{\alpha}{2\pi^2} \frac{1}{\mathcal{D}} \left[ m_F^2 \left( \frac{1}{xx'} + \frac{1}{(1-x)(1-x')} \right) + \frac{k_\perp k'_\perp}{xx'(1-x)(1-x')} e^{-i(\varphi-\varphi')} \right] \\
 E_2(x, \vec{k}; x', \vec{k}') &= \frac{\alpha}{2\pi^2} \frac{1}{\mathcal{D}} \left( m_F^2 + k_\perp k'_\perp e^{i(\varphi-\varphi')} \right) \left( \frac{1}{xx'} + \frac{1}{(1-x)(1-x')} \right) \\
 &\quad + \frac{\alpha}{2\pi^2} \frac{1}{\mathcal{D}} \left( \frac{k_\perp^2}{x(1-x)} + \frac{k'^2_\perp}{x'(1-x')} \right) \\
 E_3(x, \vec{k}; x', \vec{k}') &= -\frac{\alpha}{2\pi^2} \frac{1}{\mathcal{D}} \frac{m_f}{xx'} \left( k'_\perp e^{-i\varphi'} - k_\perp \frac{1-x'}{1-x} e^{-i\varphi} \right) \\
 E_4(x, \vec{k}; x', \vec{k}') &= -\frac{\alpha}{2\pi^2} \frac{m_f^2}{\mathcal{D}} \frac{(x'-x)^2}{xx'(1-x')(1-x)}.
 \end{aligned}$$

The energy denominator is defined as

$$\begin{aligned}
 \mathcal{D}(x, \vec{k}_\perp; x', \vec{k}'_\perp) &:= -(x-x')^2 \frac{m_F^2}{2} \left( \frac{1}{xx'} + \frac{1}{(1-x)(1-x')} \right) + 2k_\perp k'_\perp \cos(\varphi - \varphi') \\
 &\quad - (k_\perp^2 + k'^2_\perp) + (x-x') \left[ \frac{k'^2_\perp}{2} \left( \frac{1}{1-x'} - \frac{1}{x'} \right) - \frac{k_\perp^2}{2} \left( \frac{1}{1-x} - \frac{1}{x} \right) \right].
 \end{aligned}$$

### F.3 The helicity table for arbitrary $J_z$

For an arbitrary  $J_z = n$  with  $n \in Z$  one obtains, following the description given in Chapter 3, the helicity table (F.2).

final : initial	$(\lambda'_1, \lambda'_2) = \uparrow\uparrow$	$(\lambda'_1, \lambda'_2) = \uparrow\downarrow$	$(\lambda'_1, \lambda'_2) = \downarrow\uparrow$	$(\lambda'_1, \lambda'_2) = \downarrow\downarrow$
$(\lambda_1, \lambda_2) = \uparrow\uparrow$	$G_1(1, 2)$	$G_3^*(1, 2)$	$G_3(1, 2)$	0
$(\lambda_1, \lambda_2) = \uparrow\downarrow$	$G_3^*(2, 1)$	$G_2(1, 2)$	$G_4(1, 2)$	$-\tilde{G}_3(2, 1)$
$(\lambda_1, \lambda_2) = \downarrow\uparrow$	$G_3(2, 1)$	$G_4(1, 2)$	$\tilde{G}_2(1, 2)$	$-\tilde{G}_3^*(2, 1)$
$(\lambda_1, \lambda_2) = \downarrow\downarrow$	0	$-\tilde{G}_3(1, 2)$	$-\tilde{G}_3^*(1, 2)$	$\tilde{G}_1(1, 2)$

**Table F.2:** Helicity table of the effective interaction for  $J_z = \pm n$ ,  $x > x'$ .

Here, the functions  $G_i(1, 2) := G_i(x, \vec{k}_\perp; x', \vec{k}'_\perp)$  are given by

$$\begin{aligned}
 G_1(x, k_\perp; x', k'_\perp) &= m_f^2 \left( \frac{1}{xx'} + \frac{1}{(1-x)(1-x')} \right) \text{Int}(|1-n|) \\
 &\quad + \frac{k_\perp k'_\perp}{xx'(1-x)(1-x')} \text{Int}(|n|) \\
 G_2(x, k_\perp; x', k'_\perp) &= \left[ m_f^2 \left( \frac{1}{xx'} + \frac{1}{(1-x)(1-x')} \right) + \frac{k_\perp^2}{x(1-x)} + \frac{k'_\perp^2}{x'(1-x')} \right] \text{Int}(|n|) \\
 &\quad + k_\perp k'_\perp \left[ \frac{\text{Int}(|1-n|)}{xx'} + \frac{\text{Int}(|1+n|)}{(1-x)(1-x')} \right] \\
 G_3(x, k_\perp; x', k'_\perp) &= -m_f \frac{1}{xx'} \left[ k'_\perp \text{Int}(|1-n|) - k_\perp \frac{1-x'}{1-x} \text{Int}(|n|) \right] \\
 G_4(x, k_\perp; x', k'_\perp) &= -m_f^2 \frac{(x-x')^2}{xx'(1-x')(1-x)} \text{Int}(|n|).
 \end{aligned}$$

The function  $\text{Int}(n)$  is defined as

$$\text{Int}(n) := \frac{\alpha}{\pi} (-A)^{-n+1} \left( \frac{B}{k_\perp k'_\perp} \right)^n.$$

Involved in this expression are the definitions

$$\begin{aligned}
 a &= (x-x')^2 \frac{m_f^2}{2} \left( \frac{1}{xx'} + \frac{1}{(1-x)(1-x')} \right) + k_\perp^2 + k'_\perp^2 \\
 &\quad - \frac{1}{2}(x-x') \left[ k_\perp'^2 \left( \frac{1}{1-x'} - \frac{1}{x'} \right) - k_\perp^2 \left( \frac{1}{1-x} - \frac{1}{x} \right) \right]
 \end{aligned}$$

#### F.4. Helicity table of the annihilation graph

---

and

$$A = \frac{1}{\sqrt{a^2 - 4k_{\perp}^2 k'_{\perp}{}^2}},$$

$$B = \frac{1}{2}(1 - aA).$$

#### F.4 Helicity table of the annihilation graph

final:initial	$(\lambda'_1, \lambda'_2) = \uparrow\uparrow$	$(\lambda'_1, \lambda'_2) = \uparrow\downarrow$	$(\lambda'_1, \lambda'_2) = \downarrow\uparrow$	$(\lambda'_1, \lambda'_2) = \downarrow\downarrow$
$(\lambda_1, \lambda_2) = \uparrow\uparrow$	$F_1(1, 2)$	$F_3(2, 1)$	$F_3^*(2, 1)$	0
$(\lambda_1, \lambda_2) = \uparrow\downarrow$	$F_3(1, 2)$	$F_2^*(1, 2)$	$F_4(2, 1)$	0
$(\lambda_1, \lambda_2) = \downarrow\uparrow$	$F_3^*(1, 2)$	$F_4(1, 2)$	$F_2(1, 2)$	0
$(\lambda_1, \lambda_2) = \downarrow\downarrow$	0	0	0	0

**Table F.3:** Helicity table of the annihilation graph for  $J_z \geq 0$ .

The functions  $F_i(1, 2) := F_i(x, \vec{k}_{\perp}; x', \vec{k}'_{\perp})$  were calculated in Chapter 4:

$$F_1(x, k_{\perp}; x', k'_{\perp}) := \frac{\alpha}{\pi} \frac{2m^2}{\omega^*} \left( \frac{1}{x} + \frac{1}{1-x} \right) \left( \frac{1}{x'} + \frac{1}{1-x'} \right) \delta_{|J_z|,1}$$

$$F_2(x, k_{\perp}; x', k'_{\perp}) := \frac{\alpha}{\pi} \left[ \frac{2}{\omega^*} \frac{k_{\perp} k'_{\perp}}{xx'} \delta_{|J_z|,1} + 4\delta_{J_z,0} \right]$$

$$F_3(x, k_{\perp}; x', k'_{\perp}) := \frac{\alpha}{\pi} \frac{2m}{\omega^*} \lambda_1 \left( \frac{1}{x} + \frac{1}{1-x} \right) \frac{k'_{\perp}}{1-x'} \delta_{|J_z|,1}$$

$$F_4(x, k_{\perp}; x', k'_{\perp}) := -\frac{\alpha}{\pi} \left[ \frac{2}{\omega^*} \frac{k_{\perp} k'_{\perp}}{x'(1-x)} \delta_{|J_z|,1} - 4\delta_{J_z,0} \right].$$

The table for  $J_z = -1$  is obtained by inverting *all* helicities. Note that the table has non-vanishing matrix elements for  $|J_z| \leq 1$  only. This restriction is due to the angular momentum of the photon.



# Appendix G

## Numerics

To solve the integral equation (2.11), central to this work, we apply several numerical methods, which are described in the sequel.

### G.1 Transformation of the variables

The invariant front form wavefunctions coincide with the equal-time wavefunctions defined in the infinite momentum frame [93, p. 379]. Let the relative momentum of the  $i$ -th particle in a composite system be  $\vec{p}_i$ . In the center of mass system holds

$$\sum_i \vec{p}_i = 0. \quad (\text{G.1})$$

We want to express the variables  $x, \vec{k}_\perp$  in terms of the equal-time variables  $\vec{p}_\perp, p_z$ . With (G.1) we have

$$p_1^+ = E + p_z, \quad p_2^+ = E - p_z,$$

where  $E = \sqrt{m^2 + \vec{p}^2}$ . If we write the relative momentum in polar coordinates

$$\vec{p} = (\mu \sin \theta \cos \varphi, \mu \sin \theta \sin \varphi, \mu \cos \theta),$$

it is clear from the definition of the front form momentum fractions (A.1) that

$$x = \frac{1}{2} \left( 1 + \frac{\mu \cos \theta}{\sqrt{m_f^2 + \mu^2}} \right)$$

$$\vec{k}_\perp = \vec{\mu}_\perp = (\mu \sin \theta \cos \varphi, \mu \sin \theta \sin \varphi).$$

The inverse transformation is

$$\mu := \sqrt{\frac{k_\perp^2 + m^2(2x - 1)^2}{1 - (2x - 1)^2}} \quad (\text{G.2})$$

$$\cos \theta := (1 - 2x) \sqrt{\frac{k_\perp^2 + m^2}{k_\perp^2 + m^2(2x - 1)^2}}. \quad (\text{G.3})$$

## G.2. Symmetries

---

These are exactly the coordinates as used by KARMANOV [94] for the deuteron wavefunction and by SAWICKI [36, Eqs. (2.3), (2.4)]. The Jacobian reads

$$J = \frac{1}{2} \frac{m^2 + \mu^2(1 - \cos^2 \theta)}{\sqrt{m^2 + \mu^2}} \mu^2 \sin \theta.$$

For the integration measure holds

$$\int_0^1 dx \int_{-\infty}^{+\infty} d^2 k_{\perp} = \int_0^{\infty} d\mu \int_{-1}^1 d \cos \theta \int_0^{2\pi} d\varphi \frac{\mu^2}{2} \frac{m^2 + \mu^2(1 - \cos^2 \theta)}{(m^2 + \mu^2)^{3/2}}.$$

The new variable  $\mu$  is referred to as *off-shell mass*, because of

$$\frac{m_f^2 + \vec{k}_{\perp}^2}{x(1-x)} = 4(m_f^2 + \mu^2).$$

The restriction on the momenta (2.13) translates into

$$4(m_f^2 + \mu^2) \leq \Lambda^2 + 4m_f^2 \quad (\text{G.4})$$

and is therefore a restriction of the off-shell mass.

In the next paragraph the integration over the angular variable  $\varphi$  is described. After this, only two variables are left in the game:  $\mu$  and  $\cos \theta$ . The integrations over these coordinates are discretized, *i.e.* the integral is mapped onto a sum, with help of the Gauss-Legendre algorithm (cf. *e.g.* [95]). The domains of the integrations are chosen in such a way, that

$$\mu \in [0, \frac{\Lambda}{2}], \quad \cos \theta \in [-1, 1].$$

Here, abscissae and corresponding weights are denoted by

$$\begin{aligned} \mu_i, w_i & \quad i = 1..N_1 \\ \cos \theta_j, w_j & \quad j = 1..N_2. \end{aligned}$$

With  $\Lambda \rightarrow \infty$  we have to map the interval  $[0, \infty]$  for numerical integration onto a finite domain. We follow [64, p. 60, case  $\gamma$ ] and use as a mapping function

$$f(\mu) = \frac{1}{1 + \mu}.$$

The mapping of the weights is calculated straightforwardly.

## G.2 Symmetries

First, we want to restore the symmetry of the Hamiltonian matrix broken by the above transformation of the variables. In discrete variables, the transformation has the Jacobian

$$a_{ij} := \mu_i^2 \frac{m_f^2 + \mu_i^2(1 - \cos \theta_j)}{2\sqrt{m_f^2 + \mu_i^2}}. \quad (\text{G.5})$$

From this transformation an unsymmetric matrix evolves. As a consequence, the numerical effort to diagonalize it increases considerably. We symmetrize the matrix therefore by substituting for the wavefunction

$$\Psi(\mu_i, \theta_j) \longrightarrow \Phi(\mu_i, \theta_j) := \Psi \sqrt{w_i w_j a_{ij}}.$$

The so-modified matrix elements of the effective interaction are

$$\langle x, \vec{k}_\perp; \lambda_1, \lambda_2 | V_{\text{eff}} | x', \vec{k}'_\perp; \lambda'_1, \lambda'_2 \rangle \sqrt{w_i w_j w'_k w'_l a_{ij} a'_{kl}}.$$

Now, we address to the implementation of the point symmetries of the theory into the matrix elements. The Lagrangian density of QED is invariant under the transformations of time reversal  $\mathcal{T}$ , parity  $\mathcal{P}$ , and charge conjugation  $\mathcal{C}$ . Opposed to that, the Hamiltonian in front form dynamics is invariant under the latter operation only. The other operations can be used to construct further, in general more complicated, symmetries.

We consider as a further symmetry of our Hamiltonian matrix the charge conjugation, which is represented mathematically by the unitary operator  $\hat{U}_C$ . Eigenstates to this transformation have the eigenvalues  $\pi_C = \pm 1$  and the creation operators of the different particles transform as follows [96]

$$\begin{aligned} \hat{U}_C b_\lambda^\dagger(x, \vec{k}_\perp) \hat{U}_C^{-1} &= d_\lambda^\dagger(x, \vec{k}_\perp), \\ \hat{U}_C d_\lambda^\dagger(x, \vec{k}_\perp) \hat{U}_C^{-1} &= b_\lambda^\dagger(x, \vec{k}_\perp), \\ \hat{U}_C a_\lambda^\dagger(x, \vec{k}_\perp) \hat{U}_C^{-1} &= -a_\lambda^\dagger(x, \vec{k}_\perp). \end{aligned}$$

The helicities are  $\lambda = \pm 1$ . We construct out of arbitrary  $P$ -space wavefunctions with undefined charge

$$|\psi\rangle = \Psi_{e\bar{e}}(x, \vec{k}_\perp; \lambda_1, \lambda_2) b_{\lambda_1}^\dagger(x, \vec{k}_\perp) d_{\lambda_2}^\dagger(1-x, -\vec{k}_\perp) |0\rangle$$

eigenstates to the charge conjugation operator

$$\begin{aligned} |\pi_C = \pm 1\rangle &= \\ & \frac{1}{\sqrt{2}} \Psi_{e\bar{e}}(x, \vec{k}_\perp; \lambda_1, \lambda_2) \left[ b_{\lambda_1}^\dagger(x, \vec{k}_\perp) d_{\lambda_2}^\dagger(1-x, -\vec{k}_\perp) \mp b_{\lambda_2}^\dagger(1-x, -\vec{k}_\perp) d_{\lambda_1}^\dagger(x, \vec{k}_\perp) \right] |0\rangle. \end{aligned} \tag{G.6}$$

The remark is in order, that if the quantum numbers of the creation operators coincide, there is only *one* eigenstate, having the eigenvalue  $\pi_C = -1$ . This explains the different dimensions of the blocks of the Hamiltonian matrix, which are build of eigenstates to the point symmetries.

As mentioned earlier, further invariants can be constructed from the two remaining symmetries of the Lagrangian density [45]. We use

$$e^{-i\pi J_z \mathcal{P} \mathcal{T}}.$$

## G.2. Symmetries

---

In Chapter 2 of the present work we address to the special case of  $J_z = 0$ . In this case, we can use the combination  $\mathcal{H} := \mathcal{PT}$  as another symmetry. We give again the behaviour of the creation operators under the transformation via the anti-unitary operator<sup>1</sup>  $V_{\mathcal{H}}$

$$\begin{aligned}\hat{U}_{\mathcal{H}} b_s^\dagger(x, \vec{k}_\perp) \hat{U}_{\mathcal{H}}^{-1} &= (-1)^{(\lambda-1)/2} d_{-\lambda}^\dagger(x, \vec{k}_\perp), \\ \hat{U}_{\mathcal{H}} d_s^\dagger(x, \vec{k}_\perp) \hat{U}_{\mathcal{H}}^{-1} &= (-1)^{(\lambda+1)/2} b_{-\lambda}^\dagger(x, \vec{k}_\perp), \\ \hat{U}_{\mathcal{H}} a_\lambda^\dagger(x, \vec{k}_\perp) \hat{U}_{\mathcal{H}}^{-1} &= -a_{-\lambda}^\dagger(x, \vec{k}_\perp).\end{aligned}$$

Physically spoken, this operation inverts the helicities and causes a phase change, dependent on the choice of the spinors [96][97]. One can read off the eigenfunctions of the operator  $V_{\mathcal{H}}$

$$\begin{aligned}|\pi_{\mathcal{H}} = \pm 1\rangle &= \frac{1}{\sqrt{2}} \left[ \Psi_{e\bar{e}}(x, \vec{k}_\perp; \lambda_1, \lambda_2) b_{\lambda_1}^\dagger(x, \vec{k}_\perp) d_{\lambda_2}^\dagger(1-x, -\vec{k}_\perp) \right. \\ &\quad \left. \pm (-1)^{\lambda_1 + \lambda_2} \Psi_{e\bar{e}}^*(x, \vec{k}_\perp; \lambda_1, \lambda_2) b_{-\lambda_1}^\dagger(x, \vec{k}_\perp) d_{-\lambda_2}^\dagger(1-x, -\vec{k}_\perp) \right] |0\rangle.\end{aligned}\tag{G.7}$$

Applying the two point symmetries, the whole Hilbert space is decomposed into four subspaces with well-defined charge and “ $\mathcal{T}$ -parity”, and the Hamiltonian matrix becomes block-diagonal. As a consequence, only four much smaller matrices need to be diagonalized. The numerical effort decreases with the third power of the matrix dimensions, and a lot of computer time can be saved. The construction of the simultaneous eigenstates to  $\mathcal{C}$  and  $\mathcal{H}$  is supplied by the computer routine GENETIX, which generates the whole Hamiltonian matrix by using a subroutine, which calculates the unsymmetrized matrix elements.

Finally, we use for the implementation of one further symmetry the fact, that the Lagrangian density and the Hamiltonian operator of QED are invariant under rotations in the  $x$ - $y$ -plane in front form dynamics, too. Due to this, we can introduce, as another quantum number, the  $z$ -component of the total angular momentum  $J_z$ , to classify our states. The angles enter via

$$\vec{k}_\perp = \begin{pmatrix} k_\perp \cos \varphi \\ k_\perp \sin \varphi \end{pmatrix}.$$

The new effective interaction is obtained by Fourier-transforming the old one

$$\begin{aligned}\langle x, k_\perp, L_z; \lambda_1, \lambda_2 | \tilde{V}_{\text{eff}} | x', k'_\perp, L'_z; \lambda'_1, \lambda'_2 \rangle &:= \\ \frac{1}{2\pi} \int_0^{2\pi} d\varphi e^{-iL_z\varphi} \int_0^{2\pi} d\varphi' e^{iL'_z\varphi'} \langle x, k_\perp, \varphi; \lambda_1, \lambda_2 | V_{\text{eff}} | x', k'_\perp, \varphi'; \lambda'_1, \lambda'_2 \rangle.\end{aligned}$$

But, neither  $L_z$  nor  $S_z = \lambda_1 + \lambda_2$  are good quantum numbers and we set  $L_z = J_z - S_z$ . From these calculations we gain the functions of the helicity table (F.2). This functions are used in the computer code in the subroutine PHYSIX, which calculates the unsymmetrized matrix elements.

---

<sup>1</sup>It is the direct product of the unitary operator of the parity transformation and of the anti-unitary operator of the time reversal transformation  $V_{\mathcal{H}} := V_{\mathcal{P}} \oplus V_{\mathcal{T}}$ .

### G.3 Coulomb trick

The underlying structure faced in treating bound states in Quantum Electrodynamics is the Coulomb problem. Obviously, in the non-relativistic limit, the derived effective integral equation (2.11) will be mapped into the *Coulomb-Schrödinger equation*<sup>2</sup>.

In the introduction, we have already made the point that momentum coordinates are essential, because they render the exact treatment of the center of mass motion possible. A major part of the numerical problems in solving Eq. (2.11) is corresponding to the solution of Coulomb problems in momentum space. This problem was examined in detail in [64]. We present the numerical techniques applied to the treatment of integral equations with a weakly singular kernel.

In the Coulomb Schrödinger equation a kernel is involved with a point singularity which is analytically integrable. Nevertheless, the matrix elements become senseless at that very point. Therefore, we apply the so-called COULOMB trick [64], which is known as the “Nyström method” in the mathematical literature.

In momentum representation the Schrödinger equation of the hydrogen atom reads

$$\frac{\vec{p}^2}{2m}\psi(\vec{p}) - \frac{\alpha}{2\pi^2} \int d^3\vec{p}' \frac{\psi(\vec{p}')}{(\vec{p} - \vec{p}')^2} = E\psi(\vec{p}).$$

For simplicity, we consider only S-waves, *i.e.* rotationally invariant states. We can integrate out the angular variables and using Bohr units we arrive at

$$p^2\psi(p) + \frac{1}{\pi} \int dp' \frac{p'}{p} \ln \left\{ \frac{(p - p')^2}{(p + p')^2} \right\} \psi(p') = E\psi(p).$$

Next, we translate the integral with help of the Gauss-Legendre algorithm in a sum

$$p_i^2\psi(p_i) + \frac{1}{\pi} \sum_{j=1}^N w_j \frac{p_j}{p_i} \ln \left\{ \frac{(p_i - p_j)^2}{(p_i + p_j)^2} \right\} \psi(p_j) = E\psi(p_i).$$

This discretized equation has a singularity at  $p_i = p_j$ . To treat it, we add and subtract two terms which cancel exactly in the continuum limit. Both are diagonal, since the divergence occurs on the diagonal only. The new equation looks like

$$\begin{aligned} p_i^2\psi(p_i) + \frac{1}{\pi} \sum_{j=1}^N w_j \frac{p_j}{p_i} \ln \left\{ \frac{(p_i - p_j)^2}{(p_i + p_j)^2} \right\} [\psi(p_j) - g(p_i, p_j)\psi(p_i)] \\ + \frac{1}{\pi} \int_{D_1} dp' \frac{p'}{p_i} \ln \left\{ \frac{(p_i - p')^2}{(p_i + p')^2} \right\} \psi(p') = E\psi(p_i). \end{aligned} \quad (\text{G.8})$$

One convinces oneself easily, that the second term in the squared bracket, multiplied by a function  $g(p_i, p_j)$  generating better convergence, nullifies this bracket as  $p_i = p_j$ .

---

<sup>2</sup>For a proof see [73] or [92, Appendix C].

### G.3. Coulomb trick

---

For  $N \rightarrow \infty$  it is compensated exactly by the additional integral expression. It must hold

$$g(p, p) = 1.$$

Since the ground state wavefunction is known, one sets for instance

$$g(p, p') = \frac{(1 + p^2)^2}{(1 + p'^2)^2}.$$

The integral in (G.8), the *continuous part* of the Coulomb trick, will in general not be solvable analytically. It suffices instead, to evaluate it numerically with a much higher precision than achieved by doing the sum, *i.e.* the *discrete part*. Here, we obtain the function

$$f(p, p') = \ln \left\{ \frac{(p_i - p_j)^2}{(p_i + p_j)^2} \right\} [\psi(p_j) - g(p_i, p_j)\psi(p_i)].$$

It can be continued continuously into  $p = p'$  and therefore is integrable numerically much easier than the original function. There are even possibilities of improving this method [98]. The matrix is no longer symmetric. We substitute

$$\phi(p_i) := \sqrt{w_i} p_i \psi(p_i)$$

and obtain finally

$$p_i^2 \phi(p_i) + \frac{1}{\pi} \sum_{j=1}^N \sqrt{w_i w_j} \ln \left\{ \frac{(p_i - p_j)^2}{(p_i + p_j)^2} \right\} \phi(p_j) + (\text{Coulomb-Counterterms}) = E \phi(p_i).$$

The result of the manipulations is a considerable improvement of convergence, documented in Ref. [24].

# Appendix H

## Listing of the computer code

To render the verification of the results of the present work possible and to demonstrate the implementation of the techniques described throughout the text *in praxi*, we show the listing of the program, written in C.

### H.1 Description of the program

The program `Mesonix`<sup>1</sup> is constructed in a modular fashion, *i.e.* one problem corresponds to one subroutine. The whole program consists of the below parts or subroutines:

- `meta_mesonix`: This part of the program was written to render its application more convenient for the user. An input file for the main program `mesonix` is created. It contains all parameters, such as cutoff, fermion mass, number of integration points, etc. Furthermore, small program tools are supplied, which enable subsequent calls of `mesonix` to be handled directly. The function `vary_J_z`, for example, was created to calculate the spectra for different values of  $J_z$  at a fixed discretization.
- `mesonix`: The main program calls the subroutines according to the parameters of the input file `input.dat`.
- `numerix`: Using the NAGLIB-Routine `d01bcf` [99], the abscissae and weights for the numerical integrations are obtained using the Gauss-Legendre algorithm.
- `coulomb_trix`: Here, the calculation and initialization of the counterterms of the Coulomb trick are processed. It decides whether the results of a former calculation are read in from a file, or if they are (re-)calculated for a different set of parameters.

---

<sup>1</sup>Mnemonic for *mesonics*=“anything, concerning mesons”, like *numerics*=“anything, concerning the numeric aspects”. Here, a meson is defined as a fermion-antifermion system.

## H.1. Description of the program

---

- **genetix**: This routine governs the construction of the *symmetrized* Hamiltonian matrix. By using the charge conjugation symmetry  $\mathcal{C}$  and the combined parity and time reversal symmetry  $\mathcal{H}$ , four matrices which describe the interaction between the eigenstates of these symmetries, are generated.
- **asymmetrix** Analogously, this procedure governs the construction of the *unsymmetrized* Hamiltonian matrix. In the case  $J_z \neq 0$  the parity and time reversal operation is not a symmetry any more. A special treatment is necessary, which increases the numerical effort enormously.
- **physix**: The matrix elements are calculated by evaluating the function listed in the helicity tables of Appendix F. The Coulomb counterterms are introduced when all quantum numbers of the incoming and the outgoing states are identical.
- **arithmetix**: With help of the NAGLIB routine `f02abf` [99], the Hamiltonian matrix is diagonalized and the spectrum, as well as the wavefunctions are calculated and sorted (`m01caf`). It is possible to store the wavefunctions. For this, they are translated into the original normalization.
- **publix**: This routine formats and outputs the results.

All global variables are explained in the listing. The program is written in standard C, but makes no excessive use of typical C structures and should consequently be understandable to readers familiar with FORTRAN.



## Meta\_mesonix

```

/*****/
/*
/* Program      :      M E T A _ M E S O N I X
/*
/* Class       :      Main program
/*
/* Purpose     :      META_MESONIX calls MESONIX and manipulates the
/*                   input file to vary different outer parameters
/*                   via INPUT_MES.DAT.
/*
/*****/

#include <stdio.h>
#include <math.h>

double alpha;
char default_directory[80]="OUTPUT/";
char special_id[80]="_";
char *name;
FILE *fp;

void create_file(double beta, double lambda, int n1, int n2, int number,
int J_z, int trix)
/* create input file for 'mesonix.c' */
{
    double m;
    int test,Anni,print_EF;
    char *name_in = "Input_mes.dat";
    FILE *fp;

    m = 1.0; /* fermion mass */
    test = 1; /* test variable */
    Anni = 0; /* control for incl./excl. of annihilation graph */
    print_EF = 0; /* control for writing the eigenfunctions in file */

    if (J_z!=0) test += 4096; /* asymmetric case */

    fp = fopen(name_in,"w");
    fprintf(fp,"-----\n");
    fprintf(fp,"MESONIX_input_file\n");
    fprintf(fp,"-----\n\n");
    fprintf(fp,"fermion_mass=\n");
    fprintf(fp," %18.12f\n",m);
    fprintf(fp,"cut-off=\n");
    fprintf(fp," %18.12f\n",lambda);
    fprintf(fp,"coupling=\n");
    fprintf(fp," %18.12f\n",beta);
    fprintf(fp,"test=\n");
    fprintf(fp," %3d\n",test);
    fprintf(fp,"J_z=\n");
    fprintf(fp," %3d\n",J_z);
    fprintf(fp,"Anni=\n");
    fprintf(fp," %3d\n",Anni);
    fprintf(fp,"N1=\n");
    fprintf(fp," %3d\n",n1);
    fprintf(fp,"N2=\n");
    fprintf(fp," %3d\n",n2);
    fprintf(fp,"number_EV=\n");
    fprintf(fp," %3d\n",number);
    fprintf(fp,"trix=\n");
    fprintf(fp," %3d\n",trix);
    fprintf(fp,"default_directory=\n");
    fprintf(fp," %s\n",default_directory);
}

```

## H.1. Description of the program

---

```
fprintf(fp,"special_id=\n");
fprintf(fp," %s\n",special_id);
fprintf(fp,"print_EF=\n");
fprintf(fp," %3d\n",print_EF);
fprintf(fp,"-----\n");
fclose(fp);
}

void vary_coupling(int nn,int N)
/* vary the coupling ALPHA: N1=N2=nn, */
{
    int i,j,k;
    double alpha;
    FILE *f_in,*f_out;
    char *name_out = "EVs_couplinx.dat";

    f_out = fopen(name_out,"w");
    fclose(f_out);
    for (i=1; i<=N; ++i)
    {
        f_in = fopen(name,"w"); /* create output file for MESONIX */
        fclose(f_in);
        alpha = 10.0*i/N;
        printf("META_MESONIX: ALPHA = %8.5f\n\n",alpha);
        create_file(alpha,1.0,nn,nn,10,0,1);
        system("mesonix.out");
        f_in = fopen(name,"r");
        f_out = fopen(name_out,"a");
        fscanf(f_in,"%d",&k);
        fprintf("k= %3d\n",k);
        fprintf(f_out,"%18.12f\n",alpha);
        for (j=1; j<=10; ++j)
        {
            fscanf(f_in,"%lf",&alpha);
            printf("EW = %18.12f\n",alpha);
            fprintf(f_out,"%18.12f\n",alpha);
        }
        fclose(f_in);
        fclose(f_out);
    }
}

void vary_N(int begin_step, int end_step, int J_z)
/* vary number of mesh points from <begin_step> to <end_step> */
{
    int i;

    sprintf(name,"%sEigenValues/EVs%sJ%d.dat",
            default_directory,special_id,J_z);
    printf("%s\n",name);

    fp = fopen(name,"w"); /* create output file for MESONIX */
    fclose(fp);

    for (i=begin_step; i<=end_step; i+=2)
    {
        printf("\n\nMETA_MESONIX: N1 = %3d, N2 = %3d\n",i,i);
        create_file(alpha,1.0,i,i,500,J_z,0);
        system("mesonix.out");
    }
}

void special_case(double lambda, int n1, int n2, int J_z)
/* different N1, N2 */
{
```

## Appendix H. Listing of the computer code

---

```
int i;

sprintf(name, "%sEigenValues/EVs%sJ%d.dat",
        default_directory, special_id, J_z);
printf("%s\n", name);

fp = fopen(name, "w");      /* create output file for MESONIX */
fclose(fp);
printf("\n\nMETA_MESONIX:  N1 = %3d, N2 = %3d\n", n1, n2);
create_file(alpha, lambda, n1, n2, 500, J_z, 0);
system("mesonix.out");
}

void Coulomb_J_z(int end_step, int max_n)
/* calculate Coulomb counterterms */
{
    int i;

    for (i=0; i<=max_n; ++i)
    {
        printf("\n\nMETA_MESONIX:  J_z = %3d\n", i);
        sprintf(name, "%sEigenValues/EVs%sJ%d.dat",
                default_directory, special_id, i);
        fp = fopen(name, "w");      /* create output file for MESONIX */
        fclose(fp);

        create_file(alpha, 1.0, end_step, end_step, 500, i, 1);
        system("mesonix.out");
        if (i>1)
        {
            printf("\nMETA_MESONIX:  J_z = %3d\n", i);
            sprintf(name, "%sEigenValues/EVs%sJ%d.dat",
                    default_directory, special_id, -i);
            fp = fopen(name, "w");      /* create output file for MESONIX */
            fclose(fp);

            create_file(alpha, 1.0, end_step, end_step, 500, -i, 1);
            system("mesonix.out");
        }
    }
}

void special_Coulomb_J_z(int N1, int N2, int J_z)
/* calculate Coulomb counterterms for special case: (N1,N2,J_z) */
{
    printf("\n\nMETA_MESONIX:  J_z = %3d\n", J_z);
    create_file(alpha, 1.0, N1, N2, 500, J_z, 1);
    system("mesonix.out");
}

void vary_J_z(int begin_N, int end_N, int max_n)
/* vary J_z from -max_n till +max_n */
{
    int i;

    for (i=0; i<=max_n; ++i)
    {
        printf("\n\nMETA_MESONIX:  J_z = %3d\n", i);
        vary_N(begin_N, end_N, i);
        if (i>0)
        {
            printf("META_MESONIX:  J_z = %3d\n", -i);
            vary_N(begin_N, end_N, -i);
        }
    }
}
```

## H.1. Description of the program

---

```
}

double Lambda(int scale, int n)
/* returns Lambda in different scales, n=1..10 */
{
    switch (scale)
    {
        case 0: return n*1.0*6.0*alpha; break; /* Krautgaertner scale */
        case 1: return n; break; /* linear scale */
        case 2: return (15.0+5.0*n); /* linear till 65 scale*/
                break;
    }
    return 1.0; /* default */
}

void create_envirnement()
/* create directories for output */
{
    FILE *fp;

    printf("\nMETA-MESONIX-----\n\n");
    fp = fopen("create_dir","w"); /* create file testing if dir. exists */
    fprintf(fp,"if [ ! -d $1 ] \nthen mkdir $1\n");
    fprintf(fp,"echo \"create_dir: Directory '$1' created.\"\n");
    fprintf(fp,"else echo \"create_dir: Directory '$1' exists!\" \nfi");
    fclose(fp);
    name=(char *)malloc(80);
    sprintf(name,"/bin/bash create_dir %s",default_directory);
    system(name);
    sprintf(name,"/bin/bash create_dir %s%s",default_directory,
            "EigenValues/");
    system(name);
    sprintf(name,"/bin/bash create_dir %s%s",default_directory,
            "EigenFunctions/");
    system(name);
    sprintf(name,"/bin/bash create_dir %s%s",default_directory,
            "Coulomb_Trick/");
    system(name);
    system("rm -f create_dir"); /* remove batch file */
    sprintf(name,"%smesonix.log",default_directory);
    printf("Creating '%s'...\n",name);
    fp = fopen(name,"w"); /* create LOG file for MESONIX */
    fclose(fp);
    printf("-----\n\n");
}

void vary_Lambda(int J_z)
/* vary cutoff Lambda */
{
    int i,n1,n2;
    double cutoff;

    n1 = 41;
    n2 = 11;
    for (i=1; i<=5; ++i)
    {
        cutoff=Lambda(0,i);
        printf("\nMETA_MESONIX: Lambda = %10.8f\n",cutoff);
        sprintf(special_id,"_L%1d-",i-1);
        printf("%s\n",special_id);
        create_file(alpha,cutoff,n1,n2,500,J_z,1); /* Coulomb terms */
        system("mesonix.out");
        special_case(cutoff,n1,n2,J_z); /* N1!=N2 */
    }
    for (i=6; i<=10; ++i)
```

## Appendix H. Listing of the computer code

---

```
{
    cutoff=Lambda(0,i);
    printf("\n\nMETA_MESONIX:   Lambda = %10.8f\n",cutoff);
    sprintf(special_id,"_L%1d_",i-1);
    printf("%s\n",special_id);
    create_file(alpha,cutoff,n1,n2,500,J_z,1); /* Coulomb terms */
    system("mesonix.out");
    special_case(cutoff,n1,n2,J_z);          /* N1!=N2 */
}
for (i=1; i<=10; ++i)
{
    cutoff=Lambda(2,i);
    printf("\n\nMETA_MESONIX:   Lambda = %10.8f\n",cutoff);
    sprintf(special_id,"_LX%1d_",i-1);
    printf("%s\n",special_id);
    create_file(alpha,cutoff,n1,n2,500,J_z,1); /* Coulomb terms */
    system("mesonix.out");
    special_case(cutoff,n1,n2,J_z);          /* N1!=N2 */
}
}

void Lambda20(int J_z)
/* calculate for Lambda=20 m_f, N1=41, N2=11 */
{
    int n1=41;
    int n2=11;
    double cutoff=20.0;

    sprintf(special_id,"_l20n4711_");
    printf("%s\n",special_id);
    create_file(alpha,cutoff,n1,n2,500,J_z,1); /* Coulomb terms */
    system("mesonix.out");
    special_case(cutoff,n1,n2,J_z);          /* N1!=N2 */
}

void main()
{
    alpha = 1.0/137.0359895; /* coupling constant */
    alpha = 0.3;

    create_environelement(); /* create directories for output */
    Coulomb_J_z(21,3); /* calc. counterterms */
    vary_N(5,21,0); /* calc spectra as func. of N, J_z=0,...,3*/
    vary_N(5,21,1);
    vary_N(5,21,2);
    vary_N(5,21,3);
    vary_Lambda(0); /* calculate spec. for Lambda= 1,..,55 m_f*/
}
```

# Mesonix

```

/*****
/*
/* Program      :      M E S O N I X
/*
/* Class       :      Main program
/*
/* Purpose     :      MESONIX calculates the eigenstates and -values
/*                    of a system consisting of two particles with
/*                    same mass, i.e. of mesons.
/*
/*
/*****

/*****
/*
/* Structure of the code :      M E S O N I X
/*                    =====
/*
/*          MAIN PRG          SUBROUTINES          SUB-SUBROUTINES
/*          -----          -
/*
/*          main -----> NUMERIX
/*                    |
/*                    |-----> COULOMB_TRIX
/*                    |
/*                    |-----> GENETIX  -----> PHYSIX
/*                    |
/*                    |-----> ASYMMETRIX -----> PHYSIX
/*                    |
/*                    |-----> CALCULATIX
/*                    |
/*                    |-----> PUBLIX
/*
/*
/*****
/*
/* Description of the subroutines :
/* -----
/*
/*          NUMERIX      calculates the weights and abscissae for the
/*                    numerical integration
/*
/*          COULOMB_TRIX calculates/initializes the Coulomb counter terms
/*
/*          GENETIX      generates the Hamilton matrix
/*
/*          PHYSIX       provides the single matrix elements
/*
/*          CALCULATIX   diagonalizes the matrix and sorts eigenvalues
/*
/*          PUBLIX       controls the output of data
/*
/*
/*****
/*
/* Outer Parameters:
/* -----
/*
/*          J_z          = n   ; z component of total angular momentum
/*
/*          Anni         = 0/1 ; omit/include annihilation graph
/*
/*          trix         = 0/1 ; read in from file / calculate Coulomb term
/*
/*          number_EV    = m   ; write m eigenvalues in file 'EVs_Jn.dat'
/*

```

## Appendix H. Listing of the computer code

---

```
/*
/*   print_EF   = 0/1 ; do not write/do write eigenfunctions in file
/*               'EFunc_X.dat'
/*
/*=====*/
/*
/*
/*   Test Facilities of the Program :
/* -----
/*
/* bit    condition    action
/* -----
/*
/* all test    == 0    nothing will be tested
/*
/* 0 (test & 1)!= 0    NUMERIX will write the abscissae and weights of
/* the numerical integration into the file
/* 'gauss_vals.dat'
/*
/* 1 (test & 2)!= 0    GENETIX will write a off-diagonal spin table
/* in "SPIN-TABLE_MES.DAT"
/*
/* 2 (test & 4)!= 0    PUBLIX will write the eigenvalues of the block
/* matrices in EV_1_MES.DAT, EV_2_MES.DAT,
/* EV_3_MES.DAT, EV_1_MES.DAT respectively.
/*
/* *12 (test &4096)!=0    Supress the symmetries, use ASYMMETRIX
/*
/*=====*/

#include <malloc.h>
#include <stdio.h>
#include <math.h>
#include <unistd.h>
#include <signal.h>

#define PI 3.141592653589793
#define NN1 41                /* max. # of integr.points (mu) */
#define NN2 21                /* max. # of integr.points (theta) */
#define np 1                  /* constant for 'd01alf', etc. */
#define lp 4000               /* constant for 'd01alf', etc. */
#define lip 2000              /* constant for 'd01alf', etc. */
#define N_sym_1 2*(N1*N2)+2*N1 /* dimensions of blocks (symmetrix)*/
#define N_sym_2 2*(N1*N2)+2*N1
#define nagtest 1             /* use NAGLib for diag if !=0 */
#define old_CT 0              /* use old(=Krautgaertner) Coulomb */
                               /* trick if != 0 */

/* =====>          external functions          <===== */

extern long time();
/* time measurements */

extern double f02abf_( double *A, int *IA, int *NP, double *R, double *V,
                      int *IV, double *E, int *IFAIL);
/* diagonalization routine from NAGLib*/

extern double Coulomb_trick_function(double *);
/* Continous Coulomb counterterm, dependend on (mu,theta) */

extern double Coulomb_trick_integrand(double *);
/* Continous Coulomb counterterm, integrated over (theta), dependent on (mu) */

extern double Coulomb_discrete(int jm, int s1, int s2);
```

## H.1. Description of the program

---

```
/* Discrete Coulomb counterterm, dependend on spins and mu[jm] */

extern double integrand(double *);
/* Krautgartner continous Coulomb counterterm, analytically integrated over */
/* (theta), dependent on (mu) */

extern double old_continous(int jm, int jt);
/* Krautgartner continous Coulomb counterterm */

/* =====>      global variables      <===== */

double m,lambda,ALPHA,p_bohr; /* mass, cut-off, coupling, Bohr momentum */
double aa,A,B,V_seag; /* variables used in 'physix' and 'genetix' */
double x[3],k[3]; /* old variables (x,k) instead (mu,theta) */
double *mu,*wmu; /* mu: abscissae and weights for Gauss-Legendre */
double *theta,*wtheta; /* cos(theta): " " Gauss-Legendre */
double *ma,*r,*v,*e; /* variables for NAGLIB diagonalization */
double *mat_1,*r_1,*v_1,*e_1; /* variables for NAGLIB diagonalization */
double *mat_2,*r_2,*v_2,*e_2; /* variables for NAGLIB diagonalization */
double *mat_3,*r_3,*v_3,*e_3; /* variables for NAGLIB diagonalization */
double *mat_4,*r_4,*v_4,*e_4; /* variables for NAGLIB diagonalization */
double mu_global; /* Coulomb trick:global variable for C_T_function*/
double CT[4][NN1][NN2]; /* matrix for Coulomb data, first index is */
/* n = uu,ud,du,dd */

int J_z,test,N1,N2,steps,Anni; /* OUTER parameters,read in from file */
int trix,number_EV,print_EF; /* OUTER parameters,read in from file */
int EV_number; /* arithmetix: number of eigenfunction */
int IndexMatrix; /* arithmetix.c */
int IndexMat[4]; /* arithmetix.c */
int jj1,jj2; /* global variables for Coulomb trick */
int spins_parallel,spin_1; /* Coulomb trick: choose function G1 <-> G2 */
int J_z_Coulomb; /* auxiliary variable for Coulomb trick */
long time1,time2; /* var. for time measurements */
char *order; /* for NAGLib routine m01caf */
char *name_EV; /* name of file containing the eigenvalues */
char *name_log; /* name of LOG file */
char *default_directory[80]; /* read in by logix, def. dir. for output */
char *special_id[80]; /* read in by logix, special ident. for output*/
char *CT_name[4]; /* names for the Coulomb trick files */
FILE *f_log; /* File variable for 'log' file */

/* =====>      functions for error handling      <===== */

void nrerror(char error_text[])
/* standard error handler */
{
    fprintf(stderr,"Numerical Recipes run-time error...\n");
    fprintf(stderr,"%s\n",error_text);
    fprintf(stderr,"...now exiting to system...\n");
    exit(1);
}

/* =====>      functions for (de)allocation      <===== */

double *dvector(long nl, long nh)
/* allocate a double vector with subscript range v[nl..nh] */
{
    double *v;

    v=(double *)malloc((size_t) ((nh-nl+1)*sizeof(double)));
    if (!v) nrerror("allocation failure in dvector()");
    return v-nl+1;
}
```



## Appendix H. Listing of the computer code

---

```
void free_dvector(double *v, long nl, long nh)
/* free a double vector allocated with dvector() */
{
    free((char*) (v+nl-1));
}

/* =====>    inclusion of subroutines    <===== */

#include "numerix.c"
#include "physix.c"
#include "genetix.c"
#include "coulomb_trix.c"
#include "arithmetix.c"
#include "publix.c"
#include "asymmetrix.c"

/* =====>    functions used for initalization    <===== */

void init_ma(int dim)
/* initialize matrix for asymmetric NAGLib diagonalization */
{
    ma = dvector(0,dim*dim - 1);
    e  = dvector(0, dim-1);
    r  = dvector(0, dim-1);
    v  = dvector(0, dim*dim - 1);
    IndexMatrix = 0;
}

void init_mat(int dim1, int dim2, int dim3, int dim4)
/* initialize matrices 1-4 for symmetric NAGLib diagonalization */
{
    int i;

    for (i=0; i<=3; ++i) IndexMat[i] = 0;

    mat_1 = dvector(0,dim1*dim1 - 1);
    e_1   = dvector(0, dim1-1);
    r_1   = dvector(0, dim1-1);
    v_1   = dvector(0, dim1*dim1 - 1);

    mat_2 = dvector(0,dim2*dim2 - 1);
    e_2   = dvector(0, dim2-1);
    r_2   = dvector(0, dim2-1);
    v_2   = dvector(0, dim2*dim2 - 1);

    if (dim3>0)
    {
        mat_3 = dvector(0,dim3*dim3 - 1);
        e_3   = dvector(0, dim3-1);
        r_3   = dvector(0, dim3-1);
        v_3   = dvector(0, dim3*dim3 - 1);

        mat_4 = dvector(0,dim4*dim4 - 1);
        e_4   = dvector(0, dim4-1);
        r_4   = dvector(0, dim4-1);
        v_4   = dvector(0, dim4*dim4 - 1);
    }
}

void free_mat(int dim1, int dim2, int dim3, int dim4)
/* deallocate matrices 1-4 used for symmetric NAGLib diagonalization */
{
    free_dvector(mat_1,0,dim1*dim1-1);
    free_dvector(e_1,0,dim1-1);
}
```

## H.1. Description of the program

---

```
free_dvector(r_1,0,dim1-1);
free_dvector(v_1,0,dim1*dim1-1);

free_dvector(mat_2,0,dim2*dim2-1);
free_dvector(e_2,0,dim2-1);
free_dvector(r_2,0,dim2-1);
free_dvector(v_2,0,dim2*dim2-1);

if (dim3>0)
{
    free_dvector(mat_3,0,dim3*dim3-1);
    free_dvector(e_3,0,dim3-1);
    free_dvector(r_3,0,dim3-1);
    free_dvector(v_3,0,dim3*dim3-1);

    free_dvector(mat_4,0,dim4*dim4-1);
    free_dvector(e_4,0,dim4-1);
    free_dvector(r_4,0,dim4-1);
    free_dvector(v_4,0,dim4*dim4-1);
}
}

void free_ma(int dim)
/* deallocate matrices used for asymmetric NAGLib diagonalization */
{
    free_dvector(ma,0,dim*dim-1);
    free_dvector(e,0,dim-1);
    free_dvector(r,0,dim-1);
    free_dvector(v,0,dim*dim-1);
}

void read_input()
/* read in inputfile created by 'meta_mesonix.c' */
{
    FILE *fp;
    char *name_IN = "Input_mes.dat";
    char comment[80]; /* dummy variable to read out comments*/

    fp = fopen(name_IN,"r"); /* read in INPUT_MES.DAT */
    fscanf(fp,"%s",comment);
    fscanf(fp,"%s",comment);
    fscanf(fp,"%s",comment);
    fscanf(fp,"%s",comment);
    fscanf(fp,"%lf",&m); /* read in <fermion mass> */
    fscanf(fp,"%s",comment);
    fscanf(fp,"%lf",&lambda); /* read in <cut-off> */
    fscanf(fp,"%s",comment);
    fscanf(fp,"%lf",&ALPHA); /* read in <coupling> */
    fscanf(fp,"%s",comment);
    fscanf(fp,"%d",&test); /* read in <test variable> */
    fscanf(fp,"%s",comment);
    fscanf(fp,"%d",&J_z); /* read in <J_z> */
    fscanf(fp,"%s",comment);
    fscanf(fp,"%d",&Anni); /* read in control for annih. graph */
    fscanf(fp,"%s",comment);
    fscanf(fp,"%d",&N1); /* read in # mesh points <N1> */
    fscanf(fp,"%s",comment);
    fscanf(fp,"%d",&N2); /* read in # mesh points <N2> */
    fscanf(fp,"%s",comment);
    fscanf(fp,"%d",&number_EV); /* read in # of EVs written in file */
    fscanf(fp,"%s",comment);
    fscanf(fp,"%d",&trix); /* read in control for Ctrick ab initio*/
    fscanf(fp,"%s",comment);
    fscanf(fp,"%s",default_directory); /* read in <default directory> */
    fscanf(fp,"%s",comment);
}
```

## Appendix H. Listing of the computer code

---

```
fscanf(fp,"%s",special_id); /* read in <special identification> */
fscanf(fp,"%s",comment);
fscanf(fp,"%s",&print_EF); /* read in control for writing */
/* eigenfctns in file */

fclose(fp);
name_EV = (char *)malloc(120);
sprintf(name_EV,"%sEigenValues/EVs%sJ%d.dat",
        default_directory,special_id,J_z); /* create filename for EVs */
}

void logix()
/* write LOG file */
{
    name_log = (char *)malloc(120); /* name for LOG file */
    sprintf(name_log,"%smesonix.log",default_directory);
    f_log = fopen(name_log,"a");
    fprintf(f_log,"\nM E S O N I X                                LOG file\n");
    fprintf(f_log,"=====\n");
    fprintf(f_log,"PARAMETERS:\n");
    fprintf(f_log,"          m = %18.12f ; fermion mass\n",m);
    fprintf(f_log,"          lambda = %18.12f ; cut-off\n",lambda);
    fprintf(f_log,"          alpha = %18.12f ; coupling\n",ALPHA);
    fprintf(f_log,"\nOPTIONS:\n");
    fprintf(f_log,"          test = %5d ; test variable\n",test);
    fprintf(f_log,"          J_z = %5d ; ang. momentum sector\n",J_z);
    fprintf(f_log,"          Anni = %5d ; annihilation graph\n",Anni);
    fprintf(f_log,"          N1 = %5d ; number of MU values\n",N1);
    fprintf(f_log,"          N2 = %5d ; number of THETA values\n",N2);
    fprintf(f_log,"          number_EV = %5d ; number of eigenvalues\n",number_EV);
    fprintf(f_log,"\n-----\n");
    fclose(f_log);
}

void close_log_file()
/* final comment and close of LOG file */

{
    fprintf(f_log,"\n=====\n");
    fclose(f_log);
}

void allocation()
/* allocate matrices used */
{
    init_ma (4*N1*N2); /* initialize matrix for NAGLIB diag */
    if ((test&16384)!=0) init_mat(N_sym_1,N_sym_2,0,0);
    else init_mat(N1*N2,N1*N2+N1,N1*N2,N1*N2-N1);
    /* initialize matrices 1-4 for NAGLIB diag. */
    mu = dvector(1,NN1+1);
    theta = dvector(1,NN2+1);
    wmu = dvector(1,NN1+1);
    wtheta = dvector(1,NN2+1);
}

void deallocation()
/* deallocate matrices used */
{
    if ((test&16384)!=0) free_mat(N_sym_1,N_sym_2,0,0);
    else free_mat(N1*N2,N1*N2+N1,N1*N2,N1*N2-N1);
    free_ma (4*N1*N2);
}

void main()
{
    int i,j;
```

## H.1. Description of the program

---

```
FILE *fp;

printf("\nMESONIX-----\n");
read_input(); /* read in INPUT_MES.DAT */
logix(); /* write header of LOG file */
allocation(); /* allocate all objects used */
p_bohr = m*ALPHA/2; /* Bohr momentum */

if (old_CT==0 ) coulomb_trix(trix,3,N1); /* init Coulomb trick */
if (trix==0) /* if not C. trick from scratch, then ...*/
{
    fp = fopen(name_EV,"a"); /* open file for eigenvalues */
    fprintf(fp,"%3d\n",N1);
    fclose(fp);
    f_log = fopen(name_log,"a"); /* open LOG file */
    fprintf(f_log,"Time for\n");
    fclose(f_log);

    numerix(N1,N2); /* calculate weights for numerical integration */

    f_log = fopen(name_log,"a"); /* open LOG file for subroutines */
    plot_running_coupling();
    if ((test&(4096+16384)) == 0) /* J_z=0 */
    {
        genetix(); /* set up Hamilton matrix */
        arithmetix(N1*N2,N1*N2+N1,N1*N2,N1*N2-N1); /* diagonalize */
    }
    else /* J_z<>0 */
    {
        if ((test&16384) == 0) /* standard, unsymmetrized Hamiltonian */
        {
            asymmetrix(); /* set up Hamiltonian without symmetries */
            arithmetix(4*N1*N2,0,0,0);
        }
    }
    publix(); /* write eigenvalues in file */
}
close_log_file();
deallocation(); /* deallocate all objects used */
printf("\n-----\n");
}
```

## Numerix

```

/*****/
/*
/* program      :      N U M E R I X
/*
/* class       :      subroutine of MESONIX
/*
/* file name   :      "numerix.c"
/*
/* purpose    :      NUMERIX calculates the weights and abscissae
/*                    for numerical integration according to the
/*                    Gauss-Legendre-algorithm.
/*
/*-----*/
/*
/* Subroutines :      d01bcf (NAGLib) for Gauss-Legendre discretization
/*
/* Global variables :      mu[1..NN1] = abscissa values in mu direction
/*                          wmu[1..NN1] = weights in mu direction
/*                          theta[1..NN2] = abscissa values in cos(theta)
/*                          direction
/*                          wmu[1..NN2] = weights in cos(theta) direction
/*
/*****/

extern double d01bcf_( int *itype, double *a, double *b, double *c, double *d,
    int *n, double *wmu, double *mu, int *ifail);
    /* NAGLib: Gauss-Legendre discretization */

void numerix( int n1, int n2 )      /* n1 = number of mu-values
    /* n2 = number of theta-values
    /* test == 1 prints values in FILE */

/* main function: calculate weights and abscissae */
{
    int i;
    int itype, ifail;      /* for d01bcf */
    double a, b, c, d;    /* for d01bcf */
    double *weight, *abscis; /* for d01bcf */
    char *name; /* name for file in case test=1 */
    FILE *fp;

    time(&time1);
    printf("-----> NUMERIX( N1=%2d, N2 =%2d)\n",
        n1, n2);
    f_log = fopen(name_log, "a");

    /* +++++ Discretize in mu-direction, boundaries [0, lambda/2] +++++ */

    weight = dvector(0, n1-1); /* initialize fields for d01bcf */
    abscis = dvector(0, n1-1);
    itype = 0; /* parameters for d01bcf */
    a = 1/(1+lambda/2.0/p_bohr);
    b = c = d = 1.0;

    d01bcf_(&itype, &a, &b, &c, &d, &n1, weight, abscis, &ifail);
    /* Gauss-Legendre discretization */

    for (i=1; i<=n1; i++)
    {
        wmu[i] = weight[i-1]/abscis[i-1]/abscis[i-1]*p_bohr;
        mu[i] = (1/abscis[i-1]-1)*p_bohr;
    }
    free_dvector(weight, 0, n1-1);
    free_dvector(abscis, 0, n1-1);
}

```

## H.1. Description of the program

---

```
/* ==> Discretize in cos(theta)-direction, boundaries [-1,1] <== */

weight = dvector(0,n2-1);      /* initialize fields for d01bcf */
abscis = dvector(0,n2-1);
itype = 0;                    /* parameters for d01bcf */
a = -1.0;
b = c = d = 1.0;

d01bcf_(&itype, &a, &b, &c, &d, &n2, weight, abscis, &ifail);
/* Gauss-Legendre discretization */

for (i=1; i<=n2; i++)
{
    theta[i] = abscis[i-1];
    wtheta[i] = weight[i-1];
}
free_dvector(weight,0,n2-1);
free_dvector(abscis,0,n2-1);

/* =====> test==1 : write Gauss-Legendre values in a file <===== */

if ((test&1) != 0 )
{
    name = (char *)malloc(120);
    sprintf(name,"%sgauss_values.dat",default_directory); /* filename */
    fp = fopen(name,"w");
    fprintf(fp,"Gauss-Legendre integration :      MESONIX.C\n");
    fprintf(fp,"-----\n\n");
    fprintf(fp,"          mu-integration
          theta-integration\n\n");
    fprintf(fp,"  n          abscissa          weight
          abscissa          weight\n");
    fprintf(fp,"-----
          -----\n");

    for (i=1; i<=n1; i++)
    {
        fprintf(fp,"%3d |   %12.8f  %12.8f  |   %12.8f
                  %12.8f \n",i,mu[i],wmu[i],theta[i],wtheta[i]);
    }
    fprintf(fp,"-----
          -----\n");

    fclose(fp);
}

/* =====> write time used for calculation in LOG file <===== */

time(&time2);
fprintf(f_log,"          ...weights: %d sec\n",time2-time1);
fclose(f_log);
return;
}
```

## Coulomb\_trix

```

/*****
/*
/* Program      :      C O U L O M B _ T R I X
/*
/* Class       :      Subroutine
/*
/* Purpose      :      COULOMB_TRIX creates the files for MESONIX
/*                    which contain the values for the different
/*                    Coulomb tricks, for g e n e r a l J_z.
/*
/*-----
/*
/* Names of the generated files:
/*
/*          1) CTrick_J<n>_uu.dat \
/*          2) CTrick_J<n>_ud.dat \_ n = ...-2,-1,0,1,2,...
/*          3) CTrick_J<n>_du.dat /
/*          4) CTrick_J<n>_dd.dat /
/*-----
/*
/* External functions:
/* -----
/*
/*      d01alf   NAGLib integration of function with singularities
/*      d01ajf   NAGLib integration of function without sing.
/*
*****/

extern double d01alf_( double (*funktion)(double *), double *a, double *b,
                      int *npts, double points[np], double *epsabs,
                      double *epsrel,double *result, double *abserr,
                      double w[lp],int *lm, int iw[lip], int *liw,
                      int *ifail);
/* integration routine from NAGLib */

extern double d01ajf_( double (*funktion)(double *), double *a, double *b,
                      double *epsabs, double *epsrel, double *result,
                      double *abserr, double w[lp], int *lm, int iw[lip],
                      int *liw, int *ifail);
/* integration routine from NAGLib */

double old_continous(int jm, int jt)
/* old Krautgaertner Coulomb trick */
{
    int ifail,npts,iw[lip],lw,liw;
    double a,b,points[2],w[lp],abserr,epsabs,epsrel,coul_conti;

    a = 0.0;
    b = lambda/2.0;

    jj1 = jm;
    jj2 = jt;

    /* NAGLIB-ROUTINE */

    epsabs = 1e-6;
    epsrel = 1e-8;
    npts = 1;
    points[0] = mu[jm];
    liw = lip;
    lw = lp;

```

## H.1. Description of the program

---

```
    ifail = -1;

    d01alf_(integrand,&a,&b,&npts,points,&epsabs,&epsrel,
            &coul_conti,&abserr,w,&lw,iw,&liw,&ifail);
    return coul_conti;
}

double Coulomb_trick_function(double *theta_lokal)
/* continous C. trick counterterm, to be integrated over <theta> */
/* for fixed <mu> */
{
/* Parameters = global variables are:
    mu_global

    jj1,jj2
    J_z_Coulomb
    spins_parallel */
    double result,thetaa;

    thetaa = *theta_lokal;
    result = 0.0;

    x[1] = (1.0 + mu_global*thetaa/sqrt(m*m + mu_global*mu_global))/2.0;
    k[1] = mu_global*sqrt(1.0-thetaa*thetaa);
    x[2] = (1.0 + mu[jj1]*theta[jj2]/sqrt(m*m + mu[jj1]*mu[jj1]))/2.0;
    k[2] = mu[jj1]*sqrt(1.0-theta[jj2]*theta[jj2]);

    if (( fabs(x[1]-x[2]) >= 1e-8 || fabs(k[1]-k[2]) >= 1e-8 )
        && (fabs(k[1]) >= 1e-8) && (fabs(k[2]) >= 1e-8))
    {
        aa = (x[1]-x[2])*(x[1]-x[2])*m*m/2.0*(1/(1-x[2]))/(1-x[1])
            +1/x[1]/x[2]) + k[1]*k[1] + k[2]*k[2]
            + (x[1]-x[2])/2*(k[1]*k[1]*(1/(1-x[1]))-1/x[1]) -
            k[2]*k[2]*(1/(1-x[2]))-1/x[2]));

        if((aa*aa-4*k[1]*k[1]*k[2]*k[2])>0.0)
        {
            A = 1.0/sqrt( aa*aa - 4*k[1]*k[1]*k[2]*k[2] );
            B = (1.0-aa*A)/2.0;

            if (spins_parallel==1) result = G1(2,1,J_z_Coulomb);
            else result = G2(2,1,J_z_Coulomb);

            result *= 2.0*mu_global*mu_global*x[1]*(1.0-x[1])/
                sqrt(m*m + mu_global*mu_global)*
                (1+mu[jj1]*mu[jj1]*mu[jj1]/p_bohr/p_bohr/p_bohr/8.0)
                /(1+mu_global*mu_global*mu_global
                /p_bohr/p_bohr/p_bohr/8.0)/PI;
        }
    }
    return result;
}

double Coulomb_trick_integrand(double *mu_lokal)
/* C. trick counterterm, already integrated over <theta>, dependent on <mu> */
{
    /* Parameters = global variables are
        mu_global
        jj1,jj2
        J_z_Coulomb
        spins_parallel */

    int ifail,npts,iw[lp],lw,liw;
    double a,b,points[2],w[lp],abserr,epsabs,epsrel,result_coul;

```



## Appendix H. Listing of the computer code

---

```

mu_global = *mu_lokal;
a = -1.0;
b = 1.0;
epsabs = 1e-12;
epsrel = 1e-3;
npts = 1;
points[0] = theta[jj2];
liw = lip;
lw = lp;
ifail = -1;
if (fabs(mu_global - mu[jj1]) <= 1e-10)
{
    d01alf_(Coulomb_trick_function,&a,&b,&npts,points,&epsabs,
            &epsrel,&result_coul,&abserr,w,&lw,iw,&liw,&ifail);
}
else
    d01ajf_(Coulomb_trick_function,&a,&b,&epsabs,&epsrel,
            &result_coul,&abserr,w,&lw,iw,&liw,&ifail);
return result_coul;
}

double Coulomb_discrete(int jm, int s1, int s2)
/* discrete part of Coulomb trick, called by PHYSIX */
{
    int km,kt;
    double result,spinfunction;

    result = 0.0;
    for ( km = 1; km <= N1; ++km )
    {
        for ( kt = 1; kt <= N2; ++kt )
        {
            x[1] = (1.0 + mu[km]*theta[kt]/sqrt(m*m + mu[km]*mu[km]))/2.0;
            k[1] = mu[km]*sqrt(1.0-theta[kt]*theta[kt]);

            if ( fabs(x[1]-x[2]) >= 1e-8 || fabs(k[1]-k[2]) >= 1e-8 )
            {
                aa = (x[1]-x[2])*(x[1]-x[2])*m*m/2.0*(1/(1-x[2]))/(1-x[1])
                    +1/x[1]/x[2]) + k[1]*k[1] + k[2]*k[2]
                    + (x[1]-x[2])/2*(k[1]*k[1]*(1/(1-x[1]))-1/x[1]) -
                    k[2]*k[2]*(1/(1-x[2]))-1/x[2]));
                A = 1.0/sqrt( aa*aa - 4*k[1]*k[1]*k[2]*k[2] );
                B = (1.0-aa*A)/2.0;

                if (s1>0)
                {
                    if (s1==s2) spinfunction = -G1(2,1,J_z);
                    else spinfunction = -G2(2,1,J_z);
                }
                else
                {
                    if (s1==s2) spinfunction = -G1(2,1,-J_z);
                    else spinfunction = -G2(2,1,-J_z);
                }
                if (old_CT !=0) spinfunction = -G2(2,1,J_z);

                result += 1.0/PI*wtheta[kt]*wmu[km]*spinfunction
                    *2.0*mu[km]*mu[km]*x[1]*(1.0-x[1])
                    /sqrt(m*m + mu[km]*mu[km])*
                    (1+mu[jm]*mu[jm]*mu[jm]/p_bohr/p_bohr/p_bohr/
                    / (1+mu[km]*mu[km]*mu[km]/p_bohr/p_bohr/p_bohr/8);
            }
        }
    }
}
return result;

```

## H.1. Description of the program

---

```
}

void install_Coulomb_trick()
/* read data from 'CTrick_Jn_ss.dat' into CT[] */
{
    int i,j,k,l,lo[2],hi[2],error;
    double value;
    FILE *fp[4];

    error = 0;
    for (i=0; i<=3; ++i)
    {
        fp[i] = fopen(CT_name[i],"r");
        fscanf(fp[i],"%d",&lo[0]);
        fscanf(fp[i],"%d",&hi[0]);
        if (i>0 && (lo[1]!=lo[0] || hi[1]!=hi[0])) error = 1;
        lo[1]=lo[0];
        hi[1]=hi[0];
    }
    if (error!=0)
        printf(">>>> ERROR(install_Coulomb_trick): lo[i]!=lo[j]\n");
    if (hi[1]<N1)
        printf(">>>> ERROR(install_Coulomb_trick): hi[1] < N1\n");

    for (i=lo[1]; i<N1; i+=2) /* ignore first data until actual N1 */
    {
        for (l=0; l<=3; ++l) fscanf(fp[l],"%lf",&k);
        for (j=1; j<=i*i; ++j)
        {
            for (l=0; l<=3; ++l) fscanf(fp[l],"%lf",&value);
        }
    }
    for (l=0; l<=3; ++l) fscanf(fp[l],"%lf",&k);
    for (i=0; i<=N1-1; ++i) /* read out needed data */
        for (j=0; j<=N2-1; ++j)
        {
            for (l=0; l<=3; ++l)
            {
                fscanf(fp[l],"%lf",&value);
                CT[l][i][j] = value;
            }
        }
    for (l=0; l<=3; ++l) fclose(fp[l]);
}

void special_install_Coulomb_trick()
/* read data from 'CTrick_Jn_ss.dat' into CT[], special case */
{
    int i,j,k,l,n1[2],n2[2],error;
    double value;
    char *comment[80];
    FILE *fp[4];

    error = 0;
    for (i=0; i<=3; ++i)
    {
        fp[i] = fopen(CT_name[i],"r");
        fscanf(fp[i],"%s",comment);
        fscanf(fp[i],"%d",&n1[0]);
        fscanf(fp[i],"%d",&n2[0]);
        if (i>0 && (n1[1]!=n1[0] || n2[1]!=n2[0])) error = 1;
        n1[1]=n1[0];
        n2[1]=n2[0];
    }
    if (error!=0)
```

## Appendix H. Listing of the computer code

---

```
        printf(">>>> ERROR(install_Coulomb_trick): lo[i]!=lo[j]\n");
if (n1[1]<N1)
    printf(">>>> ERROR(install_Coulomb_trick): n1[1] < N1\n");

for (i=0; i<=N1-1; ++i) /* read out needed data */
    for (j=0; j<=N2-1; ++j)
    {
        for (l=0; l<=3; ++l)
        {
            fscanf(fp[l], "%lf", &value);
            CT[l][i][j] = value;
        }
    }
for (l=0; l<=3; ++l) fclose(fp[l]);
}

void special_coulomb_trix(int from_scratch)
/* calculate or initialize the Coulomb counterterms */
/* !!!!!!!!!!!!! special case N1!=N2 !!!!!!!!!!!!! */
/*-----*/
/* from_scratch != 0 --> really calculate the terms */
/* == 0 --> just install the trick */
{
    int i,j,l,NNN,counter;
    int ifail,npts,iw[lip],lw,liw;
    double a,b,points[2],w[lp],abserr,epsabs,epsrel,coul_result;
    FILE *fp[4];

    printf("\n                (special)\n");

    for (i=0; i<=3; ++i) /* create file names */
    {
        CT_name[i]=(char *)malloc(80);
        sprintf(CT_name[i], "%sCoulomb_Trick/sCTrick%sJ",
                default_directory, special_id);
        switch (i)
        {
            case 0: sprintf(CT_name[i], "%s%d_uu.dat", CT_name[i], J_z);
                    break;
            case 1: sprintf(CT_name[i], "%s%d_ud.dat", CT_name[i], J_z);
                    break;
            case 2: sprintf(CT_name[i], "%s%d_du.dat", CT_name[i], J_z);
                    break;
            case 3: sprintf(CT_name[i], "%s%d_dd.dat", CT_name[i], J_z);
                    break;
        }
    }
    if (from_scratch == 0) special_install_Coulomb_trick();
    else
    {
        for (i=0; i<=3; ++i) /* open file */
        {
            printf(">>>> INFO: Opening file '%s'\n", CT_name[i]);
            fp[i] = fopen(CT_name[i], "w");
        }
        for (i=0; i<=3; ++i) fprintf(fp[i], "Special:\n%2d\n%2d\n", N1, N2);

        numerix(N1, N2); /* calculate Gauss_Legendre values */

        for (i=1; i<=N1; ++i)
        {
            printf(" i = %2d\n", i);
            for (j=1; j<=N2; ++j)
            {
```

## H.1. Description of the program

---

```
printf(" j = %2d\n",j);
counter = 0;
for (l=1; l>=-1; l=-2)
  for (spins_parallel=1; spins_parallel>=-1;
       spins_parallel=-2)
  {
    J_z_Coulomb = l*J_z;
    x[2] = (1.0+mu[i]*theta[j]/sqrt(m*m+mu[i]*mu[i]))/2.0;
    k[2] = mu[i]*sqrt(1.0-theta[j]*theta[j]);
    jj1 = i;
    jj2 = j;
    a = 0.0;
    b = lambda/2.0;
    epsabs = 1e-6;
    epsrel = 1e-8;
    npts = 1;
    liw = lip;
    lw = lp;
    ifail = -1;
    points[0] = mu[i];
    if (J_z_Coulomb !=0 || l>0)
    {
      d01alf_(Coulomb_trick_integrand,&a,&b,&npts,
              points,&epsabs,&epsrel,&coul_result,
              &abserr,w,&lw,iw,&liw,&ifail);
      fprintf(fp[counter+spins_parallel*(1-l)/2],
              "%18.12f\n",coul_result);
      if (J_z_Coulomb==0)
        fprintf(fp[counter+2+spins_parallel],
                "%18.12f\n",coul_result);
    }
    ++counter;
  }
} /* j loop */
} /* i loop */
for (i=0; i<=3; ++i) fclose(fp[i]);
} /* END: from_scratch != 0 */
}
```

```
void coulomb_trix(int from_scratch, int lo_N, int hi_N)
/* calculate or initialize the Coulomb counterterms */
/*-----*/
/* from_scratch != 0 --> really calculate the terms */
/* == 0 --> just install the trick */
/* lo_N --> lowest discretization */
/* hi_N --> highest discretization */
{
  int i,j,l,n,NNN,counter;
  int ifail,npts,iw[lip],lw,liw;
  double a,b,points[2],w[lp],abserr,epsabs,epsrel,coul_result;
  FILE *fp[4];

  printf("\n-----> COULOMB_TRIX\n");

  if (N1!=N2) special_coulomb_trix(from_scratch);
  else
  {
    for (i=0; i<=3; ++i) /* create file names */
    {
      CT_name[i]=(char *)malloc(80);
      sprintf(CT_name[i],"%sCoulomb_Trick/CTrick%sJ",
              default_directory,special_id);
      switch (i)
      {
```

## Appendix H. Listing of the computer code

---

```
        case 0:printf(CT_name[i],"%s%d_uu.dat",CT_name[i],J_z);
                break;
        case 1:printf(CT_name[i],"%s%d_ud.dat",CT_name[i],J_z);
                break;
        case 2:printf(CT_name[i],"%s%d_du.dat",CT_name[i],J_z);
                break;
        case 3:printf(CT_name[i],"%s%d_dd.dat",CT_name[i],J_z);
                break;
    }
}
if (from_scratch == 0) install_Coulomb_trick();
else
{
    for (i=0; i<=3; ++i) /* open file */
    {
        printf(">>>> INFO: Opening file '%s'\n",CT_name[i]);
        fp[i] = fopen(CT_name[i],"w");
    }
    for (i=0; i<=3; ++i) fprintf(fp[i],"%2d\n%2d\n",lo_N,hi_N);
    for (n=lo_N; n<=hi_N; n+=2)
    {
        numerix(n,n); /* calculate Gauss_Legendre values */

        printf("Counterterms: n/hi_N = %2d/%2d\n",n,hi_N);
        for (i=0; i<=3; ++i) fprintf(fp[i],"%2d\n",n);
        for (i=1; i<=n; ++i)
        {
            printf("                i = %2d\n",i);
            for (j=1; j<=n; ++j)
            {
                printf("                j = %2d\n",j);
                counter = 0;
                for (l=1; l>=-1; l-=2)
                for (spins_parallel=1; spins_parallel>=-1;spins_parallel-=2)
                {
                    J_z_Coulomb = l*J_z;
                    x[2] = (1.0+mu[i]*theta[j]/sqrt(m*m+mu[i]*mu[i]))/2.0;
                    k[2] = mu[i]*sqrt(1.0-theta[j]*theta[j]);
                    jj1 = i;
                    jj2 = j;
                    a = 0.0;
                    b = lambda/2.0;
                    epsabs = 1e-6;
                    epsrel = 1e-8;
                    npts = 1;
                    liw = lip;
                    lw = lp;
                    ifail = -1;
                    points[0] = mu[i];
                    if (J_z_Coulomb !=0 || l>0)
                    {
                        d01alf_(Coulomb_trick_integrand,&a,&b,&npts,
                                points,&epsabs,&epsrel,&coul_result,
                                &abserr,w,&lw,iw,&liw,&ifail);
                        fprintf(fp[counter+spins_parallel*(1-l)/2],
                                "%18.12f\n",coul_result);
                        if (J_z_Coulomb==0)
                            fprintf(fp[counter+2+spins_parallel],
                                    "%18.12f\n",coul_result);
                    }
                    ++counter;
                }
            }
        }
    }
}
}
```

## H.1. Description of the program

---

```
        for (i=0; i<=3; ++i) fclose(fp[i]);
    } /* END: from_scratch != 0 */
} /* END: N1==N2 */
}

double integrand ( double *mu_c )
/* Krautgaertner counterterm, analytically integrated over <theta> */
/* (only used if <old_CT>!=0) */
{
    double e1,e1p,e11,f,g,h,kl,a,b,c,d,x_cc,k_cc,mu_cc;
    double xp1,xp2,xp3,xm1,xm2,xm3,abk;
    double q1,q2,q3,q4,q5;

    mu_cc = *mu_c;

    x_cc = (1.0 + mu[jj1]*theta[jj2]/sqrt(m*m + mu[jj1]*mu[jj1]))/2.0;
    k_cc = mu[jj1]*sqrt(1.0 - theta[jj2]*theta[jj2]);

    e1 = sqrt(m*m + mu[jj1]*mu[jj1]);
    e1p = sqrt(m*m + mu_cc*mu_cc);

    kl = e1p/e1 + e1/e1p;

    a = mu[jj1]*mu[jj1]*mu_cc*mu_cc*(4.0 +theta[jj2]*theta[jj2])*
        (e1p - e1)*(e1p-e1)/e1/e1p/e1/e1p);
    b = -2.0*(mu[jj1]*mu[jj1] + mu_cc*mu_cc)*mu[jj1]*mu_cc*theta[jj2]*kl;
    c = (mu[jj1]*mu[jj1] + mu_cc*mu_cc)*(mu[jj1]*mu[jj1] + mu_cc*mu_cc)
        -4.0*mu[jj1]*mu[jj1]*mu_cc*mu_cc*(1.0-theta[jj2]*theta[jj2]);
    d = m*m/(1.0 - x_cc)/x_cc/e1p + 2.0*mu_cc*mu_cc/e1p
        + k_cc*k_cc/2.0/e1p/x_cc/(1.0 - x_cc)
        + 0.5/(1.0 - x_cc)/x_cc/e1p*(mu[jj1]*mu[jj1] + mu_cc*mu_cc);
    e11 = 2.0*m*m/(1.0 - x_cc)/x_cc/e1p/e1p*mu_cc*(x_cc - 0.5)
        1.0/x_cc/(1.0 - x_cc)/e1p*
        (-mu[jj1]*mu_cc*theta[jj2]*kl*0.5 +
        (mu[jj1]*mu[jj1] + mu_cc*mu_cc)*mu_cc/e1p*(x_cc - 0.5));
    f = -2.0*mu_cc*mu_cc/e1p - 0.5*mu_cc*mu_cc/x_cc/(1.0 - x_cc)/
        e1p/e1p/e1p*k_cc*k_cc - 1.0/e1p/e1p/x_cc/(1.0 - x_cc)*
        mu_cc*(x_cc - 0.5)*mu[jj1]*mu_cc*theta[jj2]*kl;
    h = -0.5/x_cc/(1.0 - x_cc)/e1p;

    xp1 = a + b + c;
    xp2 = (mu_cc*mu[jj1]*theta[jj2]*kl - (mu[jj1]*mu[jj1] + mu_cc*mu_cc))*
        (mu_cc*mu[jj1]*theta[jj2]*kl - (mu[jj1]*mu[jj1] + mu_cc*mu_cc));
    xp3 = fabs(mu_cc*mu[jj1]*theta[jj2]*kl-(mu[jj1]*mu[jj1] + mu_cc*mu_cc));

    xm1 = a - b + c;
    xm2 = (mu_cc*mu[jj1]*theta[jj2]*kl + (mu[jj1]*mu[jj1] + mu_cc*mu_cc))*
        (mu_cc*mu[jj1]*theta[jj2]*kl + (mu[jj1]*mu[jj1] + mu_cc*mu_cc));
    xm3 = fabs(mu_cc*mu[jj1]*theta[jj2]*kl + (mu[jj1]*mu[jj1]
        + mu_cc*mu_cc));

    if ( (2.0*sqrt(a)*xm3 - 2.0*a + b == 0)
        ||(2.0*sqrt(a)*xp3 + 2.0*a + b == 0)) return 0;
    else
    {
        abk = 1.0/sqrt(a)*log(fabs((2.0*sqrt(a)*xp3 + 2.0*a + b)
            /(2.0*sqrt(a)*xm3 - 2.0*a + b)));
        return -1.0/PI*

```

```

        (d*abk*mu_cc*mu_cc + e11*mu_cc*mu_cc/a
        *(sqrt(xp2) - sqrt(xm2) - 0.5*b*abk)
        +f*((mu_cc*mu_cc*0.5/a - 0.75*b*mu_cc*mu_cc/a/a)*sqrt(xp2)
        -(-mu_cc*mu_cc*0.5/a - 0.75*b*mu_cc*mu_cc/a/a)*sqrt(xm2)
        +(3.0*b*b - 4.0*a*c)*abk/8.0*mu_cc*mu_cc/a/a)
        + 2.0 *h*mu_cc*mu_cc)
        *(1.0+mu[jj1]*mu[jj1]*mu[jj1]/p_bohr/p_bohr/p_bohr/8.0)
        /(1.0+mu_cc*mu_cc*mu_cc/p_bohr/p_bohr/p_bohr/8.0);
    }
}

```

## Genetix

```

/*****
/*
/* program      :      G E N E T I X
/*
/* class       :      subroutine of MESONIX
/*
/* file name   :      "genetix.c"
/*
/* purpose    :      GENETIX generates the Hamilton matrix of the
/*                   system. It uses the subroutine PHYSIX for
/*                   calculation of the single elements.
/*
/*-----*/
/*
/* External functions:
/* -----
/*
/*   physix      subroutine of 'mesonix', calculates one matrix
/*               element
/*
/*-----*/
/*****/

void genetix()
/* create 4 Hamiltonians, symmetries C,H */
{
    int jm,jt,sj1,sj2;          /* loop variables for rows */
    int im,it,si1,si2;        /* loop variables for columns */
    int j_parity,i_parity;    /* booleans for loop end */
    double element[17];       /* matrix elements[1..16] */
    double T,Sqrt2;           /* kinetic energy, 1/sqrt(2) */
    double factor_j1,factor_j2,factor_j3; /* factors for wavefunctions */
    double factor_i1,factor_i2,factor_i3;
    int jnum_1,jnum_2,jnum_3,jnum_4; /* actual Hamiltonian row */
    int inum_1,inum_2,inum_3,inum_4; /* actual Hamiltonian column */

    time(&time1);
    printf("-----> GENETIX \n");

    Sqrt2 = 1/sqrt(2.0);

    jnum_1 = jnum_2 = jnum_3 = jnum_4 = 0;

    sj1 = si1 = 1;

    /* =====> rows of Hamiltonian <===== */

    for ( jm=1; jm <= N1; ++jm) /* loop for <mu> */
    {
        for ( jt=1; jt <= (N2+1)/2; ++jt) /* loop for <theta> */
        {

```

## H.1. Description of the program

---

```
printf("jm/N1 =%2d/%2d  jt/N2 =%2d/%2d\n",jm,N1,jt,(N2+1)/2);
for ( sj2 = -1; sj2 <= 1; sj2 += 2 ) /* loop for <spin> */
{
    factor_j1 = factor_j2 = factor_j3 = 1;

    if ( 2*jt-1 != N2 )
    {
        ++jnum_1;
        ++jnum_2;
        ++jnum_3;
        ++jnum_4;

        j_parity = 0;          /* not end of loop */
    }
    else
    {
        if (sj1 == sj2)
        {
            ++jnum_1;
            ++jnum_2;
            factor_j1 = factor_j2 = Sqrt2;
            j_parity = 1; /* end of loop && s1=s2 */
        }
        else
        {
            ++jnum_2;
            ++jnum_3;
            factor_j2 = factor_j3 = Sqrt2;
            j_parity = -1; /* end of loop && s1!=s2 */
        }
    }
}

/* =====> columns of Hamiltonian <===== */

inum_1 = inum_2 = inum_3 = inum_4 = 0;

for ( im=1; im <= N1; ++im) /* loop for <mu> */
{
    for ( it=1; it <= (N2+1)/2; ++it) /* loop for <theta> */
    {
        for ( si2 = -1; si2 <= 1; si2 += 2 ) /* loop for <spin> */
        {
            factor_i1 = factor_i2 = factor_i3 = 1;

            if ( (2*it-1) != N2 )
            {
                ++inum_1;
                ++inum_2;
                ++inum_3;
                ++inum_4;

                i_parity = 0;          /* not end of loop */
            }
            else
            {
                if (s1 == si2)
                {
                    ++inum_1;
                    ++inum_2;
                    factor_i1 = factor_i2 = Sqrt2;
                    i_parity = 1; /* end of loop && s1=s2 */
                }
                else
                {
                    ++inum_2;
                }
            }
        }
    }
}
```



## Appendix H. Listing of the computer code

---

```

        ++inum_3;
        factor_i2 = factor_i3 = Sqrt2;
        i_parity = -1; /* end of loop && s1!=s2 */
    }
}

element[1] = physix(jm,jt,sj1,sj2,im,it,si1,si2);
element[2] = physix(jm,jt,sj1,sj2,im,it,-si1,-si2);
element[3] = physix(jm,jt,sj1,sj2,im,N2+1-it,si2,si1);
element[4] = physix(jm,jt,sj1,sj2,im,N2+1-it,-si2,-si1);

element[5] = physix(jm,jt,-sj1,-sj2,im,it,si1,si2);
element[6] = physix(jm,jt,-sj1,-sj2,im,it,-si1,-si2);
element[7] = physix(jm,jt,-sj1,-sj2,im,N2+1-it,si2,si1);
element[8] = physix(jm,jt,-sj1,-sj2,im,N2+1-it,-si2,-si1);

element[9] = physix(jm,N2+1-jt,sj2,sj1,im,it,si1,si2);
element[10] = physix(jm,N2+1-jt,sj2,sj1,im,it,-si1,-si2);
element[11] = physix(jm,N2+1-jt,sj2,sj1,
                    im,N2+1-it,si2,si1);
element[12] = physix(jm,N2+1-jt,sj2,sj1,
                    im,N2+1-it,-si2,-si1);

element[13] = physix(jm,N2+1-jt,-sj2,-sj1,im,it,si1,si2);
element[14] = physix(jm,N2+1-jt,-sj2,-sj1,
                    im,it,-si1,-si2);
element[15] = physix(jm,N2+1-jt,-sj2,-sj1,
                    im,N2+1-it,si2,si1);
element[16] = physix(jm,N2+1-jt,-sj2,-sj1,
                    im,N2+1-it,-si2,-si1);

/* =====> take care of phase <===== */

if (abs(si1+si2-J_z) == 2)
{
    element[2] = -element[2];
    element[3] = -element[3];
    element[14] = -element[14];
    element[15] = -element[15];
}
if (abs(sj1+sj2-J_z) == 2)
{
    element[5] = -element[5];
    element[8] = -element[8];
    element[9] = -element[9];
    element[12] = -element[12];
}
if ((abs(si1+si2-sj1-sj2) == 2) ||
    (abs(sj1+sj2-sj1-sj2) == 3))
{
    element[6] = -element[6];
    element[7] = -element[7];
    element[10] = -element[10];
    element[11] = -element[11];
}

/* Kinetic energy is diagonal */

T = 4*(mu[im]*mu[im] + m*m);

if ( (j_parity >= 0) && (i_parity >=0) )
/* CH = ++ */
{
    mat_1[IndexMat[0]] = ALPHA/4*factor_j1*factor_i1*
    (

```

## H.1. Description of the program

---

```
        element[1] + element[2] - element[3] - element[4]
    + element[5] + element[6] - element[7] - element[8]
    - element[9] - element[10] + element[11] + element[12]
    - element[13] - element[14] + element[15] + element[16]
    );
    if ( jnum_1 == inum_1 ) mat_1[IndexMat[0]] += T;
    ++IndexMat[0];
}

mat_2[IndexMat[1]] = ALPHA/4*factor_j2*factor_i2*
/* CH = +- */
(
    element[1] - element[2] - element[3] + element[4]
    - element[5] + element[6] + element[7] - element[8]
    - element[9] + element[10] + element[11] - element[12]
    + element[13] - element[14] - element[15] + element[16]
);
if ( jnum_2 == inum_2 ) mat_2[IndexMat[1]] += T;
++IndexMat[1];

if ( (j_parity <= 0) && (i_parity <=0) )
/* CH = -+ */
{
    mat_3[IndexMat[2]] = ALPHA/4*factor_j3*factor_i3*
    (
        element[1] + element[2] + element[3] + element[4]
        + element[5] + element[6] + element[7] + element[8]
        + element[9] + element[10] + element[11] + element[12]
        + element[13] + element[14] + element[15] + element[16]
    );
    if ( jnum_3 == inum_3 ) mat_3[IndexMat[2]] += T;
    ++IndexMat[2];
}
if ( (j_parity == 0) && (i_parity ==0) )
/* CH = -- */
{
    mat_4[IndexMat[3]] = ALPHA/4*
    (
        element[1] - element[2] + element[3] - element[4]
        - element[5] + element[6] - element[7] + element[8]
        + element[9] - element[10] + element[11] - element[12]
        - element[13] + element[14] - element[15] + element[16]
    );
    if ( jnum_4 == inum_4 ) mat_4[IndexMat[3]] += T;
    ++IndexMat[3];
}
} /* three column loops: <spin>,<theta>,<mu> */
}
} /* three row loops: <spin>,<theta>,<mu> */
}
}
time(&time2);
fprintf(f_log,"          ...matrix: %d sec\n",time2-time1);
return;
}
```

## Asymmetrix

```

/*****
/*
/* program      :      A S Y M M E T R I X
/*
/* class       :      subroutine of MESONIX
/*
/* file name    :      "asymmetrix.c"
/*
/* purpose     :      ASYMMETRIX generates the Hamilton matrix of the
/*                    system, but WITHOUT any use of symmetries. It is
/*                    as well a test case for the KRAUT code, as a first
/*                    step to the J_z<>0 case, which has OTHER symmetry
/*                    properties. It uses the subroutine PHYSIX for
/*                    calculation of the single elements.
/*
/*-----
/*
/* External functions:
/* -----
/*
/*   physix      subroutine of 'mesonix', calculates one matrix
/*               element
/*
/*****

void asymmetrix()
/* create Hamiltonian, no symmetries */
{
    int jm,jt,sj1,sj2; /* loop variables for rows */
    int im,it,si1,si2; /* loop variables for columns */
    double T; /* kinetic energy */
    int j_num,i_num; /* actual Hamiltonian row/column */

    printf("-----> ASYMMETRIX\n");
    j_num = 0;
    IndexMatrix = 0;

    /* =====> rows of Hamiltonian <===== */

    for ( jm=1; jm <= N1; ++jm) /* loop for <mu> */
    {
        for ( jt=1; jt <= N2; ++jt) /* loop for <theta> */
        {
            printf("jm/N1 =%2d /%2d, jt/N2=%2d /%2d\n",jm,N1,jt,N2);

            for ( sj1 = -1; sj1 <= 1; sj1 += 2 ) /* loop for <spin1> */
            {
                for ( sj2 = -1; sj2 <= 1; sj2 += 2 ) /* loop for <spin2> */
                {
                    i_num = 0;
                    ++j_num;

                /* =====> columns of Hamiltonian <===== */

                for ( im=1; im <= N1; ++im) /* loop for <mu> */
                {
                    for ( it=1; it <= N2; ++it) /* loop for <theta> */
                    {
                        for ( si1 = -1; si1 <= 1; si1 += 2 ) /* loop for <spin1> */
                        {
                            for ( si2 = -1; si2 <= 1; si2 += 2 ) /* loop for <spin2> */
                            {

```

## H.1. Description of the program

---

```
        ++i_num;
        ma[IndexMatrix] = ALPHA*physics(jm,jt,-sj1,-sj2,im,it,-si1,-si2);
        if ( j_num == i_num ) ma[IndexMatrix] += 4*(mu[im]*mu[im] + m*m);
        ++IndexMatrix; /* matrix element counter */

        } /* four column loops: <spin2>,<spin1>,<theta>,<mu> */
    }
}
} /* four row loops: <spin2>,<spin1>,<theta>,<mu> */
}
}
}
return;
}
```

## Physix

```

/*****/
/*
/* program      :    P H Y S I X
/*
/* class       :    sub-subroutine of MESONIX, subroutine of GENETIX
/*
/* file name   :    "physix.c"
/*
/* purpose    :    PHYSIX calculates one single element of the
/*                  Hamilton matrix of the system.
/*                  Takes care of singularities with Coulomb trick.
/*
/*
/*****/

double Int(int n)
/* the formula for the integral over cos(nx)/(a+b cos(x))*/
{
    double vz;

    vz=1.0;
    if (n%2==0) vz = -1.0;
    return vz*pow(A,1.0-n)*pow(B/k[1]/k[2],1.0*n);
}

double G1(int j, int i, int n)
/* diagonal matrix element, parallel spins */
{
    double help;

    if ( (k[i]==0) && (k[j]==0) ) help = 0.0;
    else
    {
        help = m*m*(1.0/x[i]/x[j]+1/(1-x[j])/(1-x[i]))*Int(abs(1-n))
            + k[i]*k[j]/x[j]/x[i]/(1-x[j])/(1-x[i])*Int(abs(n));
    }
    return help;
}

double G2(int j, int i, int n)
/* diagonal matrix element, anti-parallel spins */
{
    double help;

    help = 1/x[i]/x[j] + 1.0/(1-x[j])/(1-x[i]);
    help = (m*m*help + k[j]*k[j]/x[j]/(1-x[j])
        + k[i]*k[i]/x[i]/(1-x[i]))*Int(abs(n))+k[i]*k[j]*
        (Int(abs(1-n))/x[i]/x[j]+Int(abs(1+n))/(1-x[i])/(1-x[j]));
    return help;
}

double G3(int j, int i, int n)
/* off-diagonal matrix element */
{
    double help;

    if ( k[j]==0 ) help = 0.0;
    else help = -m/x[i]/x[j]*
        (k[i]*Int(abs(1-n))-k[j]*(1-x[i])/(1-x[j])*Int(abs(n)));
    return help;
}

double G3_star(int j, int i, int n)

```

## H.1. Description of the program

---

```
/* off-diagonal matrix element */
{
    double help;

    if ( k[j]==0 ) help = 0.0;
    else help = m/(1-x[i])/(1-x[j])*
                (k[i]*Int(abs(1-n))-k[j]*x[i]/x[j]*Int(abs(n)));
    return help;
}

double G4(int j, int i, int n)
/* off-diagonal matrix element */
{
    double help;

    help = -m*m*(x[i]-x[j])*(x[i]-x[j])/(1-x[i])/(1-x[j])
            /x[i]/x[j]*Int(abs(n));
    return help;
}

/* -----> Functions for dynamical annihilation graph <-----*/

double F1(int j, int i, int n)
/* dynamical annihilation graph: parallel spins, diagonal */
{
    double help,omega;

    help=0.0;
    if (abs(n)==1)
    {
        omega=((m*m+k[i]*k[i])/x[i]/(1.0-x[i])
                +(m*m+k[j]*k[j])/x[j]/(1.0-x[j]))/2.0;
        help=2.0*m*m/omega*(1.0/x[i]+1/(1-x[i]))*(1/x[j]+1.0/(1-x[j]));
    }
    return help;
}

double F2(int j, int i, int n)
/* dynamical annihilation graph: antiparallel spins, diagonal, I */
{
    double help,omega;

    help = 0.0;
    if (n==0) help=4.0; /* seagull graph */
    if (abs(n)==1) /* dynamic graph */
    {
        omega=((m*m+k[i]*k[i])/x[i]/(1.0-x[i])
                +(m*m+k[j]*k[j])/x[j]/(1.0-x[j]))/2.0;
        help = 2.0/omega*k[i]*k[j]/x[i]/x[j];
    }
    return help;
}

double F2_star(int j, int i, int n)
/* dynamical annihilation graph: antiparallel spins, diagonal, II */
{
    double help,omega;

    help = 0.0;
    if (n==0) help=4.0; /* seagull graph */
    if (abs(n)==1) /* dynamic graph */
    {
        omega=((m*m+k[i]*k[i])/x[i]/(1.0-x[i])
                +(m*m+k[j]*k[j])/x[j]/(1.0-x[j]))/2.0;
```

## Appendix H. Listing of the computer code

---

```
        help = 2.0/omega*k[i]*k[j]/(1.0-x[i])/((1.0-x[j]));
    }
    return help;
}

double F3(int j, int i, int n)
/* dynamical annihilation graph: spin non-diagonal */
{
    double help,omega;

help=0.0;
if (abs(n)==1)    /* dynamic graph */
{
    omega=((m*m+k[i]*k[i])/x[i]/(1.0-x[i])
+(m*m+k[j]*k[j])/x[j]/(1.0-x[j]))/2.0;
    help = 2.0*m/omega*k[i]/(1-x[i])*(1/x[j]+1.0/(1-x[j]));
}
    return help;
}

double F3_star(int j, int i, int n)
/* dynamical annihilation graph: spin non-diagonal */
{
    double help,omega;

help=0.0;
if (abs(n)==1)    /* dynamic graph */
{
    omega=((m*m+k[i]*k[i])/x[i]/(1.0-x[i])
+(m*m+k[j]*k[j])/x[j]/(1.0-x[j]))/2.0;
    help = -2.0*m/omega*k[i]/x[i]*(1/x[j]+1.0/(1-x[j]));
}
    return help;
}

double F4(int j, int i, int n)
/* dynamical annihilation graph: all spins antiparallel, non-diagonal */
{
    double help,omega;

help = 0.0;
    if (n==0) help=4.0; /* seagull graph */
if (abs(n)==1)    /* dynamic graph */
{
    omega=((m*m+k[i]*k[i])/x[i]/(1.0-x[i])+
(m*m+k[j]*k[j])/x[j]/(1.0-x[j]))/2.0;
    help = -2.0/omega*k[i]*k[j]/x[i]/(1-x[j]);
}
    return help;
}
double annihilation_spintable(int sj1, int sj2, int si1, int si2)
{
    double result;

/* Evaluation of SPIN-TABLE of dynamic annihilation graph */
/*                                     J_z == +/-1 */
/* (row-wise from top to bottom,left to right) */
/* (final is row index, initial is column index) */

result= 0.0;

if (J_z== -1)    /* 'transpose' matrix */
{
    sj1 = -sj1;
    sj2 = -sj2;
}
```

## H.1. Description of the program

---

```
        si1 = -si1;
        si2 = -si2;
    }
    if (((sj1==--1) && (sj2==--1))||((si1==--1) && (si2==--1))) return 0.0;
    else
    {
        if (sj1 > 0)          /* first and second row */
        {
            if (sj2 > 0)      /* first row */
            {
                if (si1 > 0)
                {
                    if (si2 > 0) result = F1(2,1,J_z);
                    else        result = F3(2,1,J_z);
                }
                else          result = F3_star(2,1,J_z);
            }
            else              /* second row */
            {
                if (si1 > 0)
                {
                    if (si2 > 0) result = F3_star(1,2,J_z); /* perm. */
                    else        result = F2_star(2,1,J_z);
                }
                else          result = F4(2,1,J_z);
            }
        }
        else                  /* third row */
        {
            if (si1 > 0)
            {
                if (si2 > 0) result = F3_star(1,2,J_z); /* permuted */
                else        result = F4(1,2,J_z);      /* permuted */
            }
            else              result = F2(2,1,J_z);
        }
    }
    return result;
}

double general_spintable(int sj1, int sj2, int si1, int si2)
/* spin table for J_z=n */
/* ----- */
/* (row-wise from top to bottom,left to right) */
/* (final is row index, initial is column index) */
{
    double result;

    if (sj1 > 0)          /* first and second row */
    {
        if (sj2 > 0)      /* first row */
        {
            if (si1 > 0)
            {
                if (si2 > 0) result = G1(2,1,J_z);
                else        result = G3_star(2,1,J_z);
            }
            else
            {
                if (si2 > 0) result = G3(2,1,J_z);
                else        result = 0.0;
            }
        }
        else              /* second row */
    }
```



## Appendix H. Listing of the computer code

---

```

    {
        if (si1 > 0)
        {
            if (si2 > 0) result = G3_star(1,2,J_z); /* permuted */
            else        result = G2(2,1,J_z);
        }
        else
        {
            if (si2 > 0) result = G4(2,1,J_z);
            else        result = -G3(1,2,-J_z); /* permuted */
        }
    }
}
else /* third and forth row */
{
    if (sj2 > 0) /* third row */
    {
        if (si1 > 0)
        {
            if (si2 > 0) result = G3(1,2,J_z); /* permuted */
            else        result = G4(2,1,J_z);
        }
        else
        {
            if (si2 > 0) result = G2(2,1,-J_z);
            else        result = -G3_star(1,2,-J_z); /* permuted */
        }
    }
    else /* forth row */
    {
        if (si1 > 0)
        {
            if (si2 > 0) result = 0.0;
            else        result = -G3(2,1,-J_z);
        }
        else
        {
            if (si2 > 0) result = -G3_star(2,1,-J_z);
            else        result = G1(2,1,-J_z);
        }
    }
}
if (Anni!=0) result += annihilation_spintable(sj1,sj2,si1,si2);
return result;
}

int spin2number(int s1, int s2)
/* transforms (uu,ud,du,dd) --> (0,1,2,3) */
{
    return 2-s1-s2-(1-s2)/2;
}

double physix(int jm,int jt,int sj1,int sj2,int im,int it,int si1,int si2)
/* main routine: calculates one Hamiltonian matrix element */
/*-----*/
/* parameters: (j=final, i=initial) */
/*      jm,jt = <mu>,<theta> */
/*      sj1,sj2 = <spin electron>,<spin positron> */
{
    double result,jacobian,epsilon;

    V_seag = -2; /* seagull graph */
    epsilon = 1e-8;
}

```

## H.1. Description of the program

---

```
/* =====> transformation: (mu,theta)-->(x,k) <===== */
/*                               j --> 2 */
/*                               i --> 1 */

x[2] = (1.0 + mu[jm]*theta[jt]/sqrt(m*m + mu[jm]*mu[jm]))/2.0;
k[2] = mu[jm]*sqrt(1.0-theta[jt]*theta[jt]);

/* =====> Coulomb trick <===== */

if ((jm==im) && (jt==it) && (sj1==si1) && (sj2==si2))
{
    result = 0.0; /* default */
    result = Coulomb_discrete(jm,sj1,sj2); /* discrete counterterm */
    if (old_CT!=0) result += old_continuous(jm,jt);
    else result += CT[spin2number(sj1,sj2)][jm-1][jt-1];
    /* continuous counterterm*/
}

/* =====> No Coulomb trick <===== */

else
{
    x[1] = (1.0 + mu[im]*theta[it]/sqrt(m*m + mu[im]*mu[im]))/2.0;
    k[1] = mu[im]*sqrt(1.0-theta[it]*theta[it]);

    if ( jt==it && jm==im ) return 0.0;

    /* Note: aa = -a(Kraut), 09/11/95 */
    /* ----- */
    /* -a,A,B as defined in KPW, etc. */

    aa = (x[1]-x[2])*(x[1]-x[2])*m*m/2.0*(1/(1-x[2]))/(1-x[1])
          +1/x[1]/x[2]) + k[1]*k[1] + k[2]*k[2]
          + (x[1]-x[2])/2*(k[1]*k[1]*(1/(1-x[1])-1/x[1]) -
                       k[2]*k[2]*(1/(1-x[2])-1/x[2]));
    A = 1.0/sqrt( aa*aa - 4*k[1]*k[1]*k[2]*k[2] );
    B = (1.0-aa*A)/2.0;

    jacobian = sqrt(wmu[jm]*wmu[im]*wtheta[jt]*wtheta[it])
               *mu[jm]*mu[im]*sqrt( 4*x[1]*(1-x[1])*x[2]*(1-x[2])
               /sqrt(m*m + mu[im]*mu[im])/sqrt(m*m + mu[jm]*mu[jm]));
    result = jacobian/PI*general_spintable(sj1,sj2,si1,si2);
}
return result;
}
```

## Arithmetix

```
/* ===== */
/*
/* program      :      A R I T H M E T I X
/*
/* class       :      subroutine of MESONIX
/*
/* file name    :      "arithmetix.c"
/*
/* purpose     :      ARITHMETIX diagonalizes the four block matrices
/*                    of the Hamiltonian and sorts the Eigenvalues from
/*                    small to big ones.
/*                    The eigenfunctions are written in a file, if
/*                    <print_EF>!=0
/*
/* ----- */
```

## Appendix H. Listing of the computer code

---

```

/*                                                                 */
/* External functions:                                           */
/* -----                                                       */
/* m01caf      NAGLib routine, sorts vector                       */
/*                                                                 */
/*****/

extern double m01caf_( double *r, int *m1, int *m2, char *order,
                      int *IFAIL);
/* sorting routine from NAGLib */

double normalisation(int i, int j)
/* the factor to resubstitute Phi --> Psi */
{
    double aij;

    aij = mu[i]*mu[i]*(m*m+mu[i]*mu[i]*(1.0-theta[j]))
        /2.0/sqrt(m*m+mu[i]*mu[i]);
    aij = 1.0/sqrt(wtheta[j]*wmu[i]*aij);
    if (j<(N2+1)/2) aij *= 1.0/sqrt(2.0);
    return aij;
}

double asym_normalisation(int i, int j)
/* the factor to resubstitute Phi --> Psi */
{
    double aij;

    aij = mu[i]*mu[i]*(m*m+mu[i]*mu[i]*(1.0-theta[j]))
        /2.0/sqrt(m*m+mu[i]*mu[i]);
    aij = 1.0/sqrt(wtheta[j]*wmu[i]*aij);
    aij *= 1.0/sqrt(2.0);
    return aij;
}

void store_asy_eigenfunctions()
/* write eigenfunctions of asymmetric Hamiltonian in file 'EFunc_asy_<l>.dat' */
{
    int i,j,l,n;
    char *name_EF[4];
    FILE *fp[4];

    for (l=0; l<=3; l++) name_EF[l]=(char *)malloc(120);
    for (n=0; n<=5; n++) /* <n>th eigenvalue */
    {
        for (l=0; l<=3; l++)
        {
            sprintf(name_EF[l],"sEigenFunctions/EF%1d_J%1dasy_%1d.dat",
                    default_directory,n,J_z,l);
            printf("%s\n",name_EF[l]);
            fp[l]=fopen(name_EF[l],"w");
        }
        for (i=1; i<=N1; i++)
        for (j=1; j<=N2; j++)
        {
            for (l=0; l<=3; l++)
            {
                x[l] = (1.0 + mu[i]*theta[j]/sqrt(m*m + mu[i]*mu[i]))/2.0;
                k[l] = mu[i]*sqrt(1.0-theta[j]*theta[j]);
                fprintf(fp[l],"%18.12f %18.12f %18.12f\n",x[l],k[l],
                        v[n*4*N1*N2+(i-1)*N2*4+4*(j-1)+1]*
                        asym_normalisation(i,j));
            }
        }
    }
}

```

## H.1. Description of the program

---

```
        for (l=0; l<=3; l++) fclose(fp[l]);
    } /* loop n */
}

void store_eigenfunctions()
/* write eigenfunctions in files 'EFunc_<n>.dat' */
{
    int i,j;
    char name_EF[120];
    FILE *fp1;

    /* CH = ++ */
    sprintf(name_EF,"%sEigenFunctions/EFunc_1.dat",default_directory);
    fp1=fopen(name_EF,"w");
    for (i=1; i<=N1; i++)
        for (j=1; j<=(N2+1)/2; j++)
            {
                fprintf(fp1,"%18.12f\n",v_1[(i-1)*N2+2*j-2]*normalisation(i,j));
                if (j!=(N2+1)/2) fprintf(fp1,"%18.12f\n",v_1[(i-1)*N2+2*j-1]*normalisation(i,j));
                else fprintf(fp1,"\n"); /* dummy line */
            }
        fclose(fp1);

    /* CH = +- */
    sprintf(name_EF,"%sEigenFunctions/EFunc_2.dat",default_directory);
    fp1=fopen(name_EF,"w");
    for (i=1; i<=N1; i++)
        for (j=1; j<=(N2+1)/2; j++)
            {
                fprintf(fp1,"%18.12f\n",v_2[(i-1)*(N2+1)+2*j-2]*normalisation(i,j));
                fprintf(fp1,"%18.12f\n",v_2[(i-1)*(N2+1)+2*j-1]*normalisation(i,j));
            }
        fclose(fp1);

    /* CH = -+ */
    sprintf(name_EF,"%sEigenFunctions/EFunc_3.dat",default_directory);
    fp1=fopen(name_EF,"w");
    for (i=1; i<=N1; i++)
        for (j=1; j<=(N2+1)/2; j++)
            {
                fprintf(fp1,"%18.12f\n",v_3[(i-1)*N2+2*j-2]*normalisation(i,j));
                if (j!=(N2+1)/2)
                    fprintf(fp1,"%18.12f\n",v_3[(i-1)*N2+2*j-1]*normalisation(i,j));
                else fprintf(fp1,"\n"); /* dummy line */
            }
        fclose(fp1);

    /* CH = -- */
    sprintf(name_EF,"%sEigenFunctions/EFunc_4.dat",default_directory);
    fp1=fopen(name_EF,"w");
    for (i=1; i<=N1; i++)
        {
            for (j=1; j<(N2+1)/2; j++)
                {
                    fprintf(fp1,"%18.12f\n",v_4[(i-1)*(N2-1)+2*j-2]*normalisation(i,j));
                    fprintf(fp1,"%18.12f\n",v_4[(i-1)*(N2-1)+2*j-1]*normalisation(i,j));
                }
            fprintf(fp1,"\n"); /* dummy line */
            fprintf(fp1,"\n"); /* dummy line */
        }
        fclose(fp1);

    /* =====> write (x,k) in file 'x_k.dat' <===== */
}
```

## Appendix H. Listing of the computer code

---

```
    sprintf(name_EF,"%sEigenFunctions/x_k.dat",default_directory);
    fp1 = fopen(name_EF,"w");
    for (i=1; i<=N1; ++i)
        for (j=1; j<=(N2+1)/2; ++j)
            {
                x[1] = (1.0 + mu[i]*theta[j]/sqrt(m*m + mu[i]*mu[i]))/2.0;
                k[1] = mu[i]*sqrt(1.0-theta[j]*theta[j]);
                fprintf(fp1,"%22.16f      %22.16f\n",x[1],k[1]);
                fprintf(fp1,"%22.16f      %22.16f\n",x[1],k[1]);
            }
    fclose(fp1);

    /* mu values */
    sprintf(name_EF,"%sEigenFunctions/abscissae.dat",default_directory);
    fp1 = fopen(name_EF,"w");
    for (i=1; i<=N1; i++) fprintf(fp1,"%22.16f\n",mu[i]/p_bohr);
    fclose(fp1);
}

void arithmetix(int dim_1, int dim_2, int dim_3, int dim_4)
/* main function: diagonalize Hamiltonians */
{
    int i; /* loop variable */
    int IA_nag,N_nag,IV_nag,IFAIL_nag; /* variables for NAGLib */
    int m1,m2; /* variables for m01caf */
    FILE *ffp;

    time(&time1);
    printf("\n-----> ARITHMETIX\n");

    if ((test&(4096+16384)) == 0)
    /* J_z=0 case, 4 bloc matrices */
    {
        /* =====> diagonalize the 4 bloc matrices <===== */

        IA_nag = IV_nag = N_nag = dim_1;IFAIL_nag=-1;
        f02abf_(mat_1,&IA_nag,&N_nag,r_1,v_1,&IV_nag,e_1, &IFAIL_nag);

        IA_nag = IV_nag = N_nag = dim_2;IFAIL_nag=-1;
        f02abf_(mat_2,&IA_nag,&N_nag,r_2,v_2,&IV_nag,e_2, &IFAIL_nag);

        IA_nag = IV_nag = N_nag = dim_3;IFAIL_nag=-1;
        f02abf_(mat_3,&IA_nag,&N_nag,r_3,v_3,&IV_nag,e_3, &IFAIL_nag);

        IA_nag = IV_nag = N_nag = dim_4;IFAIL_nag=-1;
        f02abf_(mat_4,&IA_nag,&N_nag,r_4,v_4,&IV_nag,e_4, &IFAIL_nag);

        ffp=fopen("EVs_1.dat","w");
        fprintf(ffp,"C=+,H=+\n");
        for (i=1; i<=dim_1; ++i) fprintf(ffp,"%18.12f\n",r_1[i-1]);
        fclose(ffp);
        ffp=fopen("EVs_2.dat","w");
        fprintf(ffp,"C=+,H=-\n");
        for (i=1; i<=dim_2; ++i) fprintf(ffp,"%18.12f\n",r_2[i-1]);
        fclose(ffp);
        ffp=fopen("EVs_3.dat","w");
        fprintf(ffp,"C=-,H=+\n");
        for (i=1; i<=dim_3; ++i) fprintf(ffp,"%18.12f\n",r_3[i-1]);
        fclose(ffp);
        ffp=fopen("EVs_4.dat","w");
        fprintf(ffp,"C=-,H=-\n");
        for (i=1; i<=dim_4; ++i) fprintf(ffp,"%18.12f\n",r_4[i-1]);
        fclose(ffp);

        for (i=1; i<=dim_1+dim_2+dim_3+dim_4; ++i)
```

## H.1. Description of the program

---

```
/* put all EVs together */
{
    if (i<=dim_1) r[i-1] = r_1[i-1];
    else
    {
        if (i<=dim_1+dim_2) r[i-1] = r_2[i-1-dim_1];
        else
        {
            if (i<=dim_1+dim_2+dim_3)
                r[i-1] = r_3[i-1-dim_1-dim_2];
            else r[i-1] = r_4[i-1-dim_1-dim_2-dim_3];
        }
    }
}
if (print_EF > 0) store_eigenfunctions();

} /* end of (test&4096==0) */
else
{
    if ((test&16384)==0) /* asymmetric Hamiltonian (1 bloc) */
    {
        printf("                (asymmetric case)\n");
        IA_nag = IV_nag = N_nag = dim_1; IFAIL_nag = -1;
        f02abf_(ma,&IA_nag,&N_nag,r,v,&IV_nag,e, &IFAIL_nag);
        if (print_EF > 0) store_asy_eigenfunctions();
    }
    else /* use C-symmetric Hamiltonian (2 blocs) */
    {
        printf("                (symmetric case)\n");

        IA_nag = IV_nag = N_nag = dim_1; IFAIL_nag = -1;
        f02abf_(mat_1,&IA_nag,&N_nag,r_1,v_1,&IV_nag,e_1,&IFAIL_nag);

        IA_nag = IV_nag = N_nag = dim_2; IFAIL_nag = -1;
        f02abf_(mat_2,&IA_nag,&N_nag,r_2,v_2,&IV_nag,e_2,&IFAIL_nag);

        /* =====> write all eigenvalues in <r[i]> <===== */

        for (i=0; i<=dim_1-1; ++i)
        {
            r[i] = r_1[i];
            printf("H_EW[%2d] = %12.8f\n",i,r_1[i-1]);
        }
        for (i=0; i<=dim_2-1; ++i)
        {
            r[dim_1+i+1] = r_2[i];
            printf("H_EW[%2d] = %12.8f\n",i,r_2[i-1]);
        }
    }
}
order = "A"; m1 = 1; m2 = dim_1+dim_2+dim_3+dim_4;
m01caf_(r,&m1,&m2,order,&IFAIL_nag); /* sort eigenvalues */

time(&time2);
fprintf(f_log,"        ...diagonalization: %d sec\n",time2-time1);
return;
}
```

## Publix

```

/*****
/*
/* program      :      P U B L I X
/*
/* class       :      subroutine of MESONIX
/*
/* file name   :      "publix.c"
/*
/* purpose    :      PUBLIX is the output routine of MESONIX.
/*
*****/

void publix()
/* write eigenvalues in file 'EVs_J<n>.dat' */
{
    int i;
    double bs, bt, chf;
    FILE *fev;

    /* loop variable */
    /* binding coefficients */
    /* pointer onto file */

    printf("-----> PUBLIX\n");
    if ((test & 4) != 0) /* write EVs of 4 blocs in different files */
    {
        printf(">>>> INFO : 2nd test bit set ON => eigenvalues in 'EV_<n>.dat'\n");

        fev = fopen("EV_1.dat", "w");
        fprintf(fev, "Sector: CH = ++\n-----\n\n", i, r_1[i]);
        for (i=0; i<=N1*N2-1; ++i) fprintf(fev, "%18.12f\n", r_1[i]);
        fclose(fev);

        fev = fopen("EV_2.dat", "w");
        fprintf(fev, "Sector: CH = +-\n-----\n\n", i, r_1[i]);
        for (i=0; i<=N1*N2+N1-1; ++i) fprintf(fev, "%18.12f\n", r_2[i]);
        fclose(fev);

        fev = fopen("EV_3.dat", "w");
        fprintf(fev, "Sector: CH = -+\n-----\n\n", i, r_1[i]);
        for (i=0; i<=N1*N2-1; ++i) fprintf(fev, "%18.12f\n", r_3[i]);
        fclose(fev);

        fev = fopen("EV_4.dat", "w");
        fprintf(fev, "Sector: CH = --\n-----\n\n", i, r_1[i]);
        for (i=0; i<=N1*N2-N1-1; ++i) fprintf(fev, "%18.12f\n", r_4[i]);
        fclose(fev);
    }
    fev = fopen(name_EV, "a"); /* open file for eigenvalues */
    i=-1;
    while ((++i<4*N1*N2)&&(i<number_EV)) fprintf(fev, "%18.12f\n", r[i]);
    for (i=4*N1*N2+1; i<=number_EV; ++i) fprintf(fev, "\n");
    /* fill with empty lines up to <number_EV> */
    fclose(fev);

    /* =====> calculate binding coefficients <===== */

    bs = 4.0/ALPHA/ALPHA*(2.0-sqrt(r[0]));
    bt = 4.0/ALPHA/ALPHA*(2.0-sqrt(r[1]));
    chf = (sqrt(r[1])-sqrt(r[0]))/ALPHA/ALPHA/ALPHA/ALPHA;
    fprintf(f_log, "\n      B_s = %12.8f\n", bs);
    fprintf(f_log, "      B_t = %12.8f\n", bt);
    fprintf(f_log, "      C_hf = %12.8f\n", chf);
    return;
}

```

# Bibliography

- [1] G. T'HOOFT, "Renormalization of Massless Yang-Mills Fields", Nucl. Phys. **B33** (1971) 173.
- [2] H.D. POLITZER, "Reliable Perturbative Results for Strong Interactions?", Phys. Rev. Lett. **30** (1973) 1346; "Asymptotic Freedom: An Approach to Strong Interactions", Phys. Rep. **C14** (1974) 129.
- [3] D.J. GROSS, F. WILCZEK, "Ultraviolet Behavior of Non-Abelian Gauge Theories", Phys. Rev. Lett. **30** (1973) 1343.
- [4] K.G. WILSON, "Confinement of Quarks", Phys. Rev. **D10** (1974) 2445.
- [5] H. YUKAWA, "On the Interaction of Elementary Particles", Proc. Phys. Math. Soc. Jap. **17** (1935) 48–57.
- [6] E. SCHRÖDINGER, "Quantisierung als Eigenwertproblem (Erste Mitteilung.)", Ann.Phys.(Leipzig) **79** (1926) 361-376; Ann.Phys.(Leipzig) **79** (1926) 489-527; Ann.Phys.(Leipzig) **80** (1926) 437-490; Ann.Phys.(Leipzig) **81** (1926) 109-139; Ann.Phys.(Leipzig) **79** (1926) 734-756.
- [7] J. L. RICHARDSON, "The heavy Quark Potential and the  $\Upsilon$ ,  $J/\psi$  Systems", Phys. Lett. **82B** (1979) 272.
- [8] W.BUCHMÜLLER, S.-H. H. TYE, "Quarkonia and Quantum Chromodynamics", Phys. Rev. **D24** (1981) 132.
- [9] S. GOTTFREY, N. ISGUR, "Mesons in a relativized quark model with chromodynamics", Phys. Rev. **D32** (1985) 189-231.
- [10] J.J. AUBERT ET AL., "Experimental Observation of a Heavy Particle  $J$ ", Phys. Rev. Lett. **33** (1974) 1404–1406.
- [11] J.E. AUGUSTIN ET AL., "Discovery of a Narrow Resonance in  $e^+e^-$  Annihilation" Phys. Rev. Lett. **33** (1974) 1406–1408.
- [12] S.W. HERB ET AL., "Observation of a Dimuon Resonance at 9.5 GeV in 400-GeV Proton-Nucleus Collisions", Phys. Rev. Lett. **39** (1977) 252–255.



## BIBLIOGRAPHY

---

- [13] M. CREUTZ, “*Quarks, Gluons and Lattices*”, Cambridge University Press, Cambridge 1983.
- [14] E.E. SALPETER, H.A. BETHE, “*A Relativistic Equation for Bound-State Problems*”, Phys. Rev. **84** (1951) 1232; E.E. SALPETER, “*Mass Corrections to the Fine Structure of Hydrogen-Like Atoms*”, Phys. Rev. **87** (1952) 328–343; Phys. Rev. **84** (1951) 1226.
- [15] D. WEINGARTEN, Nucl. Phys. (Proc. Supp.) **B34** (1994) 29; C.T.H. DAVIES, A.J. LINDSEY, K. HORNBOSTEL, G.P. LEPAGE, J. SHIGEMITSU, J. SLOAN, “ *$B_c$  and  $\Upsilon$  Spectra from Lattice NRQCD*”, hep-lat/9510052, October 1995.
- [16] D. GROMES, “*Construction of Bethe-Salpeter Wave Functions and Applications in QCD*”, Z. Phys. **C57** (1993) 631–638; “*More on Bethe Salpeter Wave Functions for Quark-Antiquark Systems*”, Preprint HD-THEP-93-15, 1993.
- [17] H. LEUTWYLER, J. STERN, “*Relativistic Dynamics on a Null Plane*”, Ann. Phys. (NY) **112** (1978) 94.
- [18] K.G. WILSON, T.S. WALHOUT, A. HARINDRANTH, W.-M. ZHANG, R.J. PERRY, “*Nonperturbative QCD: A weak-coupling treatment on the light front*”, Phys. Rev. **D49** (1994) 6720.
- [19] R.J. PERRY, “*Hamiltonian Light-Front Theory and Quantum Chromodynamics*”, in *Proceedings of Hadrons 94*, V. Herscovitz, C. Vasconcellos, Eds., World Scientific, Singapore 1995.
- [20] H.-C. PAULI, “*Solving Gauge field Theory by Discretized Light-Cone Quantization*”, submitted to Phys. Rev. **D** (1996).
- [21] S. TOMONAGA, “*On a Relativistically Invariant Formulation of the Quantum Theory of Wave Fields*”, Prog. Theoret. Phys. **1** (1946) 27–42; Z. Koba, T. TATI, S. TOMONAGA, “*On a Relativistically Invariant Formulation of the Quantum Theory of Wave Fields. II. — Case of Interacting Electromagnetic and Electron Fields —*”, Prog. Theoret. Phys. **2** (1947) 101–116; Z. Koba, T. TATI, S. TOMONAGA, “*On a Relativistically Invariant Formulation of the Quantum Theory of Wave Fields. III. — Case of Interacting Electromagnetic and Electron Fields —*”, Prog. Theoret. Phys. **2** (1947) 198–208; S. KANESAWA, S. TOMONAGA, “*On a Relativistically Invariant Formulation of the Quantum Theory of Wave Fields. VI. — Case of Interacting Electromagnetic and Meson Fields —*”, Prog. Theoret. Phys. **3** (1948) 1–13; S. KANESAWA, S. TOMONAGA, “*On a Relativistically Invariant Formulation of the Quantum Theory of Wave Fields. V. — Case of Interacting Electromagnetic and Meson Fields —*”, Prog. Theoret. Phys. **3** (1948) 101–113; S. TOMONAGA, Phys. Rev. **74** (1948) 224.

- [22] R. P. FEYNMAN, “*Space-Time Approach to Non-Relativistic Quantum Mechanics*”, Rev. Mod. Phys. **20** (1948) 367–387; “*A Relativistic Cut-Off for Classical Electrodynamics*”, Phys. Rev. **74** (1948) 739–746; “*A Relativistic Cut-Off for Quantum Electrodynamics*”, Phys. Rev. **74** (1948) 1430–1438; “*The Theory of Positrons*”, Phys. Rev. **76** (1949) 749–759; “*Space-Time Approach to Quantum Electrodynamics*”, Phys. Rev. **76** (1949) 769.
- [23] J. SCHWINGER, “*Quantum Electrodynamics. I. A Covariant Formulation*”, Phys. Rev. **74** (1948) 1439; “*Quantum Electrodynamics. II. Vacuum Polarization and Self-Energy*”, Phys. Rev. **75** (1948) 651–679.
- [24] M. KRAUTGÄRTNER, H.-C. PAULI, F. WÖLZ, “*Positronium and Heavy Quarkonia as Testing Case for DLCQ*”, Phys. Rev. **D45** (1992) 3755.
- [25] H.-C. PAULI, “*On a Numerical Exact Solution to the Many-Body Problem in One Dimension*”, Z. Phys. **A319** (1984) 303-314.
- [26] B. VAN DE SANDE, “*Renormalization and the Zero-Mode in Light-Front field Theory*”, Dissertation, Ohio State University, 1994; “*Renormalization of Tamm-Dancoff Integral Equations*”, hep-th/9210147; B. VAN DE SANDE, S.S. PINSKY, ET AL. “*Spontaneous Symmetry Breaking of  $\phi^4$  Theory in Light-Front Field Theory*”, Phys. Rev. **D48** (1993) 816-821; Phys. Rev. **D49** (1994) 2001-2013; Phys. Rev. **D51** (1994) 726-733.
- [27] P.A.M. DIRAC, “*Forms of Relativistic Dynamics*”, Rev. Mod. Phys. **21** (1949) 392.
- [28] J. SCHWINGER, “*Quantum Electrodynamics. III. The Electromagnetic Properties of the Electron — Radiative Corrections to Scattering*”, Phys. Rev. **75** (1948) 790–817.
- [29] S. WEINBERG, “*Dynamics at Infinite Momentum*”, Phys. Rev. **150** (1966) 1313.
- [30] J.B. KOGUT, D.E. SOPER, “*Quantum Electrodynamics in the Infinite-Momentum Frame*”, Phys. Rev. **D1** (1970) 2901.
- [31] S.J. CHANG, R.G. ROOT, T.M. YAN, “*Quantum field theories in the infinite momentum frame. I–III.*”, Phys. Rev. **D7** (1973) 1133;1147;1760.
- [32] N.E. LIGTERINK, “*Light-front Hamiltonian field theory: covariance and renormalization*”, Dissertation, University of Amsterdam, 1996; N.E. LIGTERINK, B.L.G. BAKKER, “*Equivalence of light-front and covariant field theory*”, Phys. Rev. **D52** (1995) 5954.
- [33] G.P. LEPAGE, S.J. BRODSKY, “*Exclusive processes in perturbative Chromodynamics*”, Phys. Rev. **D22** (1980) 2157.

- [34] S.J. Brodsky, G.P. LEPAGE, in “*Perturbative Quantum Chromodynamics*”, A.H. Mueller, Ed., World Scientific, Singapore, 1989.
- [35] H.-C. PAULI, S.J. BRODSKY, “*Solving field theory in one space and one time dimension*”, Phys. Rev. **D32** (1985) 1993; “*Discretized light-cone quantization: Solution to a field theory in one space and one time dimension*”, Phys. Rev. **D32** (1985) 2001.
- [36] M. SAWICKI, “*Solution of the light-cone equation for the relativistic bound state*”, Phys. Rev. **D32** (1985) 2666; “*Eigensolutions of the light-cone equation for a scalar field model*”, Phys. Rev. **D33** (1986) 1103.
- [37] A. HARINDRANATH, J.P. VARY, “*Solving  $\phi_2^4$  by discretized light front quantization*”, Phys. Rev. **D36** (1987) 3666.
- [38] K. HORNBOSTEL, S.J. BRODSKY, H.-C. PAULI, “*Light-Cone-Quantized QCD in 1+1 Dimensions*”, Phys. Rev. **D45** (1990) 3814; K. HORNBOSTEL, Ph.D. thesis, SLAC Report 333.
- [39] M. HEYSSLER, “*Numerische Lösungsverfahren zur  $QCD_{(1+1)}$  im Rahmen der DLCQ-Methode*”, Diplomarbeit, Heidelberg 1994.
- [40] S. ELLER, H.-C. PAULI, S.J. BRODSKY, “*DLCQ: The massless and the massive Schwinger Model*”, Phys. Rev. **35** (1987) 1493.
- [41] G. MCCARTOR, “*Schwinger Model in the light cone representation*”, Z. Phys. **C64** (1994) 349–354; “*Light cone gauge Schwinger Model*”, Z. Phys. **C52** (1991) 611–626.
- [42] S. ELSER, “*Das Spektrum der  $QED_{(1+1)}$  im Rahmen der DLCQ-Methode*”, Diplomarbeit, Heidelberg 1994.
- [43] M. VÖLLINGER, “*Über die Lichtkegel-Nullmoden in der  $QED_{(1+1)}$* ”, Diplomarbeit, Heidelberg 1996.
- [44] A. TANG, “*DLCQ: Application to Quantum Electrodynamics*”, Dissertation, SLAC-Report-351, Juni 1990; A. TANG, S.J. BRODSKY, H.-C. PAULI, “*Discretized light-cone quantization: Formalism for quantum electrodynamics*”, Phys. Rev. **D44** (1991) 1842.
- [45] M. KALUZA, H.-C. PAULI, “*Discretized light-cone quantization:  $e^+e^-(\gamma)$  Model for Positronium*”, Phys. Rev. **D45** (1992) 2968; M. KALUZA, “*Facets of solving 3+1 gauge theory with DLCQ*”, Dissertation, Heidelberg 1991.
- [46] F. WÖLZ, “*Über das Spektrum der Normalmoden in der QCD und die Theorie der effektiven Wechselwirkung nach der Tamm-Dancoff Methode*”, Dissertation (unpublished), Heidelberg 1995.

- [47] A.C. KALLONIATIS, H.-C. PAULI, S.S. PINSKY, “Towards solving QCD: The transverse zero modes in light-cone quantization”, Phys. Rev. **D52** (1995) 1176-1189.
- [48] R.M. BAYER, “Berechnung von Spektren in einem kollinearen Modell der Quantenchromodynamik”, Dissertation(unpublished), Heidelberg 1996.
- [49] B. VAN DE SANDE, M. BURCKARDT, “Tube model for light-front QCD”, Phys. Rev. **D53** (1996) 4628–4637.
- [50] B. VAN DE SANDE, S. DALLEY, “The transverse lattice in 2+1 dimensions” in B.N. KURSUNOGLU, S. MINTZ, AND A. PERLMUTTER (Eds.), “Neutrino Mass, Monopole Condensation, Dark Matter, and Gravitational Waves”, Plenum Publishing Corp., New York, to be published in 1996.
- [51] M. BURKARDT, A. LANGNAU, “Rotational invariance in light-cone quantization”, Phys. Rev. **D44** (1991) 3857–3867.
- [52] M. KALUZA, H.-J. PIRNER: “Hyperfine splitting in the light-cone Tamm-Dancoff equation of QED and QCD”, Phys. Rev. **D47** (1993) 1620-1628.
- [53] G. LEIBBRANDT, “Introduction to non-covariant gauges”, Rev. Mod. Phys. **59** (1987) 1067.
- [54] D. MUSTAKI, S.S. PINSKY, J. SHIGEMITSU, K.G. WILSON, “Perturbative renormalization of null-plane QED”, Phys. Rev. **D43** (1991) 3411-3427.
- [55] S. MANDELSTAM, “Light-cone superspace and ultraviolet finiteness of the N=4 model”, Nucl. Phys. **B213** (1983) 149; G. LEIBBRANDT, “Light-cone gauge in Yang-Mills theory”, Phys. Rev. **D29** (1984) 1699.
- [56] A. BASETTO, M. DALBOLSCO, I. LAZZIZZERA, R. SOLDATI, “Yang-Mills theories in the light-cone gauge” Phys. Rev. **D31** (1985) 2012.
- [57] A.C. KALLONIATIS, H.-C. PAULI, “Bosonic zero modes and gauge theory in discrete light-cone quantization”, Z. Phys. **C60** (1993) 255-264; “Beyond the Light-Cone Gauge in Discrete Light-Cone Quantization of Quantum Electrodynamics”, Z. Phys. **C63** (1994) 161.
- [58] T. HEINZL, S. KRUSCHE, S. SIMBÜRGER, AND E. WERNER, “Nonperturbative light cone quantum field theory beyond the tree level”, Z. Phys. **C56**, (1992) 415.
- [59] G. MCCARTOR, “Bosonic Zero Modes in Discretized Light Cone Field Theory”, Z. Phys. **C53** (1992) 679–686.
- [60] A.C. KALLONIATIS, D. ROBERTSON, “On the Discretized Light-Cone Quantization of Electrodynamics”, Phys. Rev. **D50** (1994) 5262.

- [61] S. COLEMAN, R. JACKIW, L. SUSSKIND, *Ann. Phys.* **93** (1975) 267; S. COLEMAN, *Ann. Phys.* **101** (1976) 239.
- [62] B. VAN DE SANDE, “*Convergence of Discretized Light-Cone Quantization in the Small Mass Limit*”, Preprint MPIH-V18-1996, hep-ph/9605409.
- [63] J. PIRENNE, *Arch. Sci. phys. nat.* **29** (1947) 121, 207, 265; V. BERESTETSKI, L.D. LANDAU, “*Interaction between an Electron and a Positron*”, translated from the Russian original, *JETP(USSR)* **19** (1949) 673–679; V. BERESTETSKI, “*The spectrum of Positronium*”, translated from the Russian original, *JETP(USSR)* **19** (1949) 1130–1135; R.A. FERRELL, “*The Positronium Fine Structure*”, *Phys. Rev.* **84** (1951) 858 (Letter to the editor); R.A. FERRELL, Ph.D. thesis, Princeton University, 1952.
- [64] F. WÖLZ, “*Numerische Lösung des Coulomb-Problems in der Impulsdarstellung*”, Diplomarbeit (unpublished), Heidelberg 1990.
- [65] S.J. BRODSKY, H.-C. PAULI, “*Light-Cone Quantization of Quantum Chromodynamics*” in H. MITTER, H. GAUSTERER (Eds.) : “*Recent Aspects of Quantum Fields*”, Proceedings of the XXX. Int. Universitätswochen für Kernphysik in Schladming 1991, Springer-Verlag.
- [66] P.M. MORSE, H. FESHBACH, “*Methods of Theoretical Physics*” (2 Volumes) McGraw-Hill, New York 1953.
- [67] I.J. TAMM, “*Relativistic Interaction of Elementary Particles*”, *J. Phys. (USSR)* **9** (1945) 449.
- [68] S.M. DANCOFF, “*Non-Adiabatic Meson Theory of Nuclear Forces*”, *Phys. Rev.* **78** (1950) 382.
- [69] S.N. GUPTA, W.W. REPKO, C.J. SUCHYTA, “*Muonium and positronium potentials*” *Phys. Rev.* **D40** (1989) 4100–4104.
- [70] T. KINOSHITA(Ed.), “*Quantum Electrodynamics*”, World Scientific, Singapore 1990.
- [71] K.-P. JUNGMANN, “*Kontinuierliches Multimoden-Laserspektrometer zur Zweiphotonenspektroskopie am Positronium-Atom*”, Dissertation (unpublished), Heidelberg 1985.
- [72] H.A. BETHE, E.E. SALPETER, “*Quantum Mechanics of One and Two-Electron Atoms*”, A Plenum/Rosetta Edition, Plenum Publishing Corporation, New York, 1957, 1977.
- [73] M. KRAUTGÄRTNER, “*Anwendung der DLCQ auf die QED*”, Dissertation (unpublished), Heidelberg 1992.

- [74] E. FERMI, “Über die magnetischen Momente der Atomkerne”, *Z. Phys.* **60** (1930) 320–333.
- [75] G.T. BODWIN, D.R. YENNIE, M.A. GREGORIO, “Recoil Effects in the hyperfine structure of QED bound states”, *Rev. Mod. Phys.* **57** (1985) 723–782.
- [76] F. COESTER, “Null-Plane Dynamics of Particles and Fields”, *Prog. Part. Nucl. Phys.* **29** (1992) 1–32.
- [77] K. LUBANSKI, “Sur la théorie des particules élémentaires de spin quelconque”, *Physics* **9** (1942) 310–338.
- [78] H.J. MELOSH, “Quarks: Currents and Constituents”, *Phys. Rev.* **D9** (1974) 1095–1112.
- [79] T. FULTON, P.C. MARTIN, “Two-Body System in Quantum Electrodynamics. Energy Levels of Positronium”, *Phys. Rev.* **95** (1954) 811–822.
- [80] W.D. DYKSHOORN, R. KONIUK “Ultrarelativistic bound states in spinor and scalar QED”, *Phys. Rev.* **A41** (1990) 60–63; “Spin effects in highly relativistic systems”, *Phys. Rev.* **A41** (1990) 64–67.
- [81] H.-C. PAULI in B.N. KURSUNOGLU, S. MINTZ, AND A. PERLMUTTER (Eds.), “Neutrino Mass, Monopole Condensation, Dark Matter, and Gravitational Waves”, Plenum Publishing Corp., New York, to be published in 1996.
- [82] M. BRISUDOVÁ, R.J. PERRY, “Initial bound state studies in light-front QCD”, *Phys. Rev.* **D54** (1996) 1831; “Note on restoring manifest rotational symmetry in hyperfine and fine structure in light-front QED”, [hep-th/9605363](#), 1996.
- [83] B.D. JONES, R.J. PERRY, S.D. GLAZEK, “Nonperturbative QED: An analytical treatment on the light front”, [hep-th/9605231](#), submitted to *Phys. Rev. D*.
- [84] F. WEGNER, “Flow-equations for Hamiltonians”, *Ann. Phys.* **3** (1994) 77–91.
- [85] H.J. PIRNER, private communication.
- [86] E. AMMONS, “Bloch-Wilson Renormalization of Tamm-Dancoff Light-Front QED”, *Phys. Rev.* **D54** (1996) 5153–5162.
- [87] H.-C. PAULI, private communication.
- [88] H.-C. PAULI, J. MERKEL, “On the Masses of the Physical Mesons: Solving the Effective QCD-Hamiltonian by DLCQ”, submitted to *Phys. Rev. D* (1996).
- [89] J.L. ANDERSON, P.G. BERGMANN, “Constraints in Covariant Field Theories”, *Phys. Rev.* **83** (1951) 1018.

## BIBLIOGRAPHY

---

- [90] K. SUNDERMAYER, “*Constrained Dynamics*”, Lecture Notes in Physics **169**, Springer, Berlin 1982.
- [91] P.A.M. DIRAC, “*Lectures on Quantum Mechanics*”, Belfer Graduate School of Science Monograph Series, New York 1964.
- [92] J. MERKEL, “*Über das Massenspektrum der physikalischen Mesonen: Ein effektiver QCD-Hamiltonian mit laufender Kopplungskonstante*”, Diplomarbeit, Heidelberg 1994.
- [93] V.A. KARMANOV, “*Light-front wave function of a relativistic composite system in an explicitly solvable model*”, Nucl. Phys. **B166** (1980) 378–398.
- [94] V.A. KARMANOV, “*Relativistic deuteron wave function on the light front*”, Nucl. Phys. **A362** (1981) 331–348.
- [95] W.H. PRESS, B.P. FLANNARY, S.A. TEUKOLSKY, W.T. VETTERLING, “*Numerical Recipes*”, Cambridge University Press, 1989.
- [96] C. ITZYKSON, J.B. ZUBER, “*Quantum Field Theory*”, McGraw Hill, 1980.
- [97] O. NACHTMANN, “*Konzepte und Phänomene der Elementarteilchenphysik*”, Vieweg, Braunschweig 1986.
- [98] B. VAN DE SANDE, “*On the Coulomb Singularity*”, unpublished notes.
- [99] “*The NAG Fortran Library Manual, Mark 16*”, The Numerical Algorithms Group Limited, 1993.